$\mathcal{H}^\infty$ Controller Design for Uncertain Multiple-Time-Delay Systems

HAKKI ULAŞ ÜNAL

Ph.D. Dissertation

Graduate School of Sciences

Electrical and Electronics

Engineering Program

January 2010

JÜRİ VE ENSTİTÜ ONAYI

Hakkı Ulaş ÜNAL'ın $\mathcal{H}^\infty$ **Controller Design for Uncertain Multiple-Time-Delay Systems** başlıklı **Elektrik-Elektronik Mühendisliği** Anabilim Dalı **Kontrol ve Kumanda Sistemleri** Bilim Dalındaki Doktora tezi 28-12-2009 tarihinde aşağıdaki jüri tarafından Anadolu Üniversitesi Lisansüstü Eğitim-Öğretim ve Sınav Yönetmeliğinin ilgili maddeleri uyarınca değerlendirilerek kabul edilmiştir.

	Adı -Soyadı	**İmza**
Üye (Tez Danışmanı)	**: Prof. Dr. Altuğ İFTAR**	**.....**
Üye	**: Prof. Dr. Hitay ÖZBAY**	**.....**
Üye	**: Doç. Dr. Haluk HÜSEYİN**	**.....**
Üye	**: Prof.Dr. Hüseyin AKÇAY**	**.....**
Üye	**: Doç. Dr. Alpaslan PARLAKÇI**	**.....**

Anadolu Üniversitesi Fen Bilimleri Enstitüsü Yönetim Kurulu'nun ..... tarih ve ..... sayılı kararıyla onaylanmıştır.

Enstitü Müdürü

ABSTRACT

Ph.D. Dissertation

$\mathcal{H}^\infty$ Controller Design for Uncertain Multiple-Time-Delay Systems

Hakkı Ulaş ÜNAL

Anadolu University
Graduate School of Sciences
Electrical and Electronics Engineering Program

Supervisor: Prof. Dr. Altuğ İFTAR

2010, 160 pages

In this dissertation, $\mathcal{H}^\infty$ controller design for systems with multiple uncertain time-delays is studied. In the $\mathcal{H}^\infty$ controller design for these systems, since the nominal time-delays are taken outside the generalized plant, the uncertainty block of the overall system may become non-causal. However, the $\mathcal{H}^\infty$ controller is designed by the small-gain theorem, which assumes the causality of the feedback interconnected subsystems. To alleviate this difficulty, the sufficient conditions are derived to satisfy the validity of the small-gain theorem for feedback interconnection of non-causal systems. Utilizing these results, an optimal $\mathcal{H}^\infty$ flow controller is designed for data-communication networks. Stable $\mathcal{H}^\infty$ controller design is also studied and different design approaches are presented. Furthermore, to satisfy one of the time-domain requirements of the flow controller, sufficient conditions are introduced to choose the free parameter in the structure of the designed controller.

Keywords: Multiple-time-delay systems, $\mathcal{H}^\infty$ controller design, Robust control, Non-causal systems, Stable $\mathcal{H}^\infty$ controller design, Flow control, Data-communication networks.

ÖZET

Doktora Tezi

Çoklu-Zaman-Gecikmeli Belirsiz Sistemler İçin $\mathcal{H}^\infty$ Denetleyici Tasarımı

Hakkı Ulaş ÜNAL

Anadolu Üniversitesi
Fen Bilimleri Enstitüsü
Elektrik-Elektronik Mühendisliği Anabilim Dalı

Danışman: Prof. Dr. Altuğ İFTAR

2010, 160 sayfa

Bu tezde, belirsiz çoklu zaman gecikmelerine sahip sistemler için $\mathcal{H}^\infty$ denetleyici tasarımı üzerine çalışılmıştır. Bu sistemler için $\mathcal{H}^\infty$ denetleyici tasarımı yapılırken nominal zaman gecikmeleri dışarı alındığından dolayı sistemin belirsizlik bloğu nedensel olamayabilmektedir. Fakat, $\mathcal{H}^\infty$ denetleyici tasarımı birbirine geri-besleme ile bağlı sistemlerin nedensel olduğunu kabul eden küçük-kazanç teoremi kullanılarak yapılmaktadır. Bu durumun üstesinden gelmek için, birbirine geri-besleme ile bağlı nedensel olmayan sistemlerde küçük-kazanç teoremini sağlamak için yeterli koşullar türetilmiştir. Bu sonuçlardan faydalanarak da veri-iletişim ağları için optimal $\mathcal{H}^\infty$ akış denetleyicisi tasarlanmıştır. Kararlı $\mathcal{H}^\infty$ denetleyicisi üzerine de çalışılmış ve farklı tasarım yaklaşımları sunulmuştur. Bunlara ilaveten, tasarlanan denetleyicinin zaman bölgesi kısıtlarını yapısındaki serbest parametre ile sağlaması için, serbest parametrenin seçimi için yeterli koşullar verilmiştir.

Anahtar Kelimeler: Çoklu-zaman-gecikmeli sistemler, $\mathcal{H}^\infty$ denetleyici tasarımı, Gürbüz denetim, Nedensel olmayan sistemler, Kararlı $\mathcal{H}^\infty$ denetleyici tasarımı, Akış denetimi, Veri-iletişim ağları.

ACKNOWLEDGMENTS

I would like to thank my advisor, Professor Altuğ İftar for all his understanding, support, and help during this dissertation study. This dissertation would not be possible without his experience, control, patience especially correcting my scientific errors. It is an honor for me to study under his supervision. I would also like to thank Professor Hitay Özbay for his support and contributions in Chapter 4 and Chapter 5 of this dissertation. I would also like to thank Professors Haluk Hüseyin, Hüseyin Akçay and Alpaslan Parlakçı for serving in my examination committee.

I would like to acknowledge the collaboration of Dr. Banu Ataşlar-Ayyıldız for providing some results in the fourth chapter of this dissertation.

I would like to thank Dr. Suat Gümüşsoy for all his support and encouragement since we met. I will never forget his encouragement during this dissertation.

I would like to thank one of the anonymous reviewers for his/her comments on the paper "A Small gain theorem for systems with non-causal subsystems," which was published in Automatica in November, 2008, which allowed me to correct a technical error in the proof of Theorem 1 (Theorem 3.1 in this dissertation). I would also like to thank one of the anonymous reviewers for his/her comments on the paper "Robust flow control in data-communication networks with multiple time-delays," which will appear in International Journal of Robust and Nonlinear Control in 2010, since results in Section 3.5 are based on his/her comments.

Finally, I am thankful to my parents, especially my brother, Hilmi Umut Ünal, who never withheld his support, encouragement, and help during my studies. I want to thank "Sıdıka" and Ozan Devrim Yay and all my friends who were with me while I was struggling to overcome the problems of the "life" and complete my studies.

TABLE OF CONTENTS

LIST OF FIGURES

LIST OF TABLES

NOTATION

$\mathbb{R}$	Real numbers
$\overline{\mathbb{R}}$	$\mathbb{R} \cup \{\infty\}$
$\mathbb{C}$	Complex numbers
$\mathbb{C}_-$	Open left-half plane
$\mathbb{C}_+$	Open right-half plane
$\overline{\mathbb{C}}_+$	Closed right-half plane
$\mathbb{R}^n$	n-dimensional real vector space
j	Imaginary unit, $j^2 = -1$
$\lceil \cdot \rceil$	Ceiling function
$\approx$	Approximately equal to
I	Identity matrix of appropriate dimensions
0	Zero matrix of appropriate dimensions
$\mathbf{1_k}$	$1 \times k$ matrix of all 1's
I_k	$k \times k$ identity matrix
$\text{diag}(\cdots)$	A diagonal matrix with elements on the $(\cdots)$ main diagonal
$\text{bdiag}(\cdots)$	A block diagonal matrix with blocks $(\cdots)$ on its diagonal
n_w	Dimension of a vector w
J_{zw}	$\text{bdiag}(I_{n_z}, -I_{n_w})$, for vectors z and w
a^T	Transpose of a vector a
A^T	Transpose of a matrix A
A^{-1}	Inverse of a matrix A
$\rho(A)$	Spectral radius of a matrix A

$\overline{\sigma}(A)$	Largest singular value of a matrix A
$A \geq B$	For matrices A and B, $A - B$ is positive semi-definite
$A > B$	For matrices A and B, $A - B$ is positive definite
$\|a\|$	Absolute value of a scalar a
$\|a\|_p$	p-norm of a vector a
$\|A\|_p$	Induced p-norm of a matrix A
$\left[\begin{array}{c\|c} A & B \\ \hline C & D \end{array}\right]$	Shorthand for $C(sI - A)^{-1}B + D$
$G^{\sim}(s)$	$G^T(-s)$
$G^*(s)$	$G^T(\bar{s})$,
$\mathcal{L}\{\cdot\}$	Laplace transformation
$F_l(\cdot, \cdot)$	Lower-LFT
$F_u(\cdot, \cdot)$	Upper-LFT
$HM(\cdot, \cdot)$	Homographic transformation
$\sup_{x \in X}\{f(x)\}$	Supremum of the function $f(x)$ over $x \in X$
$\inf_{x \in X}\{f(x)\}$	Infimum of the function $f(x)$ over $x \in X$
$L_p[a, \infty)$	The space of all measurable functions $f : [a, \infty) \to \mathbb{R}$ such that $\int_a^\infty \|f(t)\|^p dt < \infty$, $p \in [1, \infty)$
$\|f\|_p$	$\left[\int_a^\infty \|f(t)\|^p dt\right]^{1/p}$, where $f(t) \in L_p[a, \infty)$, $p \in [1, \infty)$
$\mathcal{RL}^\infty{}_{n \times m}$	The space of all $n \times m$ dimensional proper and real rational TFMs with no poles on the imaginary axis
$\mathcal{H}^\infty$	The space of analytic and bounded matrix functions in $\overline{\mathbb{C}}_+$
$\mathcal{RH}^\infty$	The space of analytic and bounded real rational matrix functions in $\overline{\mathbb{C}}_+$
$\|G\|_\infty$	$\sup_{\omega \in \overline{\mathbb{R}}} \overline{\sigma}(G(j\omega))$, where $G \in \mathcal{RH}^\infty$

LIST OF ACRONYMS

ABR	Available Bit Rate
ATM	Asynchronous Transfer Mode
CBR	Constant Bit Rate
FIR	Finite impulse response
HM	Homographic Transformation
LFT	Linear Fractional Transformation
LMI	Linear Matrix Inequality
LTI	Linear Time-Invariant
LTV	Linear Time-Varying
MIMO	Multi-Input Multi-Output
MISO	Multi-Input Single-Output
OBP	One-Block Problem
QoS	Quality of Service
SHP	Standard $\mathcal{H}^\infty$ Problem
SIMO	Single-Input Multi-Output
SISO	Single-Input Single-Output
TCP/IP	Transmission Control Protocol / Internet Protocol
TFM	Transfer Function Matrix
VBR	Variable Bit Rate
UBR	Unspecified Bit Rate

1 INTRODUCTION

1.1 Overview and Motivation

Time-delays appear in the dynamics of most physical systems, because the reactions of the physical systems to external actions never take place instantaneously due to the transportation and propagation phenomena. In data-communication networks, signals that are sent from the sources do not arrive instantly to the destination. In economic systems or political systems, the effects of taken decisions happen after a time interval (see [1] for a wide survey). Therefore, systems with delays abound in the world.

Handling delays in a control system is difficult and a long-standing problem, since systems with time-delay are a class of infinite-dimensional systems. It is well known that if the time-delays of the system to be controlled are "sufficiently" small, then a controller can be designed by neglecting the delays, and it may satisfy the design requirements. However, under significant time-delays, the delays can not be neglected. A controller designed by neglecting the time-delays may fail to stabilize the actual system or may exhibit poor performance. On the other hand, inserted time-delays are used to yield a stabilizing controller for many systems, e.g. oscillatory systems (see [2]).

One of the most important issues of the feedback control theory is to overcome the destabilizing effect of the existing uncertainties, which is the discrepancy between the physical plant and the mathematical model for which a controller is to be designed. In addition to these uncertainties, unmeasured noises and disturbances that act on the physical plant may destabilize the feedback system. In order to design a controller, which stabilizes the physical plant and meets the design specifications against uncertainties, robust control tools can be used. $\mathcal{H}^\infty$ control is one of the powerful robust control tools, since it utilizes the magnitude of the plant uncertainties in a proper way by the small-gain theorem which verifies the internal stability of the feedback

interconnected stable causal subsystems [3–5].

In the literature, there exists numerous robust controller design approaches for time-delay systems [1]. These controller design approaches can be classified as operator-theoretical approaches, state-space methods, and J-spectral factorization. Toker and Özbay [6] used the operator theory [7, 8] to formulate an $\mathcal{H}^\infty$-optimal controller design approach for SISO infinite-dimensional systems. This approach, however, can be used only for SISO systems. In [9], design of an $\mathcal{H}^\infty$ controller is given for SISO general time-delay systems by the Skew-Toeplitz operator approach [8]. Nagpal and Ravi [10] and Tadmor [11] used state-space methods to design an $\mathcal{H}^\infty$ controller for single-time-delay systems. In [12], J-spectral factorizations are used to solve the same problem for systems which involve a single delay. The general solution of the $\mathcal{H}^\infty$-optimal controller design problem for systems which involve multiple delays is given in [13]. In [13], the problem with multiple time-delays is decomposed into a nested sequence of simpler problems each with a single delay, called an *adobe problem*, then a controller is obtained solving each problem.

In order to design a stabilizing controller for a system with multiple time-delays by the approach of [13], the known nominal time-delays are taken outside the generalized plant. Therefore, if there exists uncertainties in the actual time-delays, then, they appear in the uncertainty block of the generalized framework. However, in this case, the uncertainty block may become non-causal and the small-gain theorem, which assumes the causality of the interconnected subsystems in the feedback loop, may not be used. Therefore, since the $\mathcal{H}^\infty$ controller design is based on the small-gain theorem, the stabilizing $\mathcal{H}^\infty$ controller can not be designed unless uncertainty block is made causal by introducing some constraints on the uncertain part of the actual time-delays. Non-causal subsystems also appear in multi-dimensional systems with non-causal spatial dynamics [14]. In the stabilizing controller design for the multi-dimensional systems with non-causal spatial dynamics, LMI and μ-frameworks are used utilizing the scaled small-gain theorem [14–18]. However, in these studies, the systems are restricted to be linear time- and space-

invariant discrete-time systems. In this dissertation, sufficient conditions will be introduced to satisfy the validity of the small-gain theorem, if at least one of the subsystems in the feedback interconnection is non-causal.

A good example for systems with multiple time-delays which possess time-varying uncertainties is data-communication networks. In data-communication networks, flow control mechanisms are used to avoid traffic congestion and satisfy a QoS level. These mechanisms are *rate-based* and *window-based* feedback mechanisms. In [19], [20], flow controllers were designed using proportional control and Smith's principle. The proposed controller in [19] ensures the congestion avoidance by keeping the queue length at the bottleneck in a desired level and high utilization of the network links whereby ensuring the positiveness of the queue length. In these studies, the actual time-delays, however, were taken constant. An $\mathcal{H}^\infty$ rate-based controller for high-speed data-communication networks was proposed in [21] using the controller design method in [6]. Later, the implementation of this controller was given in [22]. However, in these studies, the uncertain time-delays were taken constant and the controllers were designed by equalizing all the delays in the channels to the longest one. This stems from the used controller design approach proposed in [6], which was for SISO systems with a single time-delay. Using the same controller approach, a rate-based $\mathcal{H}^\infty$ flow controller design considering the uncertain time-varying time-delays was presented in [23]. In this study, different than [21, 22], separate $\mathcal{H}^\infty$ controllers were designed for channels with different delays and then the obtained controllers were weighted and blended to obtain the overall controller. Hence, the designed controllers in [23] are less conservative compared to the controllers in [21, 22], however, they are sub-optimal in the $\mathcal{H}^\infty$-sense. In [24], flow controllers were designed using the μ synthesis. In that approach, the controller was designed using the *D-K* iterations by approximating the time-delay system utilizing the Padé-approximation. In order to find an optimal solution to this problem, the approach of [13] was first considered in [25]. In the present dissertation, an optimal $\mathcal{H}^\infty$ flow controller design for high-speed data-communication networks

is given using the same approach. The performance level and the actual stability margin of the designed $\mathcal{H}^\infty$ flow controllers are presented. Furthermore, the performance improvement of the designed $\mathcal{H}^\infty$ flow controllers utilizing the non-causal uncertainty blocks compared to the causal ones, are also addressed.

The set of all stabilizing $\mathcal{H}^\infty$ controllers is parameterized by a free stable norm-bounded TFM. Utilizing the free parameter, some of the design requirements, which are not introduced in the controller design process, can be achieved by the controller. For instance, in the stable $\mathcal{H}^\infty$ controller design, first the stabilizing $\mathcal{H}^\infty$ controllers are found, and then the appropriate free parameter is sought which stabilizes the controller (e.g., [26–28]). In addition, some of the design requirements, e.g. time-domain constraints, which are not introduced in the controller design process, can be met utilizing the free parameter [29, 30]. In this dissertation, we will give the sufficient conditions to choose the free parameter denoted by Q_Λ, which ensures that the designed stabilizing controller satisfies the desired time-domain constraint, which is not taken into account in the design process.

The controllers are designed to stabilize the system and, if any, to achieve some other design requirements. In general, the designed controller may or may not be stable. If the designed controller is unstable, although it theoretically stabilizes the overall system, it is undesirable due to two reasons:

- the closed-loop system becomes highly sensitive to sensor/actuator faults, since such a fault can make the overall system unstable (a stable controller, however, guarantees overall stability under such a fault if the plant is also stable);

- an unstable controller introduces additional right-half-plane zeros, which reduce the tracking ability and disturbance rejection of the closed-loop system and makes it more sensitive to numerical errors and nonlinear effects [31]. Such effects, may indeed cause an unstable behaviour in a practical implementation.

Due to above reasons, stable controller design problem, which is also referred to as the *strong stabilization problem*, has been considered in the literature for a long time (e.g., [26, 32]). Strong stabilization problem has also been considered for time-delay systems (e.g., [33–35]). However, these studies have been limited to SISO time-delay systems. In this dissertation, stable $\mathcal{H}^\infty$ controller design algorithms for the flow control problem in data-communication networks, which is an example of multiple-time-delay systems, are given.

1.2 Dissertation Outline

In Chapter 2, standard background material are brought together to clarify the definitions, lemmas, theorems and proofs in the dissertation. First, the *chain-scattering representation* and its properties are given. Then, the adobe problem in the optimal $\mathcal{H}^\infty$ controller design for multiple-time-delay systems is defined and the general solution is given. Finally, the flow control problem in data-communication networks is introduced.

In Chapter 3, validity of the small-gain theorem for feedback interconnection of non-causal subsystems is discussed. The sufficient conditions are proposed to satisfy the validity of the small-gain theorem for non-causal subsystems. A less conservative result for the validity of the small-gain theorem is also given if the interconnected subsystems in the feedback loop are SIMO and MISO respectively. In this chapter, appearance of non-causal uncertainty blocks in the robust controller design problem is also given. Instead of designing a robust controller utilizing the non-causal uncertainty blocks, an alternative way, which considers the robust controller design of an equivalent problem with causal uncertainty blocks, is also presented. The results presented in this chapter, with the exception of those given in Section 3.5, were published in [36–39].

In Chapter 4, an optimal $\mathcal{H}^\infty$ flow controller design for data-communication networks is given utilizing the results in Chapter 3. The perfor-

mance level and actual stability margins of the designed flow controller are defined. The performance improvement obtained by utilizing the non-causal uncertainty blocks compared to the causal ones are addressed. In this chapter, the sufficient conditions are also presented to choose an appropriate free parameter Q_Λ such that the designed controller meets one of the time-domain constraints which was not introduced in the design process. Parts of the results in this chapter were published in [40–46].

In Chapter 5, utilizing the results in Chapter 4, some design algorithms that yield a stable $\mathcal{H}^\infty$ flow controller are given. A number of different approaches are given. In the first approach, a *strong* $\mathcal{H}^\infty$ *stabilization* problem is solved in order to design a stable $\mathcal{H}^\infty$ flow controller. In the second approach, another strong $\mathcal{H}^\infty$ stabilization problem is solved to design a stable $\mathcal{H}^\infty$ flow controller. However, the latter problem is more relaxed compared to the one which is to be solved in the first approach. The third approach tries to ensure the stability of the controller by stabilizing the finite-dimensional part of the controller. In the fourth approach, a stable $\mathcal{H}^\infty$ flow controller is sought by increasing the gain of the defined uncertainty weighting TFM in the problem. In the last approach, a stable $\mathcal{H}^\infty$ flow controller design problem is defined as a strong stabilization problem for finite dimensional systems utilizing the rational approximation of the infinite dimensional part of the controller. Parts of the results in this chapter were published in [47–49].

In Chapter 6, the concluding remarks and possible future studies are given.

2 BACKGROUND

In this chapter, important background material and definitions to be used in subsequent chapters are presented. In Section 2.1, the chain-scattering representation of systems and its properties are given. In addition, *J-lossless* systems, which play an important role in Section 2.2, are introduced. In Section 2.2, the adobe problem is defined to obtain the optimal $\mathcal{H}^\infty$ controller design for systems with multiple time-delays. In Section 2.3, the flow control problem in data-communication networks is introduced.

2.1 Chain-scattering Framework and J-lossless Systems

The standard $\mathcal{H}^\infty$ optimal control problem setup is given in Figure 2.1a. Here, the vectors z, w, y, u represent, respectively, the regulated outputs, the exogenous signals, the measured outputs, the control inputs, and $\widehat{P}$ denotes the TFM containing the plant to be controlled and weighting functions, if any, to satisfy some design criteria, and K is the controller to be designed. Note that, for the system in Figure 2.1a,

$$z = \widehat{P}_{11}w + \widehat{P}_{12}u \tag{2.1}$$

$$y = \widehat{P}_{21}w + \widehat{P}_{22}u, \tag{2.2}$$

where $\widehat{P}$ is partitioned as $\widehat{P} = \begin{bmatrix} \widehat{P}_{11} & \widehat{P}_{12} \\ \widehat{P}_{21} & \widehat{P}_{22} \end{bmatrix}$. If $\widehat{P}_{21}$ is square and has a proper inverse, then (2.2) can be written as

$$w = -\widehat{P}_{21}^{-1}\widehat{P}_{22}u + \widehat{P}_{21}^{-1}y\ . \tag{2.3}$$

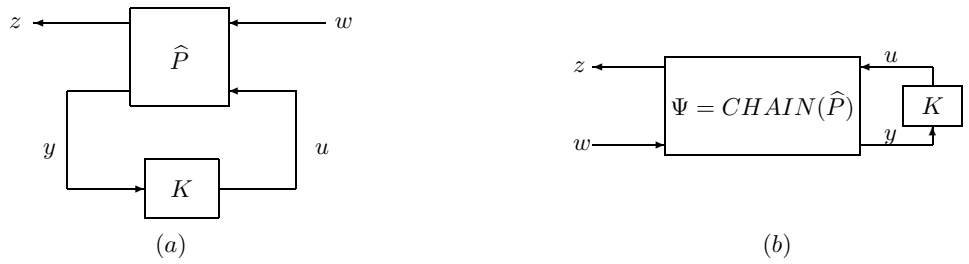

Figure 2.1: a) Generalized framework b) It's chain-scattering representation

By replacing w in (2.1) by (2.3), we obtain

$$\begin{aligned} z &= (\widehat{P}_{12} - \widehat{P}_{11}\widehat{P}_{21}^{-1}\widehat{P}_{22})u + \widehat{P}_{11}\widehat{P}_{21}^{-1}y \\ w &= -\widehat{P}_{21}^{-1}\widehat{P}_{22}u + \widehat{P}_{21}^{-1}y \ . \end{aligned}$$

Therefore, if we define

$$\Psi := \begin{bmatrix} \widehat{P}_{12} - \widehat{P}_{11}\widehat{P}_{21}^{-1}\widehat{P}_{22} & \widehat{P}_{11}\widehat{P}_{21}^{-1} \\ -\widehat{P}_{21}^{-1}\widehat{P}_{22} & \widehat{P}_{21}^{-1} \end{bmatrix} =: \begin{bmatrix} \Psi_{11} & \Psi_{12} \\ \Psi_{21} & \Psi_{22} \end{bmatrix} , \tag{2.4}$$

the system in Figure 2.1a can be represented as in Figure 2.1b, where Ψ is called the chain-scattering representation of $\widehat{P}$ and denoted by $\Psi = CHAIN(\widehat{P})$ [50].

The $\mathcal{H}^\infty$ optimal control problem for the system described in Figure 2.1a is to design a stabilizing controller K which minimizes the $\mathcal{H}^\infty$ norm of the closed loop TFM from w to z. The closed-loop TFM from w to z in Figure 2.1a, called T_{zw}, can be written as;

$$T_{zw} =: F_l(\widehat{P}, K) = \widehat{P}_{11} + \widehat{P}_{12}K(I - \widehat{P}_{22}K)^{-1}\widehat{P}_{21}, \tag{2.5}$$

where $F_l(\cdot,\cdot)$ is the lower-LFT [5]. If the chain-scattering representation is considered, the closed-loop TFM in Figure 2.1b, from w to z, can be written as [50]:

$$T_{zw} =: HM(\Psi, K) = (\Psi_{11} + \Psi_{12}K)(\Psi_{21} + \Psi_{22}K)^{-1}. \tag{2.6}$$

Thus $F_l(\widehat{P}, K) = HM(\Psi, K)$. If Ψ in (2.4) is invertible, and the closed-loop TFM $Q := HM(\Psi, K)$ is known, then K is easily obtained as [50]:

$$K = HM(\Psi^{-1}, Q) \ . \tag{2.7}$$

The main reason for using the chain scattering representation is for its simplicity in representing cascade connections. Indeed, the cascade connection in chain scattering representation corresponds to star-product representation in the generalized framework. The star product of systems plays a crucial role in the $\mathcal{H}^\infty$ controller design, since all the stabilizing controllers can be parameterized as $K = F_l(J, Q)$, where J is obtained from the solutions of two algebraic Riccati equations, and $Q \in \mathcal{H}^\infty$ is a free parameter such that $\|Q\|_\infty < \gamma$,

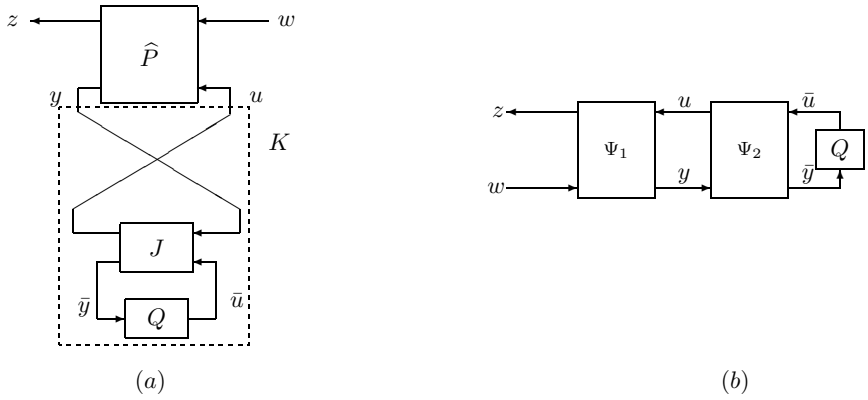

Figure 2.2: *a*) Star product of systems, *b*) Cascade connection in chain-scattering representation

where the stabilizing controller K achieves $\|F_l(P,K)\|_\infty < \gamma$ (see [5] for details). Then the overall system in Figure 2.1*b* can be described as shown in Figure 2.2*a*. Suppose that, J is partitioned as $J = \begin{bmatrix} J_{11} & J_{12} \\ J_{21} & J_{22} \end{bmatrix}$, where J_{21} is invertible. Then, if Ψ_1 and Ψ_2 are the corresponding chain-scattering representation of the systems $\widehat{P}$ and J, then the system in Figure 2.2*a* can be represented as in Figure 2.2*b*. The cascade connection of two chain scattering representations Ψ_1 and Ψ_2, as shown in Figure 2.2*b*, is represented as the product $\Psi_1\Psi_2$ of each chain scattering representations. Furthermore, the closed-loop TFM in Figure 2.2*b*, from w to z is obtained as

$$HM(\Psi_1, HM(\Psi_2, Q)) = HM(\Psi_1\Psi_2, Q)\ . \tag{2.8}$$

However, the same closed-loop TFM in Figure 2.2*a*, from w to z is obtained as; $F_l(\widehat{P}, F_l(J,Q))$ which is more complicated compared to (2.8), since its expansion may not be expressed as the product of two functions, in general.

For the chain-scattering representation of the proper TFM $\widehat{P}$, it is assumed that $\widehat{P}_{21}$ is square and invertible, i.e., $\text{rank}(\widehat{P}_{21}(s)_{|_{s=\infty}}) = n_w = n_y$. However, $\widehat{P}_{21}$ may not be square in general and in this case the chain-scattering representation of $\widehat{P}$ does not exist. If $\widehat{P}_{21}$ is not square but full row rank, $\text{rank}(\widehat{P}_{21}(s)_{|_{s=\infty}}) = n_y < n_w$, then the plant can be augmented by a fictitious

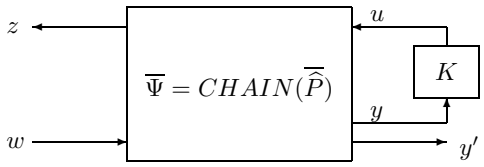

Figure 2.3: Chain scattering representation of output augmented system

measured output y' of dimension $n_w - n_y$ given by

$$y' = \widehat{P}'_{21} w + \widehat{P}'_{22} u, \tag{2.9}$$

such that $\begin{bmatrix} \widehat{P}_{21} \\ \widehat{P}'_{21} \end{bmatrix}^{-1} =: \begin{bmatrix} \widehat{P}^{\dagger}_{21} & \widehat{P}^{\perp}_{21} \end{bmatrix}$ exists, where $\widehat{P}^{\dagger}_{21}$ is $n_w \times n_y$ and $\widehat{P}^{\perp}_{21}$ is $n_w \times (n_w - n_y)$. Then the augmented plant $\overline{\widehat{P}}$ can be described by

$$\begin{bmatrix} z \\ y \\ y' \end{bmatrix} = \overline{\widehat{P}} \begin{bmatrix} w \\ u \end{bmatrix} = \left[\begin{array}{c:c} \widehat{P}_{11} & \widehat{P}_{12} \\ \hdashline \widehat{P}_{21} & \widehat{P}_{22} \\ \hdashline \widehat{P}'_{21} & \widehat{P}'_{22} \end{array}\right] \begin{bmatrix} w \\ u \end{bmatrix},$$

and then the chain-scattering representation of the augmented plant $\overline{\widehat{P}}$ can be represented as shown in Figure 2.3, where

$$\overline{\Psi} = \begin{bmatrix} \widehat{P}_{12} - \widehat{P}_{11}(\widehat{P}^{\dagger}_{21}\widehat{P}_{22} + \widehat{P}^{\perp}_{21}\widehat{P}'_{22}) & \widehat{P}_{11}\widehat{P}^{\dagger}_{21} & \widehat{P}_{11}\widehat{P}^{\perp}_{21} \\ -(\widehat{P}^{\dagger}_{21}\widehat{P}_{22} + \widehat{P}^{\perp}_{21}\widehat{P}'_{22}) & \widehat{P}^{\dagger}_{21} & \widehat{P}^{\perp}_{21} \end{bmatrix}.$$

Lossless systems will play an important role in the following sections. The $\mathcal{H}^{\infty}$ controller design utilizing the chain-scattering approach is also based on the J-lossless factorization [50]. In order to clarify the lossless systems, some definitions, a lemma, and a theorem are given below.

Definition 2.1. A TFM G is said to be stable if it is analytic in $\overline{\mathbb{C}}_+$.

Definition 2.2. An invertible TFM G is said to be bistable if both it and its proper inverse are analytic in $\overline{\mathbb{C}}_+$.

Definition 2.3. The transpose of a real rational TFM $G(s)$ with state-space realization $G(s) = \left[\begin{array}{c|c} A & B \\ \hline C & D \end{array}\right]$ is denoted by $G^T(s) = \left[\begin{array}{c|c} A^T & C^T \\ \hline B^T & D^T \end{array}\right]$.

Definition 2.4. [50] A TFM G is said to be *unitary* if it satisfies

$$G^{\sim}G = I.$$

Definition 2.5. [50] A unitary TFM G is said to be lossless if it is stable.

Definition 2.6. [50] A TFM $\Theta \in \mathcal{RL}^{\infty}_{(n_z+n_w)\times(n_u+n_y)}$ is said to be (J_{zw}, J_{uy})-unitary, if

$$\Theta^{\sim} J_{zw} \Theta = J_{uy}. \tag{2.10}$$

Definition 2.7. [50] A (J_{zw}, J_{uy})-unitary TFM $\Theta(s)$ is said to be (J_{zw}, J_{uy})-lossless, if

$$\Theta^{*}(s) J_{zw} \Theta(s) \leq J_{uy}, \ \ \forall \ s \in \overline{\mathbb{C}}_{+}. \tag{2.11}$$

The interpretation of (J_{zw}, J_{uy})-lossless or (J_{zw}, J_{uy})-unitary systems arises in the chain-scattering framework.

Lemma 2.1. *[50] A TFM Θ is (J_{zy}, J_{uy})-unitary (lossless) if and only if it is a chain-scattering representation of a unitary (lossless) matrix.*

Theorem 2.1. *[50] Assume that Θ is a (J_{zy}, J_{uy})-unitary TFM. Then, there exists a TFM Q such that $HM(\Theta, Q)$ is stable and $\|HM(\Theta, Q)\|_{\infty} < 1$ if and only if Θ is (J_{zy}, J_{uy})-lossless. In that case, $\|HM(\Theta, Q)\|_{\infty} < 1$ if and only if Q is stable and $\|Q\|_{\infty} < 1$.*

2.2 Adobe Problem in $\mathcal{H}^{\infty}$ Controller Design for Multiple-Time-Delay Systems

In this section, an optimal $\mathcal{H}^{\infty}$ controller design for systems with multiple input/output delays proposed in [13] is reviewed. The controller design problem for systems with multiple time-delays is solved by decomposing the problem into a nested sequence of problems, called adobe problems, each of which involves a single delay. The solution of the problem is then obtained by tailoring the solutions of subproblem in a proper way.

For the sake of clarity, some definitions are introduced. Consider a real rational TFM $G(s)$ with state-space realization

$$G(s) = \left[\begin{array}{c|c} A & B \\ \hline C & D \end{array}\right].$$

Definition 2.8. The square real matrix A is called Hurwitz if all the eigenvalues of A are in $\mathbb{C}_-$.

Definition 2.9. (A, B) is said to be stabilizable if the matrix $\left[\begin{array}{cc} A - \lambda I & B \end{array}\right]$ has full row rank for all $\lambda \in \overline{\mathbb{C}}_+$, and (C, A) is detectable if (A^T, C^T) is stabilizable.

Lemma 2.2. *If D is square and non-singular, then the inverse of $G(s)$ is given by*

$$G^{-1}(s) = \left[\begin{array}{c|c} A - BD^{-1}C & -BD^{-1} \\ \hline D^{-1}C & D^{-1} \end{array}\right].$$

Definition 2.10. A TFM Q is called contractive, if Q belongs to $\mathcal{H}^\infty$ and $\|Q\|_\infty < 1$.

Definition 2.11. For an $n \times n$ real matrix A and real symmetric matrices Q and R, the $2n \times 2n$ matrix $H = \left[\begin{array}{cc} A & R \\ -Q & -A^T \end{array}\right]$ is called a Hamiltonian matrix. Furthermore, the algebraic Riccati equation associated with H is

$$A^T X + XA + XRX + Q = 0.$$

Theorem 2.2. *[51] Suppose that Q, M, and R are matrices such that M and Q are symmetric. Then the following are equivalent:*

- *Both the matrix inequalities $Q > 0$ and $M - RQ^{-1}R^T > 0$ hold.*
- $\left[\begin{array}{cc} M & R \\ R^T & Q \end{array}\right] > 0$ *is satisfied.*

Definition 2.12. A Hamiltonian matrix H without purely imaginary eigenvalues is said to be in the domain of the Riccati operator, denoted as dom(Ric), if

there exist square $n \times n$ matrices H_- and X such that $\begin{bmatrix} I \\ X \end{bmatrix} H_- = H \begin{bmatrix} I \\ X \end{bmatrix}$, where H_- is Hurwitz. In this case, the function Ric is defined as: Ric: $H \to X$. Thus, X=Ric(H).

Definition 2.13. π_h is called the "completion operator" [13], and it is defined as $\pi_h \left(e^{-hs} \left[\begin{array}{c|c} A & B \\ \hline C & 0 \end{array}\right] \right) = \left[\begin{array}{c|c} A & B \\ \hline Ce^{-Ah} & 0 \end{array}\right] - e^{-hs} \left[\begin{array}{c|c} A & B \\ \hline C & 0 \end{array}\right]$, which describes an FIR filter of duration h. In addition, the impulse response of this FIR filter, $g(t)$, is :

$$g(t) = \begin{cases} Ce^{A(t-h)}B\,, & 0 \le t < h \\ 0\,, & \text{otherwise} \end{cases} . \tag{2.12}$$

The $\mathcal{H}^\infty$ controller design setup for a system with multiple time-delays is depicted in Figure 2.4. Here, it is assumed that the TFM P has a state-space representation as:

$$P = \left[\begin{array}{c|cc} A & B_1 & B_2 \\ \hline C_1 & D_{11} & D_{12} \\ C_2 & D_{21} & D_{22} \end{array}\right], \tag{2.13}$$

and the following hold:

(i) (A, B_2) is stabilizable

(ii) (C_2, A) is detectable

(iii) $\begin{bmatrix} A - j\omega I & B_2 \\ C_1 & D_{12} \end{bmatrix}$ has full column rank $\forall\ \omega \in \overline{\mathbb{R}}$

(iv) $\begin{bmatrix} A - j\omega I & B_1 \\ C_2 & D_{21} \end{bmatrix}$ has full row rank $\forall\ \omega \in \overline{\mathbb{R}}$.

The assumptions (i)–(iv) are called standard $\mathcal{RH}^\infty$ assumptions. The delay blocks in Figure 2.4 are assumed to be diagonal such as

$$\Lambda_u(s) = \begin{bmatrix} e^{-h_{u,q}s} I_{m_q} & & & \\ & \ddots & & \\ & & e^{-h_{u,1}s} I_{m_1} & \\ & & & I_{m_0} \end{bmatrix}, \tag{2.14}$$

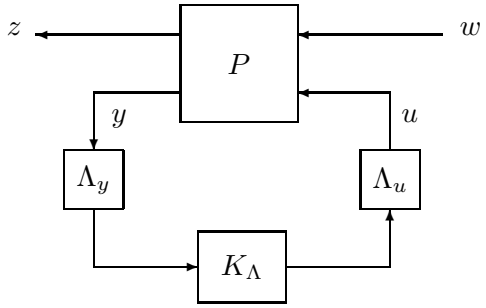

Figure 2.4: Four-block problem

where $0 < h_{u,1} < \ldots < h_{u,q}$, $\sum_{i=0}^{q} m_i = n_u$, and

$$\Lambda_y(s) = \begin{bmatrix} I_{p_0} & & & \\ & e^{-h_{y,1}s} I_{p_1} & & \\ & & \ddots & \\ & & & e^{-h_{y,r}s} I_{p_r} \end{bmatrix}, \tag{2.15}$$

with $0 < h_{y,1} < \cdots < h_{y,r}$ $\sum_{i=0}^{r} p_i = n_y$. The standard $\mathcal{H}^\infty$ problem for the system depicted in Figure 2.4 can be posed as finding a proper stabilizing K_Λ such that $K := \Lambda_u K_\Lambda \Lambda_y$ internally stabilizes the system and guarantees that

$$\|F_l(P, \Lambda_u K_\Lambda \Lambda_y)\|_\infty < \gamma \tag{2.16}$$

for a given $\gamma > 0$.

In the approach of [13], the four-block $\mathcal{H}^\infty$ problem with multiple time-delays is reduced to a one-block $\mathcal{H}^\infty$ problem with multiple time-delays. To do this, firstly, the solution of the delay-free counterpart of the four-block $\mathcal{H}^\infty$ problem is obtained. Then, utilizing this solution and properties of chain-scattering representation, the four-block $\mathcal{H}^\infty$ problem with multiple delays is posed as a one-block problem with multiple delays.

To obtain the solution for the delay-free counterpart of the four-block $\mathcal{H}^\infty$ problem, let us define the followings:

- $\gamma_z := \|(I - D_{12}(D_{12}^T D_{12})^{-1} D_{12}^T) D_{11}\|_2$
- $\gamma_w := \|D_{11}(I - D_{21}^T (D_{21} D_{21}^T)^{-1} D_{21})\|_2$.

Let us introduce the following Hamiltonian matrices H_X, H_Y

$$\begin{aligned} H_X &= \begin{bmatrix} A & 0 \\ -C_1^T C_1 & -A^T \end{bmatrix} - \begin{bmatrix} B_1 & B_2 \\ -C_1^T D_{11} & -C_1^T D_{12} \end{bmatrix} \\ &\quad \begin{bmatrix} D_{11}^T D_{11} - \gamma^2 I & D_{11}^T D_{12} \\ D_{12}^T D_{11} & D_{12}^T D_{12} \end{bmatrix}^{-1} \begin{bmatrix} D_{11}^T C_1 & B_1^T \\ D_{12}^T C_1 & B_2^T \end{bmatrix}, \end{aligned} \tag{2.17}$$

$$\begin{aligned} H_Y &= \begin{bmatrix} A^T & 0 \\ -B_1 B_1^T & -A \end{bmatrix} - \begin{bmatrix} C_1^T & C_2^T \\ -B_1 D_{11}^T & -B_1 D_{12}^T \end{bmatrix} \\ &\quad \begin{bmatrix} D_{11} D_{11}^T - \gamma^2 I & D_{11} D_{21}^T \\ D_{21} D_{11}^T & D_{21} D_{21}^T \end{bmatrix}^{-1} \begin{bmatrix} D_{11} B_1^T & C_1 \\ D_{21} B_1^T & C_2 \end{bmatrix}. \end{aligned} \tag{2.18}$$

Utilizing the above definitions, there exists a solution for the delay-free version of the problem depicted in Figure 2.4 if and only if the following conditions hold

i) $\max\{\gamma_z, \gamma_w\} < \gamma$

ii) $H_X \in \text{dom(Ric)}$ and $X := Ric(H_X) \geq 0$

iii) $H_Y \in \text{dom(Ric)}$ and $Y := Ric(H_Y) \geq 0$

iv) $\rho(XY) < \gamma^2$.

Define the following matrices:

$$F = \begin{bmatrix} F_1 \\ F_2 \end{bmatrix} = -\Theta_z^{-1} \left(\begin{bmatrix} B_1^T \\ B_2^T \end{bmatrix} X + \begin{bmatrix} D_{11}^T \\ D_{12}^T \end{bmatrix} C_1 \right) \tag{2.19}$$

$$L = \begin{bmatrix} L_1 & L_2 \end{bmatrix} = \left(Y \begin{bmatrix} C_1^T & C_2^T \end{bmatrix} + B_1 \begin{bmatrix} D_{11}^T & D_{21}^T \end{bmatrix} \right) \Theta_w^{-1}, \tag{2.20}$$

where $\Theta_z = \begin{bmatrix} D_{11}^T D_{11} - \gamma^2 I & D_{11}^T D_{12} \\ D_{12}^T D_{11} & D_{12}^T D_{12} \end{bmatrix}$, $\Theta_w = \begin{bmatrix} D_{11} D_{11}^T - \gamma^2 I & D_{11} D_{21}^T \\ D_{21} D_{11}^T & D_{21} D_{21}^T \end{bmatrix}$.
If the solvability conditions given above are satisfied, then the matrix $Z := (I - \gamma^{-2} YX)^{-1}$ is well-defined and the matrices

$$A_F = A + B_1 F_1 + B_2 F_2 \tag{2.21}$$

$$A_L = A + L_1 C_1 + L_2 C_2, \tag{2.22}$$

are Hurwitz. Using these definitions, let us introduce

$$G_\infty(s) := D_\infty \left[\begin{array}{c|c} A_L & B_\infty \\ \hline C_\infty Z & I \end{array}\right], \tag{2.23}$$

where

$$B_\infty := \left[\begin{array}{cc} -(B_2 + L_1 D_{12} + L_2 D_{22}) & L_2 \end{array}\right]$$

$$C_\infty := \left[\begin{array}{c} F_2 \\ -C_2 + D_{21} F_1 + D_{22} F_2 \end{array}\right]$$

and nonsingular D_∞ satisfies

$$D_\infty^T J_{uy} D_\infty = -\gamma^2 \left[\begin{array}{cc} D_{12}^T & D_{22}^T \\ 0 & -I \end{array}\right] \Theta_w^{-1} \left[\begin{array}{cc} D_{12} & 0 \\ D_{22} & -I \end{array}\right]. \tag{2.24}$$

It can be shown [50] that

$$G_\infty(s)^{-1} = \left[\begin{array}{c|c} A_F & -Z B_\infty \\ \hline C_\infty & I \end{array}\right] D_\infty^{-1}, \tag{2.25}$$

which is stable, hence, G_∞ is bistable.

Using the above definitions, the delay-free version of the problem in Figure 2.4, i.e. $\Lambda_u = I$ and $\Lambda_y = I$, is to find a proper stabilizing K which results in

$$Q := HM(G_\infty, K) \tag{2.26}$$

is contractive. From (2.7), the stabilizing controllers K can be obtained from (2.26) as

$$K = HM(G_\infty^{-1}, Q), \tag{2.27}$$

where Q is a free contractive parameter.

In delay case, the used inversion property above may not be used, since existing Λ_u and Λ_y in K, $K = \Lambda_u K_\Lambda \Lambda_y$, results in non-causal K_Λ in general. However, to obtain a solution for the four-block $\mathcal{H}^\infty$ problem with multiple time-delays the problem can alternatively be posed as to find a stabilizing controller K_Λ which yields contractive $Q = HM(G_\infty, \Lambda_u K_\Lambda \Lambda_y)$. This problem can be depicted as in Figure 2.5. Utilizing the properties of the chain-scattering

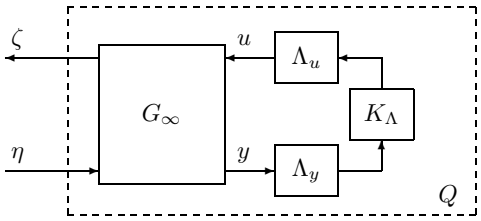

Figure 2.5: One block problem

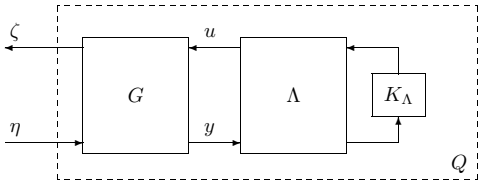

Figure 2.6: Alternative representation of one block problem

representation, an alternative representation for the problem setup shown in Figure 2.5 can be obtained as in Figure 2.6, where

$$G(s) := G_\infty(s)D_\infty^{-1} = \left[\begin{array}{c|c} A_L & B_\infty D_\infty^{-1} \\ \hline D_\infty C_\infty Z & I \end{array}\right], \tag{2.28}$$

and

$$\begin{aligned} \Lambda &= e^{-h_{y,r}s}\mathrm{bdiag}(\Lambda_u, \Lambda_y^{-1}) \\ &= \left[\begin{array}{cccc} e^{-h_{q+r}s}I_{n_{q+r}} & & & \\ & \ddots & & \\ & & e^{-h_1 s}I_{n_1} & \\ & & & I_{n_0} \end{array}\right], \end{aligned} \tag{2.29}$$

where $h_{q+r} > \cdots > h_1 > 0$. Here, $h_{q+r} = h_{u,q} + h_{y,r}$, where $h_{u,i}$ $(i = 1, \ldots, q)$ and $h_{y,j}$ $(j = 1, \ldots, r)$ are defined in (2.14) and (2.15).

Now, the problem is reduced to the one-block $\mathcal{H}^\infty$ problem:

OBP(G, Λ): Find a proper stabilizing controller K_Λ such that

$$\|HM(G\Lambda, K_\Lambda)\|_\infty < 1, \tag{2.30}$$

where G is bistable with $\lim_{s\to\infty} G(s) = I$, as in (2.28), and Λ is a diagonal delay block, as in (2.29) [13].

An adobe delay problem is described as OBP(G_a,Λ_a) where Λ_a, called *adobe delay*, has a special form as: $\Lambda_a := \begin{bmatrix} e^{-h_a s} I_{\mu_a} & 0 \\ 0 & I_{\rho_a} \end{bmatrix}$ such that $\mu_a < n_u + n_y$ and $\mu_a + \rho_a = n_u + n_y$. In this problem, G_a is a bistable TFM

$$G_a = \left[\begin{array}{c|cc} A_a & B_{\mu_a} & B_{\rho_a} \\ \hline C_{\mu_a} & I_{\mu_a} & 0 \\ C_{\rho_a} & 0 & I_{\rho_a} \end{array}\right], \tag{2.31}$$

where the partitioning is compatible with that of Λ_a [13]. OBP(G_a, Λ_a) is to find a stabilizing controller K_a such that $Q_a = HM(G_a\Lambda_a, K_a)$ is contractive. To obtain the solution for OBP(G_a, Λ_a), let us define the following as in [13]:

$$J_{\mu_a} := \begin{bmatrix} I_{\mu_a} & 0 \end{bmatrix} J_{uy} \begin{bmatrix} I_{\mu_a} \\ 0 \end{bmatrix}$$

$$J_{\rho_a} := \begin{bmatrix} 0 & I_{\rho_a} \end{bmatrix} J_{uy} \begin{bmatrix} 0 \\ I_{\rho_a} \end{bmatrix}$$

$$H_a := \begin{bmatrix} A_a - B_{\rho_a} C_{\rho_a} & -B_{\rho_a} J_{\rho_a} B_{\rho_a}^T \\ -C_{\mu_a}^T J_{\mu_a} C_{\mu_a} & -A_a^T + C_{\rho_a}^T B_{\rho_a}^T \end{bmatrix}$$

$$\Sigma(t) = \begin{bmatrix} \Sigma_{11}(t) & \Sigma_{12}(t) \\ \Sigma_{21}(t) & \Sigma_{22}(t) \end{bmatrix} := e^{H_a t},$$

and $\Sigma_a = \begin{bmatrix} \Sigma_{a11} & \Sigma_{a12} \\ \Sigma_{a21} & \Sigma_{a22} \end{bmatrix} := \Sigma(h_a)$.

Theorem 2.3. *[13] The solution for OBP(G_a, Λ_a) exists if and only if $\Sigma_{22}(t)$ is nonsingular for all $t \in [0, h_a]$ and the controller K_a solves OBP(G_a, Λ_a) if and only if*

$$K_a = HM\left(\begin{bmatrix} I & 0 \\ \Pi_a & I \end{bmatrix} \widetilde{G}_a^{-1}, \widetilde{Q}_a\right), \tag{2.32}$$

where

$$\widetilde{G}_a := \left[\begin{array}{c|c} A_a & \Sigma_{a22}^T B_{\mu_a} + \Sigma_{a12}^T C_{\mu_a}^T J_{\mu_a} \quad B_{\rho_a} \\ \hline C_{\mu_a} \Sigma_{a22}^{-T} & \\ C_{\rho_a} - J_{\rho_a} B_{\rho_a}^T \Sigma_{a22}^{-1} \Sigma_{a21} & I_{\mu_a + \rho_a} \end{array}\right], \tag{2.33}$$

is finite-dimensional and bistable,

$$\Pi_a(s) := \pi_{h_a}\left(e^{-h_a s}\left[\begin{array}{cc|c} & & B_{\mu_a} \\ & H_a & -C_{\mu_a}^T J_{\mu_a} \\ \hline C_{\rho_a} & J_{\rho_a} B_{\rho_a}^T & 0 \end{array}\right]\right) \tag{2.34}$$

is a FIR filter of duration h_a, and $\widetilde{Q}_a$ is contractive, but otherwise arbitrary.

Utilizing the solution given by (2.32) for the OBP(G_a, Λ_a), the solution to the $OBP(G, \Lambda)$, where Λ is the joint delay operator that contains $q + r$ descendantly ordered delay-blocks can be obtained in $q + r$ iterations. The i^{th} iteration involves solving the adobe delay problem $OBP(G_i, \Lambda_i)$, where

$$\Lambda_i := \left[\begin{array}{cc} e^{-(h_i - h_{i-1})s} I_{\mu_i} & 0 \\ 0 & I_{\rho_i} \end{array}\right], \quad \rho_i = \sum_{j=0}^{i-1} n_j \tag{2.35}$$

and bistable G_i's are generated by the following sequence:

$$G_i = \widetilde{G}_{i-1}, \tag{2.36}$$

where $G_1 = G$, which is partitioned compatibly with $\Lambda_1 = \left[\begin{array}{cc} e^{-h_1 s} I_{\mu_1} & 0 \\ 0 & I_{\rho_1} \end{array}\right]$, similar to G_a in (2.31). After obtaining the solutions of OBP(G_i, Λ_i), for $i = 1, \ldots, q + r$, the solution to OBP(G, Λ) is obtained by the following theorem.

Theorem 2.4. *[13] The problem $OBP(G, \Lambda)$ is solvable if and only if all $OBP(G_i, \Lambda_i)$ for $i = 1, \ldots, q + r$ are solvable. In that case, the stabilizing controller K can be parameterized as*

$$K = HM(\Pi_\Lambda G_\Lambda^{-1}, Q_\Lambda), \tag{2.37}$$

where $G_\Lambda = \widetilde{G}_{q+r}$ is bistable and finite dimensional and the TFM

$$\Pi_\Lambda = \Lambda^{-1} \prod_{i=1}^{q+r} \Lambda_i \left[\begin{array}{cc} I & 0 \\ \Pi_i & I \end{array}\right]$$

is bistable. The TFM Q_Λ is contractive but otherwise arbitrary.

2.3 Flow Control Problem in Data-communication Networks

During the past decades, increasing demands on utilization of different traffic sources such as data, voice, video, have resulted in a large growth in the size and diversity of communication networks. However, this growth has brought problems along with it, thereby, managing and controlling the networks to satisfy reliable service to the users have become more difficult.

In telephone networks, which are good examples of circuit switching systems, constant transmission rate is satisfied during connection. However, the network is underutilized since the communication links are hold by the established connections. In modern computer networks, packet-switching technology is used. This technology improves the link utilization, since, unlike the circuit-switching, the packet is transmitted over the communication links without reserving any unused bandwidth. On the other hand, this technology does not assure quality of the real data transmission. The ATM technology merges the benefits of both circuit-switching and packet-switching technologies.

The network service model defines the characteristics of end-to-end transport of data between one "edge" of the network and the other. Today's internet provides only a single service model, the datagram service [52]. It is known as *best-effort-service* and provides unreliable QoS. Meanwhile, the ATM network provides multiple service models: CBR, VBR, UBR, and ABR services, which satisfy minimum data-transmission and provide feedback for the congestion notification.

One of the major problems of nowadays' modern communications is congestion. Congestion occurs when demand exceeds the network capacity and causes long queueing delays, packet dropping, and retransmission. Flow control methodologies are used to avoid congestion by regulating the data transmission from sources to destinations. Window-based flow control mechanism is used in packet-switching networks, meanwhile, rate-based flow control

mechanism is used in ATM networks. In the rate-based flow control approach, the flow control is implemented at the bottleneck node and adjusts the rate of data that is sent from sources to the bottleneck node to avoid traffic congestion.

In the literature, there exist numerous rate-based flow controller design approaches. The challenging aspect of the flow controller design is the existence of time-delays. Since the flow controller is implemented at the bottleneck node, which is designed to regulate the data rates of the sources, a time-delay occurs between the time a rate command signal is issued and the actual time this rate command arrives to the source, called *backward time-delay*. In addition, the data packets sent from the source does not arrive the bottleneck node instantly, hence, there exists a time delay between the time a data packet is sent from the source and the actual time this packet arrives, called *forward time-delay*. The total time-delay is the sum of backward and forward time-delays, called *round trip time-delay*. These delays are usually uncertain and time-varying.

3 SMALL-GAIN THEOREMS

One of the most important results in the control literature is the celebrated small gain condition introduced in the 1960's [3, 4, 53]. This condition lets one to verify the stability of a feedback interconnection of two stable systems (e.g., see [54]). In the 1980's this condition became a basic part of the robust control theory (e.g., see [5]). Various results have been obtained based on this condition. However, all of the results published to date consider interconnection of causal (in time) systems only.

Although most physical systems satisfy the causality (in time) assumption, the need to consider non-causal systems may arise in some problems. One of the problems is the robust controller design problem for systems with uncertain time-delays, which will be considered in the next chapter. Another problem arises in multidimensional systems, which are not causal in spatial coordinates [14].

This chapter is organized as follows. In Section 3.1, the motivation behind the study to show the validity of the small-gain theorem for non-causal systems is discussed. In Section 3.2, sufficient conditions to satisfy the validity of the small-gain theorem for interconnection of two stable systems, at least one of which is non-causal, are given. In Section 3.3, a more relaxed condition is introduced for the feedback interconnection of two subsystems one of which is MISO and the other is SIMO. In Section 3.4, the utilization of non-causal uncertainty blocks in the robust controller design problem for multiple-time-delay systems is addressed. Considering different uncertainty representations of the finite-dimensional part of the system, a new *strong small-gain condition* is introduced to utilize the non-causal uncertainty blocks in the $\mathcal{H}^\infty$ controller design. In Section 3.5, an alternative approach to robust controller design for the system in Section 3.4 is given by replacing the non-causal uncertainty blocks with causal ones. This chapter ends with a summary of the results derived.

3.1 Existence of Non-Causal Uncertainty Blocks in the $\mathcal{H}^\infty$ Controller Design for Systems with Multiple Time-Delays

Consider a plant with input and output delays, represented by the input-output map $G = \Lambda_y G_f \Lambda_u$, where Λ_u and Λ_y are diagonal operators with delay elements on the diagonal. Each input or output delay is assumed to be in the form $\tau_i^\bullet(t) = h_i^\bullet + \delta_i^\bullet(t)$, where t is the time variable, $h_i^\bullet$ is the known constant *nominal* delay, $\delta_i^\bullet(t)$ is the time-varying unknown delay uncertainty, and $\bullet$ stands for either u or y, where u refers to input signals and y refers to output signals. Therefore, τ_i^u corresponds to the delay in the i^{th} input channel, and τ_i^y corresponds to the delay in the i^{th} output channel. G_f is the *finite-dimensional part* of the plant, possibly including time-varying uncertainties. The nominal part of G_f, however, is assumed to be linear and time-invariant. The uncertainties in the time-delays are assumed to satisfy either

$$0 \leq \delta_i^\bullet(t) < \delta_i^{\bullet,\max} \tag{3.1}$$

or

$$|\delta_i^\bullet(t)| < \delta_i^{\bullet,\max} \tag{3.2}$$

for a given positive bound $\delta_i^{\bullet,\max}$ (in addition, time derivative of $\delta_i^\bullet(t)$ may also be bounded). It is further assumed that $\tau_i^\bullet(t) \geq 0$ (i.e., $\delta_i^\bullet(t) \geq -h_i^\bullet$) for all t.

A controller design problem, which guarantees the robust stability and certain performance conditions may be set-up as shown in Figure 3.1a, where Δ is an LTV uncertainty block representing uncertainties in the time-delays and in the finite-dimensional part of the plant (if any), M is the generalized plant representing the nominal plant G_f with input/output delays and weighting functions, if any, and K is the controller to be designed using an $\mathcal{H}^\infty$-optimization approach (e.g., [5]). To design an $\mathcal{H}^\infty$-optimal controller for the problem depicted in Figure 3.1a, the known constant nominal time-delays are taken outside of the generalized plant as depicted in Figure 3.1b to use the approach given in Section 2.2. Here, Λ_u^0 and Λ_y^0, respectively, denote the

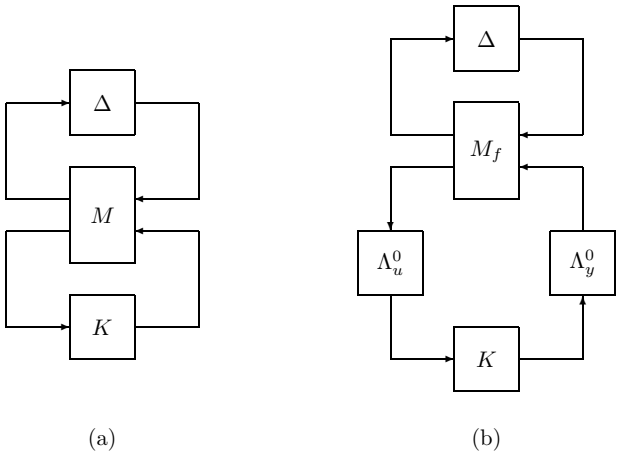

Figure 3.1: Robust control problem; a) Generalized plant includes time-delays; b) Time delays are taken outside the generalized plant [36]

nominal parts of Λ_u and Λ_y, M_f is a finite-dimensional generalized plant, Δ again represents the uncertainties, which is different than the one shown in Figure 3.1a.

When this approach is undertaken, however, the uncertainty block, Δ, turns out to be non-causal, if uncertainties in the delays are assumed to be bounded as in (3.2) (see Chapter 4). In this case, a difficulty arises in the $\mathcal{H}^\infty$ controller design, since it uses the small-gain theorem [3–5], which assumes the causality of the systems. To overcome this difficulty, it may be assumed that the uncertainties are bounded as in (3.1). Therefore, Δ turns out to be causal, and the $\mathcal{H}^\infty$ optimal controller can be designed. However, this assumption, requires taking $h_i^\bullet$'s as the minimum delays, rather than nominal, which are most probable, and taking the bound $\delta_i^{\bullet,\max}$ larger (twice as much) compared to the case in (3.2). This, in turn, introduces conservativeness in the robust controller design and the performance is optimized not for the actual nominal plant, but for the plant which has minimum delays. By using the results presented in the following sections, it may be possible to let Δ be non-causal and thus use (3.2) rather than (3.1). This should reduce the conservatism and improve performance.

3.2 A Small-Gain Theorem for Feedback Systems with Non-Causal Subsystems

In this section, the sufficient conditions are given to satisfy the internal stability of a feedback interconnection of two stable systems, at least one of which is non-causal. The results presented in this section have been published in [36]. For the sake of completeness, some definitions and a lemma, borrowed from [55], are first introduced .

Definition 3.1. Given $p \in [1, \infty)$, $a = \begin{bmatrix} a_1 & \cdots & a_n \end{bmatrix}^T \in \mathbb{R}^n$, and a positive integer n, the set $L_p^n[a, \infty)$ consists of all n-tuples $f = \begin{bmatrix} f_1 & \cdots & f_n \end{bmatrix}^T$, with $f_i \in L_p[a_i, \infty)$ for $i = 1, \ldots, n$. The norm on $L_p^n[a, \infty)$ is defined as $\|f\|_p := \left[\sum_{i=1}^{n} \|f_i\|_p^2\right]^{1/2}$.

Remark 3.1. The initial time a is assumed to be same for each component of a vector function in an L_p^n space, in many references, including [55]. Therefore, the usual notation for an L_p^n space is $L_p^n[a, \infty)$, where $a \in \mathbb{R}$. However, throughout the dissertation, to represent non-causal systems with different time-advances in each channel, each component of a should be different. Therefore, the notation is generalized as above.

Definition 3.2. Suppose $f = \begin{bmatrix} f_1 & \cdots & f_n \end{bmatrix}^T$, where $f_i : [a_i, \infty) \to \mathbb{R}$ $i = 1, \ldots, n$. Then, for each finite T, $f_T := \begin{bmatrix} (f_T)_1 & \cdots & (f_T)_n \end{bmatrix}^T$, called the *truncation* of f, where $(f_T)_i : [a_i, \infty) \to \mathbb{R}$ $(i = 1, \ldots, n)$ is defined as

$$(f_T)_i(t) := \begin{cases} 0, & \forall t \geq a_i, \text{ if } T < a_i \\ f_i(t), & a_i \leq t \leq T \\ 0, & t > T \geq a_i \end{cases} .$$

Definition 3.3. The set $L_{pe}^n[a, \infty)$, where $a = \begin{bmatrix} a_1 & \cdots & a_n \end{bmatrix}^T$, consists of all $f = \begin{bmatrix} f_1 & \cdots & f_n \end{bmatrix}^T$, where $f_i : [a_i, \infty) \to \mathbb{R}$ $(i = 1, \ldots, n)$, with the property that $f_T \in L_p^n[a, \infty)$ for all finite T, and is called the *extension* of L_p^n or the *extended* L_p^n*-space.*

Lemma 3.1. *For each real* $p \in [1, \infty)$ *and* $f \in L_{pe}^n[a, \infty)$,

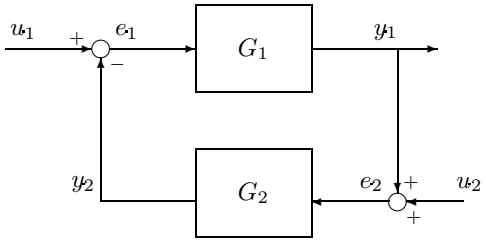

Figure 3.2: Feedback system [36]

(i) $\|f_T\|_p$ *is a non-decreasing function of* T*,*

(ii) $f \in L_p^n[a,\infty)$ *if and only if there exists a finite constant* m *such that* $\|f_T\|_p \leq m$*, for all finite* T*; in which case,* $\|f\|_p = \lim_{T\to\infty} \|f_T\|_p$*.*

Proof. See [55]. □

Definition 3.4. A mapping $A : L_{pe}^{n_1}[a_1,\infty) \to L_{pe}^{n_2}[a_2,\infty)$, where $a_1 \in \mathbb{R}^{n_1}$ and $a_2 \in \mathbb{R}^{n_2}$, is said to be L_p*-stable with finite gain* (L_p-sfg) if there exist non-negative finite constants γ, called the *gain* of A, and b, called the *bias* of A, such that, $\|Ax\|_p \leq \gamma\|x\|_p + b$, for all $x \in L_p^{n_1}[a_1,\infty)$.

Definition 3.5. A mapping $A : L_{pe}^{n_1}[a_1,\infty) \to L_{pe}^{n_2}[a_2,\infty)$ is said to be *causal* if $(Af)_T = (Af_T)_T$, for all finite T, $\forall f \in L_{pe}^{n_1}[a_1,\infty)$.

We consider the feedback configuration shown in Figure 3.2, where $u_1 \in L_p^{n_1}[a_1,\infty)$, $e_1, y_2 \in L_{pe}^{n_1}[a_1,\infty)$, $u_2 \in L_p^{n_2}[a_2,\infty)$, and $e_2, y_1 \in L_{pe}^{n_2}[a_2,\infty)$. We assume that $G_1 : L_{pe}^{n_1}[a_1,\infty) \to L_{pe}^{n_2}[a_2,\infty)$ and $G_2 : L_{pe}^{n_2}[a_2,\infty) \to L_{pe}^{n_1}[a_1,\infty)$ are L_p-sfg, respectively with gain γ_1 and γ_2 and bias b_1 and b_2; i.e.,

$$\|G_1e_1\|_p \leq \gamma_1\|e_1\|_p + b_1 \ , \qquad \forall e_1 \in L_p^{n_1}[a_1,\infty) \tag{3.3}$$

and

$$\|G_2e_2\|_p \leq \gamma_2\|e_2\|_p + b_2 \ , \qquad \forall e_2 \in L_p^{n_2}[a_2,\infty) \tag{3.4}$$

When G_1 and G_2 satisfy (3.3) and (3.4) and are both causal, the small gain condition [3,55], $\gamma_1\gamma_2 < 1$, proves the stability of the closed-loop system shown in Figure 3.2. This result, however, does not directly extend to the case when at least one of the blocks is non-causal, as shown by the following example.

Example 3.1. *[36] Consider the feedback configuration shown in Figure 3.2. Let, for some $a \in \mathbb{R}$ and $h > 0$, $G_1 : L_{pe}[a, \infty) \to L_{pe}[a-h, \infty)$ and $G_2 : L_{pe}[a-h, \infty) \to L_{pe}[a, \infty)$ be defined as $y_1(t) = \gamma_1 e_1(t+h)$, $\forall t \geq a-h$, and $y_2(t) = \gamma_2 e_2(t)$, $\forall t \geq a$ (the input of G_2 at times $a-h \leq t < a$ does not have any effect on its output), respectively, where γ_1 and γ_2 are positive finite constants. It can easily be shown that, for $i = 1, 2$, G_i is L_p-sfg with gain γ_i and bias zero. Note that*

$$y_1(t) = \gamma_1 \left[u_1(t+h) - \gamma_2 \left(u_2(t+h) + y_1(t+h) \right) \right] , \qquad t \geq a-h$$

This gives

$$y_1(t+h) = -\frac{1}{\gamma_1 \gamma_2} y_1(t) + v_1(t) , \qquad t \geq a-h$$

where $v_1(t) := \frac{1}{\gamma_2} u_1(t+h) - u_2(t+h)$, $t \geq a-h$, is an external signal. Similarly,

$$y_2(t+h) = -\frac{1}{\gamma_1 \gamma_2} y_2(t) + v_2(t) , \qquad t \geq a$$

where $v_2(t) := u_1(t+h) + \frac{1}{\gamma_1} u_2(t)$, $t \geq a$. These show that the closed-loop map from $u = \begin{bmatrix} u_1 \\ u_2 \end{bmatrix}$ to $y = \begin{bmatrix} y_1 \\ y_2 \end{bmatrix}$ (thus also the map from u to $e = \begin{bmatrix} e_1 \\ e_2 \end{bmatrix}$) is L_p-sfg if and only if $\gamma_1 \gamma_2 > 1$. Interestingly, this implies that this closed-loop system is stable only if the small gain condition, $\gamma_1 \gamma_2 < 1$, is **not** *satisfied.* □

Now, we assume that at least one of the blocks in Figure 3.2 is non-causal, but the two cascade connections of these blocks (i.e., the two systems obtained by breaking the loop in Figure 3.2 (i) at e_1, (ii) at e_2) are both casual; i.e., G_1 and G_2 satisfy

$$(G_1 G_2 e_2)_T = \left((G_1 G_2) (e_2)_T \right)_T , \qquad \forall e_2 \in L_{pe}^{n_2}[a_2, \infty) \tag{3.5}$$

and

$$(G_2 G_1 e_1)_T = \left((G_2 G_1) (e_1)_T \right)_T , \qquad \forall e_1 \in L_{pe}^{n_1}[a_1, \infty) \tag{3.6}$$

for all T. This condition is satisfied, for example, when G_1 is such that, for some $h > 0$, its output at time t depends on its input up to time $t+h$, i.e., G_1 satisfies $(G_1 e_1)_T = \left(G_1 (e_1)_{T+h} \right)_T$, $\forall T$, $\forall e_1 \in L_{pe}^{n_1}[a_1, \infty)$, and G_2 involves a

pure delay which is not less than h, i.e., G_2 satisfies $(G_2 e_2)_{T+h} = (G_2 (e_2)_T)_{T+h}$, $\forall T$, $\forall e_2 \in L_{pe}^{n_2}[a_2, \infty)$.

We also assume that G_1 and G_2 satisfy

$$\left\| \left(G_1 \left(e_1^1 \pm e_1^2 \right) \right)_T \right\|_p \leq \left\| \left(G_1 \left(e_1^1 \right) \right)_T \right\|_p + \left\| \left(G_1 \left(e_1^2 \right) \right)_T \right\|_p \ , \tag{3.7}$$

$\forall e_1^1, e_1^2 \in L_{pe}^{n_1}[a_1, \infty)$ and

$$\left\| \left(G_2 \left(e_2^1 \pm e_2^2 \right) \right)_T \right\|_p \leq \left\| \left(G_2 \left(e_2^1 \right) \right)_T \right\|_p + \left\| \left(G_2 \left(e_2^2 \right) \right)_T \right\|_p \ , \tag{3.8}$$

$\forall e_2^1, e_2^2 \in L_{pe}^{n_2}[a_2, \infty)$, for all T. We note that the class of systems which satisfy relations (3.7) and (3.8) are fairly large. In particular, these relations are satisfied by any linear G_1 and G_2, since in this case $(G_1 (e_1^1 \pm e_1^2))_T = (G_1 (e_1^1))_T \pm (G_1 (e_1^2))_T$ and $(G_2 (e_2^1 \pm e_2^2))_T = (G_2 (e_2^1))_T \pm (G_2 (e_2^2))_T$, $\forall e_1^1, e_1^2 \in L_{pe}^{n_1}[a_1, \infty)$, $\forall e_2^1, e_2^2 \in L_{pe}^{n_2}[a_2, \infty)$, and for all T (desired result then follows by the triangular inequality for $\| \cdot \|_p$).

Theorem 3.1. *[36] Consider the feedback configuration shown in Figure 3.2. Let G_1 and G_2 satisfy (3.3)–(3.8). Suppose $\gamma_1 \gamma_2 < 1$. Then the closed-loop system, i.e., the map from $u = \begin{bmatrix} u_1 \\ u_2 \end{bmatrix}$ to $y = \begin{bmatrix} y_1 \\ y_2 \end{bmatrix}$ (or to $e = \begin{bmatrix} e_1 \\ e_2 \end{bmatrix}$), is L_p-sfg.*

Proof. From Figure 3.2 we have

$$\begin{aligned} \|(y_1)_T\|_p &= \| (G_1 e_1)_T \|_p \leq \| (G_1 u_1)_T \|_p + \| (G_1 G_2 e_2)_T \|_p \\ &\leq \|G_1 u_1\|_p + \| (G_1 G_2) (e_2)_T \|_p \\ &\leq \gamma_1 \|u_1\|_p + b_1 + \gamma_1 \gamma_2 \| (e_2)_T \|_p + \gamma_1 b_2 + b_1 \\ &\leq \gamma_1 \|u_1\|_p + \gamma_1 \gamma_2 \|u_2\|_p + \gamma_1 \gamma_2 \| (y_1)_T \|_p + c_1 \end{aligned}$$

where $c_1 := \gamma_1 b_2 + 2 b_1$ and we used Lemma 3.1, (3.3)–(3.5), (3.7), and the *triangular inequality* [55] for $\| \cdot \|_p$. Since $\gamma_1 \gamma_2 < 1$, this implies that

$$\|(y_1)_T\|_p \leq \frac{\gamma_1}{1 - \gamma_1 \gamma_2} \|u_1\|_p + \frac{\gamma_1 \gamma_2}{1 - \gamma_1 \gamma_2} \|u_2\|_p + \frac{c_1}{1 - \gamma_1 \gamma_2} \ . \tag{3.9}$$

Since the right-hand-side of the above inequality is independent of T, by Lemma 3.1, $y_1 \in L_p^{n_2}[a_2, \infty)$ and, given $\|u_1\|_p$ and $\|u_2\|_p$, the right-hand-side

of (3.9) is an upper bound for $\|y_1\|_p$. Similarly, by using (3.6) instead of (3.5), and (3.8) instead of (3.7), we can also obtain

$$\|(y_2)_T\|_p \leq \frac{\gamma_2}{1-\gamma_1\gamma_2}\|u_2\|_p + \frac{\gamma_1\gamma_2}{1-\gamma_1\gamma_2}\|u_1\|_p + \frac{c_2}{1-\gamma_1\gamma_2}\,, \tag{3.10}$$

where $c_2 := \gamma_2 b_1 + 2b_2$. This in turn implies that $y_2 \in L_p^{n_1}[a_1, \infty)$. Consequently, since $e_1 = u_1 - y_2$ and $e_2 = u_2 + y_1$, $e_1 \in L_p^{n_1}[a_1, \infty)$ and $e_2 \in L_p^{n_2}[a_2, \infty)$. Furthermore, the right-hand-side of (3.10) is an upper bound for $\|y_2\|_p$. Moreover, (3.9) and (3.10) also imply that

$$\begin{aligned}
\|y\|_p &= \left(\|y_1\|_p^2 + \|y_2\|_p^2\right)^{\frac{1}{2}} \\
&\leq \frac{1}{1-\gamma_1\gamma_2}\left(\gamma_1(1+\gamma_2)\|u_1\|_p + \gamma_2(1+\gamma_1)\|u_2\|_p + c_1 + c_2\right) \\
&\leq \gamma\|u\|_p + b
\end{aligned}$$

which implies that the closed-loop map from u to y is L_p-sfg with gain

$$\gamma := \sqrt{2}\max\left(\frac{\gamma_1(1+\gamma_2)}{1-\gamma_1\gamma_2}\,,\ \frac{\gamma_2(1+\gamma_1)}{1-\gamma_1\gamma_2}\right)$$

and bias $b := \dfrac{c_1+c_2}{1-\gamma_1\gamma_2}$. Similarly, it can also be shown that, under the hypothesis, the closed-loop map from u to e is also L_p-sfg with gain

$$\hat{\gamma} := \sqrt{2}\max\left(\frac{1+\gamma_1}{1-\gamma_1\gamma_2}\,,\ \frac{1+\gamma_2}{1-\gamma_1\gamma_2}\right)$$

and bias b. □

3.3 A Small-Gain Theorem for Feedback Connection of a SIMO System with a MISO System

In the previous section, the sufficient conditions to satisfy the internal stability of the feedback interconnection of two stable subsystems, at least one of which is non-causal, were presented. The main result, Theorem 3.1, was based on the assumption of the causality of cascade connections of subsystems. However, this condition may not be satisfied in the flow controller design problem, considered in the next chapter. The flow control problem considered there is for a network with a single bottleneck node fed by n sources. Thus, to show

the validity of the small-gain theorem for this problem, the feedback system in Figure 3.2 should be arranged as a feedback interconnection of a SIMO system with a MISO system. Hence, a less conservative result can be found in comparison to the result derived in Section 3.2, since the systems in the feedback connection have known structure. The results presented in this section have been published in [37]

Let us consider the feedback system in Figure 3.2, where it is assumed that $G_1 : L_{pe}^n[a,\infty) \to L_{pe}[\bar{a},\infty)$ and $G_2 : L_{pe}[\bar{a},\infty) \to L_{pe}^n[a,\infty)$ are L_p-sfg and linear. Furthermore, the causality assumption (3.5) is also assumed to be satisfied. The other causality assumption, (3.6), however, is not necessarily satisfied. In the following theorem, instead of (3.6), a more relaxed condition is introduced. It is shown that this condition is also sufficient for stability in the present case.

Theorem 3.2. *[37] Consider the feedback configuration shown in Figure 3.2, where $u_1 \in L_p^n[a,\infty)$, $e_1, y_2 \in L_{pe}^n[a,\infty)$, $u_2 \in L_p[\bar{a},\infty)$, $e_2, y_1 \in L_{pe}[\bar{a},\infty)$, where $a \in \mathbb{R}^n$ and $\bar{a} \in \mathbb{R}$. Let $G_1 : L_{pe}^n[a,\infty) \to L_{pe}[\bar{a},\infty)$ and $G_2 : L_{pe}[\bar{a},\infty) \to L_{pe}^n[a,\infty)$. Assume that both G_1 and G_2 are linear (thus (3.7) and (3.8) are satisfied) and L_p-sfg with gain γ_1 and γ_2 respectively and bias zero (thus (3.3) and (3.4) are satisfied with $b_1 = b_2 = 0$). For $i = 1,\ldots,n$, let $G_{1i} : L_{pe}[a_i,\infty) \to L_{pe}[\bar{a},\infty)$ denote the map from the i^{th} input of G_1 to its output and $G_{2i} : L_{pe}[\bar{a},\infty) \to L_{pe}[a_i,\infty)$ denote the map from the input of G_2 to its i^{th} output (i.e., $G_1 = \begin{bmatrix} G_{11} & \cdots & G_{1n} \end{bmatrix}$ and $G_2 = \begin{bmatrix} G_{21} & \cdots & G_{2n} \end{bmatrix}^T$). Suppose that G_1G_2 is causal (i.e., (3.5) is satisfied). Also suppose that $G_{2i}G_{1i}$ is causal, i.e.,*

$$(G_{2i}G_{1i}e_{1i})_T = ((G_{2i}G_{1i})(e_{1i})_T)_T \ , \qquad \forall e_{1i} \in L_{pe}[a_i,\infty) \ , \tag{3.11}$$

$\forall T$, for all $i = 1,\ldots,n$. Moreover, suppose that $\gamma_1\gamma_2 < 1$. Then the closed-loop system, i.e., the map from $u = \begin{bmatrix} u_1^T & u_2^T \end{bmatrix}^T$ to $y = \begin{bmatrix} y_1^T & y_2^T \end{bmatrix}^T$ (or to $e = \begin{bmatrix} e_1^T & e_2^T \end{bmatrix}^T$), is L_p-sfg.

Proof. As in the proof of Theorem 3.1, taking $u_1 \in L_p^n[a,\infty)$ and $u_2 \in$

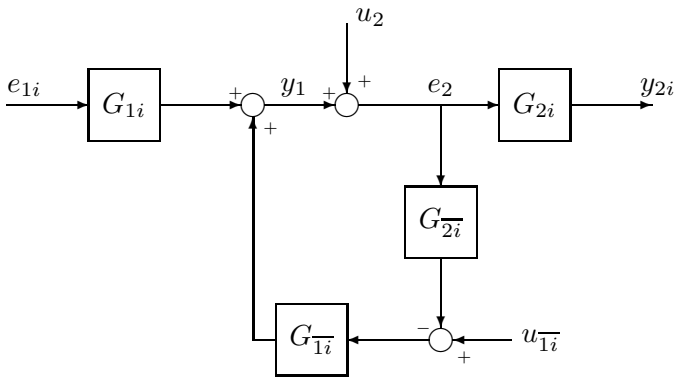

Figure 3.3: Feedback system with the loop broken at e_{1i} [37]

$L_p[\bar{a}, \infty)$, using (3.3)–(3.5) (with $b_1 = b_2 = 0$) and the linearity of G_1, it can be shown that

$$\|(y_1)_T\|_p \leq \frac{\gamma_1}{1-\gamma_1\gamma_2}\|u_1\|_p + \frac{\gamma_1\gamma_2}{1-\gamma_1\gamma_2}\|u_2\|_p \; . \tag{3.12}$$

Since the right-hand-side of this inequality is independent of T, $y_1 \in L_p[\bar{a}, \infty)$ and, given $\|u_1\|_p$ and $\|u_2\|_p$, the right-hand-side of (3.12) is an upper bound for $\|y_1\|_p$.

To obtain a similar result for y_2, instead of breaking the loop at e_1, as in the proof of Theorem 3.1, we will break the loop at each individual channel of e_1. Note that, when the loop is broken at the i^{th} channel of e_1, the system shown in Figure 3.3 is obtained, where $G_{\overline{1i}}$, $G_{\overline{2i}}$, and $u_{\overline{1i}}$ respectively denote G_1, G_2, and u_1 with their i^{th} element removed.

Let γ_{ij} denote the gain of G_{ij} (thus $\gamma_i = \sqrt{\sum_{j=1}^{n} \gamma_{ij}^2}$) for $j = 1, \ldots, n$, $i = 1, 2$. Note that, by Schwarz inequality (by viewing γ_i as the 2-norm of $\begin{bmatrix} \gamma_{i1} & \cdots & \gamma_{in} \end{bmatrix}^T$, $i = 1, 2$),

$$\sum_{j=1}^{n} \gamma_{1j}\gamma_{2j} \leq \gamma_1\gamma_2 \; . \tag{3.13}$$

From Figure 3.3,

$$e_2 = \frac{1}{1 + \sum\limits_{j=1, j\neq i}^{n} G_{1j}G_{2j}} \left(u_2 + \sum_{j=1, j\neq i}^{n} G_{1j}u_{1j} + G_{1i}e_{1i} \right) \; . \tag{3.14}$$

Note that the feedback loop from the output of G_{1i} to the input of G_{2i} in Figure 3.3 is well-posed, since, by (3.13) and the assumption $\gamma_1\gamma_2 < 1$, its loop gain is $\sum_{j=1,j\neq i}^{n} \gamma_{1j}\gamma_{2j} < 1$. Furthermore, by (3.11), the map $\sum_{j=1,j\neq i}^{n} G_{1j}G_{2j}$ is causal. Therefore, the system with map $\dfrac{1}{1+\sum_{j=1,j\neq i}^{n} G_{1j}G_{2j}}$ is causal. Moreover, an upper bound on its gain is $\rho_i := \dfrac{1}{1-\sum_{j=1,j\neq i}^{n} \gamma_{1j}\gamma_{2j}}$.

Now, using (3.3) and (3.4) (with $b_1 = b_2 = 0$), the linearity of G_1 and G_2, the fact that $u_{1j} \in L_p[a_j, \infty), u_2 \in L_p[\bar{a}, \infty)$, and (3.11), from Figure 3.3, we obtain

$$\begin{aligned}
\|(y_{2i})_T\|_p &= \| \left(G_{2i}e_2\right)_T \|_p \\
&\leq \rho_i \left(\| \left(G_{2i}u_2\right)_T \|_p + \sum_{j=1,j\neq i}^{n} \| \left(G_{2i}G_{1j}u_{1j}\right)_T \|_p + \| \left(G_{2i}G_{1i}e_{1i}\right)_T \|_p \right) \\
&\leq \rho_i \left(\|G_{2i}u_2\|_p + \sum_{j=1,j\neq i}^{n} \|G_{2i}G_{1j}u_{1j}\|_p + \| \left(G_{2i}G_{1i}\right)\left(e_{1i}\right)_T \|_p \right) \\
&\leq \rho_i \left(\gamma_{2i}\|u_2\|_p + \gamma_{2i}\sum_{j=1}^{n} \gamma_{1j}\|u_{1j}\|_p + \gamma_{2i}\gamma_{1i}\|(y_{2i})_T\|_p \right) \ , \qquad (3.15)
\end{aligned}$$

where $e_{1i} = u_{1i} - y_{2i}$ is also used in the last step. Using $\gamma_1\gamma_2 < 1$, from (3.13) we obtain $\gamma_{1i}\gamma_{2i} < 1 - \sum_{j=1,j\neq i}^{n} \gamma_{1j}\gamma_{2j}$ or $\rho_i\gamma_{2i}\gamma_{1i} = \dfrac{\gamma_{1i}\gamma_{2i}}{1-\sum_{j=1,j\neq i}^{n} \gamma_{1j}\gamma_{2j}} < 1$. Therefore, from (3.15) we obtain

$$\|(y_{2i})_T\|_p \leq \frac{\gamma_{2i}}{1-\sum_{j=1}^{n} \gamma_{1j}\gamma_{2j}} \left(\|u_2\|_p + \sum_{j=1}^{n} \gamma_{1j}\|u_{1j}\|_p \right) \ . \qquad (3.16)$$

Since the right-hand-side of this inequality is independent of T, $y_{2i} \in L_p[a_i, \infty)$ and, given $\|u_{1j}\|_p$, $j = 1, \ldots, n$, and $\|u_2\|_p$, the right-hand-side of (3.16) is an upper bound for $\|y_{2i}\|_p$. Repeating this for each $i = 1, \ldots, n$, it is concluded that $y_2 \in L_p^n[a, \infty)$. Consequently, since $e_1 = u_1 - y_2$ and $e_2 = u_2 + y_1$, $e_1 \in L_p^n[a, \infty)$ and $e_2 \in L_p[\bar{a}, \infty)$. Furthermore, from (3.12) and (3.16), we also obtain

$$\|y\|_p = \left(\|y_1\|_p^2 + \sum_{i=1}^{n} \|y_{2i}\|_p^2 \right)^{\frac{1}{2}} \leq \gamma\|u\|_p \qquad (3.17)$$

where

$$\gamma := \frac{\sqrt{\gamma_1\gamma_2\left(\gamma_1\gamma_2 + \gamma_1 + \gamma_2\right) + \max\left(\gamma_1^2\ ,\ \gamma_2^2\right)}}{1-\gamma_1\gamma_2} \ .$$

This implies that the closed-loop map from u to y is L_p-sfg. Similarly, it can also be shown that the closed-loop map from u to e is also L_p-sfg. Thus, the desired result follows. □

3.4 Utilization of Non-Causal Uncertainty Blocks in the Robust Controller Design Problem for Systems with Multiple Time-Delays

In the previous two sections, the sufficient conditions were given for the validity of the small-gain theorem for feedback interconnected non-causal subsystems. As stated in Section 3.1, non-causal uncertainty blocks may arise if the approach of [13] is used in the robust controller design problem for multiple-time-delay systems. In this section, it is shown how the non-causal uncertainty blocks arise in the $\mathcal{H}^\infty$ controller design problem for systems with multiple time-delays. In addition, utilization of non-causal uncertainty blocks in the robust controller design is given under different uncertainty representations of the finite dimensional part of the actual plant. To show the appearance of non-causal uncertainty blocks in the problem setup, firstly, the structure of the uncertainty blocks is derived in Subsection 3.4.1. Then, in Subsections 3.4.2–3.4.5, a number of different representations for the uncertainties in the finite-dimensional part of the actual plant are given. In Subsection 3.4.6, it is shown that the design of an $\mathcal{H}^\infty$-optimal controller for a plant whose uncertainties may be represented in one of these forms is possible utilizing the special time-advance form of the resulting uncertainty blocks with the introduced strong small-gain condition. Results presented in this section have been published in [38] and [39].

3.4.1 Appearance of non-causal uncertainty blocks in robust controller design

In this subsection, appearance of non-causal uncertainty blocks in the robust controller design for systems with multiple time-delays by the approach of [13] is given.

Definition 3.6. For a time function (including a constant) $\tau : [t_0, \infty) \to \mathbb{R}$, we let D_τ denote the delay operator by τ; i.e., if $r = D_\tau s$, then

$$r(t) = \begin{cases} s(t - \tau(t)) \,, & t - \tau(t) \geq t_0 \\ 0 \,, & t - \tau(t) < t_0 \end{cases} \quad , \qquad t \geq t_0 \,.$$

If $\tau = \begin{bmatrix} \tau_1 & \cdots & \tau_n \end{bmatrix}^T$, then $D_\tau := \mathrm{diag}(D_{\tau_1}, \ldots, D_{\tau_n})$; i.e., if $r = D_\tau s$, then

$$r_i(t) = \begin{cases} s_i(t - \tau_i(t)) \,, & t - \tau_i(t) \geq t_0 \\ 0 \,, & t - \tau_i(t) < t_0 \end{cases} \quad , \qquad t \geq t_0 \,, \quad i = 1, \ldots, n \,.$$

Note that, if $\tau = h + \delta$, with $h \geq 0$, $\delta(t_0) = 0$, and $|\dot{\delta}(t)| < 1$, $\forall t \geq t_0$, then, for $t \geq t_0$, $D_\tau = D_h D_\delta = D_\delta D_h$.

Let us consider the robust controller design problem for a MIMO linear plant, whose each input and each output is subject to an uncertain time-varying time-delay. To design a stabilizing controller by the approach of [13], the problem should be stated in the generalized $\mathcal{H}^\infty$-framework as depicted in Figure 3.4. Here, Δ is a linear (but possibly time-varying) norm-bounded block which represents uncertainties, K is the controller to be designed, Λ_u and Λ_y respectively represent the nominal input and output time-delays, as in (2.14) and (2.15), $G = \left[\begin{array}{c|cc} A & B_1 & B_2 \\ \hline C_1 & D_{11} & D_{12} \\ C_2 & D_{21} & D_{22} \end{array}\right]$ is the generalized plant from $\begin{bmatrix} w \\ \overline{u} \end{bmatrix}$ to $\begin{bmatrix} z \\ \overline{y} \end{bmatrix}$, which is LTI, finite dimensional, and satisfies the standard $\mathcal{RH}^\infty$ assumptions ((i)–(iv) given in Section 2.2).

In this set-up, if K stabilizes the nominal system (i.e., the system in Figure 3.4 with $\Delta = 0$) and makes the L_2-induced norm of the TFM from w

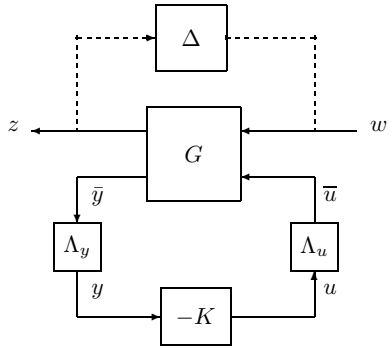

Figure 3.4: Generalized plant [38]

to z less than or equal to some γ, then assuming that Δ is causal, the small gain theorem implies that the actual system is robustly stable for all Δ whose L_2-induced norm is less than $1/\gamma$. However, by the approach of [13], Δ may become non-causal if uncertain part of the actual time-delay is assumed to be negative. If Δ is non-causal, then robustly stabilizing controller K can be designed if the sufficient conditions given in the previous sections are satisfied. However, as shown in [38], these conditions may not always be satisfied.

To show the appearance of non-causal uncertainty blocks in the $\mathcal{H}^\infty$ framework, consider a linear plant, Ω, with n_u inputs and n_y outputs. We assume that the i^{th} input is subject to a time-varying time-delay of $\tau_i^u(t) = h_i^u + \delta_i^u(t)$, where h_i^u is the known time-invariant nominal part and $\delta_i^u(t)$ is the unknown time-varying uncertain part. Similarly, the i^{th} output is subject to a time-varying time-delay of $\tau_i^y(t) = h_i^y + \delta_i^y(t)$, where h_i^y is the known time-invariant nominal part and $\delta_i^y(t)$ is the unknown time-varying uncertain part. It is assumed that

$$\max_{t \geq t_0} \{-\delta_i^\bullet(t)\} \leq \bar{\delta}_i^\bullet \leq h_i^\bullet \,, \qquad i = 1, \ldots, n_\bullet, \tag{3.18}$$

for some $\bar{\delta}_i^\bullet > 0$, where $\bullet$ represents either u or y. Furthermore it is assumed that

$$|\delta_i^\bullet(t)| < \hat{\delta}_i^\bullet, \;\; |\dot{\delta}_i^\bullet(t)| < \beta_i^\bullet, \;\; \forall t \geq t_0, \;\; \text{and} \;\; \delta_i^\bullet(t_0) = 0, \tag{3.19}$$

for some bounds $\hat{\delta}_i^\bullet > 0$ and $0 < \beta_i^\bullet < 1$, $i = 1, \ldots, n_\bullet$. We also assume that, apart from these delays, the plant is time-invariant and finite-dimensional. Then, the actual plant can be represented as $\Omega = D_{\tau^y} P D_{\tau^u}$, where $\tau^\bullet :=$

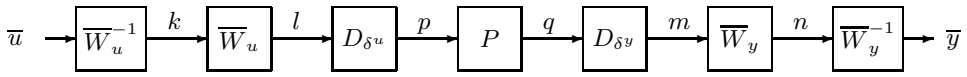

Figure 3.5: Representation of Π [38]

$\left[\begin{array}{ccc} \tau_1^\bullet & \cdots & \tau_{n_\bullet}^\bullet \end{array} \right]^T$ and P is LTI and finite-dimensional. By defining $\Pi := D_{\delta^y} P D_{\delta^u}$, where $\delta^\bullet := \left[\begin{array}{ccc} \delta_1^\bullet & \cdots & \delta_{n_\bullet}^\bullet \end{array} \right]^T$, the plant can also be represented as $\Omega = \Lambda_y \Pi \Lambda_u$, where $\Lambda_\bullet := D_{h^\bullet}$, where $h^\bullet := \left[\begin{array}{ccc} h_1^\bullet & \cdots & h_{n_\bullet}^\bullet \end{array} \right]^T$.

To model the uncertain part of Ω considering the bounds and variations of the uncertain time-varying time-delays, one possible way is to introduce the weighting matrices $\overline{W}_\bullet = \mathrm{diag}(\overline{w}_1^\bullet, \ldots, \overline{w}_{n_\bullet}^\bullet)$, where $\overline{w}_i^\bullet(s) = \dfrac{a_i^\bullet s + 1}{s + b_i^\bullet}$, where $a_i^\bullet, b_i^\bullet > 0$ are design parameters, to represent Π as in Figure 3.5. The transfer function $\overline{w}_i^u(s)$ in Figure 3.5, $i = 1, \ldots, n_u$, can be represented in state-space form as follows:

$$\begin{aligned} \dot{x}_i^u(t) &= -b_i^u x_i^u(t) + (1 - a_i^u b_i^u) k_i(t), \\ l_i(t) &= x_i^u(t) + a_i^u k_i(t), \end{aligned} \tag{3.20}$$

where $x_i^u(t)$ is the state variable and k_i and l_i are the i^{th} element of k and l, respectively. For $i = 1, \ldots, n_u$, the i^{th} element of p in Figure 3.5 can be written as:

$$p_i(t) = l_i(t - \delta_i^u(t)) = x_i^u(t - \delta_i^u(t)) + a_i^u k_i(t - \delta_i^u(t)). \tag{3.21}$$

If the solution of $x_i^u(t)$ is substituted in $p_i(t)$, (3.21) can be written as;

$$\begin{aligned} p_i(t) &= \int_0^{t-\delta_i^u(t)} k_i(\upsilon) d\upsilon - b_i^u \int_0^{t-\delta_i^u(t)} l_i(\upsilon) d\upsilon + a_i^u k_i(t - \delta_i^u(t)) \\ &= \int_0^{t-\delta_i^u(t)} k_i(\upsilon) d\upsilon - \int_0^t k_i(\upsilon) d\upsilon + \int_0^t k_i(\upsilon) d\upsilon \\ &\quad -b_i^u \int_0^{t-\delta_i^u(t)} l_i(\upsilon) d\upsilon + b_i^u \int_0^t l_i(\upsilon) d\upsilon - b_i^u \int_0^t l_i(\upsilon) d\upsilon \\ &\quad +a_i^u k_i(t - \delta_i^u(t)) \\ &= -\int_{t-\delta_i^u(t)}^t e_i^u(\upsilon) d\upsilon + \int_0^t e_i^u(\upsilon) d\upsilon + a_i^u k(t - \delta_i^u(t)), \end{aligned} \tag{3.22}$$

where $e_i^u(t) := k_i^u(t) - b_i^u l_i^u(t)$ and without loss of generality we assume $t_0 = 0$. Let us define $\widetilde{w}_i^u(s) := \dfrac{s(1 - a_i^u b_i^u)}{s + b_i^u}$, then $e_i^u(s) = \widetilde{w}_i^u(s) k_i^u(s)$. Therefore,

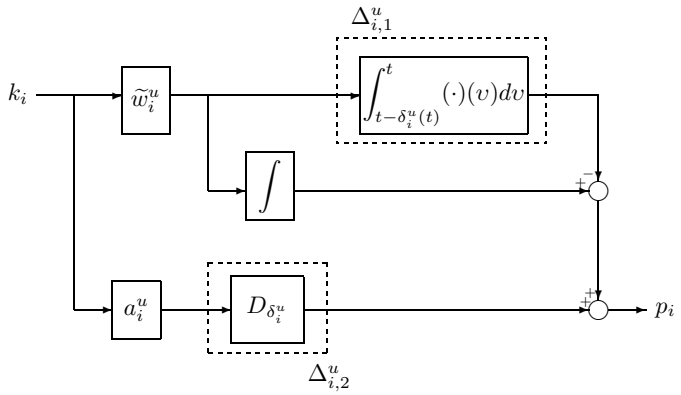

Figure 3.6: Mapping from k_i to p_i [38]

utilizing (3.22), the mapping from the i^{th} element of k to the i^{th} element of p can be depicted as in Figure 3.6. To find a bound on the uncertainty block $\Delta^u_{i,1}$, let us define

$$v_i(t) := \int_{t-\delta^u_i(t)}^{t} e^u_i(\nu)d\nu \leq \int_{t-\delta^u_i(t)}^{t} |e^u_i(\nu)|d\nu.$$

Let $r^u_i(t) := |e^u_i(t)|$, $i = 1, \cdots, n_u$, then, from the assumption in (3.19)

$$|v_i(t)| \leq \left| \int_{t-\delta^u_i(t)}^{t} r^u_i(\nu)d\nu \right| \leq \begin{cases} |\hat{v}_i(t)|, & \text{if} \quad \delta^u_i(t) \geq 0 \\ |\overline{v}_i(t)|, & \text{if} \quad \delta^u_i(t) \leq 0 \end{cases}, \tag{3.23}$$

where $\hat{v}_i(t) := \int_{t-\hat{\delta}^u_i}^{t} r^u_i(\nu)d\nu$, and $\overline{v}_i(t) := \int_{t}^{t+\hat{\delta}^u_i} r^u_i(\nu)d\nu$. Taking Laplace transformations of $\hat{v}_i(t)$ and $\overline{v}_i(t)$,

$$\hat{v}_i(s) = \frac{e^{\hat{\delta}^u_i s} - 1}{s} r^u_i(s) \tag{3.24}$$

$$\overline{v}_i(s) = \frac{e^{-\hat{\delta}^u_i s} - 1}{s} r^u_i(s). \tag{3.25}$$

From (3.24) and (3.25), both $\|\hat{v}_i(t)\|_2$ and $\|\overline{v}_i(t)\|_2$ are less than or equal $\hat{\delta}^u_i \|r^u_i(t)\|_2$, $i = 1, \cdots, n_u$. Therefore, from (3.23), $\|v_i(t)\|_2 \leq \hat{\delta}^u_i \|r^u_i(t)\|_2 = \hat{\delta}^u_i \|e^u_i(t)\|_2$, since $\int_0^\infty |r^u_i(t)|^2 dt = \int_0^\infty |(|e^u_i(t)|)|^2 dt = \int_0^\infty |e^u_i(t)|^2 dt$ for $i = 1, \ldots, n_u$. Hence, $\|\Delta^u_{i,1}\|_2 \leq \hat{\delta}^u_i$, $i = 1, \ldots, n_u$.

To find a norm bound on $\Delta^u_{i,2}$, as in [23], let us define for $i = 1, \ldots, n_\bullet$,

$$\lambda^\bullet_i := \upsilon - \delta^\bullet_i(\upsilon) =: f^\bullet_i(\upsilon). \tag{3.26}$$

The relation in (3.26) implies that

$$\frac{d\lambda_i^\bullet}{d\upsilon} = 1 - \frac{d\delta_i^\bullet(\upsilon)}{d\upsilon} := 1 - g_i^\bullet(\lambda_i^\bullet). \tag{3.27}$$

Since by (3.19), $\left|\frac{d\delta_i^\bullet(\upsilon)}{d\upsilon}\right| < 1$, therefore, $\frac{df_i^\bullet(\upsilon)}{d\upsilon} > 0$. The latter inequality implies that $\upsilon = f_i^{\bullet -1}(\lambda_i^\bullet)$. From (3.26), $g_i^\bullet(\lambda_i^\bullet) = \left.\frac{d\delta_i^\bullet(\upsilon)}{d\upsilon}\right|_{\upsilon = f_i^{\bullet -1}(\lambda_i^\bullet)}$. Therefore, if $d(t) := c(t - \delta_i^u(t))$, $i = 1, \ldots, n_u$, then,

$$\begin{aligned}\int_0^\infty |d(t)|^2 dt &= \int_0^\infty |c(t-\delta_i^u(t))|^2 dt = \int_0^\infty |c(\lambda_i^u)|^2 \frac{d\lambda_i^u}{1 - g_i^u(\lambda_i^u)} \\ &< \frac{1}{1-\beta_i^u}\int_0^\infty |c(\lambda_i^u)|^2 d\lambda_i^u,\end{aligned} \tag{3.28}$$

hence, $\|\Delta_{i,2}^u\|_2 < \frac{1}{\sqrt{1-\beta_i^u}}$. As shown in Figure 3.6, $\Delta_{i,1}^u$ and $\Delta_{i,2}^u$ are non-causal, since $\Delta_{i,1}^u$ becomes a non-causal integral block and $\Delta_{i,2}^u$ becomes a time-advance block for $\delta_i^u(t) < 0$. The maximum time-advance in both $\Delta_{i,1}^u$ and $\Delta_{i,2}^u$ is $\max_{t\geq 0}\{-\delta_i^u(t)\} > 0$. However, by (3.18), it is bounded by $\bar{\delta}_i^u \leq h_i^u$. Let us define $\Delta_i^u := \begin{bmatrix} 1 & \Delta_{i,1}^u & \Delta_{i,2}^u \end{bmatrix}$, which is norm-bounded, and $w_i^u(s) := \begin{bmatrix} \frac{1-a_i^u b_i^u}{a_i^u s + 1} & -\frac{s(1-a_i^u b_i^u)}{a_i^u s+1} & a_i^u \frac{s+b_i^u}{a_i^u s+1} \end{bmatrix}^T$, which is stable. Now, defining $\Delta_u := \text{bdiag}(\Delta_1^u, \ldots, \Delta_{n_u}^u)$ and $W_u := \text{bdiag}(w_1^u, \ldots, w_{n_u}^u)$, the mapping from $\overline{u}$ to p in Figure 3.5 can be obtained as $\Delta_u W_u$.

Using the similar procedure, the mapping from q to $\bar{y}$ can be obtained as follows. The transfer function $\overline{w}_j^y(s)$ in Figure 3.5, $j = 1, \ldots, n_y$, can be represented in state-space form:

$$\begin{aligned}\dot{x}_j^y(t) &= -b_j^y x_j^y(t) + (1 - a_j^y b_j^y) m_j(t), \\ n_j(t) &= x_j^y(t) + a_j^y m_j(t),\end{aligned} \tag{3.29}$$

where $x_j^y(t)$ is the state variable and m_j and n_j are the j^{th} element of m and n, respectively. In Figure 3.5, $m_j(t) = q_j(t - \delta_j^y(t))$. Therefore, the solution of $x_j^y(t)$ in (3.29) can be written as below;

$$x_j^y(t) = -b_j^y \int_0^t x_j^y(\upsilon) d\upsilon + (1 - a_j^y b_j^y) \int_0^t q_j(\upsilon - \delta_j^y(\upsilon)) d\upsilon$$

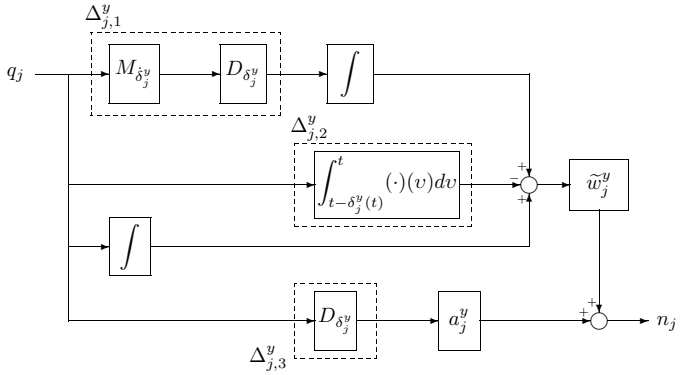

Figure 3.7: Mapping from q_j to n_j [38]

$$
\begin{aligned}
= \; & -b^y_j \int_0^t x^y_j(\upsilon)d\upsilon + (1-a^y_j b^y_j)\left[\int_0^t q_j(\upsilon-\delta^y_j(\upsilon))d\upsilon - \right. \\
& \int_0^{t-\delta^y_j(t)} q_j(\lambda^y_j)d\lambda^y_j + \int_0^{t-\delta^y_j(t)} q_j(\upsilon)d\upsilon + \int_0^t q_j(\upsilon)d\upsilon \\
& \left. - \int_0^t q_j(\upsilon)d\upsilon\right]. \qquad (3.30)
\end{aligned}
$$

From (3.26), since $\int_0^{t-\delta^y_j(t)} q_j(\lambda^y_j)d\lambda^y_j = \int_0^t (1-g^y_j(\upsilon-\delta^y_j(\upsilon)))q_j(\upsilon-\delta^y_j(\upsilon))d\upsilon$, (3.30) can be written as;

$$
\begin{aligned}
x^y_j(t) \; = \; & -b^y_j \int_0^t x^y_j(\upsilon)d\upsilon + (1-a^y_j b^y_j)\int_0^t (g^y_j q_j)(\upsilon-\delta^y_j(\upsilon))d\upsilon \\
& -(1-a^y_j b^y_j)\int_{t-\delta^y_j(t)}^t q_j(\upsilon)d\upsilon + (1-a^y_j b^y_j)\int_0^t q_j(\upsilon)d\upsilon \\
= \; & -b^y_j \int_0^t x^y_j(\upsilon)d\upsilon + (1-a^y_j b^y_j)(Tq_j)(t), \qquad (3.31)
\end{aligned}
$$

where $(Tq_j)(t) := \left[\int_0^t D_{\delta^y_j}[g^y_j q_j](\upsilon)d\upsilon - \int_{t-\delta^y_j(t)}^t q_j(\upsilon)d\upsilon + \int_0^t q_j(\upsilon)d\upsilon\right]$. If the Laplace transform of both sides in (3.31) are taken, then

$$x^y_j(s) = \frac{s(1-a^y_j b^y_j)}{s+b^y_j}\mathcal{L}\{(Tq_j)(t)\}.$$

Let us define $\widetilde{w}^y_j(s) := \dfrac{s(1-a^y_j b^y_j)}{s+b^y_j}$ and $\widetilde{q}^y_j(s) := \mathcal{L}\{(Tq_j)(t)\}$. Then, $x^y_j(s) = \widetilde{w}^y_j(s)\widetilde{q}^y_j(s)$. Since $n_j(t) = x^y_j(t) + m_j(t) = x^y_j(t) + a^y_j q_j(t-\delta^y_j(t))$, the mapping from the j^{th} element of q to the j^{th} element of n can be depicted as in Figure 3.7, where $M_{\dot{\delta}^y_j}$ represents multiplication with $\dot{\delta}^y_j$. Using the relation in (3.26) and (3.27) , $\|\Delta^y_{j,1}\|_2 < \dfrac{\beta^y_j}{\sqrt{1-\beta^y_j}}$ (see also [23]), $\|\Delta_{j,2}\|_2 \leq \widehat{\delta}^y_j$ and

$\|\Delta^y_{j,3}\|_2 < \dfrac{1}{\sqrt{1-\beta^y_j}}$, $j = 1, \ldots, n_y$. Here, all $\Delta^y_{j,l}$, $l = 1, 2, 3$, are non-causal for $\delta^y_j(t) < 0$, since $\Delta^y_{j,1}$ becomes a time-advance block, $\Delta^y_{j,2}$ becomes a non-causal integral block, and $\Delta^y_{j,3}$ becomes a time-advance block. The maximum time-advance in all $\Delta^y_{j,l}$, $l = 1, 2, 3$, is $\max_{t\geq 0}\{-\delta^y_j(t)\} > 0$, in general and, by (3.18), is bounded by $\bar{\delta}^y_j \leq h^y_j$. Defining $\Delta_y := \text{bdiag}(\Delta^y_1, \ldots, \Delta^y_{n_y})$, where $\Delta^y_j := \begin{bmatrix} 1 & \Delta^y_{j,1} & \Delta^y_{j,2} & \Delta^y_{j,3} \end{bmatrix}^T$ is norm-bounded, and $W_y := \text{bdiag}(w^y_1, \ldots, w^y_{n_y})$, where $w^y_j(s) := \begin{bmatrix} \dfrac{1-a^y_j b^y_j}{a^y_j s+1} & \dfrac{1-a^y_j b^y_j}{a^y_j s+1} & -\dfrac{s(1-a^y_j b^y_j)}{a^y_j s+1} & a^y_j \dfrac{s+b^y_j}{a^y_j s+1} \end{bmatrix}$ is stable, the mapping from q to $\overline{y}$ in Figure 3.5 can be obtained as $W_y\Delta_y$. Therefore, Π can be written as:

$$\Pi = W_y \Delta_y P \Delta_u W_u \, . \tag{3.32}$$

In the following subsections, the robust controller design for the actual plant Ω, whose finite-dimensional part is shown in one of the four different uncertainty representations, is presented.

3.4.2 Additive uncertainty representation

Let

$$P = P^0 + W_1 \widetilde{\Delta} W_2, \tag{3.33}$$

where P^0 is the nominal plant (apart from the time-delays), W_1 and W_2 are the stable uncertainty weights, and $\widetilde{\Delta}$ is the stable uncertainty block. Then, (3.32) can be written as

$$\Pi = W_y \Delta_y P^0 \Delta_u W_u + W_y \Delta_y W_1 \widetilde{\Delta} W_2 \Delta_u W_u \, .$$

Let us assume that P^0 has a left co-prime factorization,

$$P^0 = M^{-1} N \tag{3.34}$$

in $\mathcal{H}^\infty$, where M is diagonal. Since $W_y\Delta_y$ and M^{-1} are both diagonal (hence they commute), Π can be written as

$$\begin{aligned} \Pi \;\; = \;\; & P^0 + W_y \Delta_y W_1 \widetilde{\Delta} W_2 \Delta_u W_u \\ & + \begin{bmatrix} W_y \Delta_y & -I_{n_y} \end{bmatrix} \begin{bmatrix} M^{-1}N & 0 \\ 0 & M^{-1}N \end{bmatrix} \begin{bmatrix} \Delta_u W_u \\ I_{n_u} \end{bmatrix} \end{aligned}$$

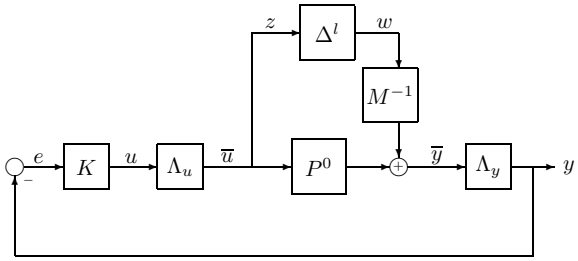

Figure 3.8: Feedback Configuration with left co-prime factorization [39]

$$= \quad P^0 + M^{-1}\overline{W}_y\overline{\Delta}_a^l\overline{W}_u = P^0 + M^{-1}\Delta_a^l \ , \tag{3.35}$$

where $\overline{\Delta}_a^l := \text{bdiag}(\Delta_y N \Delta_u, \Delta_y M W_1 \widetilde{\Delta} W_2 \Delta_u, N)$, $\overline{W}_y := \begin{bmatrix} W_y & W_y & -I_{n_y} \end{bmatrix}$, and $\overline{W}_u := \begin{bmatrix} W_u' & W_u' & I_{n_u} \end{bmatrix}^T$. Since $\overline{W}_y, \overline{W}_u$, and $\overline{\Delta}_a^l$ are norm-bounded, $\Delta_a^l := \overline{W}_y\overline{\Delta}_a^l\overline{W}_u$ is also norm-bounded and its norm is bounded by the norms of $W_\bullet$ (which depends on design parameters $a_i^\bullet$ and $b_i^\bullet$), M, W_1, W_2, N, and by the norm bounds of $\widetilde{\Delta}$ and $\Delta_\bullet$ (which depends on $\hat{\delta}_i^\bullet$ and $\beta_i^\bullet$). Then, the feedback configuration to control the actual plant can be represented as shown in Figure 3.8, where $\Delta^l = \Delta_a^l$. Note that Figure 3.8 is equivalent to Figure 3.4 with $\Delta = \Delta^l$ and

$$G = \begin{bmatrix} 0 & I_{n_u} \\ M^{-1} & P^0 \end{bmatrix} \ , \tag{3.36}$$

which satisfies the standard $\mathcal{RH}^\infty$ assumptions ((i)–(iv) given in Section 2.2) as long as the actual realization of P^0 is stabilizable and detectable. Moreover, Figure 3.8 is also equivalent to Figure 3.2, where $G_1 = \Delta_a^l$ and $G_2 = \Lambda_u K(I + \Lambda_y P^0 \Lambda_u K)^{-1}\Lambda_y M^{-1} = \Lambda_u K(M + \Lambda_y N \Lambda_u K)^{-1}\Lambda_y$. G_1 and G_2 are both linear and, since Δ_a^l is stable and K is designed to stabilize the nominal plant, G_1 and G_2 are also both stable. Note that, the maximum time-advance from the i^{th} input of $G_1 = \Delta_a^l = W_y\Delta_y(N + MW_1\widetilde{\Delta}W_2)\Delta_u W_u - N$ to its j^{th} output is bounded by $\bar{\delta}_i^u + \bar{\delta}_j^y$, since W_1, W_2, $\widetilde{\Delta}$, M, and N are causal. On the other hand, note that, due to Λ_u and Λ_y, $G_2 = \Lambda_u K(M + \Lambda_y N \Lambda_u K)^{-1}\Lambda_y$ involves a pure delay of $h_i^u + h_j^y$ from its j^{th} input to its i^{th} output.

Alternatively, if P^0 does not have a left-coprime factorization (3.34) where M is diagonal, but has a right-coprime factorization,

$$P^0 = \widetilde{N}\widetilde{M}^{-1} \tag{3.37}$$

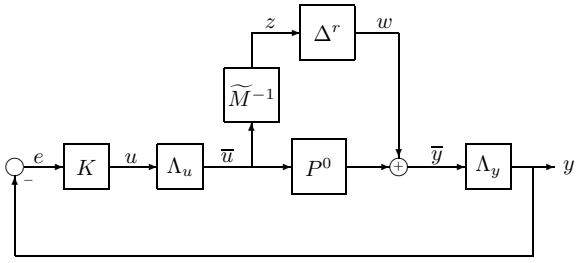

Figure 3.9: Feedback configuration with right co-prime factorization [39]

in $\mathcal{H}^\infty$ where $\widetilde{M}$ is diagonal, then

$$\begin{aligned}\Pi &= P^0 + W_y\Delta_y W_1\widetilde{\Delta}W_2\Delta_u W_u \\ &+ \begin{bmatrix} W_y\Delta_y & -I_{n_y} \end{bmatrix}\begin{bmatrix} \widetilde{N}\widetilde{M}^{-1} & 0 \\ 0 & \widetilde{N}\widetilde{M}^{-1} \end{bmatrix}\begin{bmatrix} \Delta_u W_u \\ I_{n_u} \end{bmatrix} \\ &= P^0 + \overline{W}_y\overline{\Delta}_a^r\overline{W}_u\widetilde{M}^{-1} = P^0 + \Delta_a^r\widetilde{M}^{-1}\,, \end{aligned} \tag{3.38}$$

where $\Delta_a^r := \overline{W}_y\overline{\Delta}_a^r\overline{W}_u$, where $\overline{\Delta}_a^r := \text{bdiag}(\Delta_y\widetilde{N}\Delta_u, \Delta_y W_1\widetilde{\Delta}W_2\widetilde{M}\Delta_u, \widetilde{N})$. Furthermore, Δ_a^r is norm-bounded and its bound can be calculated in terms of the norms of $W_\bullet$, $\widetilde{M}$, W_1, W_2, $\widetilde{N}$, and the norm bound of $\Delta_\bullet$ and $\widetilde{\Delta}$. Then the feedback configuration to control the actual plant can be represented as shown in Figure 3.9, where $\Delta^r = \Delta_a^r$. Furthermore, this feedback configuration is equivalent to the one given in Figure 3.4 with $\Delta = \Delta^r$ and

$$G = \begin{bmatrix} 0 & \widetilde{M}^{-1} \\ I_{n_y} & P^0 \end{bmatrix}\,, \tag{3.39}$$

which satisfies the standard $\mathcal{RH}^\infty$ assumptions ((i)–(iv) given in Section 2.2) as long as the actual realization of P^0 is stabilizable and detectable. Figure 3.9 is also equivalent to Figure 3.2, where $G_1 = \Delta_a^r$ and $G_2 = \widetilde{M}^{-1}\Lambda_u K\Lambda_y(I + P^0\Lambda_u K\Lambda_y)^{-1} = \Lambda_u\widetilde{M}^{-1}K(I + \Lambda_y P^0\Lambda_u K)^{-1}\Lambda_y$. In this feedback configuration, G_1 and G_2 are both linear and, since Δ_a^r is stable and K is designed to stabilize the nominal plant, G_1 and G_2 are both stable. Furthermore, the maximum time-advance from the i^{th} input of $G_1 = \Delta_a^r = W_y\Delta_y(\widetilde{N} + W_1\widetilde{\Delta}W_2\widetilde{M})\Delta_u W_u - \widetilde{N}$ to its j^{th} output is bounded by $\bar{\delta}_i^u + \bar{\delta}_j^y$, since W_1, W_2, $\widetilde{\Delta}$, $\widetilde{M}$, and $\widetilde{N}$ are causal. On the other hand, due to Λ_u and Λ_y, $G_2 = \Lambda_u\widetilde{M}^{-1}K(I + \Lambda_y P^0\Lambda_u K)^{-1}\Lambda_y$ involves a pure delay of $h_i^u + h_j^y$ from its j^{th} input to its i^{th} output.

3.4.3 Multiplicative input uncertainty representation

Let

$$P = P^0(I_{n_u} + W_1\widetilde{\Delta}W_2), \tag{3.40}$$

where W_1 and W_2 are stable uncertainty weights and $\widetilde{\Delta}$ is the stable uncertainty block. Then

$$\Pi = W_y\Delta_y P^0\Delta_u W_u + W_y\Delta_y P^0 W_1\widetilde{\Delta}W_2\Delta_u W_u \ .$$

Let us assume that, P^0 has a factorization in $\mathcal{H}^\infty$ as given in (3.34) where M is diagonal. Then

$$\begin{aligned}
\Pi &= P^0 + W_y\Delta_y P^0 W_1\widetilde{\Delta}W_2\Delta_u W_u \\
&\quad + \begin{bmatrix} W_y\Delta_y & -I_{n_y} \end{bmatrix} \begin{bmatrix} M^{-1}N & 0 \\ 0 & M^{-1}N \end{bmatrix} \begin{bmatrix} \Delta_u W_u \\ I_{n_u} \end{bmatrix} \\
&= P^0 + M^{-1}\overline{W}_y\overline{\Delta}^l_{m_i}\overline{W}_u = P^0 + M^{-1}\Delta^l_{m_i} \ ,
\end{aligned} \tag{3.41}$$

where $\overline{\Delta}^l_{m_i} := \text{bdiag}(\Delta_y N\Delta_u, \Delta_y N W_1\widetilde{\Delta}W_2\Delta_u, N)$, $\overline{W}_y$ and $\overline{W}_u$ are same as in Subsection 3.4.2, and $\Delta^l_{m_i} := \overline{W}_y\overline{\Delta}^l_{m_i}\overline{W}_u$. Note that, $\Delta^l_{m_i}$ is norm-bounded (norm bound depends on the norms of $W_\bullet$, W_1, W_2, N, and the norm bounds of $\Delta_\bullet$, $\widetilde{\Delta}$). Furthermore, representation of Π in (3.41) for the perturbed plant in (3.40) is the same as in (3.35). Therefore, the feedback configuration to control the actual plant which is represented by multiplicative input perturbation, can be represented as in Figure 3.8, where $\Delta^l = \Delta^l_{m_i}$.

Since the structure of Π in (3.41) is same as in (3.35), the generalized plant in the $\mathcal{H}^\infty$-framework in this case is same as in (3.36). Furthermore, the feedback configuration for this set up (Figure 3.8 with $\Delta^l = \Delta^l_{m_i}$) can also be shown as in Figure 3.2, where $G_1 = \Delta^l_{m_i}$ and $G_2 = \Lambda_u K(M + \Lambda_y N\Lambda_u K)^{-1}\Lambda_y$. Note that, G_1 and G_2 are both linear and, since $\Delta^l_{m_i}$ is stable and K stabilizes the nominal plant, G_1 and G_2 are also stable. Since $(I_{n_u} + W_1\widetilde{\Delta}W_2)$ and N are causal, the maximum time-advance from the i^{th} input of $G_1 = \Delta^l_{m_i} = W_y\Delta_y N(I_{n_u} + W_1\widetilde{\Delta}W_2)\Delta_u W_u - N$ to its j^{th} output is bounded by $\bar{\delta}^u_i + \bar{\delta}^y_j$. Furthermore, as above, $G_2 = \Lambda_u K(M + \Lambda_y N\Lambda_u K)^{-1}\Lambda_y$ involves a pure delay of $h^u_i + h^y_j$ from its j^{th} input to its i^{th} output.

3.4.4 Multiplicative output uncertainty representation

Let

$$P = (I_{n_y} + W_1 \widetilde{\Delta} W_2) P^0, \tag{3.42}$$

where W_1 and W_2 are stable uncertainty weights and $\widetilde{\Delta}$ is the stable uncertainty block. Then

$$\Pi = W_y \Delta_y P^0 \Delta_u W_u + W_y \Delta_y W_1 \widetilde{\Delta} W_2 P^0 \Delta_u W_u \ .$$

Let us assume that, P^0 has a factorization in $\mathcal{H}^\infty$ as given in (3.37) where $\widetilde{M}$ is diagonal. Then

$$\begin{aligned} \Pi &= P^0 + W_y \Delta_y W_1 \widetilde{\Delta} W_2 P^0 \Delta_u W_u \\ &\quad + \begin{bmatrix} W_y \Delta_y & -I_{n_y} \end{bmatrix} \begin{bmatrix} \widetilde{N}\widetilde{M}^{-1} & 0 \\ 0 & \widetilde{N}\widetilde{M}^{-1} \end{bmatrix} \begin{bmatrix} \Delta_u W_u \\ I_{n_u} \end{bmatrix} \\ &= P^0 + \overline{W}_y \overline{\Delta}^r_{m_o} \overline{W}_u \widetilde{M}^{-1} = P^0 + \Delta^r_{m_o} \widetilde{M}^{-1} \ , \end{aligned} \tag{3.43}$$

where $\overline{\Delta}^r_{m_o} := \text{bdiag}(\Delta_y \widetilde{N} \Delta_u, \Delta_y W_1 \widetilde{\Delta} W_2 \widetilde{N} \Delta_u, \widetilde{N})$, $\overline{W}_y$ and $\overline{W}_u$ are same as in Subsection 3.4.2, and $\Delta^r_{m_o} := \overline{W}_y \overline{\Delta}^r_{m_o} \overline{W}_u$. Note that, $\Delta^r_{m_o}$ is also norm-bounded and the feedback configuration to control the actual plant can be represented as in Figure 3.9, where $\Delta^r = \Delta^r_{m_o}$.

Since Π in (3.43) has the same structure as in (3.38), then the generalized plant to design a robust controller for this plant is the same as in (3.39). Furthermore, this configuration is also equivalent to the one shown in Figure 3.2 with $G_1 = \Delta^r_{m_o}$ and $G_2 = \Lambda_u \widetilde{M}^{-1} K (I + \Lambda_y P^0 \Lambda_u K)^{-1} \Lambda_y$, which are both linear and stable. Furthermore, the maximum time-advance from the i^{th} input of G_1 to its j^{th} output is bounded by $\bar{\delta}^u_i + \bar{\delta}^y_j$ and G_2 involves a pure delay of $h^u_i + h^y_j$ from its j^{th} input to its i^{th} output.

3.4.5 Multiplicative input/output uncertainty representation

Let

$$P = (I_{n_y} + W_{y_1} \widetilde{\Delta}^y W_{y_2}) P^0 (I_{n_u} + W_{u_1} \widetilde{\Delta}^u W_{u_2}), \tag{3.44}$$

where $\widetilde{\Delta}^{\bullet}$ are stable uncertainty blocks and $W_{\bullet_k}$ are stable uncertainty weights ($\bullet$ represents either u or y and $k = 1, 2$). Let us assume that either

(a) $W_{y_1}\widetilde{\Delta}^{y}W_{y_2}$ is diagonal and P^0 has a factorization in $\mathcal{H}^{\infty}$ as given in (3.34) where M is diagonal or

(b) $W_{u_1}\widetilde{\Delta}^{u}W_{u_2}$ is diagonal and P^0 has a factorization in $\mathcal{H}^{\infty}$ as given in (3.37) where $\widetilde{M}$ is diagonal.

In case (a) we have

$$\begin{aligned}\Pi &= W_y\Delta_y P^0\Delta_u W_u + W_y\Delta_y P^0 W_{u_1}\widetilde{\Delta}^{u}W_{u_2}\Delta_u W_u \\ &\quad + W_y\Delta_y W_{y_1}\widetilde{\Delta}^{y}W_{y_2}P^0\Delta_u W_u + P^0 - P^0 \\ &\quad + W_y\Delta_y W_{y_1}\widetilde{\Delta}^{y}W_{y_2}P^0 W_{u_1}\widetilde{\Delta}^{u}W_{u_2}\Delta_u W_u \\ &= P^0 + M^{-1}\Delta^l_{m_{io}}\ , \end{aligned} \tag{3.45}$$

where $\Delta^l_{m_{io}} := \widetilde{W}_y\widetilde{\Delta}^l_{m_{io}}\widetilde{W}_u$. In $\Delta^l_{m_{io}}$, the weighting matrices is of the form $\widetilde{W}_y := \begin{bmatrix} W_y & W_y & W_y & W_y & -I_{n_y}\end{bmatrix}$, $\widetilde{W}_u := \begin{bmatrix} W'_u & W'_u & W'_u & W'_u & I_{n_u}\end{bmatrix}^T$ and the uncertainty block is, $\widetilde{\Delta}^l_{m_{io}} := \text{bdiag}\Big(\Delta_y N\Delta_u\ ,\ \Delta_y NW_{u_1}\widetilde{\Delta}^{u}W_{u_2}\Delta_u\ ,$ $\Delta_y W_{y_1}\widetilde{\Delta}^{y}W_{y_2}N\Delta_u\ ,\ \Delta_{44}\ ,\ N\Big)$, where $\Delta_{44} := \Delta_y W_{y_1}\widetilde{\Delta}^{y}W_{y_2}NW_{u1}\widetilde{\Delta}^{u}W_{u_2}\Delta_u$. Since $\Delta_{\bullet}$, $\widetilde{\Delta}^{\bullet}$, $W_{\bullet}$, N, and $W_{\bullet_k}$ are norm-bounded, $\Delta^l_{m_{io}}$ is norm-bounded. Since Π in (3.45) is in additive form as in (3.35), the feedback configuration in Figure 3.8 with $\Delta^l = \Delta^l_{m_{io}}$ can be used to control the actual plant. Furthermore, the generalized plant in the $\mathcal{H}^{\infty}$-framework is the same as in (3.36). Moreover, this configuration is equivalent to the one given in Figure 3.2 with $G_1 = \Delta^l_{m_{io}}$ and $G_2 = \Lambda_u K(M+\Lambda_y N\Lambda_u K)^{-1}\Lambda_y$. In this feedback configuration, G_1 and G_2 are linear and since $\Delta^l_{m_{io}}$ is stable and K stabilizes the nominal plant, G_1 and G_2 are also stable. Moreover, the maximum time-advance from the i^{th} input of G_1 to its j^{th} output is bounded by $\bar{\delta}^u_i + \bar{\delta}^y_j$ and G_2 involves a pure delay of $h^u_i + h^y_j$ from its j^{th} input to its i^{th} output.

On the other hand, in case (b) we have

$$\Pi = P^0 + \Delta^r_{m_{io}}\widetilde{M}^{-1}, \tag{3.46}$$

where $\Delta^r_{m_{io}}$ is same as $\Delta^l_{m_{io}}$ with N replaced by $\widetilde{N}$. Thus, $\Delta^r_{m_{io}}$ is also norm-bounded. Since Π in (3.46) is in additive form as in (3.38), the feedback configuration in Figure 3.9 with $\Delta^r = \Delta^r_{m_{io}}$ can be used to control the actual plant. Furthermore, the generalized plant in the $\mathcal{H}^\infty$-framework is same as in (3.39). Moreover, this configuration is equivalent to the one given in Figure 3.2 with $G_1 = \Delta^r_{m_{io}}$ and $G_2 = \Lambda_u \widetilde{M}^{-1} K (I + \Lambda_y P^0 \Lambda_u K)^{-1} \Lambda_y$, which are both linear and stable. Moreover, the maximum time-advance from the i^{th} input of G_1 to its j^{th} output is bounded by $\bar{\delta}^u_i + \bar{\delta}^y_j$ and G_2 involves a pure delay of $h^u_i + h^y_j$ from its j^{th} input to its i^{th} output.

From the results of this subsection, it is also evident that in the case of multiplicative input uncertainty representation (presented in Subsection 3.4.3), a right co-prime factorization, rather than a left co-prime factorization, can be used if $W_1 \widetilde{\Delta} W_2$ in (3.40) is diagonal. Similarly, in the case of multiplicative output uncertainty representation (presented in Subsection 3.4.4), a left co-prime factorization, rather than a right co-prime factorization, can be used if $W_1 \widetilde{\Delta} W_2$ in (3.42) is diagonal.

3.4.6 Utilization of the non-causal uncertainty blocks

So far, for a number of different uncertainty representations, we have shown that the feedback configuration to design a stabilizing optimal $\mathcal{H}^\infty$-controller can be represented as in Figure 3.2, where G_1 and G_2 are both linear (thus (3.7) and (3.8) are satisfied) and stable (thus (3.3) and (3.4) are satisfied for some γ_1 and γ_2 and $b_1 = b_2 = 0$). Furthermore, in each case, G_1, which in general is non-causal, has the property that the maximum time-advance from its i^{th} input to its j^{th} output is bounded by $\bar{\delta}^u_i + \bar{\delta}^y_j$ and G_2 has the property that it involves a pure delay of $h^u_i + h^y_j$ from its j^{th} input to its i^{th} output. This implies that the maximum time-advance from the j^{th} input of $G_1 G_2$ to its i^{th} output is

$$\max_{k=1,\ldots,n_u} \left\{ \bar{\delta}^y_i + \bar{\delta}^u_k - h^u_k - h^y_j \right\} \leq \bar{\delta}^y_i - h^y_j \,, \tag{3.47}$$

where the inequality follows from the fact that, by (3.18), $\bar{\delta}_k^u \leq h_k^u$, for $k = 1, \ldots, n_u$. Note that, (3.47) may be positive, unless $\bar{\delta}_i^y \leq h_j^y$ for all i, j. This means that (3.5) may not be satisfied in general. The above properties of G_1 and G_2 also implies that the maximum time-advance from the j^{th} input of G_2G_1 to its i^{th} output is

$$\max_{k=1,\ldots,n_y} \left\{ \bar{\delta}_j^u + \bar{\delta}_k^y - h_k^y - h_i^u \right\} \leq \bar{\delta}_j^u - h_i^u \,, \tag{3.48}$$

where the inequality follows from the fact that, by (3.18), $\bar{\delta}_k^y \leq h_k^y$, for $k = 1, \ldots, n_y$. Note that, (3.48) may also be positive, unless $\bar{\delta}_j^u \leq h_i^u$ for all i, j. This implies that (3.6) may also not be satisfied in general. Although (3.5) and (3.6) may not be satisfied, if the strong small-gain conditions, given in the following theorem, are satisfied then the internal stability of the feedback system in Figure 3.2 is guaranteed.

Theorem 3.3. *[39] Consider the feedback configuration shown in Figure 3.2. Let $G_1 : L_{pe}^{n_1}[a_1, \infty) \to L_{pe}^{n_2}[a_2, \infty)$ and $G_2 : L_{pe}^{n_2}[a_2, \infty) \to L_{pe}^{n_1}[a_1, \infty)$ be both linear and L_p-sfg with gain γ_1 and γ_2 respectively, where $n_1 = n_u$ and $n_2 = n_y$. Denote the j^{th} column of G_k ($k = 1, 2$) by G_{kj}^u ($j = 1, \ldots, n_k$) and its i^{th} row by G_{ki}^y ($i = 1, \ldots, n_{\bar{k}}$, $\bar{k} := k - (-1)^k$). Let $\gamma_{ki}^{\bullet}$ denote the gain of $G_{ki}^{\bullet}$. Suppose that the maximum time-advance from the j^{th} input of $\Gamma_1 := G_1G_2$ to its i^{th} output is bounded by (3.47) and the maximum time-advance from the j^{th} input of $\Gamma_2 := G_2G_1$ to its i^{th} output is bounded by (3.48), where $\bar{\delta}_i^y \leq h_i^y$, $i = 1, \ldots, n_2$, and $\bar{\delta}_j^u \leq h_j^u$, $j = 1, \ldots, n_1$. Moreover, suppose that the strong small-gain conditions for G_1G_2 and G_2G_1,*

$$\sqrt{\sum_{i=1}^{n_2} \left(\gamma_{1i}^y\right)^2} \sqrt{\sum_{i=1}^{n_2} \left(\gamma_{2i}^u\right)^2} < 1 \quad \text{and} \quad \sqrt{\sum_{i=1}^{n_1} \left(\gamma_{2i}^y\right)^2} \sqrt{\sum_{i=1}^{n_1} \left(\gamma_{1i}^u\right)^2} < 1 \tag{3.49}$$

are both satisfied. Then the closed-loop system, i.e., the map from $u = \begin{bmatrix} u_1 \\ u_2 \end{bmatrix}$ to $y = \begin{bmatrix} y_1 \\ y_2 \end{bmatrix}$ in Figure 3.2, is L_p-sfg.

Proof. Let $u_1 \in L_p^{n_1}[a_1,\infty)$ and $u_2 \in L_p^{n_2}[a_2,\infty)$. From Schwarz inequality, (3.49) implies that

$$\sum_{i=1}^{n_2} \gamma_{1i}^y \gamma_{2i}^u \leq \sqrt{\sum_{i=1}^{n_2} \left(\gamma_{1i}^y\right)^2} \sqrt{\sum_{i=1}^{n_2} \left(\gamma_{2i}^u\right)^2} < 1 \tag{3.50}$$

$$\sum_{i=1}^{n_1} \gamma_{1i}^u \gamma_{2i}^y \leq \sqrt{\sum_{i=1}^{n_1} \left(\gamma_{2i}^y\right)^2} \sqrt{\sum_{i=1}^{n_1} \left(\gamma_{1i}^u\right)^2} < 1 \tag{3.51}$$

Let y_{ki} denote the i^{th} element of y_k ($k = 1, 2$, $i = 1, \ldots, n_{\bar{k}}$). Then, from Figure 3.2

$$\begin{aligned} y_{11} &= v_{11} - G_{11}^y G_{21}^u y_{11} - \ldots - G_{11}^y G_{2n_2}^u y_{1n_2} \\ &\vdots \\ y_{1n_2} &= v_{1n_2} - G_{1n_2}^y G_{21}^u y_{11} - \ldots - G_{1n_2}^y G_{2n_2}^u y_{1n_2} \end{aligned} \tag{3.52}$$

where v_{1i} is the i^{th} element of $v_1 := G_1 u_1 - G_1 G_2 u_2$. Note that, since $u_1 \in L_p^{n_1}[a_1,\infty)$, $u_2 \in L_p^{n_2}[a_2,\infty)$, and both G_1 and G_2 are L_p-sfg, $v_1 \in L_p^{n_2}[a_2,\infty)$. Also note that, $G_{1n_2}^y G_{2n_2}^u$ is the $n_2{}^{\text{th}}$ diagonal element of Γ_1. Therefore, the maximum time-advance in $G_{1n_2}^y G_{2n_2}^u$ is bounded by $\bar{\delta}_{n_2}^y - h_{n_2}^y \leq 0$, which means that $G_{1n_2}^y G_{2n_2}^u$ is causal. Furthermore, by (3.50), its gain is $\gamma_{1n_2}^y \gamma_{2n_2}^u < 1$. Therefore, from the last expression in (3.52), we obtain

$$y_{1n_2} = \left(1 + G_{1n_2}^y G_{2n_2}^u\right)^{-1} \left[v_{1n_2} - G_{1n_2}^y G_{21}^u y_{11} - \ldots - G_{1n_2}^y G_{2(n_2-1)}^u y_{1(n_2-1)}\right] \tag{3.53}$$

where $\left(1 + G_{1n_2}^y G_{2n_2}^u\right)^{-1}$ is causal and an upper bound on its gain is $\frac{1}{1-\gamma_{1n_2}^y \gamma_{2n_2}^u}$. By substituting (3.53) into the $(n_2-1)^{\text{st}}$ expression in (3.52), we obtain

$$\begin{aligned} y_{1(n_2-1)} \;=\; & v_{1(n_2-1)} - G_{1(n_2-1)}^y G_{2n_2}^u \left(1 + G_{1n_2}^y G_{2n_2}^u\right)^{-1} v_{1n_2} - \tilde{G}_1 y_{11} \\ & - \ldots - \tilde{G}_{n_2-1} y_{1(n_2-1)} \,, \end{aligned} \tag{3.54}$$

where $\tilde{G}_i := G_{1(n_2-1)}^y G_{2i}^u - G_{1(n_2-1)}^y G_{2n_2}^u \left(1 + G_{1n_2}^y G_{2n_2}^u\right)^{-1} G_{1n_2}^y G_{2i}^u$, for $i = 1, \ldots, n_2-1$. Consider $\tilde{G}_{n_2-1}$. Note that $G_{1(n_2-1)}^y G_{2(n_2-1)}^u$ is the $(n_2-1)^{\text{st}}$ diagonal element of Γ_1, and hence (by the same argument given above for the $n_2{}^{\text{th}}$ diagonal element) is causal. Furthermore, $G_{1(n_2-1)}^y G_{2n_2}^u$ and $G_{1n_2}^y G_{2(n_2-1)}^u$ are respectively the maps from the $n_2{}^{\text{th}}$ input to the $(n_2-1)^{\text{st}}$ output and from $(n_2-1)^{\text{st}}$ input to the $n_2{}^{\text{th}}$ output of Γ_1. Therefore, since $\left(1 + G_{1n_2}^y G_{2n_2}^u\right)^{-1}$ is causal,

the maximum time-advance in $G^y_{1(n_2-1)}G^u_{2n_2}\left(1+G^y_{1n_2}G^u_{2n_2}\right)^{-1}G^y_{1n_2}G^u_{2(n_2-1)}$ is bounded by $\bar{\delta}^y_{n_2-1}-h^y_{n_2}+\bar{\delta}^y_{n_2}-h^y_{n_2-1}\leq 0$. Consequently, $\tilde{G}_{n_2-1}$ is causal. Furthermore, its gain is bounded by

$$\gamma^y_{1(n_2-1)}\gamma^u_{2(n_2-1)}+\frac{\gamma^y_{1(n_2-1)}\gamma^u_{2n_2}\gamma^y_{1n_2}\gamma^u_{2(n_2-1)}}{1-\gamma^y_{1n_2}\gamma^u_{2n_2}}=\frac{\gamma^y_{1(n_2-1)}\gamma^u_{2(n_2-1)}}{1-\gamma^y_{1n_2}\gamma^u_{2n_2}}<1\ ,$$

where the last inequality follows from the fact that, by (3.50),

$$\gamma^y_{1(n_2-1)}\gamma^u_{2(n_2-1)}+\gamma^y_{1n_2}\gamma^u_{2n_2}<1.$$

This implies that $y_{1(n_2-1)}$ can be solved from (3.54). Then, it can be substituted into the third equation from the bottom in (3.52). Continuing in this way, it is arrived at

$$y_{11}=\bar{G}v_1-\tilde{G}y_{11}\ , \tag{3.55}$$

where $\tilde{G}$ is causal and has gain less than 1. Therefore, $y_{11}=\left(1+\tilde{G}\right)^{-1}\bar{G}v_1$, where $\left(1+\tilde{G}\right)^{-1}\bar{G}$ is L_p-sfg. Furthermore, since the map from $u=\begin{bmatrix}u_1\\u_2\end{bmatrix}$ to v_1 is also L_p-sfg, this implies that the map from u to y_{11} is L_p-sfg. By changing the order of substitutions above, it can also be shown that the maps from u to y_{1i}, $i=2,\ldots,n_2$, are also L_p-sfg. Consequently, the map from u to $y_1=\begin{bmatrix}y_{11}&\cdots&y_{1n_2}\end{bmatrix}^T$ is L_p-sfg. Similarly, it can be shown that, the map from u to $y_2=\begin{bmatrix}y_{21}&\cdots&y_{2n_1}\end{bmatrix}^T$ is L_p-sfg. This implies that the map from u to $y=\begin{bmatrix}y_1\\y_2\end{bmatrix}$ is L_p-sfg. □

Now, utilizing the strong small-gain condition, an optimal $\mathcal{H}^\infty$ controller can be designed to stabilize the actual plant Ω against all uncertain time-varying time-delays. For example, let us consider the controller design for the feedback system depicted in Figure 3.8. Let $\hat{\gamma}^u_{1i}$ be the upper bound on γ^u_{1i}, for $i=1,\ldots,n_1$ and $\hat{\gamma}^y_{1i}$ be the upper bound on γ^y_{1i}, where $i=1,\ldots,n_2$, where γ^y_{1i} and γ^u_{1i} are defined as in Theorem 3.3. Both $\hat{\gamma}^u_{1i}$ and $\hat{\gamma}^y_{1i}$ can be calculated from the uncertainty representations. Furthermore, note that, $\gamma^y_{2i}\leq\gamma_2$, $i=1,\ldots,n_1$, and $\gamma^u_{2i}\leq\gamma_2$, $i=1,\ldots,n_2$, where γ_2 is the $\mathcal{H}^\infty$ norm of the

closed-loop TFM from w to z in Figure 3.8. Therefore, the designed controller, K, which stabilizes the nominal system in Figure 3.8 for $\Delta^l = 0$ also robustly stabilizes the actual plant, if K is chosen such that γ_2 satisfies

$$\gamma_2 < \frac{1}{\max\left\{\sqrt{n_2 \sum_{i=1}^{n_2} (\hat{\gamma}_{1i}^y)^2}, \sqrt{n_1 \sum_{i=1}^{n_1} (\hat{\gamma}_{1i}^u)^2}\right\}}.$$

A similar approach can also be taken for the system shown in Figure 3.9.

3.5 Removing Non-Causal Uncertainty Blocks in Robust Controller Design Setup

In this section, we discuss how to replace the non-causal uncertainty blocks, which appear as shown in the previous section, by causal blocks in the robust controller design setup. This approach gives an alternative way to directly using non-causal blocks.

The mapping from $\bar{u}$ to p in Figure 3.5 is $\Delta_u W_u$ (see Subsection 3.4.1), where $\Delta_u = \text{bdiag}(\Delta_1^u, \ldots, \Delta_{n_u}^u)$, where $\Delta_i^u = \begin{bmatrix} 1 & \Delta_{i,1}^u & \Delta_{i,2}^u \end{bmatrix}$ is non-causal for all $i = 1, \ldots, n_u$. In this mapping, $W_u = \text{bdiag}(w_1^u, \ldots, w_{n_u}^u)$, where $w_i^u(s) = \begin{bmatrix} \frac{1 - a_i^u b_i^u}{a_i^u s + 1} & -\frac{s(1 - a_i^u b_i^u)}{a_i^u s + 1} & a_i^u \frac{s + b_i^u}{a_i^u s + 1} \end{bmatrix}^T$ $(i = 1, \ldots, n_u)$. Utilizing the structure of Δ_i^u and w_i^u, the mapping from the i^{th} element of $\bar{u}$ to the i^{th} element of p, can be expressed as $\widehat{w}_i^u + \overline{\Delta}_i^u \overline{w}_i^u$, where

$$\widehat{w}_i^u := \frac{1 - a_i^u b_i^u}{a_i^u s + 1}$$

$$\overline{\Delta}_i^u := \begin{bmatrix} \Delta_{i,1}^u & \Delta_{i,2}^u \end{bmatrix}$$

$$\overline{w}_i^u(s) = \begin{bmatrix} -\frac{s(1 - a_i^u b_i^u)}{a_i^u s + 1} & a_i^u \frac{s + b_i^u}{a_i^u s + 1} \end{bmatrix}^T,$$

for $i = 1, \ldots, n_u$. Now, let us define $\overline{\Delta}_u := \text{bdiag}\left(\overline{\Delta}_1^u, \cdots, \overline{\Delta}_{n_u}^u\right)$, $\overline{W}_u := \text{bdiag}\left(\overline{w}_1^u, \cdots, \overline{w}_{n_u}^u\right)$, and $\widehat{W}_u := \text{diag}\left(\widehat{w}_1^u, \ldots, \widehat{w}_{n_u}^u\right)$, then the mapping from $\bar{u}$ to p is $\overline{\Delta}_u \overline{W}_u + \widehat{W}_u$.

Similarly, let us consider the mapping from q to $\bar{y}$ in Figure 3.5, which is $W_y\Delta_y$ (see Subsection 3.4.1). In the mapping, $W_y = \text{bdiag}(w_1^y, \ldots, w_{n_y}^y)$, where $w_j^y(s) = \begin{bmatrix} \frac{1-a_j^y b_j^y}{a_j^y s+1} & \frac{1-a_j^y b_j^y}{a_j^y s+1} & -\frac{s(1-a_j^y b_j^y)}{a_j^y s+1} & a_j^y \frac{s+b_j^y}{a_j^y s+1} \end{bmatrix}$, and $\Delta_y = \text{bdiag}(\Delta_1^y, \ldots, \Delta_{n_y}^y)$, where $\Delta_j^y = \begin{bmatrix} 1 & \Delta_{j,1}^y & \Delta_{j,2}^y & \Delta_{j,3}^y \end{bmatrix}^T$ is non-causal for all $j = 1, \ldots, n_y$. Using the structure of Δ_y and W_y, the mapping from the j^{th} element of q to the j^{th} element of $\bar{y}$ can be obtained as $\overline{w}_j^y \overline{\Delta}_j^y + \widehat{w}_j^y$, where

$$\overline{\Delta}_j^y := \begin{bmatrix} \Delta_{j,1}^y & \Delta_{j,2}^y & \Delta_{j,3}^y \end{bmatrix}^T$$

$$\overline{w}_j^y(s) := \begin{bmatrix} \frac{(1-a_j^y b_j^y)}{a_j^y s+1} & -\frac{s(1-a_j^y b_j^y)}{a_j^y s+1} & a_j^y \frac{s+b_j^y}{a_j^y s+1} \end{bmatrix}$$

and

$$\widehat{w}_j^y := \frac{1-a_j^y b_j^y}{a_j^y s+1},$$

for $j = 1, \ldots, n_y$. Now, let us define $\overline{\Delta}_y := \text{bdiag}\left(\overline{\Delta}_1^y, \ldots, \overline{\Delta}_{n_y}^y\right)$, $\overline{W}_y := \text{bdiag}\left(\overline{w}_1^y, \ldots, \overline{w}_{n_y}^y\right)$ and $\widehat{W}_y := \text{diag}\left(\widehat{w}_1^y, \ldots, \widehat{w}_{n_y}^y\right)$. Then, the mapping from q to $\bar{y}$ can be written as $\widehat{W}_y + \overline{W}_y\overline{\Delta}_y$.

Therefore, Π in (3.32), assuming that the finite dimensional part of the plant does not involve any uncertainties, i.e., $P = P^0$, can be written alternatively as below;

$$\Pi = (\overline{W}_y\overline{\Delta}_y + \widehat{W}_y)P^0(\overline{\Delta}_u\overline{W}_u + \widehat{W}_u). \tag{3.56}$$

The feedback configuration for the actual plant Ω can be depicted as in Figure 3.10. In this configuration, $\Lambda_u(s) = \text{diag}(e^{-h_1^u s}, \cdots, e^{-h_{n_u}^u s})$ and $\Lambda_y(s) = \text{diag}(e^{-h_1^y s}, \cdots, e^{-h_{n_y}^y s})$. To design a robust stabilizing controller for the actual plant Ω by the approach of [13], the feedback configuration depicted in Figure 3.10 can be represented as in the generalized framework (Figure 3.4), where $z = \begin{bmatrix} z_1 \\ z_2 \end{bmatrix}$, $w = \begin{bmatrix} w_1 \\ w_2 \end{bmatrix}$,

$$\Delta = \begin{bmatrix} \Delta_u & 0 \\ 0 & \Delta_y \end{bmatrix}, \tag{3.57}$$

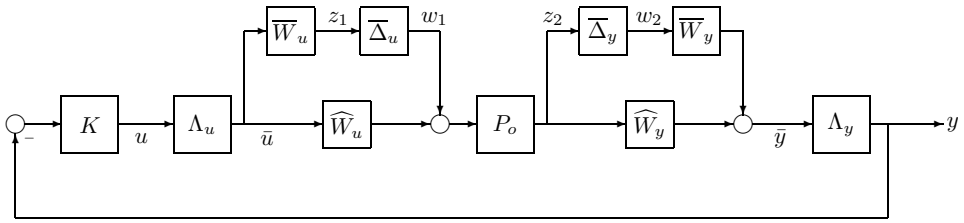

Figure 3.10: Feedback configuration for the actual plant Ω

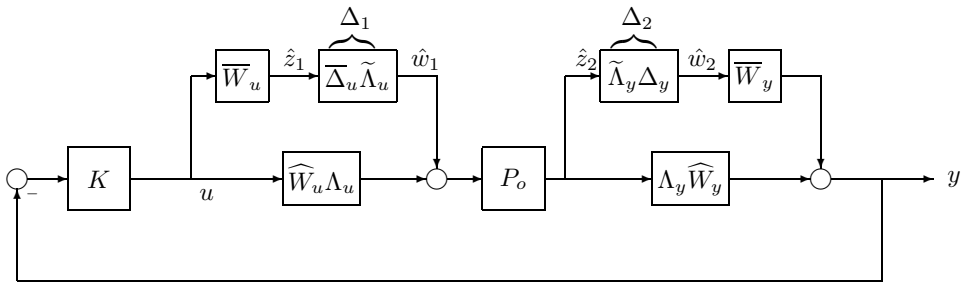

Figure 3.11: Equivalent system

which is non-causal, and

$$G = \begin{bmatrix} 0 & 0 & \overline{W}_u \\ P^0 & 0 & P^0\widehat{W}_u \\ \widehat{W}_y P^0 & \overline{W}_y & \widehat{W}_y P^0 \widehat{W}^u \end{bmatrix}. \tag{3.58}$$

Now, by using algebraic manipulations, an equivalent of the feedback system in Figure 3.10 can be obtained as depicted in Figure 3.11. Here, $\widetilde{\Lambda}_u(s) = \text{bdiag}(e^{-h_1^u s}I_2, \ldots, e^{-h_{n_u}^u s}I_2)$ and $\widetilde{\Lambda}_y(s) = \text{bdiag}(e^{-h_y^u s}I_3, \ldots, e^{-h_{n_y}^y s}I_3)$. In this case $\Delta_1 := \overline{\Delta}_u\widetilde{\Lambda}_u$ and $\Delta_2 := \widetilde{\Lambda}_y\overline{\Delta}_y$ are causal. The input-output relation of the feedback configuration in Figure 3.11 can be expressed as follows:

$$\begin{bmatrix} \hat{z}_1 \\ \hat{z}_2 \\ \hdashline y \end{bmatrix} = \left[\begin{array}{cc:c} 0 & 0 & \overline{W}_u \\ P^0 & 0 & P^0\widehat{W}_u\Lambda_u \\ \hdashline \Lambda_y\widehat{W}_y P^0 & \overline{W}_y & \Lambda_y\widehat{W}_y P^0\widehat{W}_u\Lambda_u \end{array}\right] \begin{bmatrix} \hat{w}_1 \\ \hat{w}_2 \\ \hdashline u \end{bmatrix} =: G_1 \left[\begin{array}{c} \hat{w}_1 \\ \hat{w}_2 \\ \hdashline u \end{array}\right]. \tag{3.59}$$

In this case, the approach of [13] can not be applied to design an $\mathcal{H}^\infty$-optimal controller for the system G_1, since Λ_u does not appear in the mapping from u to $\hat{z}_1$ and Λ_y does not appear in the mapping from $\hat{w}_2$ to y. That is,

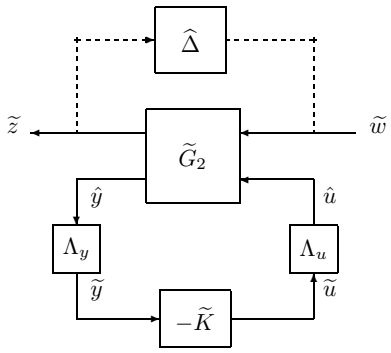

Figure 3.12: Generalized plant for G_2

the delay blocks in (3.59) can not be removed from the generalized plant G_1 to set-up the generalized framework as shown in Figure 2.4.

Now, let us define the augmented plant G_2 instead of G_1 as shown below:

$$G_2 := \begin{bmatrix} 0 & 0 & \overline{W}_u\Lambda_u \\ P^0 & 0 & P^0\widehat{W}_u\Lambda_u \\ \Lambda_y\widehat{W}_yP^0 & \Lambda_y\overline{W}_y & \Lambda_y\widehat{W}_yP^0\widehat{W}_u\Lambda_u \end{bmatrix},$$

where,

$$\begin{bmatrix} \widetilde{z}_1 \\ \widetilde{z}_2 \\ \widetilde{y} \end{bmatrix} := G_2 \begin{bmatrix} \widetilde{w}_1 \\ \widetilde{w}_2 \\ \widetilde{u} \end{bmatrix}. \tag{3.60}$$

Therefore, the generalized $\mathcal{H}^\infty$-framework for G_2 can be set-up as shown in Figure 3.12, where $\widetilde{G}_2 := \begin{bmatrix} 0 & 0 & \overline{W}_u \\ P^0 & 0 & P^0\widehat{W}_u \\ \widehat{W}_yP^0 & \overline{W}_y & \widehat{W}_yP^0\widehat{W}_u \end{bmatrix}$, $\widetilde{z} := \begin{bmatrix} \widetilde{z}_1 \\ \widetilde{z}_2 \end{bmatrix}$, $\widetilde{w} := \begin{bmatrix} \widetilde{w}_1 \\ \widetilde{w}_2 \end{bmatrix}$, and $\widehat{\Delta} = \text{bdiag}(\Delta_1, \Delta_2)$, which is causal. Now, an $\mathcal{H}^\infty$-optimal controller can be designed for the generalized plant $\widetilde{G}_2$ by the approach of [13], where $\widetilde{G}_2$ satisfies the standard $\mathcal{RH}^\infty$ assumptions ((i)–(iv) given in Section 2.2) as long as the actual realization of $\widehat{W}_yP^0\widehat{W}_u$ is stabilizable and detectable.

In the sequel, it will be shown that the designed controller, which

internally stabilizes the nominal system in Figure 3.12 (with $\widehat{\Delta} = 0$) and achieves $\|F_l(\widetilde{G}_2, -\Lambda_u \widetilde{K} \Lambda_y)\|_\infty < 1/\|\widehat{\Delta}\|_2$, also stabilizes the feedback system in Figure 3.11, which is equivalent to the actual system, and achieves that the norm of the closed-loop TFM from $\widehat{w} := \begin{bmatrix} \widehat{w}_1 \\ \widehat{w}_2 \end{bmatrix}$ to $\widehat{z} := \begin{bmatrix} \widehat{z}_1 \\ \widehat{z}_2 \end{bmatrix}$ in Figure 3.11 is less than $\dfrac{1}{\|\Delta\|_2}$.

Let us assume that the designed controller $\widetilde{K}$ internally stabilizes the system in Figure 3.12 and achieves that $\|F_l(\widetilde{G}_2, -\Lambda_u \widetilde{K} \Lambda_y)\|_\infty < 1/\|\widehat{\Delta}\|_2$. In Figure 3.12, $\widehat{\Delta}$ is causal and has the same L_2-induced norm with the non-causal uncertainty block Δ given in (3.57) since

$$\begin{aligned}
\|\widehat{\Delta}\|_2 &= \left\| \begin{bmatrix} \Delta_u \Lambda_u & 0 \\ 0 & \Lambda_y \Delta_y \end{bmatrix} \right\|_2 = \left\| \begin{bmatrix} I & 0 \\ 0 & \Lambda_y \end{bmatrix} \begin{bmatrix} \Delta_u & 0 \\ 0 & \Delta_y \end{bmatrix} \begin{bmatrix} \Lambda_u & 0 \\ 0 & I \end{bmatrix} \right\|_2 \\
&= \left\| \begin{bmatrix} \Delta_u & 0 \\ 0 & \Delta_y \end{bmatrix} \right\|_2 = \|\Delta\|_2.
\end{aligned}$$

From Figure 3.12 and (3.60),

$$\widetilde{y} = (I + \Lambda_y \widehat{W}_y P^0 \widehat{W}_u \Lambda_u \widetilde{K})^{-1} \begin{bmatrix} \Lambda_y \widehat{W}_y P^0 & \Lambda_y \overline{W}_y \end{bmatrix} \widetilde{w}.$$

Therefore,

$$\begin{aligned}
\widetilde{z} &= \begin{bmatrix} 0 & 0 \\ P^0 & 0 \end{bmatrix} \widetilde{w} + \begin{bmatrix} \overline{W}_u \Lambda_u \\ P^0 \widehat{W}_u \Lambda_u \end{bmatrix} \widetilde{u} \\
&= \begin{bmatrix} 0 & 0 \\ P^0 & 0 \end{bmatrix} \widetilde{w} - \begin{bmatrix} \overline{W}_u \Lambda_u \\ P^0 \widehat{W}_u \Lambda_u \end{bmatrix} \widetilde{K} \widetilde{y} \\
&= \begin{bmatrix} 0 & 0 \\ P^0 & 0 \end{bmatrix} \widetilde{w} - \left(\begin{bmatrix} \overline{W}_u \Lambda_u \\ P^0 \widehat{W}_u \Lambda_u \end{bmatrix} \widetilde{K} \right. \\
&\qquad \left. (I + \Lambda_y \widehat{W}_y P^0 \widehat{W}_u \Lambda_u \widetilde{K})^{-1} \begin{bmatrix} \Lambda_y \widehat{W}_y P^0 & \Lambda_y \overline{W}_y \end{bmatrix} \right) \widetilde{w} \\
&= F_l(\widetilde{G}_2, -\Lambda_u \widetilde{K} \Lambda_y) \widetilde{w}.
\end{aligned}$$

Let us define $S := (I + \Lambda_y \widehat{W}_y P^0 \widehat{W}_u \Lambda_u \widetilde{K})^{-1}$, then

$$F_l(\widetilde{G}_2, -\Lambda_u \widetilde{K} \Lambda_y) = \begin{bmatrix} -\overline{W}_u \Lambda_u \widetilde{K} S \Lambda_y \widehat{W}_y P^0 & -\overline{W}_u \Lambda_u \widetilde{K} S \Lambda_y \overline{W}_y \\ P^0 (I - \widehat{W}_u \Lambda_u \widetilde{K} S \Lambda_y \widehat{W}_y P^0) & -P^0 \widehat{W}_u \Lambda_u \widetilde{K} S \Lambda_y \overline{W}_y \end{bmatrix}. \quad (3.61)$$

Now, to show that the designed stabilizing controller $\widetilde{K}$ also stabilizes the actual system, or its equivalent depicted in Figure 3.11, let us replace K in Figure 3.11 with $\widetilde{K}$. Then,

$$\begin{aligned}
\hat{z}_1 &= \overline{W}_u u && (3.62)\\
\hat{z}_2 &= P^0 w_1 + P^0 \widehat{W}_u \Lambda_u u && (3.63)\\
y &= \Lambda_y \widehat{W}_y P^0 \hat{w}_1 + \overline{W}_y \hat{w}_2 + \Lambda_y \widehat{W}_y P^0 \widehat{W}_u \Lambda_u u \ ,
\end{aligned}$$

where $u = -\widetilde{K} y$. Therefore,

$$\begin{aligned}
y &= (I + \Lambda_y \widehat{W}_y P^0 \widehat{W}_u \Lambda_u \widetilde{K})^{-1} \left[\begin{array}{cc} \Lambda_y \widehat{W}_y P^0 & W_y \end{array} \right] \hat{w} && (3.64)\\
u &= -\widetilde{K}(I + \Lambda_y \widehat{W}_y P^0 \widehat{W}_u \Lambda_u \widetilde{K})^{-1} \left[\begin{array}{cc} \Lambda_y \widehat{W}_y P^0 & \overline{W}_y \end{array} \right] \hat{w}.
\end{aligned}$$

Using (3.62)–(3.64), the closed-loop TFM from $\widehat{w}$ to $\widehat{z}$ in Figure 3.11 can be obtained as:

$$\begin{aligned}
\hat{z} &= \left[\begin{array}{cc} 0 & 0 \\ P^0 & 0 \end{array} \right] \hat{w} - \left[\begin{array}{c} \overline{W}_u \\ P^0 \widehat{W}_u \end{array} \right] \Lambda_u \widetilde{K} \Lambda_y \bar{y} \\
&= \left[\begin{array}{cc} 0 & 0 \\ P^0 & 0 \end{array} \right] \hat{w} - \left(\left[\begin{array}{c} \overline{W}_u \\ P^0 \widehat{W}_u \end{array} \right] \Lambda_u \widetilde{K} \Lambda_y \right. \\
&\qquad \left. (I + \widehat{W}_y P^0 \widehat{W}_u \Lambda_u \widetilde{K} \Lambda_y)^{-1} \left[\begin{array}{cc} \widehat{W}_y P^0 & \overline{W}_y \end{array} \right] \right) \hat{w} \\
&= \left[\begin{array}{cc} -\overline{W}_u \widetilde{K} S \Lambda_y \widehat{W}_y P^0 & -\overline{W}_u \widetilde{K} S \widehat{W}_y \\ P^0 - P^0 \overline{W}_u \Lambda_u \widetilde{K} S \Lambda_y \widehat{W}_y P^0 & -P^0 \overline{W}_u \Lambda_u \widetilde{K} S \widehat{W}_y \end{array} \right] \hat{w} \\
&=: T_{zw} \hat{w} && (3.65)
\end{aligned}$$

From (3.61) and (3.65),

$$F_l(G_2, \Lambda_u \widetilde{K} \Lambda_y) = \left[\begin{array}{cc} \widetilde{\Lambda}_u & 0 \\ 0 & I \end{array} \right] T_{zw} \left[\begin{array}{cc} I & 0 \\ 0 & \widetilde{\Lambda}_y \end{array} \right], \qquad (3.66)$$

where $\widetilde{\Lambda}_u \overline{W}_u = \overline{W}_u \Lambda_u$ and $\overline{W}_y \widetilde{\Lambda}_y = \Lambda_y \overline{W}_y$. Therefore, $F_l(\widetilde{G}_2, -\Lambda_u \widetilde{K} \Lambda_y)$ is stable if and only if T_{zw} in (3.65) is stable [56]. In addition, since $\widetilde{\Lambda}_u$ and $\widetilde{\Lambda}_y$ are inner functions, $\|F_l(\widetilde{G}_2, \Lambda_u \widetilde{K} \Lambda_y)\|_\infty = \|T_{zw}\|_\infty$.

As a summary, in this section, to avoid utilization of non-causal uncertainty blocks in the robust controller design, an equivalent problem with

causal blocks is solved by using algebraic manipulations. As shown above, the designed controller which stabilizes the augmented plant also stabilizes the equivalent of the actual plant. In addition, the closed-loop $\mathcal{H}^\infty$ norm constraints are also satisfied.

3.6 Summary

In this chapter, the sufficient conditions to satisfy the validity of the small-gain theorem for interconnected subsystems, at least one of which is non-causal, were given. Using these results, non-causal uncertainty blocks can be used in the $\mathcal{H}^\infty$ controller design for systems with multiple time-delays

It was shown that, even though all the physical systems are causal, the uncertainty representation of the multiple-time-delay systems in the robust controller design set-up may be non-causal. To show the appearance of non-causal uncertainty blocks in the robust controller design, an uncertainty model for systems with multiple uncertain time-delays was derived. However, it should be noted that the uncertainty structure of the systems with multiple time-delays derived in Subsection 3.4.1, is not unique. Different structures may be obtained using different manipulations. As shown in Subsection 3.4.6, the presented sufficient conditions in Sections 3.2 and 3.3 to satisfy the validity of the small-gain theorem may not be satisfied in general. To overcome this situation, the strong small-gain condition was defined which allows the use of non-causal uncertainty blocks to represent the uncertainties in the time-delays and design robust controllers for multiple-time-delay systems. Hence, to design an $\mathcal{H}^\infty$-optimal controller using the approach of [13] for a multiple-time-delay system, where its finite dimensional part is subject to uncertainties, it is sufficient to show that the designed controller, which stabilizes the nominal system, makes the $\mathcal{H}^\infty$ norm of the resulting closed-loop TFM in Figure 3.4 such that the strong small-gain conditions for $p = 2$ are satisfied.

In Section 3.5, an alternative approach was presented in the robust

controller design by replacing non-causal uncertainty blocks with the causal ones. To achieve this, an equivalent problem, which had causal uncertainty blocks, to the actual problem, which had non-causal uncertainty blocks, was defined by using algebraic manipulations. Then, to design a robust stabilizing controller by the approach of [13] for the equivalent problem, an augmented problem was defined. As a result, by [56], it was shown that the designed stabilizing controller for the augmented plant also stabilizes the actual plant. Furthermore, it satisfies the closed-loop $\mathcal{H}^\infty$ norm constraint.

4 ROBUST FLOW CONTROLLER DESIGN

An arising problem in today's data-communication networks is traffic congestion. Congestion occurs at a node of the network when the sources send data packets to that node at a rate more than the capacity of the outgoing link. In this case, this node is called a bottleneck node. If congestion occurs at the bottleneck node of the network, long queueing delays and overflow of buffer can happen which result in loss of data. To overcome these problems, rate of data packets sent from the sources to the bottleneck node should be controlled.

One of the available mechanisms to control the rate of data that is sent from the sources to the bottleneck node to avoid congestion occurrence is flow control. In general, there are two flow control methods: rate-based [57–59] and window-based [60, 61]. Although window-based control is widely used for end to end congestion control in TCP/IP networks, rate-based control is preferred for edge to edge control in newer generation networks [62, 63].

In the rate-based flow control method, the controller is implemented at the bottleneck node and calculates a rate command for each source to adjust the rate of data that is sent from the sources to the bottleneck node in order to regulate the queue length for congestion avoidance. The challenge in the flow controller design is the existence of uncertain time-varying time-delays. Both the control signal issued by the flow controller to adjust the rate of data packets that will be sent from the sources and the data packets that will be sent from sources to the bottleneck node are subject to these delays. Moreover, in general, existence of more than one source feeding a bottleneck results in multiple time-delays. To design a flow controller to achieve congestion avoidance despite the presence of uncertain time-varying time-delays, one of the robust control tools, $\mathcal{H}^\infty$ control can be used.

In this chapter, an optimal $\mathcal{H}^\infty$ flow controller design for data-communication networks with multiple uncertain time-delays is given. In Section 4.1,

the derivation of the mathematical model of the network is given. In Section 4.2, the flow control problem is defined. The optimal $\mathcal{H}^\infty$ flow controller design is given in Section 4.3. To illustrate the performance of the controller designed by the approach proposed in Section 4.3, simulation studies are given in Section 4.4. In Section 4.5, the performance and stability margins of the designed flow controller are examined. In Section 4.6, the benefits of utilizing non-causal uncertainty blocks compared to causal ones are presented. In Section 4.7, sufficient conditions are derived to choose the free parameter of the controller to meet one of the time-domain constraints. In the last section, a summary of the results is presented.

4.1 Network Model

In this section, the flow control problem in a data-communication network with n sources feeding a single bottleneck node is considered. For the model of the network, we will use a continuous flow model, which is called the *fluid-flow* model. The network model presented in this section and the control problem defined in the next section, as well as its solution given in Section 4.3, have been published in [43].

The dynamics of the queue length are given as [23]:

$$\dot{q}(t) = \sum_{i=1}^{n} r_i^b(t) - c(t) \tag{4.1}$$

where,

$q(t)$ is the queue length at the bottleneck node at time t,

$r_i^b(t)$ is the rate of data received by the bottleneck node at time t from the i^{th} source, $i = 1, \ldots, n$,

$c(t)$ is the outgoing rate of data from the bottleneck node at time t, which equals to the capacity of the outgoing link when $q(t)$ is positive. When $q(t) = 0$, $c(t)$ is the outgoing link capacity if $\sum_{i=1}^{n} r_i^b(t)$ is greater than or equal to the outgoing link capacity, otherwise, $c(t) = \sum_{i=1}^{n} r_i^b(t)$.

The total amount of data received at the bottleneck node from the i^{th} source, $i = 1, \ldots, n$, by time t is given as [23]:

$$\int_0^t r_i^b(\varphi)d\varphi = \begin{cases} \int_0^{t-\tau_i^f(t)} r_i^s(\varphi)d\varphi\,, & t-\tau_i^f(t) \geq 0 \\ 0\,, & t-\tau_i^f(t) < 0 \end{cases}, \tag{4.2}$$

where

$r_i^s(t)$ is the rate of data sent from the i^{th} source at time t.

Let us define

$r_i^c(t) := r_i(t - \tau_i^b(t))$ as the rate command received by the i^{th} source at time t, where

$r_i(t)$ is the rate command for the i^{th} source issued by the controller, which is to be implemented at the bottleneck node, at time t.

By taking the derivative of both sides of (4.2) and using $r_i^s(t) = r_i^c(t) = r_i(t-\tau_i^b(t))$, the rate of data received by the bottleneck node, $r_i^b(t)$, is given in terms of the rate command issued by the controller at time t, $r_i(t)$, as follows:

$$r_i^b(t) = \begin{cases} (1-\dot{\delta}_i^f(t))r_i(t-\tau_i(t)), & t-\tau_i^f(t) \geq 0 \\ 0, & t-\tau_i^f(t) < 0 \end{cases}. \tag{4.3}$$

Here, $\tau_i(t) = \tau_i^b(t) + \tau_i^f(t)$ is the round-trip time-delay, where

$\tau_i^b(t) = h_i^b + \delta_i^b(t)$ is the backward time-delay at time t, which is the time required for the rate command to reach the i^{th} source. Here, h_i^b is the nominal time-invariant known backward time-delay, and $\delta_i^b(t)$ is the time-varying backward time-delay uncertainty,

$\tau_i^f(t) = h_i^f + \delta_i^f(t)$ is the forward time-delay at time t, which is the time required for the data sent from the i^{th} source to reach the bottleneck node. Here, h_i^f is the nominal time-invariant known forward time-delay, and $\delta_i^f(t)$ is the time-varying forward time-delay uncertainty.

The nominal round-trip time-delay for the i^{th} channel of the system is $h_i = h_i^b + h_i^f$, and the time-varying round-trip time-delay uncertainty is $\delta_i(t) = \delta_i^b(t) + \delta_i^f(t)$. It is assumed that the uncertainties are bounded as follows:

$$|\delta_i(t)| < \delta_i^+, \quad |\dot{\delta}_i(t)| < \beta_i, \quad |\dot{\delta}_i{}^f(t)| < \beta_i^f \tag{4.4}$$

for some bounds $\delta_i^+ > 0$ and $0 < \beta_i^f \leq \beta_i < 1$. It is further assumed that, $\delta_i(t)$ is such that $\tau_i(t) \geq 0$ at all times. In a real application, there also exist some *hard constraints*, such as non-negativity constraints and upper bounds on the queue length and data rates. In this work, we assume that these constraints are always satisfied for the purpose of controller design.

Remark 4.1. The term $\dot{\delta}_i^f$ in (4.3) arises from differentiation of (4.2). It is the *jitter* effect and a characteristic of networks with a time-varying delay.

4.2 Control Problem

In any defined control problem, firstly, the design requirements should be posed. In the flow control problem, the aim is to design a controller, for the above described system, to regulate the queue length $q(t)$ at the bottleneck node against the presence of uncertain time-varying time-delays. Hence, the controller to be designed should robustly stabilize the system against all existing time-varying uncertainties in the time-delays which satisfy (4.4). Besides robustness, assuming that $\lim_{t\to\infty} c(t) = c_\infty$ exists, the controller should also achieve the *tracking* requirement:

$$\lim_{t\to\infty} q(t) = q_d \ , \tag{4.5}$$

and the *weighted fairness* [23] requirement:

$$\lim_{t\to\infty} r_i(t) = \alpha_i c_\infty \ , \qquad i = 1, \ldots, n \ . \tag{4.6}$$

Here, q_d is the *desired queue length* and $\alpha_i > 0$, $i = 1, \ldots, n$, are the fairness weights [23], which satisfy $\sum_{i=1}^n \alpha_i = 1$.

To state the robust flow control problem, let us consider the mathematical model of the plant to be controlled. The uncertainty part of the plant can be modelled as follows. From (4.1) and (4.3), $q(t)$ can be written as:

$$q(t) = \int_0^t \left[\sum_{i=1}^{n} (1 - \dot{\delta}_i^f(\nu)) r_i(\nu - \tau_i(\nu)) - c(\nu) \right] d\nu \ + q(0) \ . \tag{4.7}$$

Let us define the *nominal queue length* as:

$$q_0(t) := \int_0^t \left[\sum_{i=1}^{n} r_i(\nu - h_i) - c(\nu) \right] d\nu \ + q(0) \ . \tag{4.8}$$

Therefore, the *uncertainty in the queue length* can be defined as $\delta_q(t) := q(t) - q_0(t)$. Then,

$$\begin{aligned} \delta_q(t) &= \sum_{i=1}^{n} \int_0^t \Big[(1 - \dot{\delta}_i^f(\nu)) r_i(\nu - \tau_i(\nu)) - r_i(\nu - h_i) \Big] \, d\nu \\ &= \sum_{i=1}^{n} \int_0^t \Big[(1 - \dot{\delta}_i^f(\nu)) r_i^h(\nu - \delta_i(\nu)) - r_i^h(\nu) \Big] \, d\nu \ , \end{aligned} \tag{4.9}$$

where $r_i^h(t) := r_i(t - h_i)$.

Similar to Section 3.4, let us define $\lambda_i := \nu - \delta_i(\nu) =: f_i(\nu)$. Then

$$\frac{d\lambda_i}{d\nu} = 1 - \frac{d\delta_i}{d\nu} = 1 - g_i(\lambda_i) \tag{4.10}$$

where

$$g_i(\lambda) := \left. \frac{d\delta_i}{d\nu} \right|_{\nu = f_i^{-1}(\lambda)} .$$

Since the uncertain part of the actual time-delay has the property $\dot{\delta}_i(t) < 1$, by (4.10), $\dfrac{df_i(\nu)}{d\nu} > 0$. Thus, $\nu = f_i^{-1}(\lambda)$ exists.

Let us assume that $\delta_i(0) = 0$. From (4.10), $d\nu = \dfrac{d\lambda_i}{1 - g_i(\lambda_i)}$, therefore, the uncertainty in the queue length, (4.9), can be rewritten as:

$$\begin{aligned} \delta_q(t) &= \sum_{i=1}^{n} \left[\int_0^t (1 - \dot{\delta}_i^f(\nu)) r_i^h(\nu - \delta_i(\nu)) \, d\nu - \int_0^t r_i^h(\nu) \, d\nu \right] \\ &= \sum_{i=1}^{n} \left[\int_0^t (1 - \dot{\delta}_i^f(\nu)) r_i^h(\nu - \delta_i(\nu)) \, d\nu - \int_0^t r_i^h(\nu) \, d\nu \right. \\ &\qquad \left. + \int_0^{t - \delta_i(t)} r_i^h(\nu) \, d\nu - \int_0^{t - \delta_i(t)} r_i^h(\lambda_i) \, d\lambda_i \right] \end{aligned}$$

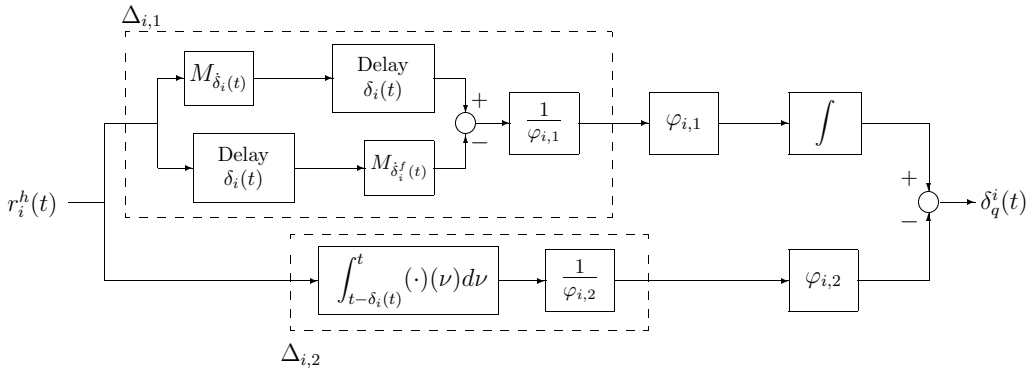

Figure 4.1: Uncertainty model [42]

$$
\begin{aligned}
&= \sum_{i=1}^{n} \left[\int_0^t (1-\dot{\delta}_i^f(\nu)) r_i^h(\nu-\delta_i(\nu))\, d\nu - \int_{t-\delta_i(t)}^{t} r_i^h(\nu)\, d\nu \right. \\
&\qquad \left. - \int_0^t r_i^h(\nu-\delta_i(\nu)) \left[1-g_i(\nu-\delta_i(\nu))\right]\, d\nu \right] \\
&= \sum_{i=1}^{n} \left[\int_0^t \left[g_i(\nu-\delta_i(\nu)) - \dot{\delta}_i^f(\nu) \right] r_i^h(\nu-\delta_i(\nu))\, d\nu \right. \\
&\qquad \left. - \int_{t-\delta_i(t)}^{t} r_i^h(\nu)\, d\nu \right].
\end{aligned}
$$

We now have $\delta_q(t) = \sum_{i=1}^{n} \delta_q^i(t)$, where $\delta_q^i(t)$ is the output of the system shown in Figure 4.1. In Figure 4.1, $\Delta_{i,1}$ and $\Delta_{i,2}$ are possibly non-causal uncertain LTV blocks, since it is assumed that:

$$|\delta_i(t)| < \delta_i^+. \tag{4.11}$$

To find a bound on the uncertainty blocks, let us consider (3.28), which implies that the L_2-induced norms of the delay blocks $\delta_i(t)$ are less than $\dfrac{1}{\sqrt{1-\beta_i}}$. Thus, the L_2-induced norm of $\Delta_{i,1}$ is less than $\left(\frac{\beta_i+\beta_i^f}{\sqrt{1-\beta_i}}\right)\frac{1}{\varphi_{i,1}}$, since we have $|g_i| < \beta_i$ and $|\dot{\delta}_i^f| < \beta_i^f$. Then, defining $\varphi_{i,1} = \sqrt{2}\dfrac{\beta_i+\beta_i^f}{\sqrt{1-\beta_i}}$, the L_2-induced norm of the LTV block $\Delta_{i,1}$ is less than $\frac{1}{\sqrt{2}}$.

To find a bound on the norm of $\Delta_{i,2}$, let us consider the relation in (3.23), which implies that the L_2-induced norm of $\Delta_{i,2}$ is less than or equal $\dfrac{\delta_i^+}{\varphi_{i,2}}$. Thus, choosing $\varphi_{i,2} = \sqrt{2}\delta_i^+$, the L_2-induced norm of $\Delta_{i,2}$ becomes less

than or equal $\frac{1}{\sqrt{2}}$. Then, the L_2-induced norm of $\Delta_i := \begin{bmatrix} \Delta_{i,1} \\ \Delta_{i,2} \end{bmatrix}$ is less than 1.

In Figure 4.1, the uncertainty blocks are non-causal in general. In fact, the delay blocks in Figure 4.1 are time-advance blocks and the integral is a non-causal integral when $\delta_i(t) < 0$. In [40–42] robust flow controllers were designed using the small-gain theorem in [5]. However, the controller design was achieved by assuming that the uncertain part of the time-delays are always non-negative:

$$0 \leq \delta_i(t) < \delta_i^+ \tag{4.12}$$

for some positive bound δ_i^+. By this assumption, the time-delay in the i^{th} channel becomes the minimum possible time-delay, rather than the nominal time-delay. In this case, the optimization problem is defined not for the actual nominal plant, but for the plant with minimum possible time-delays. Furthermore, this also requires taking the bounds δ_i^+ larger, robustness range must be larger which results in conservativeness in the robust controller design. Therefore, assumption (4.12) brings two drawbacks. In order to overcome these drawbacks, bounds (4.11), rather than (4.12) should be used and either the problem can be converted to an equivalent problem without using non-causalities (see Section 3.5) or the problem can directly be considered by using non-causal uncertainty blocks by utilizing Theorem 3.2 to design an $\mathcal{H}^\infty$-optimal flow controller. Here, we will take the latter approach.

To define the overall problem, without loss of generality, let us assume that $h_1 \geq h_2 \geq \ldots > h_n \geq 0$. Let N be the number of distinct h_i's and let us rename the nominal time-delays as $\bar{h}_1 > \bar{h}_2 > \ldots > \bar{h}_N \geq 0$ so that all $\bar{h}_i$'s are distinct. For this, let $\bar{h}_1 = h_1$, $\bar{h}_2 = h_{i_2}$, where i_2 is the smallest index such that $h_{i_2} < h_1$, $\bar{h}_3 = h_{i_3}$, where i_3 is the smallest index such that $h_{i_3} < h_{i_2}$, and so on. Also let l_i $(i = 1, \ldots, N)$ be the number of channels with nominal round trip time-delay $\bar{h}_i$. Then, $\sum_{i=1}^{N} l_i = n$.

Now, we can describe the overall system as shown in Figure 4.2,

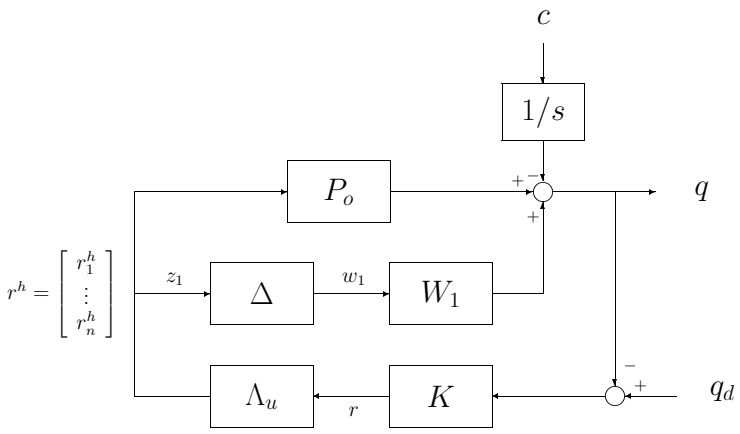

Figure 4.2: Overall system [43]

where $P_o(s) = \frac{1}{s}\mathbf{1}_n$ is the nominal plant, K is the controller to be designed, $\Lambda_u(s) = \text{bdiag}\left(e^{-\bar{h}_1 s} I_{l_1}, \ldots, e^{-\bar{h}_N s} I_{l_N}\right)$ represents the nominal time-delays, which are taken outside the plant in order to apply the approach of [13], $W_1(s) = \left[\overline{W}_1(s) \cdots \overline{W}_n(s)\right]$, where $\overline{W}_i(s) = \left[\frac{\varphi_{i,1}}{s} \;\; \varphi_{i,2}\right]$, and

$$\Delta = \text{bdiag}\left(\begin{bmatrix} \Delta_{1,1} \\ \Delta_{1,2} \end{bmatrix}, \ \ldots \ , \begin{bmatrix} \Delta_{n,1} \\ \Delta_{n,2} \end{bmatrix}\right)$$

represents the uncertainties in the system. By using Theorem 3.2, we can apply the small-gain theorem as long as $\tau_i(t) := h_i + \delta_i(t) \geq 0$, $\forall t \geq 0$, $\forall i$, which is naturally satisfied since round-trip time-delays can not actually be time-advances. By Theorem 3.2, if we choose K to stabilize the system with $\Delta = 0$ and make the L_2-induced norm of the system from w_1 to z_1 in Figure 4.2 less than 1, then the overall system is robustly stable for all uncertainties satisfying (4.4).

To show the utilization of Theorem 3.2 in the robust flow controller design, as it was published in [37], let us define $\tilde{W}_1(s) := \dfrac{s}{s+\epsilon} W_1(s)$, for some $\epsilon > 0$. Then, as it was shown in [37], by suppressing external signals (which do not have any effect on closed-loop stability), the system shown in Figure 4.2 can be represented as in Figure 3.2, where $G_1 = \tilde{W}_1 \Delta$ and $G_2 = \Lambda_u T$, where $T := K\left(1 + P_o \Lambda_u K\right)^{-1} \dfrac{s+\epsilon}{s}$ is the closed-loop TFM from $\tilde{w}_1 := \tilde{W}_1 w_1$ to $-r$.

Now, we can consider the system in Figure 3.2 for G_1 and G_2 defined

above. Since $\tilde{W}_1$ and Δ are stable, (3.3) is satisfied. Furthermore, since K is chosen to stabilize the closed-loop nominal system (system shown in Figure 4.2 with $\Delta = 0$), the transfer function from w_1 to r is stable. Thus, in particular, $-K\left(1 + P_o\Lambda_u K\right)^{-1}\frac{\varphi_{1,1}}{s}$, which is the transfer function from the first entry of w_1 to r and is strictly proper, is stable (the pole at zero is canceled by the pole of P_o). This implies that T is also stable. Therefore, since Λ_u is stable, G_2 is also stable, and hence (3.4) is also satisfied. (3.7) and (3.8) are satisfied since G_1 and G_2 are both linear.

In order to show that (3.5) is satisfied, let us consider the cascade connection of G_1 with G_2. Note that $G_1G_2 = \tilde{W}_1\Delta\Lambda_u T$, where $\Delta\Lambda_u = \text{bdiag}\left(\Delta_1\lambda_1, \ldots, \Delta_n\lambda_n\right)$, where $\lambda_i(s) := e^{-h_i s}$ is the i^{th} diagonal element of $\Lambda_u(s)$. Also note that (see Figure 4.1), the maximum time-advance in Δ_i is $\max_{t\geq 0}\{-\delta_i(t)\}$, which is not greater than h_i, since the actual time-delays can not be time-advance, i.e. $\tau_i(t) := h_i + \delta_i(t) \geq 0$, $\forall t \geq 0$, $\forall i$. Thus, since λ_i is a pure delay of h_i, for $i = 1, \ldots, n$, each element of $\Delta\Lambda_u$, hence $\Delta\Lambda_u$ itself, is causal. Since $\tilde{W}_1$ and T are also causal, this implies that G_1G_2 is causal, and hence (3.5) is satisfied.

To show that (3.11) is satisfied, note that $G_{1i} = \tilde{W}_{i,1}\Delta_{i,1} + \tilde{W}_{i,2}\Delta_{i,2}$, where $\tilde{W}_{i,1}(s) := \frac{\varphi_{i,1}}{s+\epsilon}$ and $\tilde{W}_{i,2}(s) := \frac{s\varphi_{i,2}}{s+\epsilon}$. It was indicated above that the maximum time-advance in $\Delta_{i,1}$ and $\Delta_{i,2}$ is not greater than h_i. Since $\tilde{W}_{i,1}$ and $\tilde{W}_{i,2}$ are causal, the maximum time-advance in G_{1i} is not greater than h_i. On the other hand, $G_{2i} = \lambda_i t_i$, where t_i is the i^{th} element of T, which is causal. Therefore, since λ_i is a pure delay of h_i, $G_{2i}G_{1i}$ is causal for all $i = 1, \ldots, n$, and hence (3.11) is satisfied. Therefore, by Theorem 3.2, the small gain theorem can be applied to our system.

In the above, it is assumed that the controller K is chosen to stabilize the system with $\Delta = 0$ and make the L_2-induced norm of the system from w_1 to z_1 in Figure 4.2 less than 1. However, if K stabilizes the system with $\Delta = 0$ and make the L_2-induced norm of the system from w_1 to z_1 in Figure 4.2 less than some $\gamma > 0$, then the overall system is robustly stable for all Δ with

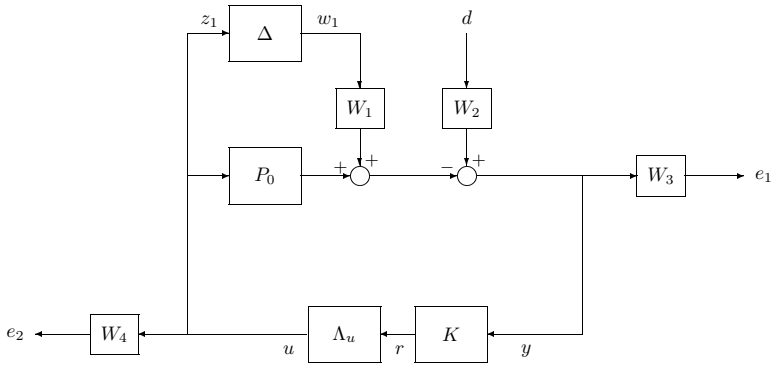

Figure 4.3: System for the mixed sensitivity minimization problem [25]

L_2-induced norm less than $\frac{1}{\gamma}$. The uncertainty block Δ would have L_2-induced norm less than $\frac{1}{\gamma}$ if, for example, $|\delta_i(t)| < \frac{\delta_i^+}{\gamma}$, $|\dot{\delta}_i(t)| < \tilde{\beta}_i$, and $|\dot{\delta}_i{}^f(t)| < \tilde{\beta}_i^f$, $i = 1, \ldots, n$, where $0 < \tilde{\beta}_i^f \leq \tilde{\beta}_i < 1$ are such that $\dfrac{\tilde{\beta}_i + \tilde{\beta}_i^f}{\sqrt{1-\tilde{\beta}_i}} = \dfrac{\beta_i + \beta_i^f}{\gamma\sqrt{1-\beta_i}}$.

4.3 Optimal $\mathcal{H}^\infty$ Controller Design

To solve the control problem defined in the previous section, we consider a mixed sensitivity minimization problem for the system shown in Figure 4.3. Here, $W_2(s) = \frac{1}{s}$, $W_3(s) = \frac{\sigma_1}{s}$, and

$$W_4(s) = \frac{\sigma_2}{s} \begin{bmatrix} \frac{\alpha_2}{\alpha_1} & -1 & 0 & & 0 \\ \frac{\alpha_3}{\alpha_1} & 0 & -1 & & 0 \\ \vdots & \vdots & & \ddots & \vdots \\ \frac{\alpha_n}{\alpha_1} & 0 & 0 & & -1 \end{bmatrix},$$

where $\sigma_1 > 0$ and $\sigma_2 > 0$ are design parameters. Furthermore, $d := \dot{q}_d - c$, e_1 is the integral of the error, $y := q_d - q$, and is introduced to achieve tracking (4.5), and e_2 is introduced to achieve the weighted fairness requirement (4.6).

Here, the weighting matrix W_1, which was introduced in the previous section, is used to normalize the uncertainty block. Weights W_2 and W_3 are introduced to reject disturbances (in the variations of q_d and c) and achieve the tracking requirement (4.5). The weighting matrix W_4 is introduced to achieve the weighted fairness requirement (4.6). Design parameters σ_1 and σ_2, which

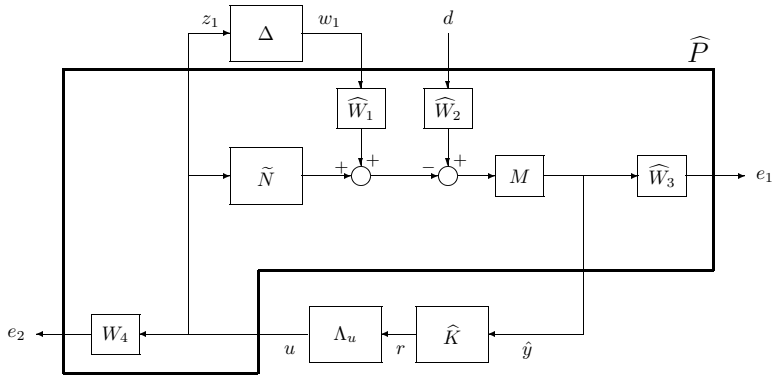

Figure 4.4: Equivalent system for the mixed sensitivity minimization problem [42]

appear respectively in W_3 and W_4, can be used to assign relative importance to tracking and weighted fairness respectively.

Note that, the nominal plant, P_o, has a pole at the origin. Furthermore, the integral terms in the weights W_2, W_3, and W_4 force K to have integral action, [5]. Therefore, the sensitivity function of the closed-loop system in Figure 4.3 has a double zero at the origin, which causes uncontrollable pole-zero cancelations to occur between the weights and the sensitivity. To avoid this problem, we let $P_o(s) = \widetilde{M}^{-1}(s)\widetilde{N}(s)$, where $\widetilde{N}(s) = \frac{1}{s+\epsilon}\mathbf{1}_n$ and $\widetilde{M}(s) = \frac{s}{s+\epsilon}$, where $\epsilon > 0$ is arbitrary. By using this factorization and making some simple block diagram manipulations, the system in Figure 4.3 is transformed to the system in Figure 4.4, where $M(s) = \frac{(s+\epsilon)^2}{s^2}$, $\widehat{W}_1(s) = \widetilde{M}(s)W_1(s)$, $\widehat{W}_2(s) = \frac{1}{s+\epsilon}$, $\widehat{W}_3(s) = \frac{\sigma_1}{s+\epsilon}$, and

$$\widehat{K}(s) = \frac{s}{s+\epsilon}K(s)\ . \tag{4.13}$$

Therefore, the problem is now transformed into the general four block problem of Figure 4.5, where the general plant is described as

$$\left[\begin{array}{c} z \\ \hdashline \hat{y} \end{array}\right] := \left[\begin{array}{c} z_1 \\ e_1 \\ e_2 \\ \hdashline \hat{y} \end{array}\right] = \left[\begin{array}{cc:c} 0 & 0 & I \\ -\widehat{W}_3M\widehat{W}_1 & \widehat{W}_3M\widehat{W}_2 & -\widehat{W}_3M\widetilde{N} \\ 0 & 0 & W_4 \\ \hdashline -M\widehat{W}_1 & M\widehat{W}_2 & -M\widetilde{N} \end{array}\right] \left[\begin{array}{c} w_1 \\ d \\ \hdashline u \end{array}\right]$$

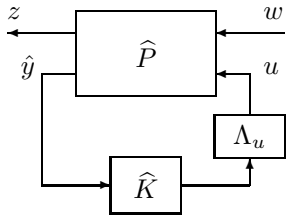

Figure 4.5: General four-block problem [42]

$$=: \quad \widehat{P} \left[\begin{array}{c} w \\ \hdashline u \end{array}\right]. \tag{4.14}$$

Now, the problem can be posed as to design a stabilizing controller $\widehat{K}$ which achieves that $\|F_l(\widehat{P}, \Lambda_u \widehat{K})\|_\infty < \gamma$, for minimum possible γ, where $F_l(\widehat{P}, \Lambda_u \widehat{K})$ is the closed-loop TFM from w to z in Figure 4.5. Let us define the *normalized plant* $\widehat{P}_\gamma := \left[\begin{array}{cc} \gamma^{-1} I & 0 \\ 0 & I \end{array}\right] \widehat{P} =: \left[\begin{array}{cc} P_{\gamma_{11}} & P_{\gamma_{12}} \\ P_{\gamma_{21}} & P_{\gamma_{22}} \end{array}\right]$, so that the stabilizing controller $\widehat{K}$ must satisfy $\|F_l(\widehat{P}_\gamma, \Lambda_u \widehat{K})\|_\infty < 1$.

As it was done in [13], the above defined 4-block problem can be reduced to a 1-block problem by using chain scattering representations. It can be shown that $P_{\gamma_{12}}(j\omega)$ has full column rank and $P_{\gamma_{21}}(j\omega)$ has full row rank for all $\omega \in \overline{\mathbb{R}}$, which guarantees existence of a solution in the delay-free case (i.e., when $\Lambda_u = I$) for sufficiently large γ. Since $P_{\gamma_{21}}(j\omega)$ has full row rank, using output augmentation, as pointed in Section 2.1, we can obtain the chain-scattering representation of the augmented plant. To do this, let us introduce an output augmentation by defining $\overline{y} := \overline{P}_{\gamma_{21}} w + \overline{P}_{\gamma_{22}} u$, where $\left[\begin{array}{c} P_{\gamma_{21}} \\ \overline{P}_{\gamma_{21}} \end{array}\right]$ is invertible. Then, the augmented plant, $\overline{\widehat{P}}_\gamma := \left[\begin{array}{cc} P_{\gamma_{11}} & P_{\gamma_{12}} \\ P_{\gamma_{21}} & P_{\gamma_{22}} \\ \overline{P}_{\gamma_{21}} & \overline{P}_{\gamma_{22}} \end{array}\right]$, has a chain-scattering representation $\Psi := CHAIN(\overline{\widehat{P}}_\gamma)$, which in turn has a (J_{zw}, J_{uw})-lossless factorization

$$\Psi =: \Theta\Omega\,, \tag{4.15}$$

as shown in Figure 4.6, where Θ is (J_{zw}, J_{uw})-lossless and Ω is unimodular [50].

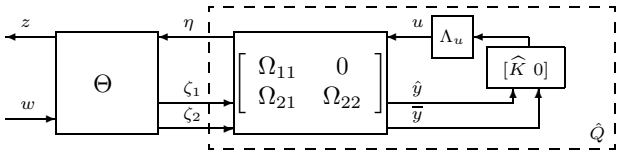

Figure 4.6: New problem definition under chain-scattering representation [42]

Furthermore, Ω is decomposed as $\Omega = \begin{bmatrix} \Omega_{11} & 0 \\ \Omega_{21} & \Omega_{22} \end{bmatrix}$, where Ω_{11} is $(n_u + n_{\hat{y}}) \times (n_u + n_{\hat{y}})$ dimensional and bistable.

In Figure 4.6, the closed-loop TFM from w to z is $HM\left(\Theta, \widehat{Q}\right)$, where $\widehat{Q} := HM\left(\Omega, \Lambda_u \begin{bmatrix} \widehat{K} & 0 \end{bmatrix}\right)$. Since Θ is (J_{zw}, J_{uw})-lossless, from Theorem 2.1, $HM(\Theta, \widehat{Q})$ is contractive if and only if $\widehat{Q}$ is contractive. Therefore, the problem of finding a stabilizing controller $\widehat{K}$ such that $F_l(\widehat{P}_\gamma, \Lambda_u \widehat{K})$ is contractive is equivalent to finding a stabilizing controller $\widehat{K}$ such that $\widehat{Q}$ is contractive, since $F_l(\widehat{P}_\gamma, \Lambda_u \widehat{K}) = HM(\Theta, \widehat{Q})$. Furthermore, we can write $\widehat{Q} = \begin{bmatrix} Q & 0 \end{bmatrix}$, where $Q := HM(\Omega_{11}, \Lambda_u \widehat{K})$. Therefore, the problem of finding a stabilizing controller $\widehat{K}$ for the system in Figure 4.5 is reduced to finding a stabilizing controller $\widehat{K}$ such that $Q = HM(\Omega_{11}, \Lambda_u \widehat{K})$ is contractive. Since $HM(\Omega_{11}, \Lambda_u \widehat{K}) = HM(\Omega_{11}\Lambda, \widehat{K})$, where $\Lambda = \text{bdiag}(\Lambda_u, 1)$, the problem is reduced to finding a stabilizing controller $\widehat{K}$ such that $Q = HM(\Omega_{11}\Lambda, \widehat{K})$ is contractive. This problem is defined as a one block problem (OBP) (see Section 2.2). Following [13], to obtain a causal stabilizing controller, we can write $Q = HM(\Omega_{11}\Lambda, \widehat{K}) = HM(\Omega_{11}\Omega_{11_\infty}^{-1}\Lambda, K_\gamma)$, where $\Omega_{11_\infty} := \lim_{s\to\infty} \Omega_{11}(s)$ and $K_\gamma := HM(\Lambda^{-1}\Omega_{11_\infty}\Lambda, \widehat{K})$. In our case, we can choose Ω in (4.15) such that

$$\Omega_{11_\infty} := \lim_{s\to\infty} \Omega_{11}(s) = \begin{bmatrix} I_n & 0 \\ 0 & \frac{\gamma}{\sqrt{D_{21} D_{21}^T}} \end{bmatrix} , \tag{4.16}$$

where $D_{21} := \lim_{s\to\infty} P_{\gamma_{21}}(s)$. Then, $\Lambda^{-1}\Omega_{11_\infty}\Lambda = \Omega_{11_\infty}$, and thus we would have

$$K_\gamma := HM(\Lambda^{-1}\Omega_{11_\infty}\Lambda, \widehat{K}) = HM(\Omega_{11_\infty}, \widehat{K}) . \tag{4.17}$$

Defining $G := \Omega_{11}\Omega_{11_\infty}^{-1}$, the problem can be written as:

OBP(G, Λ): Find a stabilizing controller K_γ satisfying $\|HM(G\Lambda, K_\gamma)\|_\infty < 1$.

The solution to this problem is found by a sequence of iterations presented in Section 2.2, which is based on the approach given in [13]. In each iteration, a problem which is called an adobe delay problem is solved. Utilizing the procedure in Section 2.2, the solution to OBP(G, Λ) can be obtained as shown in the sequel.

The problem OBP(G, Λ), is solved in N steps assuming that $\bar{h}_N > 0$. However, if $\bar{h}_N = 0$, then it is solved in $N - 1$ steps.

Step 1: Assuming $\bar{h}_N > 0$ (if $\bar{h}_N = 0$, we directly start with step 2, using $\widetilde{\Lambda}_1 := \Lambda$ and $\widetilde{G}_1 := G$), let $\Lambda =: \Lambda_1\widetilde{\Lambda}_1$, where $\Lambda_1(s) := \begin{bmatrix} e^{-\bar{h}_N s} I_{\mu_1} & 0 \\ 0 & I_{\rho_1} \end{bmatrix}$, where $\mu_1 = \sum_{i=1}^{N} l_i = n$ and $\rho_1 = n + 1 - \mu_1 = 1$. Then, using (2.8), $HM(G\Lambda, K_\gamma) = HM\left(G\Lambda_1, HM(\widetilde{\Lambda}_1, K_\gamma)\right)$. Letting

$$K_1 := HM\left(\widetilde{\Lambda}_1, K_\gamma\right) , \tag{4.18}$$

the problem becomes determining a stabilizing controller K_1 which results in $\|HM(G\Lambda_1, K_1)\|_\infty < 1$, which is the problem discussed in Section 2.2. Therefore, by (2.32), its solution is

$$K_1 = HM\left(\begin{bmatrix} I & 0 \\ \Pi_1 & I \end{bmatrix} \widetilde{G}_1^{-1}, \widetilde{Q}_1\right) , \tag{4.19}$$

where Π_1 and $\widetilde{G}_1$ are respectively determined as $\widetilde{G}_a$ and Π_a in (2.33) and (2.34), respectively, and $\widetilde{Q}_1$ must be contractive. Using (2.7),

$$\widetilde{Q}_1 = HM\left(\widetilde{G}_1 \begin{bmatrix} I & 0 \\ -\Pi_1 & I \end{bmatrix}, K_1\right) , \tag{4.20}$$

where K_1 is given by (4.18). Hence, by (2.8) and using (4.18), $\widetilde{Q}_1$ in (4.20) can be written as:

$$\widetilde{Q}_1 = HM\left(\widetilde{G}_1\widetilde{\Lambda}_1, \widetilde{K}_1\right) , \tag{4.21}$$

where

$$\widetilde{K}_1 := HM\left(\widetilde{\Lambda}_1^{-1} \begin{bmatrix} I & 0 \\ -\Pi_1 & I \end{bmatrix} \widetilde{\Lambda}_1, K_\gamma\right) . \tag{4.22}$$

Therefore, using (4.21), the remaining problem is to determine a stabilizing controller $\widetilde{K}_1$ such that $\left\| HM\left(\widetilde{G}_1\widetilde{\Lambda}_1, \widetilde{K}_1\right)\right\|_\infty < 1$, which is considered in the next step.

Step 2: Let $\widetilde{\Lambda}_1 =: \Lambda_2\widetilde{\Lambda}_2$, where $\Lambda_2(s) := \begin{bmatrix} e^{-\left(\bar{h}_{N-1}-\bar{h}_N\right)s}I_{\mu_2} & 0 \\ 0 & I_{\rho_2} \end{bmatrix}$, where $\mu_2 = \sum_{i=1}^{N-1} l_i = n - l_N$ and $\rho_2 = n + 1 - \mu_2 = 1 + l_N$. Then, using (2.8), $HM\left(\widetilde{G}_1\widetilde{\Lambda}_1, \widetilde{K}_1\right) = HM\left(\widetilde{G}_1\Lambda_2, HM\left(\widetilde{\Lambda}_2, \widetilde{K}_1\right)\right)$. Letting

$$K_2 := HM\left(\widetilde{\Lambda}_2, \widetilde{K}_1\right) , \tag{4.23}$$

the problem becomes determining a stabilizing controller K_2 which yields $\|HM(\widetilde{G}_1\Lambda_2, K_2)\|_\infty < 1$, which is the problem discussed in Section 2.2. Therefore, by (2.32), its solution is

$$K_2 = HM\left(\begin{bmatrix} I & 0 \\ \Pi_2 & I \end{bmatrix}\widetilde{G}_2^{-1}, \widetilde{Q}_2\right) , \tag{4.24}$$

where Π_2 and $\widetilde{G}_2$ are respectively determined as $\widetilde{G}_a$ and Π_a in (2.33) and (2.34), respectively, and $\widetilde{Q}_2$ must be contractive. Using (2.7),

$$\widetilde{Q}_2 = HM\left(\widetilde{G}_2\begin{bmatrix} I & 0 \\ -\Pi_2 & I \end{bmatrix}, K_2\right) , \tag{4.25}$$

where K_2 is given by (4.23). Hence, by (2.8) and using (4.23), $\widetilde{Q}_2$ in (4.25) can be written as:

$$\widetilde{Q}_2 = HM\left(\widetilde{G}_2\widetilde{\Lambda}_2, \widetilde{K}_2\right) , \tag{4.26}$$

where

$$\widetilde{K}_2 := HM\left(\widetilde{\Lambda}_2^{-1}\begin{bmatrix} I & 0 \\ -\Pi_2 & I \end{bmatrix}\widetilde{\Lambda}_2, \widetilde{K}_1\right) . \tag{4.27}$$

Therefore, using (4.26), the remaining problem is to determine a stabilizing controller $\widetilde{K}_2$ such that $\left\| HM\left(\widetilde{G}_2\widetilde{\Lambda}_2, \widetilde{K}_2\right)\right\|_\infty < 1$, which is considered in the next step.

$\vdots$

Step N: Let $\widetilde{\Lambda}_{N-1} =: \Lambda_N \widetilde{\Lambda}_N$, where $\Lambda_N(s) := \begin{bmatrix} e^{-\left(\bar{h}_1 - \bar{h}_2\right)s} I_{\mu_N} & 0 \\ 0 & I_{\rho_N} \end{bmatrix}$, where $\mu_N = \sum_{i=1}^{1} l_i = l_1$ and $\rho_N = n+1-\mu_N = 1+\sum_{i=2}^{N} l_i$. Note that, $\widetilde{\Lambda}_N = I$. Then, using (2.8), $HM\left(\widetilde{G}_{N-1}\widetilde{\Lambda}_{N-1}, \widetilde{K}_{N-1}\right) = HM\left(\widetilde{G}_{N-1}\Lambda_N, HM\left(\widetilde{\Lambda}_N, \widetilde{K}_{N-1}\right)\right)$. Letting

$$K_N := HM\left(\widetilde{\Lambda}_N, \widetilde{K}_{N-1}\right) , \tag{4.28}$$

the problem becomes determining a stabilizing controller K_N which results in $\|HM(\widetilde{G}_{N-1}\Lambda_N, K_N)\|_\infty < 1$, which is the problem discussed in Section 2.2. Therefore, by (2.32), its solution is

$$K_N = HM\left(\begin{bmatrix} I & 0 \\ \Pi_N & I \end{bmatrix} \widetilde{G}_N^{-1}, \widetilde{Q}_N\right) , \tag{4.29}$$

where Π_N and $\widetilde{G}_N$ are respectively determined as $\widetilde{G}_a$ and Π_a in (2.33) and (2.34), respectively, and $\widetilde{Q}_N$ must be contractive, but otherwise arbitrary. Note that, since $\widetilde{\Lambda}_N = I$, (4.28) gives $K_N = \widetilde{K}_{N-1}$.

Now, using (2.7), from (4.22) we obtain

$$K_\gamma = HM\left(\widetilde{\Lambda}_1^{-1}\begin{bmatrix} I & 0 \\ \Pi_1 & I \end{bmatrix} \widetilde{\Lambda}_1, \widetilde{K}_1\right) . \tag{4.30}$$

Similarly, from (4.27) we obtain

$$\widetilde{K}_1 = HM\left(\widetilde{\Lambda}_2^{-1}\begin{bmatrix} I & 0 \\ \Pi_2 & I \end{bmatrix} \widetilde{\Lambda}_2, \widetilde{K}_2\right) . \tag{4.31}$$

Substituting (4.31) into (4.30) and using (2.8) we obtain

$$K_\gamma = HM\left(\widetilde{\Lambda}_1^{-1}\begin{bmatrix} I & 0 \\ \Pi_1 & I \end{bmatrix} \widetilde{\Lambda}_1\widetilde{\Lambda}_2^{-1}\begin{bmatrix} I & 0 \\ \Pi_2 & I \end{bmatrix} \widetilde{\Lambda}_2, \widetilde{K}_2\right) . \tag{4.32}$$

Proceeding like this, through the first $N-1$ steps and using the fact that $\widetilde{K}_{N-1} = K_N$, which is given by (4.29), we obtain

$$\begin{aligned} K_\gamma \;=\; HM\Bigg(&\widetilde{\Lambda}_1^{-1}\begin{bmatrix} I & 0 \\ \Pi_1 & I \end{bmatrix} \widetilde{\Lambda}_1 \cdots \widetilde{\Lambda}_{N-1}^{-1}\begin{bmatrix} I & 0 \\ \Pi_{N-1} & I \end{bmatrix} \\ &\widetilde{\Lambda}_{N-1}\begin{bmatrix} I & 0 \\ \Pi_N & I \end{bmatrix} \widetilde{G}_N^{-1}, \widetilde{Q}_N\Bigg) . \end{aligned} \tag{4.33}$$

On noting that $\widetilde{\Lambda}_1^{-1} = \Lambda^{-1}\Lambda_1$, $\widetilde{\Lambda}_1\widetilde{\Lambda}_2^{-1} = \Lambda_2$, ..., $\widetilde{\Lambda}_{N-2}\widetilde{\Lambda}_{N-1}^{-1} = \Lambda_{N-1}$, and $\widetilde{\Lambda}_{N-1} = \Lambda_N$, as in (2.37), we can rewrite (4.33) as

$$K_\gamma = HM(\Pi_\Lambda G_\Lambda^{-1}, Q_\Lambda) \,, \tag{4.34}$$

where $\Pi_\Lambda := \Lambda^{-1}\prod_{i=1}^{N}\Lambda_i \begin{bmatrix} I & 0 \\ \Pi_i & I \end{bmatrix}$ is a system which involves delays and FIR filters (note that time-advances introduced by Λ^{-1} are all cancelled by Λ_i's; i.e., Π_Λ is causal), $G_\Lambda := \widetilde{G}_N$ is a finite-dimensional and bistable system, and $Q_\Lambda := \widetilde{Q}_N$ is such that $\|Q_\Lambda\|_\infty < 1$, but otherwise arbitrary.

Once the stabilizing controller K_γ is found as in (4.34), using (2.8) and (2.7), the stabilizing controller $\widehat{K}$ is found by inverting (4.17) and the desired stabilizing controller K is found from (4.13) as

$$K(s) = \frac{s+\epsilon}{s} HM\left(\Omega_{11_\infty}^{-1}\Pi_\Lambda(s)G_\Lambda^{-1}(s), Q_\Lambda(s)\right) \,. \tag{4.35}$$

By decomposing Π_k's as

$$\Pi_1 =: \begin{bmatrix} \Pi_{11}^1 & \Pi_{12}^1 & \cdots & \Pi_{1N}^1 \end{bmatrix} \,,$$

where Π_{1j}^1 is $1 \times l_j$ dimensional,

$$\Pi_2 =: \begin{bmatrix} \Pi_{11}^2 & \Pi_{12}^2 & \cdots & \Pi_{1(N-1)}^2 \\ \Pi_{21}^2 & \Pi_{22}^2 & \cdots & \Pi_{2(N-1)}^2 \end{bmatrix} \,,$$

where Π_{1j}^2 is $l_N \times l_j$ and Π_{2j}^2 is $1 \times l_j$ dimensional, ..., and

$$\Pi_N =: \begin{bmatrix} \Pi_{11}^N \\ \Pi_{21}^N \\ \vdots \\ \Pi_{N1}^N \end{bmatrix} \,,$$

where Π_{j1}^N is $l_{j+1} \times l_1$ $(j = 1, \ldots, N-1)$ and Π_{N1}^N is $1 \times l_1$ dimensional, the stabilizing controller K can be implemented as shown in Figure 4.7. Here, $\kappa\frac{s+\epsilon}{s}$ is a proportional-integral term, where

$$\kappa := \frac{\gamma}{\sqrt{D_{21}D_{21}^T}} = \frac{\gamma}{\sqrt{2\sum_{i=1}^{n}\left(\delta_i^+\right)^2}} \,,$$

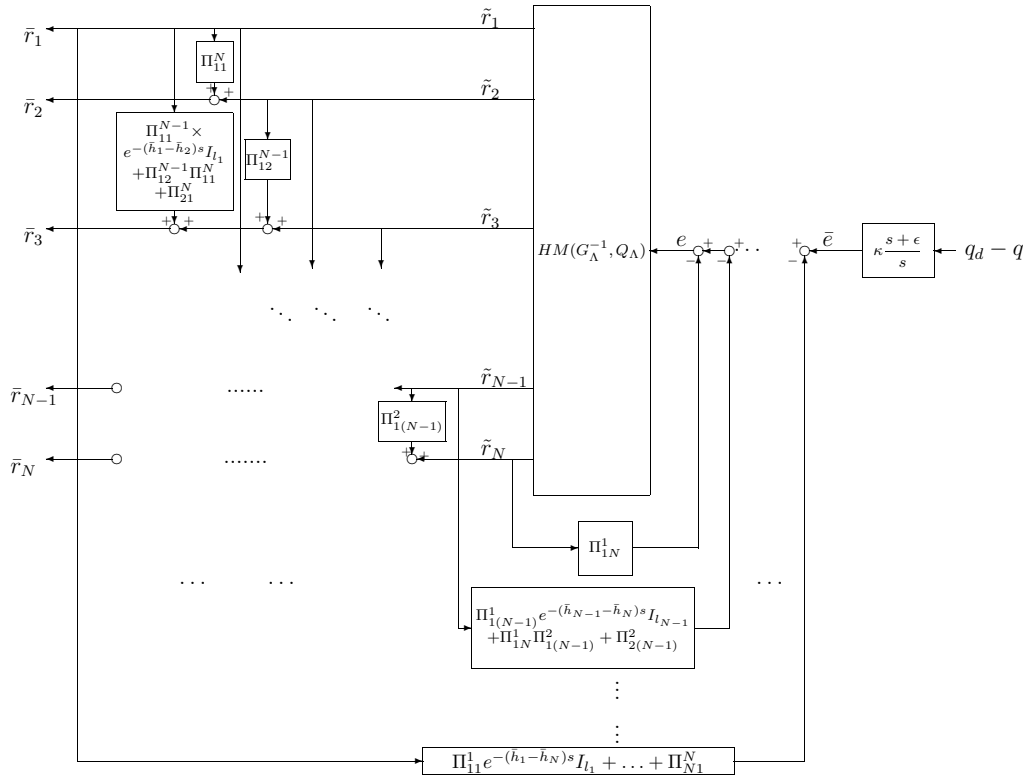

Figure 4.7: The implementation of the controller K [43]

$HM(G_\Lambda^{-1}, Q_\Lambda)$ is a finite-dimensional system parameterized by Q_Λ, which is assumed to be finite-dimensional and must be contractive, and each Π_{ij}^k is an FIR filter. Furthermore,

$$\bar{r}_1 := \begin{bmatrix} r_1 \\ \vdots \\ r_{l_1} \end{bmatrix}, \quad \bar{r}_2 := \begin{bmatrix} r_{l_1+1} \\ \vdots \\ r_{l_1+l_2} \end{bmatrix}, \quad \ldots, \quad \bar{r}_N := \begin{bmatrix} r_{\sum_{i=1}^{N-1} l_i+1} \\ \vdots \\ r_n \end{bmatrix}.$$

In the above, we assumed that $\gamma > 0$ is such that there exists a solution to the adobe delay problem at each step. In order to find minimum such γ and the corresponding stabilizing controller, i.e., to determine the *optimal* controller $K_{opt}(s) = \frac{s+\epsilon}{s}\widehat{K}_{opt}(s)$, where stabilizing $\widehat{K}_{opt}$ solves

$$\inf_{\widehat{K}} \|F_l(\widehat{P}, \Lambda_u \widehat{K})\|_\infty =: \gamma^{opt}, \tag{4.36}$$

we first find the minimum γ, call it γ^0, for which there exists a (J_{zw}, J_{uw})-lossless factorization (4.15). If step 1 also has a solution for this γ, we let

$\gamma^1 = \gamma^0$. Otherwise, we increase γ and determine the minimum γ, call it γ^1, for which there exists a solution to the adobe delay problem of step 1. After solving step k ($k = 1, \ldots, N-1$), and thus determining γ^k, if step $k+1$ also has a solution for this γ, we let $\gamma^{k+1} = \gamma^k$. Otherwise, we increase γ and determine the minimum γ, call it γ^{k+1}, for which there exists a solution to the adobe delay problem of step $k+1$ (of course, we resolve all the previous steps for this new γ). In this way, γ^{opt} in (4.36) is determined as γ^N at the end of step N. The stabilizing controller given by (4.35) for $\gamma = \gamma^{opt}$ is the stabilizing optimal controller.

Examining Figure 4.7, the controller to be implemented involves a proportional-integral term (the right-most block in Figure 4.7), which can simply be realized as

$$\dot{x}(t) = \kappa\epsilon(q_d(t) - q(t))$$
$$\bar{e}(t) = x(t) + \kappa(q_d(t) - q(t))$$

where x is the scalar state variable. This block is followed by an LTI block with TFM $HM(G_\Lambda^{-1}, Q_\Lambda)$ put in a feedback loop with N FIR filters. FIR filters are also connected from the k^{th} output of this block to $(k+1)^{\text{th}}$, ..., N^{th} output ($k = 1, \ldots, N-1$). The state-space dimension of the LTI block with TFM $HM(G_\Lambda^{-1}, Q_\Lambda)$ is equal to $n_{G_\Lambda^{-1}} + n_{Q_\Lambda}$, where $n_{G_\Lambda^{-1}}$ and n_{Q_Λ} are the state-space dimension of G_Λ^{-1} and Q_Λ, respectively. It can be shown by tracking back the design steps given above, the state-space dimension of G_Λ^{-1} is the same as the state-space dimension of $G := \Omega_{11}\Omega_{11_\infty}^{-1}$. In addition, since $\Omega_{11_\infty}^{-1}$ is a constant matrix, the state-space dimension of G, hence G_Λ^{-1}, is the same as the state-space dimension of Ω_{11}. The state-space dimension of Ω_{11} equals to the state-space dimension of the general plant in (4.14), since Ω_{11} is obtained as G in (2.28), which is obtained by solving (2.17) and (2.18) for the corresponding generalized plant. Since the second and fourth row blocks of the generalized system in (4.14) can be realized as a second order system and $n-1$ states are needed to realize the third block, the state-space dimension of the generalized plant, hence, Ω_{11}, is $n+1$. Therefore, for a constant Q_Λ,

the state-space dimension of the LTI block with TFM $HM(G_\Lambda^{-1}, Q_\Lambda)$ equals to $n+1$. If the central controller is considered, i.e., $Q_\Lambda = 0$, a state-space realization of $HM(G_\Lambda^{-1}, Q_\Lambda)$ can be written as

$$\dot{x}(t) = (A_a - \Sigma_{a22}^T B_{\mu_a} C_{\mu_a} \Sigma_{a22}^{-T} - \Sigma_{a12}^T C_{\mu_a}^T J_{\mu_a} C_{\mu_a} \Sigma_{a22}^{-T}) x(t) + B_{\rho_a} e(t)$$
$$\widetilde{r}(t) = -C_{\mu_a} \Sigma_{a22}^{-T} x(t),$$

where $\widetilde{r} := \begin{bmatrix} \widetilde{r}_1^T & \widetilde{r}_2^T & \cdots & \widetilde{r}_{N-1}^T & \widetilde{r}_N^T \end{bmatrix}^T$, $x(t)$ is the $n+1$ dimensional state vector, and the appearing matrices are as defined in Section 2.2, corresponding to Step N. Furthermore, each FIR filter, whose impulse response is in the form of (2.12), can easily be realized in discrete-time using $\frac{h}{\tau}$ delay elements, where h is the length of the impulse response and τ is the sampling period. Therefore, the implementation of the overall controller is relatively simple.

4.4 Time Domain Performance of the Designed Flow Controller

In this section, we consider the time-domain performance of the controllers designed by the approach proposed in the previous section. In addition, the designed controllers are compared to the controllers designed by the approach of [23]. Simulations are carried out as in [43], but the cases considered here are different than those in [43]. Simulations are done using MATLAB/SIMULINK package, where non-linear effects (hard constraints) are also taken into account. Although the controller was designed using a fluid-flow model, a more realistic discrete model is used for the simulations. In the simulations, all the links are assumed to have 100 Mbits/second physical capacity. Data flow is assumed to consist of discrete data packets of size 1 Mbits and each packet is modeled as a pulse with 10 milliseconds width. Control packets, which carry rate information from the bottleneck node to the sources, on the other hand, have much smaller sizes. It is assumed that the designed controller, which is implemented at the bottleneck, sends a control packet to each source at every 5 milliseconds. Each source updates its data sending

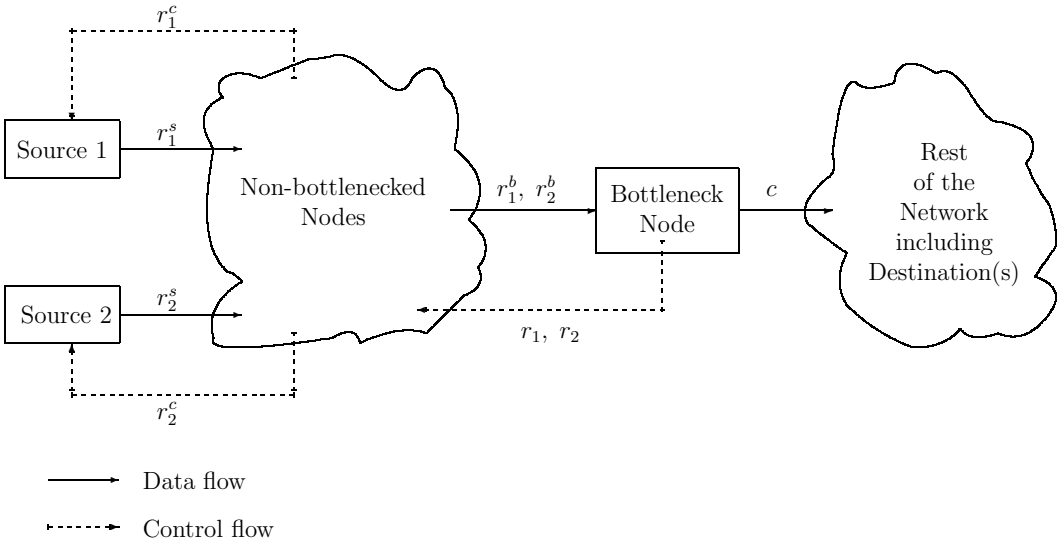

Figure 4.8: Topology of the example network [43]

rate when it receives a new control packet. However, control packets may not be received at equal intervals due to the presence of time-varying backward time-delays. This causes that data sending rates may not be updated at equal intervals. In all simulations, simulation step size is taken as 1 millisecond.

We consider a network with two sources as shown in Figure 4.8. The nominal time-delays (in seconds), controller design parameters, and the resulting optimal sensitivity level, γ^{opt}, for each case are shown in Table 4.1. In all cases, we take $Q_\Lambda = 0$ and $h_i^f = h_i^b = \frac{1}{2}h_i$, $i = 1, 2$. In all cases, the buffer size (maximum queue length) is taken as 60 packets and the desired queue length, q_d, is taken as half of this value, 30 packets. The rate limits of the sources are taken as 150 packets/second in all cases except Case 5. The capacity of the outgoing link is taken as 90 packets/second in all cases. The uncertain part of the actual time-delays (in seconds) are shown in Table 4.2. The simulation results of the controllers designed by the approach of Section 4.3 are shown in Figures 4.9–4.16. In all figures, q is the queue length, $q(t)$ (whose scale is shown on the right-hand-side of each graph), and $\mathrm{r}_i^{\mathrm{s}}$, for $i = 1, 2$, is the actual rate, $r_i^s(t) := \min\left(\max\left(r_i^c(t), 0\right), d_i\right)$, of data sent from source i at time t, where d_i is the rate limit of source i and $r_i^c(t) = r_i(t - \tau_i^b(t))$ is the rate command received at source i at time t.

Table 4.1: Controller design parameters and γ^{opt}

Case	h_1	h_2	δ_1^+	δ_2^+	β_1	β_2	β_1^f	β_2^f	α_1	α_2	σ_1	σ_2	γ^{opt}
1,2,5	3	1	1/2	1	0.6	0.4	0.2	0.1	$\frac{2}{3}$	$\frac{1}{3}$	0.25	0.25	5.126
3	3	1	2	1	0.6	0.4	0.2	0.1	$\frac{2}{3}$	$\frac{1}{3}$	0.25	0.25	7.061
4	1	1	1/2	1	0.6	0.4	0.2	0.1	$\frac{2}{3}$	$\frac{1}{3}$	1	0.25	3.792

Table 4.2: The uncertain part of the actual time-delays

Case	i	$\delta_i^b(t)$	$\delta_i^f(t)$
1, 4, 5	1	0.2+0.3sin($\frac{2\pi}{40}t$)	0.1+0.1sin($\frac{2\pi}{100}t$)
	2	0.6+0.3 sin($\frac{2\pi}{50}t$)	0.1+0.1sin($\frac{2\pi}{100}t$)
2, 3	1	1.5+0.8sin($\frac{2\pi}{40}t$)	0.15+0.15sin($\frac{2\pi}{100}t$)
	2	0.6+0.3sin($\frac{2\pi}{50}t$)	0.1+0.1sin($\frac{2\pi}{100}t$)

Case 1: This is the central case, which will be used to compare all other simulation results. In Figure 4.9, the queue length remains almost zero up to around 18 seconds, which is the time required for the incoming rates to reach the capacity of the outgoing link. Then, queue length settles around 40 seconds following an overshoot. The high-frequency oscillations in the queue length are due to discrete arrival/departure of packets (those oscillations would not be seen if a fluid-flow model was used, see simulation results in Sections 4.6, 4.7). Moreover, existence of time-varying forward time-delays also cause oscillations. As shown in Figure 4.9, at steady-state, the queue length oscillates around its desired value, q_d, and the flow rates oscillate around the values given by (4.6). In addition, the controller is more conservative on rate 1, than it is on rate 2. The reason for this is that the nominal delay of channel 1 is higher than that of channel 2.

Case 2: In this case, we have the same controller as in Case 1, however, the actual delay in channel 1 is increased. As shown in Figure 4.10, this results in

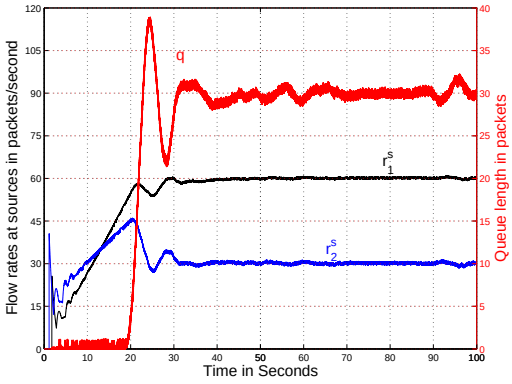

Figure 4.9: Results for Case 1

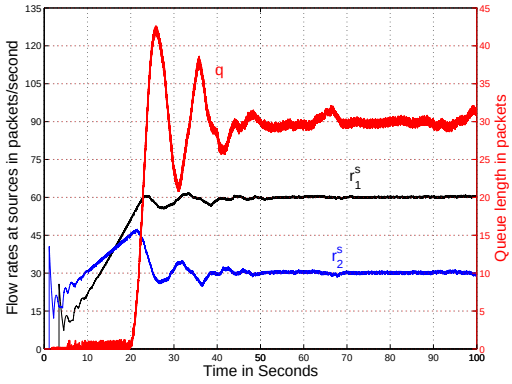

Figure 4.10: Results for Case 2

an increase on the settling time and the overshoot.

Case 3: We increased the value of the design parameter δ_1^+ four times as shown in Table 4.1. This makes the resulting controller more robust, but more conservative. As shown in Figure 4.11, when we apply the same actual delays as in Case 2, the queue length settles later than the settling time of the queue length in Figure 4.10 with a smaller overshoot.

Case 4: We take equal nominal delays in the channels. By comparing Figure 4.12 to 4.9, the response of the controller in Figure 4.12 is faster compared to the one in Figure 4.9. The reason of the faster response is that the nominal time-delay in the 1st channel is less than the one in the 1st channel of Case 1. In addition, apart from the ratio α_1/α_2, the rate response of the controller is the same in both channels.

Case 5: The rate limits of the sources are decreased to 50 packets/second. This causes the rate of the first source to saturate as shown in Figure 4.13. However, the controller increases the rate of the second source to compensate. Due to this extra compensation, however, the response here is slower compared to the central case.

To compare our controller to the controller proposed in [23], we designed controllers using the approach of [23] using the design parameters (except σ_1 and σ_2, which are not used in the approach of [23], where tracking and robustness are achieved by solving a two-block problem and fairness is achieved

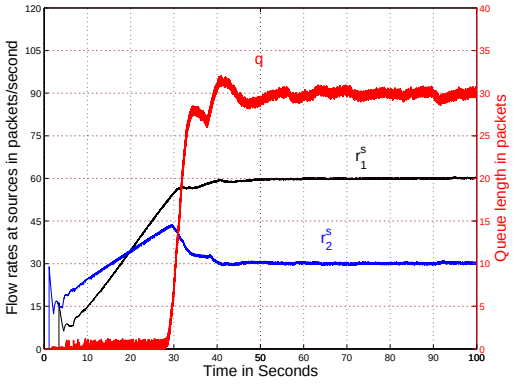

Figure 4.11: Results for Case 3

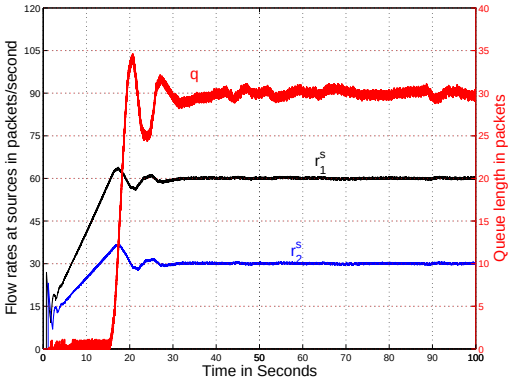

Figure 4.12: Results for Case 4

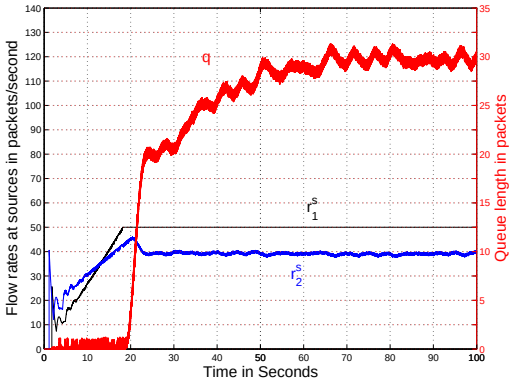

Figure 4.13: Results for Case 5

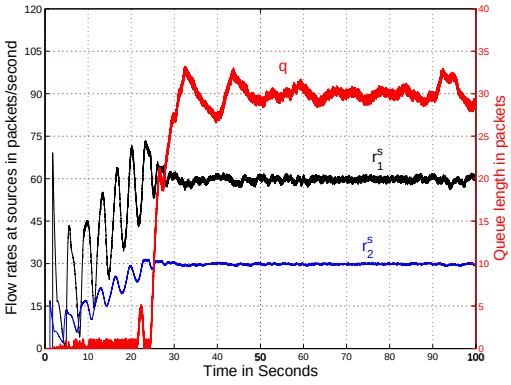

Figure 4.14: Results of [23] for Case 1

by including the fairness weights in the controller derivation) shown in Table 4.1. The response of the controllers designed by the approach of [23] is given in Figures 4.14–4.16 for cases 1–3 above. As seen by comparing Figure 4.14 to Figure 4.9, the response of the controller designed by the approach of [23] is slower and has less overshoot compared to one designed by the approach presented in the previous section. This difference indicates that the controller designed by the approach of [23] is conservative compared to one designed by the approach of Section 4.3.

As seen in Figure 4.15, the controller designed by the approach of [23] can not stabilize the actual system if the uncertain part of the actual time-delays in Case 1 are increased as in Case 2 given in Table 4.2. However, as seen in Figure 4.10, the controller designed by the approach proposed in Section 4.3 stabilizes the actual system and achieves the performance requirements. In

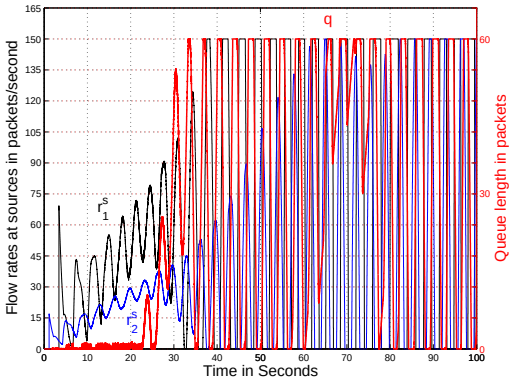

Figure 4.15: Results of [23] for Case 2

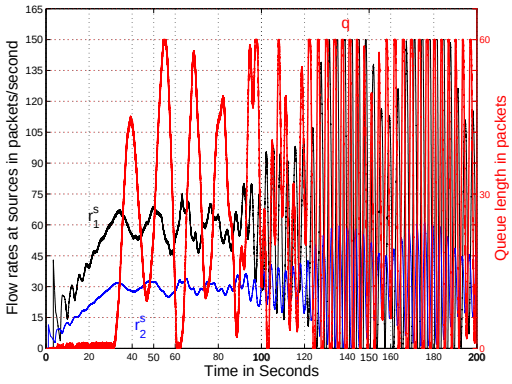

Figure 4.16: Results of [23] for Case 3

Figure 4.16, the response of the controller, which is designed by the approach of [23] for larger δ_1^+ compared to previous one, is shown. However, the designed controller still can not stabilize the actual system. On the other hand, as shown in Figure 4.11, the controller designed by the approach proposed in Section 4.3 stabilizes the actual system and achieves the design requirements. Hence, the controllers designed by the approach of Section 4.3 exhibit better robustness properties compared to the ones designed by the approach of [23].

4.5 Performance Level and Stability Margins of the Designed Flow Controller

In this section, performance level and actual stability margins of the flow controller designed by the approach of Section 4.3 are presented. Analysis carried out in this section have been published in [44], but the example network considered here is different than the one in [44].

The stabilizing $\mathcal{H}^\infty$ flow controller K designed by the approach proposed in Section 4.3 internally stabilizes the nominal system in Figure 4.3, where $\Delta = 0$, and makes the $\mathcal{H}^\infty$ norm of the closed-loop TFM from w to z in Figure 4.3, called T_{zw}, less than a given $\gamma > 0$. By defining $S := (1+P_o\Lambda_u K)^{-1}$, the closed-loop TFM T_{zw} in Figure 4.3 can be written as given below;

$$T_{zw} = \begin{bmatrix} -\Lambda_u KSW_1 & \Lambda_u KSW_2 \\ -W_3 SW_1 & W_3 SW_2 \\ -W_4\Lambda_u KSW_1 & W_4\Lambda_u KSW_2 \end{bmatrix}. \tag{4.37}$$

Therefore, the designed stabilizing controller K should satisfy;

$$\left\| \begin{bmatrix} \Lambda_u KSW_1 & \Lambda_u KSW_2 \\ W_3 SW_1 & W_3 SW_2 \\ W_4\Lambda_u KSW_1 & W_4\Lambda_u KSW_2 \end{bmatrix} \right\|_\infty < \gamma, \tag{4.38}$$

for a given $\gamma > 0$.

Since the optimal controller (besides stabilization) is designed to achieve the minimum sensitivity level, γ^{opt}, its reciprocal, $\dfrac{1}{\gamma^{opt}}$, is defined as the *performance level* of the designed optimal controller K^{opt}. Therefore, the performance level indicates how much the performance requirements are satisfied with the designed robustly stabilizing optimal controller.

The designed flow controller should robustly stabilize (internally) the feedback system in Figure 4.2 for all possible Δ. By the small-gain theorem, Theorem 3.2, since the non-causal uncertainty block Δ is norm-bounded, $\|\Delta\|_2 < 1$, the controller K robustly stabilizes the actual system if it stabilizes the nominal feedback system (the system in Figure 4.2 with $\Delta = 0$) and satisfies $\|\Lambda_u K(1 + P_o\Lambda_u K)^{-1}W_1\|_\infty \leq 1$. Furthermore, since Λ_u is an inner function, the latter condition is equivalent to

$$\|K(1 + P_o\Lambda_u K)^{-1}W_1\|_\infty \leq 1. \tag{4.39}$$

Therefore, the designed controller robustly stabilizes the actual system against all uncertain time-varying time-delays satisfying (4.4) if the stabilizing optimal controller K^{opt} satisfies (4.39). Since K^{opt} satisfies $\|T_{zw}\|_\infty = \gamma^{opt}$, from (4.37), $\|\Lambda_u KSW_1\|_\infty = \|KSW_1\|_\infty =: \rho \leq \gamma^{opt}$. Therefore, the designed controller robustly stabilizes the overall feedback system for $\|\Delta\|_2 < \dfrac{1}{\rho}$. Note that $\|\Delta\|_2 < 1$ when the stability margins on $\delta_i(t)$, $\dot{\delta}_i(t)$, and $\dot{\delta}_i^f(t)$ are respectively δ_i^+, β_i and β_i^f (see Section 4.2). Therefore, $\|\Delta\|_2 < \dfrac{1}{\rho}$ is satisfied if the

actual stability margins on $\delta_i(t)$, $\dot{\delta}_i(t)$, and $\dot{\delta}_i^f(t)$ are respectively changed to δ_i^{act}, β_i^{act} and $\beta_i^{f^{\text{act}}}$, where

$$\delta_i^{\text{act}} = \frac{1}{\rho}\delta_i^+ \tag{4.40}$$

and

$$\frac{\beta_i^{\text{act}} + \beta_i^{f^{\text{act}}}}{\sqrt{1-\beta_i^{\text{act}}}} = \frac{\beta_i + \beta_i^f}{\rho\sqrt{1-\beta_i}} \tag{4.41}$$

are satisfied for $i = 1, \cdots, n$. Note that there are infinitely many solutions for β_i^{act} and $\beta_i^{f^{\text{act}}}$ in (4.41). The system is robustly stable for any one of these solutions. To obtain unique solutions, we introduce the additional constraint

$$\frac{\beta_i^{f^{\text{act}}}}{\beta_i^{\text{act}}} = \frac{\beta_i^f}{\beta_i}\,. \tag{4.42}$$

In order to show the performance level and the actual stability margins of the designed optimal $\mathcal{H}^\infty$ flow controllers while design parameters δ_i^+, β_i, β_i^f $(i = 1, 2)$ change in given intervals, we consider a network with two sources as depicted in Figure 4.8. In the controller design, the nominal time-delays are assumed to be $h_1 = 3$ tu and $h_2 = 1$ tu, where tu stands for the time unit. The flow controllers are designed for $\beta_1 = \beta_2$, which varies in the interval $[0, 0.99]$, while $\delta_1^+ = \delta_2^+$ varies in the interval $[0.01, 1]$ and three cases for β_i^f, $\beta_i^f = 0$, $\beta_i^f = \beta_i/2$, and $\beta_i^f = \beta_i$, $(i = 1, 2)$ are considered. Fairness weights are chosen as $\alpha_1 = 2/3$, and $\alpha_2 = 1/3$ and other design parameters are chosen as $\sigma_1 = \sigma_2 = 0.25$.

The performance level of the designed optimal $\mathcal{H}^\infty$ controller is given in Figure 4.17. As shown in Figure 4.17, increasing any one of the design parameters, β_i, β_i^f, or δ_i^+, decreases the performance level of the designed controller. This stems from the fact that increasing these design parameters implies that the assumed uncertainty range is enlarged. Therefore, as expected, as the uncertainty range is enlarged the controller gives more priority to robustness and trades this off from performance. In addition, as β_i approaches to 1, which implies that $\dot{\delta}_i(t)$ may become close to 1, the performance level of the designed controller decreases to 0. In fact, if $\dot{\delta}_i(t) = 1$, the rate commands calculated at time t do not have any effect on the queue length at any time. Therefore, in this case, the controller may be said to have no performance.

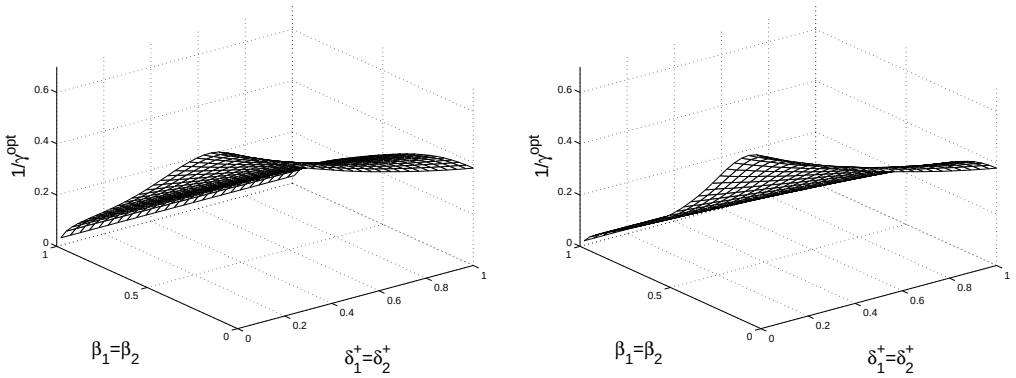

(a) $\beta_i^f = 0$ (b) $\beta_i^f = \beta_i/2$

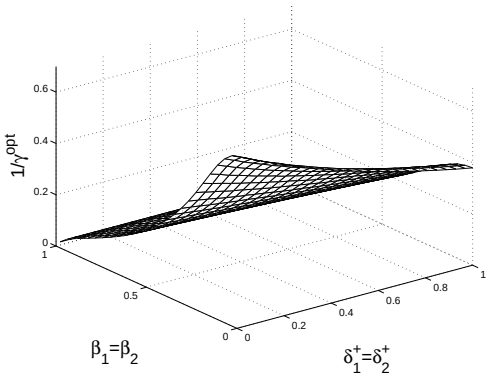

(c) $\beta_i^f = \beta_i$

Figure 4.17: Performance levels of the designed optimal $\mathcal{H}^\infty$ flow controllers

The actual stability margin on $\dot{\delta}_i(t)$, β_i^{act}, of the designed $\mathcal{H}^\infty$ controllers is given in Figure 4.18. As seen in the figure, as β_i increases, β_i^{act} increases without seriously being affected by δ_i^+. Moreover, β_i^{act} value for any corresponding β_i and δ_i^+ values in Figure 4.18 decreases as β_i^f increases.

The actual stability margin on $\delta_i(t)$, δ_i^{act}, of the designed $\mathcal{H}^\infty$ controllers is given in Figure 4.19. As seen in the figure, as δ_i^+ increases, δ_i^{act} increases almost independently from β_i for small β_i values. However, as β_i approaches to 1, δ_i^{act} approaches to 0. As stated above, since the controller looses its effect as β_i approaches to 1, its robustness properties vanishes.

Finally, the actual stability margin on $\dot{\delta}_i^f(t)$, $\beta_i^{f^{act}}$, of the designed controller is given in Figure 4.20, as δ_i^+ and β_i^f are changed, for two cases

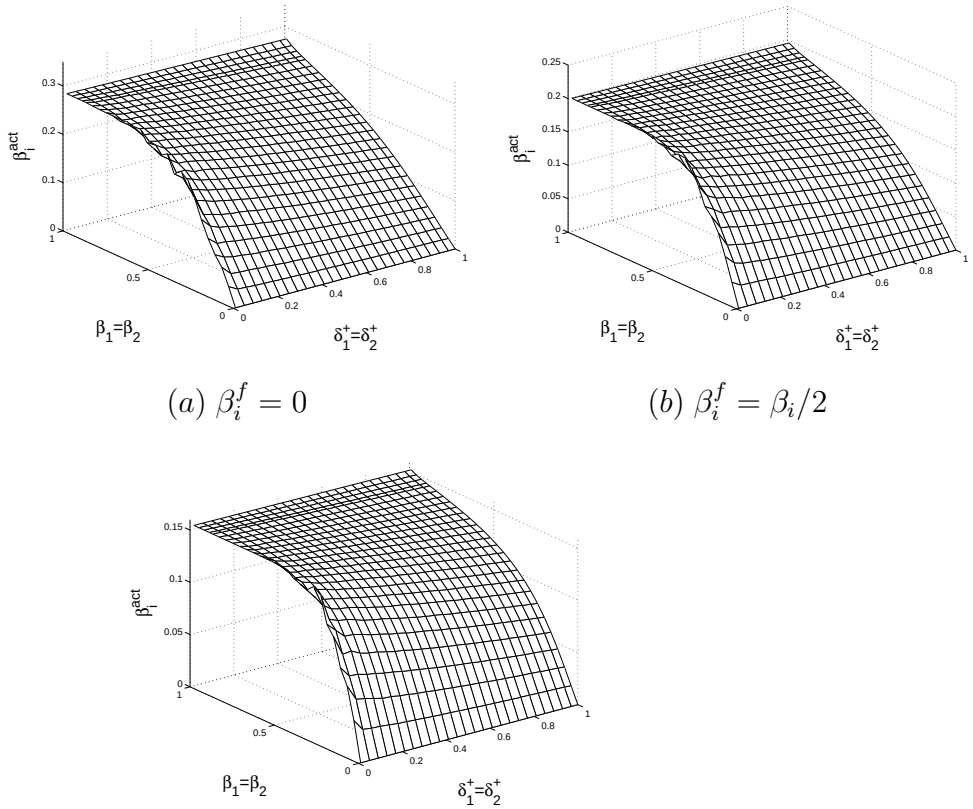

(a) $\beta_i^f = 0$ (b) $\beta_i^f = \beta_i/2$

(c) $\beta_i^f = \beta_i$

Figure 4.18: Actual stability margin on $\dot{\delta}_i(t)$ for the designed optimal $\mathcal{H}^\infty$ flow controllers

of β_i, $\beta_i = \beta_i^f$ and $\beta_i = 2\beta_i^f$. It should be noted that, in the latter case, since $\beta_i < 1$, β_i^f is changed up to 0.495, so that $\beta_i \leq 0.99$. As shown in Figure 4.20, $\beta_i^{f^{act}}$ increases as β_i^f increases without seriously being affected by δ_i^+. Furthermore, for a fixed β_i^f, increasing β_i decreases $\beta_i^{f^{act}}$.

To summarize, as the values of the design parameters β_i, β_i^f, and δ_i^+ are increased, stability margins of the designed controller increase, meanwhile its performance level decreases, in general. However, for β_i values, which are close to 1, performance and actual stability margin on $\delta_i(t)$ of the controller decreases drastically.

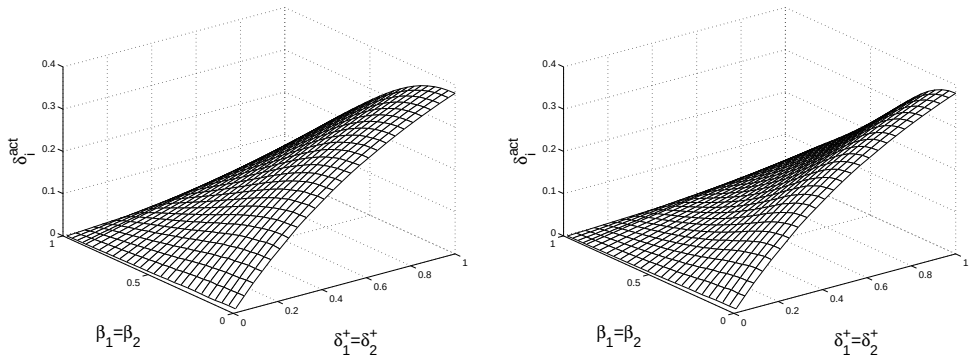

$(a)\ \beta_i^f = 0$ $(b)\ \beta_i^f = \beta_i/2$

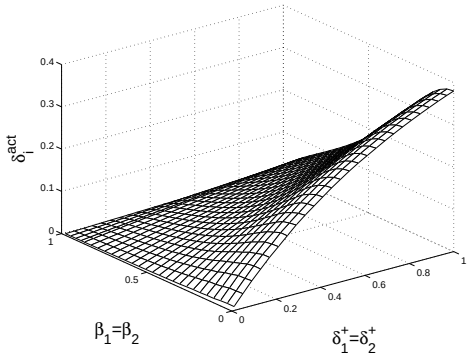

$(c)\ \beta_i^f = \beta_i$

Figure 4.19: Actual stability margin on $\delta_i(t)$ for the designed optimal $\mathcal{H}^\infty$ flow controllers

4.6 Performance and Robustness of Flow Controllers Designed Using Non-Causal Uncertainty Blocks

To present the benefits of utilizing non-causal uncertainty blocks in the stabilizing robust flow controller design, (i.e., using (4.11) instead of (4.12) and allowing non-causal uncertainty blocks) performance levels and stability margins of the stabilizing controllers designed by the approach given in Section 4.3 can be compared to the stabilizing controllers designed by the approach of [40–42]. For brevity, throughout this section, the controller design using the approach proposed in [40–42], is called the *causal approach* and the controller design using the approach proposed in Section 4.3 is called the *non-causal ap-*

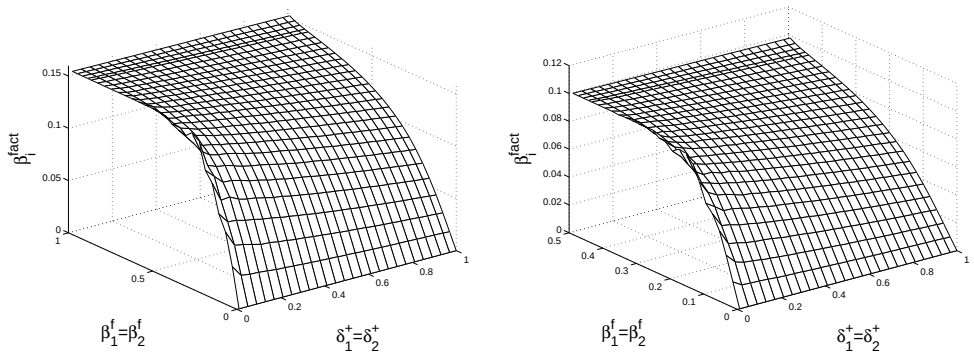

$(a)\ \beta_i = \beta_i^f$ $(b)\ \beta_i = 2\beta_i^f$

Figure 4.20: Actual stability margin on $\dot{\delta}_i^f(t)$ for the designed optimal $\mathcal{H}^\infty$ flow controllers

proach. In both approaches, the designed controller, K^{opt}, internally stabilizes the system and satisfies $\inf_{K=K^{\text{opt}}} \|T_{zw}\|_\infty =: \gamma^{opt}$ (for a different γ^{opt} for each approach), where T_{zw} is given in (4.37). Analysis carried out in this section is the same as in [45], however, the cases considered here are different than those considered in [45].

To compare the performance level, the stability margins, and time-domain performance of the flow controllers designed by the two approaches, a network with two sources, as depicted in Figure 4.8, is considered. For a satisfactory comparison, five different cases for the possible time delays in each channel are considered. The nominal time-delays and the uncertainty bounds for each channel in each case are given in Table 4.3. In each case, the actual time-delay in channel i is assumed to vary from $\tau_i^{\text{nom}} - \delta_i^{\max}$ to $\tau_i^{\text{nom}} + \delta_i^{\max}$. Therefore, for the causal approach we take

$$h_i = \tau_i^{\text{nom}} - \delta_i^{\max} \quad \text{and} \quad \delta_{\text{i}}^+ = 2\delta_{\text{i}}^{\max}\ , \quad \text{i} = 1, 2, \tag{4.43}$$

and for the non-causal approach we take

$$h_i = \tau_i^{\text{nom}} \quad \text{and} \quad \delta_{\text{i}}^+ = \delta_{\text{i}}^{\max}\ , \quad \text{i} = 1, 2. \tag{4.44}$$

The other controller design parameters are given in Table 4.4.

Table 4.3: Nominal time-delays and uncertainty bounds

	τ_1^{nom}	τ_2^{nom}	$\delta_1^{\max}$	$\delta_2^{\max}$
Case 1	1.0	1.0	0.25	0.25
Case 2	1.0	1.0	0.5	0.5
Case 3	2.0	2.0	0.5	0.5
Case 4	2.0	1.0	0.5	0.75
Case 5	3.0	1.0	1.0	0.75

Table 4.4: Controller design parameters for all cases

β_1	β_2	β_1^f	β_2^f	α_1	α_2	σ_1	σ_2
0.2	0.1	0.01	0.01	2/3	1/3	0.5	0.5

The performance level and actual stability margins of the controller designed by the causal and non-causal approach for each case are given in Tables 4.5 and 4.6, respectively. In addition to actual stability margins, the value of ρ, which is the $\mathcal{H}^\infty$ norm of the closed-loop TFM from w_1 to z_1 in Figure 4.2, for the designed controller for each case is also given. Moreover, in these tables, the length of the full stability range of the controllers designed by the both approaches is given. The length of the full stability range of the controller designed by the non-causal approach and the causal approach are $2\delta_i^{\text{act}}$ and δ_i^{act}, respectively.

As seen in the tables, the value of $1/\gamma^{opt}$ under non-causal approach is greater compared to causal approach in each case. This implies that, the controller designed by the non-causal approach has better performance property compared to the causal one. In addition, in all cases, the value of ρ under non-causal approach is smaller compared to causal approach in each case. Hence, all of the actual stability margins are greater under the non-causal approach compared to the causal approach. This implies that the controller designed by the non-causal approach is more robust than the controller designed by the causal approach against changes in the time-delays and their derivatives. Moreover,

Table 4.5: Performance level and stability margins for the causal approach

	$\frac{1}{\gamma^{\text{opt}}}$	ρ	δ_1^{act}	δ_2^{act}	β_1^{act}	β_2^{act}	$\beta_1^{f^{\text{act}}}$	$\beta_2^{f^{\text{act}}}$
Case 1	0.5540	1.8034	0.2773	0.2773	0.1165	0.0568	0.0058	0.0057
Case 2	0.4442	2.2501	0.4444	0.4444	0.0946	0.0458	0.0047	0.0046
Case 3	0.2767	3.6059	0.2773	0.2773	0.0601	0.0288	0.0030	0.0029
Case 4	0.3196	3.1249	0.3200	0.4800	0.0690	0.0332	0.0035	0.0033
Case 5	0.2403	4.1527	0.4816	0.3612	0.0524	0.0251	0.0026	0.0025

Table 4.6: Performance level and stability margins for the non-causal approach

	$\frac{1}{\gamma^{\text{opt}}}$	ρ	$2\delta_1^{\text{act}}$	$2\delta_2^{\text{act}}$	β_1^{act}	β_2^{act}	$\beta_1^{f^{\text{act}}}$	$\beta_2^{f^{\text{act}}}$
Case 1	0.6010	1.6609	0.3010	0.3010	0.1259	0.0615	0.0063	0.0061
Case 2	0.4854	2.0561	0.4864	0.4864	0.1030	0.0500	0.0051	0.0050
Case 3	0.3046	3.2762	0.3052	0.3052	0.0660	0.0317	0.0033	0.0032
Case 4	0.3451	2.8961	0.3453	0.5179	0.0743	0.0357	0.0037	0.0036
Case 5	0.2621	3.8135	0.5250	0.3930	0.0569	0.0272	0.0028	0.0027

in the non-causal approach, the guaranteed stability range for the variations in the time-delays is centered around the nominal time-delays, since the controller designed by the non-causal approach guarantees stability in the range $\tau_i^{\text{nom}} - \delta_i^{\text{act}} < \tau_i(t) < \tau_i^{\text{nom}} + \delta_i^{\text{act}}$, as long as $|\dot{\tau}_i(t)| < \beta_i^{\text{act}}$ and $|\dot{\tau}_i^f(t)| < \beta_i^{f^{\text{act}}}$ are also satisfied. On the other hand, assuming $|\dot{\tau}_i(t)| < \beta_i^{\text{act}}$ and $|\dot{\tau}_i^f(t)| < \beta_i^{f^{\text{act}}}$, the controller designed by the causal approach guarantees stability in the range $\tau_i^{\text{nom}} - \delta_i^{\max} < \tau_i(t) < \tau_i^{\text{nom}} - \delta_i^{\max} + \delta_i^{\text{act}}$. The guaranteed stability ranges for the five cases considered above are shown in Table 4.7 for both approaches. It is seen that in many cases the guaranteed stability range under the causal approach does not even include the nominal time-delay.

As seen in the tables given above, and also examined in [45] for different cases, the flow controllers designed by the non-causal approach exhibit better performance and robustness compared to ones designed by the causal approach. Now, let us consider the time-domain performance of the designed

Table 4.7: Time-delay range for guaranteed stability

	Channel 1		Channel 2	
	Causal	Non-Causal	Causal	Non-Causal
Case 1	(0.75, 1.0273)	(0.8495, 1.1505)	(0.75, 1.0273)	(0.8495, 1.1505)
Case 2	(0.5, 0.9444)	(0.7568, 1.2432)	(0.5, 0.9444)	(0.7568, 1.2432)
Case 3	(1.5, 1.7773)	(1.8474, 2.1526)	(1.5, 1.7773)	(1.8474, 2.1526)
Case 4	(1.5, 1.82)	(1.8274, 2.1727)	(0.25, 0.73)	(0.7410, 1.2590)
Case 5	(2.0, 2.482)	(2.475, 3.525)	(0.25, 0.611)	(0.607, 1.393)

controllers by both approaches. In order to compare the time-domain performance of the controllers designed by the causal approach to ones designed by the non-causal approach, a number of simulations will be carried out. We consider the same example network and the same cases for the nominal time delays and uncertainty bounds given in Table 4.3. The controller design parameters h_i and δ_i^+ are calculated as given in (4.43) and (4.44), for the causal and non-causal approaches respectively. The other controller design parameters are given in Table 4.4. The simulations are done using MATLAB/SIMULINK package, where non-linear effects are also taken into account. The buffer size (maximum queue length) is taken as 60 packets, the desired queue length, q_d, is taken as 30 packets, the capacity of the outgoing link (which equals to $c(t)$ when $q(t) > 0$) is taken as 90 packets/tu, where tu stands for the time-unit, and the rate limits of the sources are taken as 150 packets/tu in all cases. We consider a total of 8 different cases, where the actual time-delays (in tu) are shown in Table 4.8. In this table, Case ka, Case kb, etc. refer to a case where the controller designed for Case k of Table 4.3 is used ($k = 1, 2 \ldots, 5$). The minimum and maximum values of $\tau_i(t) := \tau_i^b(t) + \tau_i^f(t)$ are also shown in the last two columns of Table 4.8.

The simulation results are shown in Figures 4.21–4.28. In all figures, part (a) shows the results obtained for the controller designed using the causal approach and part (b) shows the results obtained for the controller designed using the non-causal approach. In all graphs, q is the queue length, $q(t)$ (whose

Table 4.8: Actual time-delays

	i	$\tau_i^b(t)$	$\tau_i^f(t)$	$\tau_i^{\min}$	$\tau_i^{\max}$
Case 1a	1	$0.48+0.04\sin(\frac{2\pi}{40}t)$	$0.48+0.02\sin(\frac{2\pi}{100}t)$	0.9	1.02
	2	$0.47+0.04\sin(\frac{2\pi}{50}t)$	$0.48+0.02\sin(\frac{2\pi}{100}t)$	0.89	1.01
Case 1b,2a	1	$0.5+0.2\sin(\frac{2\pi}{40}t)$	$0.5+0.1\sin(\frac{2\pi}{100}t)$	0.70	1.3
	2	$0.6+0.1\sin(\frac{2\pi}{50}t)$	$0.5+0.1\sin(\frac{2\pi}{100}t)$	0.9	1.3
Case 3a	1	$1.2+ 0.1\sin(\frac{2\pi}{40}t)$	$0.8+0.1\sin(\frac{2\pi}{100}t)$	1.8	2.2
	2	$1.1+0.05\sin(\frac{2\pi}{50}t)$	$0.9+0.05\sin(\frac{2\pi}{100}t)$	1.9	2.1
Case 4a	1	$0.9+0.08\sin(\frac{2\pi}{40}t)$	$0.7+0.01\sin(\frac{2\pi}{100}t)$	1.51	1.69
	2	$0.3+0.1\sin(\frac{2\pi}{50}t)$	$0.2+0.05\sin(\frac{2\pi}{100}t)$	0.35	0.65
Case 4b	1	$1.1+0.1\sin(\frac{2\pi}{40}t)$	$0.9+0.05\sin(\frac{2\pi}{100}t)$	1.85	2.15
	2	$0.6+0.1\sin(\frac{2\pi}{50}t)$	$0.4+0.1\sin(\frac{2\pi}{100}t)$	0.8	1.2
Case 4c	1	$1.9+0.2\sin(\frac{2\pi}{40}t)$	$1.0+0.1\sin(\frac{2\pi}{100}t)$	2.6	3.2
	2	$0.8+0.1\sin(\frac{2\pi}{50}t)$	$0.6+0.05\sin(\frac{2\pi}{100}t)$	1.25	1.55
Case 5a	1	$2.5+0.1\sin(\frac{2\pi}{40}t)$	$1.0+0.05\sin(\frac{2\pi}{100}t)$	3.35	3.75
	2	$0.8+0.1\sin(\frac{2\pi}{50}t)$	$0.6+0.05\sin(\frac{2\pi}{100}t)$	1.25	1.55

scale is shown on the right-hand-side of each graph), and $\mathrm{r}_i^{\mathrm{s}}$ is the actual rate at which data is send from source i, $i = 1, 2$, (whose scale is shown on the left-hand-side of each graph).

Case 1a: In this case, the actual time-delays vary within the guaranteed stability range of the controllers designed by the causal and non-causal approaches. As seen in Figure 4.21, both controllers stabilize the actual system and achieve the tracking (4.5) and the weighted fairness (4.6) requirements. As seen by comparing Figure 4.21(a) to (b), the response of the controller designed by the non-causal approach is faster compared to the controller designed by the causal approach

Case 1b: In this case, we apply the same controller designed for Case 1a, however, the actual time-delays vary within a wider range compared to the actual time-delays in Case 1a. In addition, the range in this case is outside

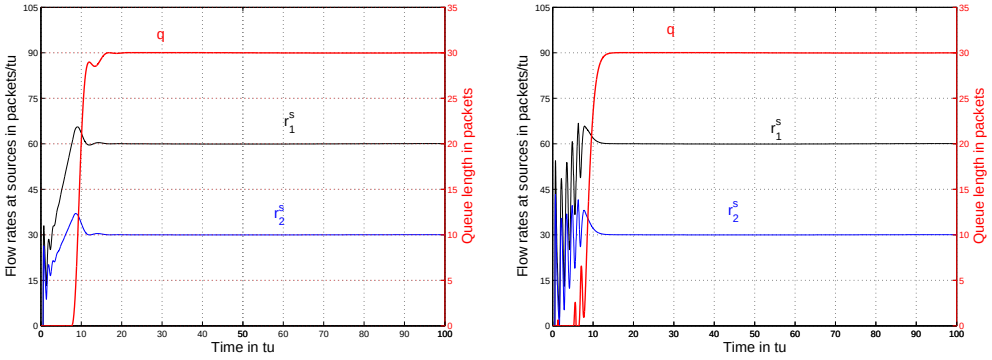

(a) (b)

Figure 4.21: Simulation results for Case 1a

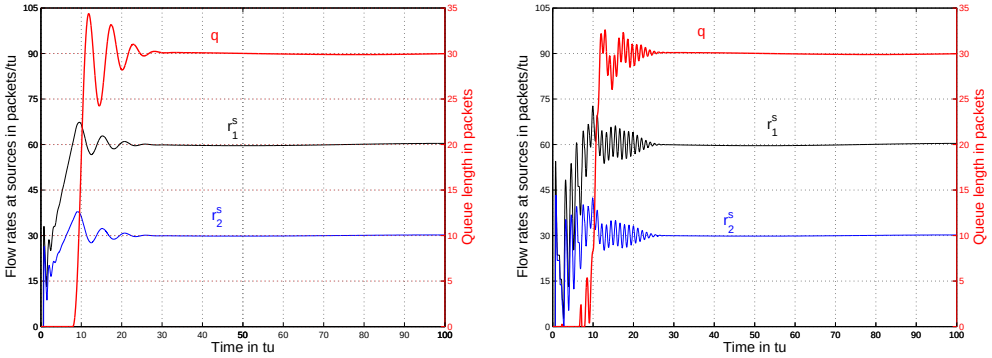

(a) (b)

Figure 4.22: Simulation results for Case 1b

the guaranteed stability range of both controllers. However, both controllers stabilize the actual system and achieve the design requirements, as seen in Figure 4.22. The response of the controller designed by the causal approach has larger overshoots and longer settling time compared to the response of the controller designed by the non-causal approach. Non-causal approach, on the other hand, provides a more oscillatory transient response.

Case 2a: In this case, the used controllers provide a wider range of variations in the actual time-delays compared to Cases 1a and 1b. Similar to Case 1b, the actual time-delays in this case are outside of the guaranteed stability range of both controllers, however, they stabilize the actual system and achieve the design requirements as shown in Figure 4.23. As seen in Figure 4.23, the response

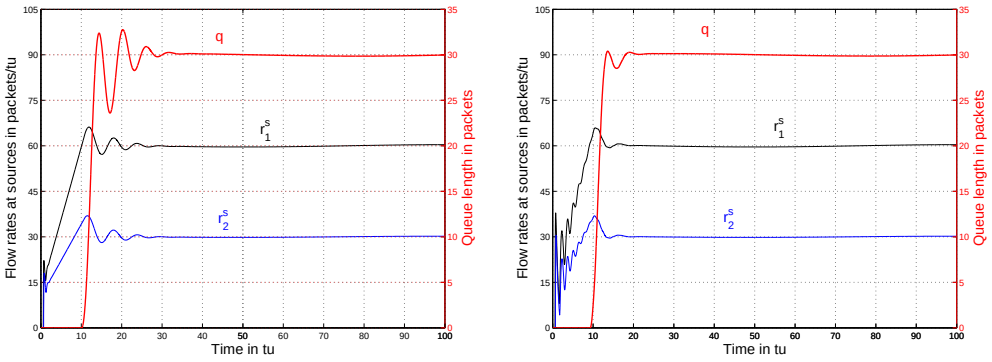

(a) (b)

Figure 4.23: Simulation results for Case 2a

of the controller designed by the non-causal approach is faster compared to the controller designed by the causal approach. In addition, the queue length in Figure 4.23(b) settles to the desired queue length with smaller overshoots and undershoots compared to the queue length in Figure 4.23(a).

Case 3a: In this case, the actual time-delays vary around the nominal time-delays given in Table 4.3, and within the guaranteed stability range of the controller designed by the non-causal approach. However, they are outside the guaranteed stability range of the controller designed by the causal approach. As seen in Figure 4.24(b), the controller designed by the non-causal approach stabilizes the actual system and achieves the design requirements. However, the controller designed by the causal approach can not stabilize the system as shown in Figure 4.24(a).

Case 4a: In this case, the actual time-delays lie within the guaranteed stability range of the controller designed by the causal approach, however, outside the guaranteed stability range of the controller designed by the non-causal approach. However, as seen in Figure 4.25(b), the controller designed by the non-causal approach stabilizes the actual system and achieves the design requirements with a small overshoot. As seen in Figure 4.25(a), the controller designed by the causal approach achieves the design requirements with a smoother response compared to the response of the controller designed by the non-causal approach.

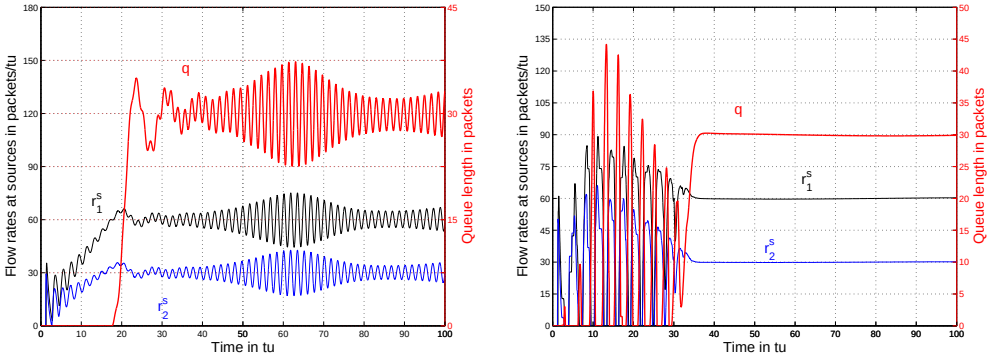

(a) (b)

Figure 4.24: Simulation results for Case 3a

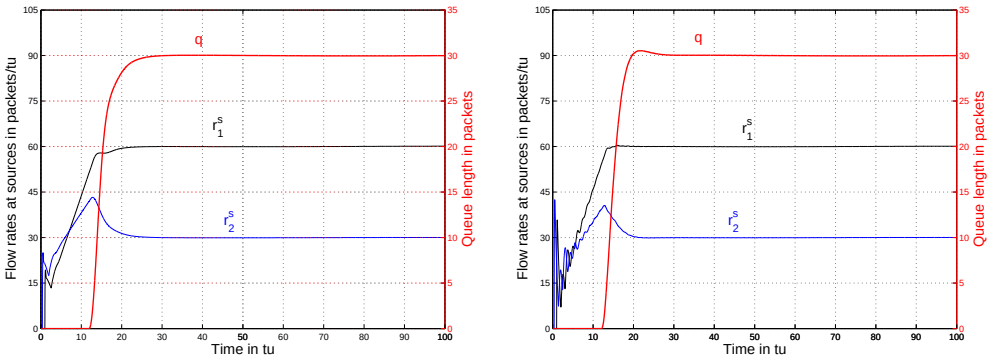

(a) (b)

Figure 4.25: Simulation results for Case 4a

Case 4b: In this case, the actual time-delays lie in the guaranteed stability range of the controller designed by the non-causal approach, however, outside the guaranteed stability range of the controller designed by the causal approach. As seen in Figure 4.26(a), the controller designed by the causal approach stabilizes the actual system with larger overshoots and undershoots compared to the controller designed by the non-causal approach. Moreover, the settling time of the controller designed by the causal approach is longer compared to that of the controller designed by the non-causal approach.

Case 4c: In this case, the actual time-delays are outside the guaranteed stability range of both controllers. As seen in Figure 4.27(a), the controller designed by the causal approach does not stabilize the system, however, as shown in

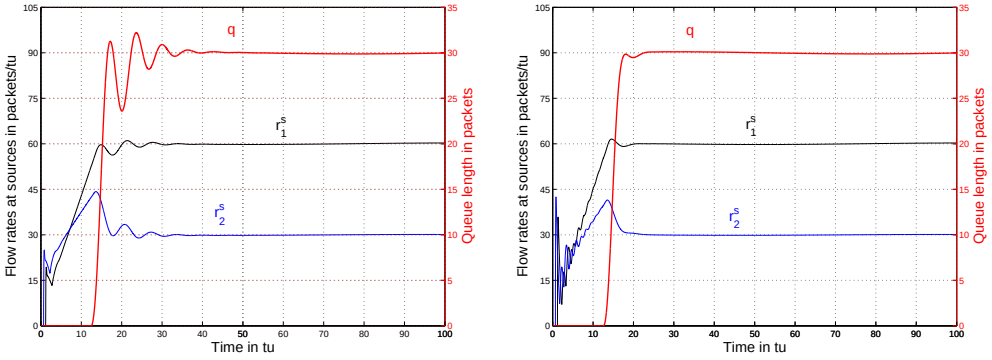

(a) (b)

Figure 4.26: Simulation results for Case 4b

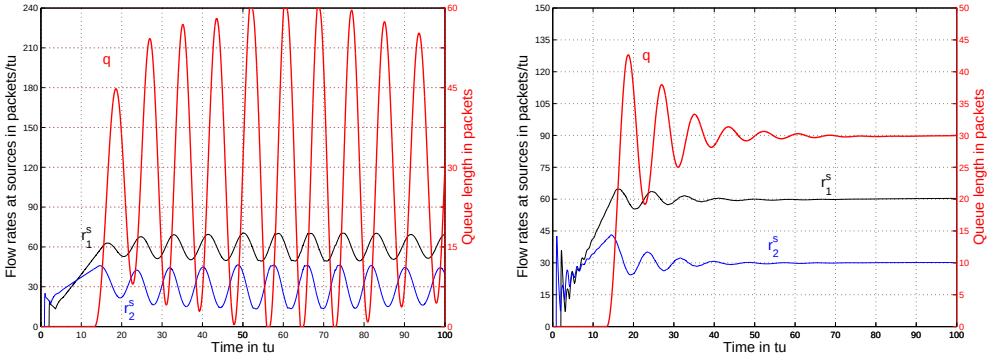

(a) (b)

Figure 4.27: Simulation results for Case 4c

Figure 4.27(b), the controller designed by the non-causal approach stabilizes the actual system and achieves all the design requirements.

Case 5a: In this case, similar to Case 4c, the actual time delays are outside the guaranteed range of both controllers. However, the used controllers satisfy a wider range of variations in the actual time-delays compared to Case 4c. As seen in Figure 4.28, both controllers stabilize the system, however, the controller designed by the non-causal approach has a faster response with less overshoots.

As seen in the simulation results (not only the ones presented here, but also many others), the non-causal approach in general produces faster responses with smaller overshoots compared to the causal approach. Further-

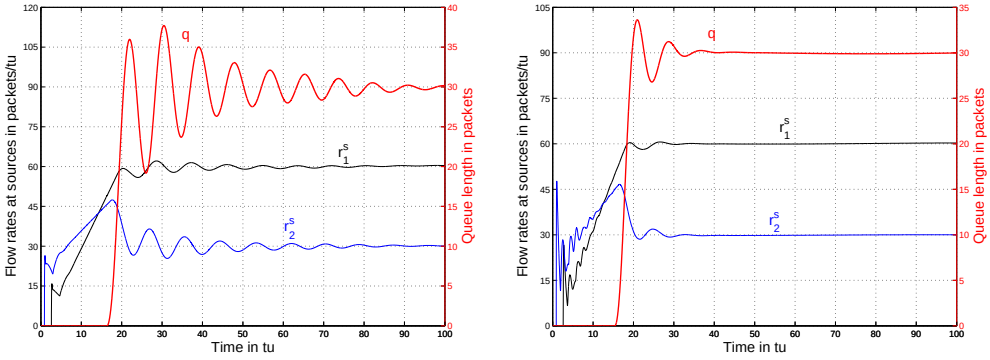

(a) (b)

Figure 4.28: Simulation results for Case 5a

more, the controllers designed by the non-causal approach have better stability robustness, in general (e.g, see Case 3a, Case 4c, Case 5a). Moreover, due to their faster response, controllers designed by the non-causal approach produce smaller steady-state oscillations in many cases (e.g., see Case 2a, Case 5a). The presented simulation results for different cases and actual time-delays in [37,45] indicate the same results.

4.7 Robust Controller Design for Data-Communication Networks to Satisfy Fair Capacity Sharing

In order to design a robust flow controller, which achieves the design objectives introduced in Section 4.2, a controller was designed to satisfy the internal stability of the nominal system in Figure 4.3 ($\Delta = 0$) and minimize the $\mathcal{H}^\infty$ norm of the closed-loop TFM from $w = \begin{bmatrix} w_1^T & d^T \end{bmatrix}^T$ to $z = \begin{bmatrix} z_1^T & e_1^T & e_2^T \end{bmatrix}^T$, called T_{zw}, in Figure 4.3. The signals z_1, e_1, and e_2 in Figure 4.3 were introduced, respectively, for the robustness, tracking, and weighted fairness requirements. An internally stabilizing robust flow controller can alternatively be designed to minimize the $\mathcal{H}^\infty$ norm of the closed-loop TFM from w to $\hat{z} := \begin{bmatrix} z_1^T & e_1^T \end{bmatrix}^T$, called $T_{\hat{z}w}$. The weighted fairness requirement is not considered in the latter $\mathcal{H}^\infty$ minimization problem. However, by utilizing the parametrization of the controller, (4.35), a contractive parameter Q_Λ can

be chosen appropriately, if it is possible, such that the weighted fairness requirement is achieved by the controller. Note that the $\mathcal{H}^\infty$ norm of the TFM $T_{\hat{z}w}$ for the controller, which is designed to minimize the $\mathcal{H}^\infty$ norm of the TFM $T_{\hat{z}w}$ is less than or equal to the $\mathcal{H}^\infty$ norm of the TFM $T_{\hat{z}w}$ for the controller, which is designed to minimize the $\mathcal{H}^\infty$ norm of the TFM T_{zw}. Hence, the controller, which is designed to minimize the $\mathcal{H}^\infty$ norm of the TFM $T_{\hat{z}w}$ and achieves the weighted fairness requirement by a chosen appropriate Q_Λ, if it exists, may be more robust and have better tracking properties compared to the controller designed to minimize the $\mathcal{H}^\infty$ norm of the TFM T_{zw}.

In this section, we give the sufficient conditions to choose the free parameter Q_Λ in the structure of the controller (see Section 4.3), which minimizes the $\mathcal{H}^\infty$ norm of the TFM $T_{\hat{z}w}$ to satisfy the robustness and tracking requirement (4.5), also meets the weighted fairness requirement (4.6). Therefore, to design such a flow controller a new mixed sensitivity minimization problem is defined as depicted in Figure 4.29. In this problem, there does not exist a weighting function to achieve the weighted fairness requirement by the controller compared to the mixed sensitivity minimization problem defined in Section 4.3, i.e., e_2 in Figure 4.3 does not exist in Figure 4.29. Using the $\mathcal{H}^\infty$ controller design procedure given in Section 4.3, an optimal $\mathcal{H}^\infty$ flow controller can be designed for the system depicted in Figure 4.29. In the sequel, the sufficient conditions are given to choose an appropriate Q_Λ such that the designed controller for the mixed sensitivity minimization problem depicted in Figure 4.29 meets the weighted fairness requirement. The results presented in this section have been published in [46]. However, the example cases considered here are different than those in [46].

From the structure of the designed flow controller in Section 4.3, the designed controller K in Figure 4.7 can be written in the Laplace domain as:

$$K(s) = R(s)H(s)\left[1 + D(s)H(s)\right]^{-1}\kappa\frac{s+\epsilon}{s}, \tag{4.45}$$

where

$$H(s) = HM(G_\Lambda^{-1}, Q_\Lambda) \tag{4.46}$$

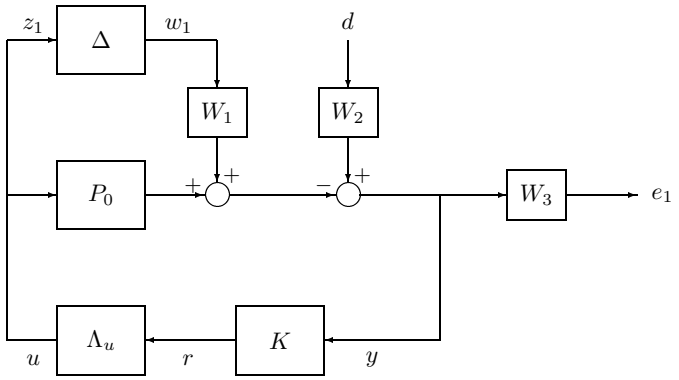

Figure 4.29: Mixed sensitivity minimization problem [46]

$$R(s) = \begin{bmatrix} I_{l_1} & 0 & 0 & \cdots & 0 \\ \Pi_{11}^{N} & I_{l_2} & \ddots & \ddots & \vdots \\ \Pi_{11}^{N-1} e^{-(\bar{h}_1 - \bar{h}_2)s} I_{l_1} & \Pi_{12}^{N-1} & I_{l_3} & \ddots & 0 \\ +\Pi_{12}^{N-1}\Pi_{11}^{N} + \Pi_{21}^{N} & & & & \\ & \ddots & \ddots & \ddots & \vdots \\ & & & \Pi_{1(N-1)}^{2} & I_{l_N} \end{bmatrix} \tag{4.47}$$

$$D(s) = \begin{bmatrix} \Pi_{11}^{1} e^{-(\bar{h}_1 - \bar{h}_N)s} I_{l_1} + \cdots + \Pi_{N1}^{N} & \cdots & \Pi_{1N}^{1} \end{bmatrix}.$$

Let K_j be the j^{th} element of the designed controller K, given in (4.45). Then, from Figure 4.2, since $q_d(t) = q_d$, a constant (hence $q_d(s) = \frac{1}{s} q_d$), the j^{th} element of $r(s)$, $r_j(s)$, can be written as:

$$r_j(s) = K_j(s) \left(1 + P_o(s)\Lambda_u(s)K(s)\right)^{-1} \frac{1}{s} \left(q_d + c(s)\right), \tag{4.48}$$

where it is assumed that $\Delta = 0$. Similar to Section 4.2, it was assumed that $\lim_{t\to\infty} c(t) = c_\infty$. The weighted fairness requirement, (4.6), implies that $\lim_{t\to\infty} \sum_{j=1}^{n} r_j(t) = c_\infty$. Utilizing this fact and the final value theorem [64], i.e., $\lim_{t\to\infty} r_j(t) = \lim_{s\to 0} s r_j(s)$, an equivalent expression to the weighted fairness requirement can be written as

$$\lim_{s\to 0} \frac{K_j(s)}{K_1(s) + \cdots + K_n(s)} = \alpha_j \ , \qquad j = 1, \ldots, n, \tag{4.49}$$

where $\sum_{j=1}^{n} \alpha_j = 1$.

To write (4.49) in terms of Q_Λ, let us partition the TFM G_Λ^{-1} compatibly with Q_Λ such that $G_\Lambda^{-1}(s) =: \begin{bmatrix} G_{11} & G_{12} \\ G_{21} & G_{22} \end{bmatrix}$, where G_{11} is $n \times n$ dimensional and G_{22} is 1×1 dimensional. Let us define

$$H_n(s) := G_{11}(s)Q_\Lambda(s) + G_{12}(s) \tag{4.50}$$

and $H_d(s) := G_{21}(s)Q_\Lambda(s) + G_{22}(s)$. Then, $H(s)$ in (4.46) can be written as $H(s) = H_n(s)H_d^{-1}(s)$. Now, if $R_j(s)$ denotes the j^{th} row of $R(s)$ in (4.47), the j^{th} element of the controller $K(s)$, $K_j(s)$, can be written as,

$$K_j(s) = R_j(s)H_n(s)\frac{\kappa(s+\epsilon)}{s\left(H_d(s) + D(s)H_n(s)\right)}. \tag{4.51}$$

If $K_j(s)$ in (4.51) is substituted in (4.49), then it is obtained that

$$R(0)H_n(0) = \alpha \mathbf{1}_n R(0)H_n(0), \tag{4.52}$$

where $\alpha := [\alpha_1 \ \cdots \ \alpha_n]^T$. Let us define $Z := R(0) - \alpha \mathbf{1}_n R(0)$. Therefore, (4.52) implies that $ZH_n(0) = 0$. However, since $R(0)$ is nonsingular and $\mathbf{1}_n\alpha = 1$, there exists a nonzero x such that $Zx = 0$, i.e. Z is singular. In addition, the rank of Z is $n-1$. Hence, x is unique up to a multiplication by a scalar.

Now, using the above definitions, we can derive the sufficient conditions to choose the appropriate Q_Λ. Let x be a nonzero vector such that $Zx = 0$. Therefore, there exists a scalar parameter ψ such that $H_n(0) = \psi x$. From (4.50), if Q_Λ is chosen to satisfy

$$G_{11}(0)Q_\Lambda(0) = \psi x - G_{12}(0), \tag{4.53}$$

or

$$Q_\Lambda(0) = G_{11}^{-1}(0)\left(\psi x - G_{12}(0)\right), \tag{4.54}$$

if $G_{11}(0)$ is nonsingular, then the designed stabilizing controller K for the mixed sensitivity minimization problem depicted in Figure 4.29 also satisfies the weighted fairness condition. However, the free parameter Q_Λ in the controller structure should be contractive. Since $\|Q_\Lambda\|_\infty \geq \overline{\sigma}\left(Q_\Lambda(0)\right)$, $Q_\Lambda(0)$ should also satisfy that $\overline{\sigma}\left(Q_\Lambda(0)\right) < 1$. Therefore, for an arbitrary ψ, if there

exists any contractive Q_Λ such that $Q_\Lambda(0)$ satisfies (4.53) or (4.54), then the designed flow controller for the problem depicted in Figure 4.29 satisfies the weighted fairness requirement. Hence, if there exists a contractive $Q_\Lambda(0)$ which satisfies (4.53) or (4.54), one can choose $Q_\Lambda(s) = Q_\Lambda(0)$, i.e., a constant matrix.

However, there may not exist any ψ such that $\overline{\sigma}\left(Q_\Lambda(0)\right) < 1$. In this case, there may not exist any Q_Λ which satisfies the weighted fairness condition for the given γ and α values. In this case, either new α_i values may be chosen to find appropriate Q_Λ or the sensitivity level may be increased and ψ is sought for the new designed controller.

To illustrate the performance of the controllers designed by the approach proposed in this section, a network with two sources, as depicted in Figure 4.8, is considered. The nominal time-delays are assumed to be $h_1 = 3$ tu and $h_2 = 1$ tu, where tu stands for the time unit. Other design parameters are taken as $\delta_1^+ = 0.5$, $\delta_2^+ = 1.0$, $\beta_1 = 0.2$, $\beta_2 = 0.3$, $\beta_1^f = 0.2$, $\beta_2^f = 0.1$, $\sigma_1 = 0.25$. To evaluate the performance of the designed controllers by the approach proposed in this section, the optimal flow controllers are also designed by the approach of Section 4.3 for the same design parameters with $\sigma_2 = 0.25$. The simulations are done using MATLAB/SIMULINK package, where the desired queue length, q_d, is taken as 30 packets and the buffer size (maximum queue length) is taken as 60 packets. Moreover, the capacity of the outgoing link is taken as 90 packets/tu and the rate limits for the sources are taken as 150 packets/tu. The uncertain part of the actual time-delays used in the simulations are given in Table 4.9. In all cases, $h_i^b = h_i^f = \frac{1}{2}h_i$, $i = 1, 2$. The simulation results for both controllers designed by the approach in Section 4.3 and in this section are given in Figures 4.30–4.31. In both figures, (a) represents the response of the controller designed by the approach presented in this section and (b) represents the response of the controller designed by the approach of Section 4.3. In addition, in all figures, q (whose scale is on the right) is the queue length and $\mathrm{r}_i^{\mathrm{s}}$ (whose scale is on the left) is the actual flow rate at source i, for $i = 1, 2$.

Table 4.9: Uncertain part of the actual time-delays

i	$\delta_i^b(t)$	$\delta_i^f(t)$
1	$0.5+0.7\sin(\frac{2\pi}{50}t)$	$0.1+0.1\sin(\frac{2\pi}{100}t)$
2	$0.6+0.9\sin(\frac{2\pi}{40}t)$	$0.1+0.2\sin(\frac{2\pi}{80}t)$

Case 1: In this case, the controllers are designed for $\alpha_1 = \frac{2}{3}$, $\alpha_2 = \frac{1}{3}$. Utilizing the approach proposed in this section, the optimal $\mathcal{H}^\infty$ flow controller is obtained for the optimal sensitivity level $\gamma^{n^{opt}}$, where $\gamma^{n^{opt}} = 3.530$. In order to achieve the weighted fairness requirement by the controller designed here, the contractive Q_Λ is obtained by (4.54), where ψ varies between -10 and 10. The ψ value achieving the minimum $\overline{\sigma}(Q_\Lambda(0))$, which is also less than 1, is chosen and Q_Λ is obtained as $Q_\Lambda = [0.297 \;\; 0.954]^T$ for $\psi = 0.3$. By the approach of Section 4.3, the optimal $\mathcal{H}^\infty$ flow controller is obtained for γ^{opt_1}, where $\gamma^{opt_1} = 3.920$. In the optimal controller, Q_Λ is taken as $Q_\Lambda = 0$. As seen in Table 4.10, the controller designed by the approach proposed here yields greater $\dfrac{1}{\rho}$ compared to the controller designed by the approach of Section 4.3, where ρ is the $\mathcal{H}^\infty$ norm of the closed-loop TFM from w_1 to z_1 in Figure 4.2. Therefore, by (4.40) and (4.41), the actual stability margins of the controller designed by the approach proposed here are larger compared to the ones designed by the approach of Section 4.3. Hence, the controller designed by the approach proposed here has better robustness property compared to the one which is designed by the approach of Section 4.3.

The response of the designed controllers by both approaches are presented in Figure 4.30. As seen in this figure, both controllers robustly stabilize the actual system and achieve the tracking (4.5) and the weighted fairness (4.6) requirements. The controller designed by the approach proposed here achieves the weighted fairness requirement at the steady-state. However, by the approach of Section 4.3, since the weighted fairness requirement was included in the $\mathcal{H}^\infty$ minimization problem, the controller tries to achieve the

Table 4.10: Upper bound on the L_2 induced norm of Δ and $\mathcal{H}^\infty$ norm of the TFM $T_{\hat{z}w}$

Case	The controller is designed by the	$\frac{1}{\rho}$	$\|T_{\hat{z}w}\|_\infty$
1	approach proposed in this section	0.289	3.530
	approach of Section 4.3	0.259	3.867
2	approach proposed in this section	0.288	3.530
	approach of Section 4.3	0.273	3.680

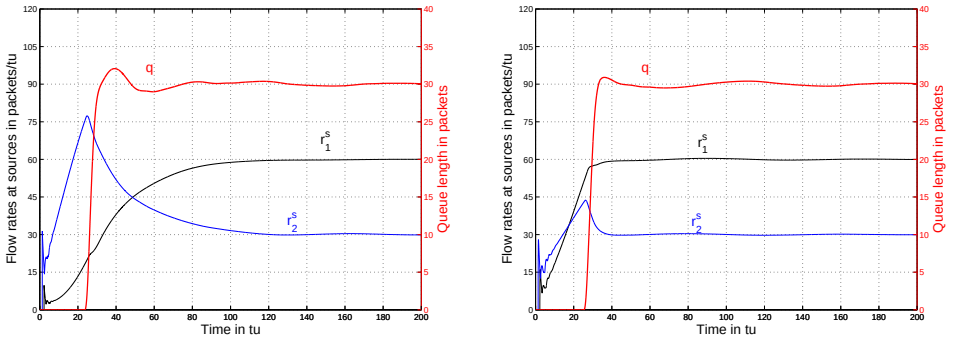

Figure 4.30: Time-domain response of the controllers designed for Case 1

weighted fairness requirement while achieving the robustness and the tracking requirements. Hence, as seen by comparing Figure 4.30(a) to (b), the flow rates in Figure 4.30(a) settle later than the flow rates in Figure 4.30(b). The flow rate at source 2 in Figure 4.30(a) rises faster compared to the flow rate at source 1 in Figure 4.30(a) to achieve the tracking requirement, due to the smaller nominal time-delay in channel 2 compared to the one in channel 1. As seen in Table 4.10, the $\mathcal{H}^\infty$ norm of the TFM $T_{\hat{z}w}$, for the controller designed here is less than the $\mathcal{H}^\infty$ norm of the TFM $T_{\hat{z}w}$, for the controller designed by the approach of Section 4.3, which is an expected result. Therefore, the robust controller designed by the approach proposed here may have a faster queue response compared to the one designed by the approach of Section 4.3. Thus, as seen by comparing Figure 4.30(a) to (b) , the queue length in Figure 4.30(a)

leaves 0 before the queue length in Figure 4.30(b).

Case 2: In this case, the controllers are designed for $\alpha_1 = \frac{1}{3}$, $\alpha_2 = \frac{2}{3}$. The designed stabilizing optimal controller by the approach proposed here is obtained for the same $\gamma^{n^{opt}}$ value, where $\gamma^{n^{opt}} = 3.530$. To achieve the weighted fairness requirement by the controller designed here, the contractive Q_Λ is obtained by the same procedure as in Case 1. Hence, Q_Λ is obtained as $Q_\Lambda = [0.323 \;\; 0.943]^T$, where ψ in (4.54) is obtained as $\psi = 0.77$. The stabilizing optimal controller designed by the approach of Section 4.3 is obtained at γ^{opt_2}, where $\gamma^{opt_2} = 3.730$, and Q_Λ is taken as $Q_\Lambda = 0$. Similar to Case 1, as seen in Table 4.10, the controller designed by the approach proposed here stabilizes the actual system for a wider uncertainty set and yields smaller $\mathcal{H}^\infty$ norm for the TFM $T_{\hat{z}w}$ compared to that of the controller designed by the approach of Section 4.3.

The response of the designed controllers by both approaches is presented in Figure 4.31. As seen in Figure 4.31, similar to Case 1, the flow rates in Figure 4.31(b) settle before the flow rates in Figure 4.31(a), and the queue length in Figure 4.31(a) leaves from 0 before the queue length in Figure 4.31(b). In this case, different than Case 1, source 2, which is subject to a smaller nominal time-delay compared to source 1 (and hence responds faster than source 1, as explained in Case 1), shares more of the network capacity at the steady-state. Therefore, the flow rates at sources in Figure 4.31 settle before the flow rates at sources in Figure 4.30.

As shown by the presented simulations above, the controllers designed by the approach proposed here stabilize the actual system and achieve the tracking and the weighted fairness requirements. In addition, the controllers designed here have better robustness properties and a faster queue response compared to the controllers designed by the approach of Section 4.3. However, since the controller designed here achieves the weighted fairness requirement at the steady-state, flow rates of data for the controller designed here settle later than the ones for the controller designed by the approach of Section 4.3.

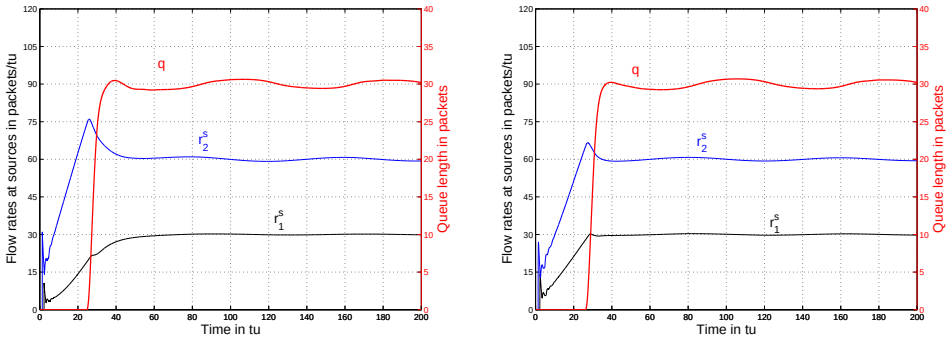

Figure 4.31: Time-domain response of the controllers designed for Case 2

4.8 Summary

In this chapter, a stabilizing optimal $\mathcal{H}^\infty$ flow controller design for data-communication networks with multiple time-delays was considered by utilizing non-causal uncertainty blocks. A stabilizing controller was designed by solving an $\mathcal{H}^\infty$ optimization problem using the method of [13]. Unlike [23], where only a suboptimal solution could be found, the present approach allows designing an optimal controller. In order to illustrate the time-domain performance of the designed flow controllers by the approach presented in Section 4.3, simulations were done in Section 4.4. In these simulations, a discrete model was used rather than the fluid-flow model which was used in the controller design. As shown in the presented simulations, the designed flow controllers drive the queue length at the bottleneck node to the desired level as required by (4.5) against the presence of uncertain time-varying time-delays and satisfy that the network capacity is shared fairly among the sources, according to (4.6). Moreover, to show the performance improvement of the flow controllers designed by the approach presented in Section 4.3, the designed flow controllers were compared to the controllers designed by the approach of [23]. As shown by the simulations, the response of the controller designed by the approach of [23] is slower compared to the response of the controller designed by the approach in Section 4.3. In addition, the controller designed by the approach of [23] can produce an unstable response for certain relatively large

uncertainties in the time-delays while the controller designed by the approach presented in Section 4.3 can stabilize the system. This shows that the controller designed by the approach proposed in Section 4.3 has better robustness properties than the controller of [23]. These results are also obtained in [43] considering a number of simulations. One of the important differences between the approach presented in Section 4.3 and the approach of [23] is the existence of design parameters σ_1 and σ_2, which bring flexibility in the controller design.

The performance level and stability margins of the optimal $\mathcal{H}^\infty$ flow controllers were examined in Section 4.5. As discussed in Section 4.5, also in [44], to improve the robustness of the flow controllers designed by the approach proposed in Section 4.3, the design parameters β_i, β_i^f, and δ_i^+ should be chosen large enough, except that β_i should not be chosen close to 1. However, these design parameters must be kept small in order to improve the performance of the flow controllers.

As shown in Section 4.6, the controllers obtained by the non-causal approach presented in Section 4.3 have better performance and robustness properties compared to the controllers obtained by the causal approach of [40–42]. A number of simulations were done using MATLAB/SIMULINK package, where nonlinearities of the model were also taken into account. Similar to the results in [37], [45], the controllers designed by the non-causal approach produced faster responses with smaller overshoots compared to the controllers designed by the causal approach in all cases. In addition, it was shown that the controller designed by the causal approach can produce an unstable response while the controller designed by the non-causal approach stabilizes the system. Therefore, the controllers designed by the non-causal approach have better robustness properties, in general.

In Section 4.7, the sufficient conditions were presented to choose an appropriate Q_Λ to yield a controller, which was designed to achieve only the robustness and the tracking requirements, also achieves the weighted fairness requirement. By the approach proposed in Section 4.7, the flow controllers

were designed to satisfy less number of objectives compared to the controllers designed by the approach of Section 4.3, since the remaining objective was met by choosing the appropriate contractive parameter Q_Λ. This yields that the controller designed by the approach of Section 4.7 has greater actual stability margins than the actual stability margins of the controller designed by the approach of Section 4.3. In addition, the approach of Section 4.7 produces a controller with a faster tracking response compared to the controller obtained by the approach of Section 4.3. Hence, the controllers designed by the approach of Section 4.7 have better robustness and tracking properties compared to the controllers designed by the approach of Section 4.3. To illustrate the performance of the controllers designed by the approach proposed in Section 4.7, simulation studies were performed using MATLAB/SIMULINK package. As seen in the simulation results, the controllers designed by the approach proposed in Section 4.7 stabilize the actual system and achieve the tracking and the weighted fairness requirements.

5 STABLE $\mathcal{H}^\infty$ FLOW CONTROLLER DESIGN

In controller design, the first requirement is to guarantee the internal stability of the closed-loop system. Therefore, resulting stabilizing controllers may be unstable. However, unstable controllers introduce additional right half-plane zeros to the closed loop system, which degenerate the tracking and disturbance rejection abilities of the closed-loop system, and result unpredictable response in presence of sensor faults and non-linear effects. In addition, since the designed optimal/suboptimal controllers for infinite dimensional systems are irrational in general (see [6, 65, 66] also Section 4.3), their rational approximation may not be obtained easily, if the designed irrational stabilizing controller is unstable [65]. Therefore, stable controllers are often desired, if it is possible. In addition, the stable controller design has also strong connections with the simultaneous stabilization problem [31].

The necessary and sufficient condition for the existence of a stable controller for a given plant is whether the plant satisfies the parity interlacing property, (p.i.p) [31]. A plant is said to satisfy the p.i.p if the number of its poles between any pair of its real right half-plane blocking zeros is even [31].

Stable $\mathcal{H}^\infty$ controller design is more difficult compared to the stable controller design, since the designed controller should also achieve some $\mathcal{H}^\infty$ norm constraints. In the literature, there exist numerous stable and stable $\mathcal{H}^\infty$ controller design approaches for finite dimensional systems (e.g. [26], [28] and references therein). However, if time-delay systems are considered, there exists only a few papers. The sufficient and necessary conditions for the existence of a stable controller for SISO systems with a single time-delay were presented in [33]. In [34], stable controller design approach was presented for a SISO system with a single time-delay by using the interpolation approach. Stable $\mathcal{H}^\infty$ controller design for a general SISO system with multiple-time-delays was

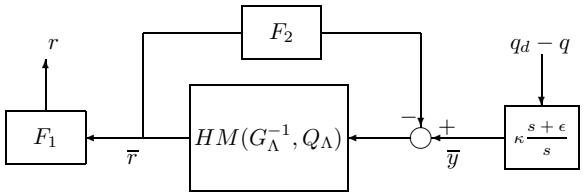

Figure 5.1: Structure of the controller K [47]

presented recently in [9, 35].

In this chapter, a number of different stable $\mathcal{H}^\infty$ flow controller design algorithms are presented. In Section 5.1, the stable $\mathcal{H}^\infty$ flow controller design problem is posed. In Section 5.2, a stable $\mathcal{H}^\infty$ flow controller design is proposed which is based on the small-gain theorem [3–5]. In Section 5.3, a less conservative methodology compared to the one in Section 5.2 is presented. In Section 5.4, two algorithms based on stabilization of the finite-dimensional part of the controller are proposed. In Section 5.5, the proposed algorithm is based on seeking a stable $\mathcal{H}^\infty$ flow controller by increasing the gain of the uncertainty weight in the robust control problem setup. In Section 5.6, firstly, two different rational approximations of an FIR filter are summarized, then, three different stable $\mathcal{H}^\infty$ flow controller design methodologies are presented, each of which is based on solving the strong stabilization problem by utilizing a rational approximation of the existing FIR block in the controller structure.

5.1 Stable $\mathcal{H}^\infty$ Flow Controller Design for Systems with Multiple Time-Delays

In this section, stable $\mathcal{H}^\infty$ flow controller design problem is stated. In order to pose the problem clearly, let us consider the structure of the controller depicted in Figure 5.1, which is the simplified representation of Figure 4.7. Here, F_1 and F_2 are stable blocks which consist of delays and FIR filters.

Any controller K, including K^{opt}, obtained by the approach proposed

in Chapter 4, is unstable due to the integral term (see Figure 5.1), which is required to ensure the tracking requirement. However, the rest of the controller, i.e., the part from $\bar{y}$ to r in Figure 5.1 may or may not be stable. When this part is unstable, due to nonlinearities in the system (i.e., the hard constraints), an unstable behaviour may be observed, at least for certain actual time-delays and/or initial conditions (see [42] and Section 5.3 for example cases). In order to avoid such undesirable behaviour, stable $\mathcal{H}^\infty$ flow controllers may be designed, since stable controllers are less sensitive to the unmodelled dynamics. In the following sections, design methodologies are proposed which ensure that the TFM from $\bar{y}$ to r in Figure 5.1 is stable. For brevity, in the sequel, stable $\mathcal{H}^\infty$ flow controller means that the TFM from $\bar{y}$ to r in Figure 5.1 is stable.

5.2 Stable $\mathcal{H}^\infty$ Flow Controller Design Methodology by Utilizing the Small-Gain Theorem

In this section, a design methodology to obtain a stable $\mathcal{H}^\infty$ flow controller to solve the problem presented in the previous section is proposed. The stable controller is obtained by utilizing the contractive free parameter Q_Λ, which is to be designed to stabilize the TFM from $\bar{y}$ to r in Figure 5.1 while keeping its contractiveness. Such Q_Λ may or may not exist for a given sensitivity level γ. Therefore, the proposed approach is based on seeking a contractive Q_Λ, which stabilizes the TFM from $\bar{y}$ to r in Figure 5.1, by increasing the sensitivity level γ, starting from the optimal sensitivity level, γ^{opt}. The results presented in this section have been published in [47].

In Figure 5.1, since F_1 and F_2 blocks consist of time-delays and FIR filters, both F_1 and F_2 are stable. Therefore, $\gamma_{F_2} := \|F_2\|_\infty$ is finite. Since F_1 is bistable, the mapping from $\bar{y}$ to r is stable if and only if the mapping from $\bar{y}$ to $\bar{r}$ is stable. Hence, by the small-gain theorem (e.g., see [5]), the mapping from $\bar{y}$ to $\bar{r}$ is stable if $HM(G_\Lambda^{-1}, Q_\Lambda)$ is stable and $\|HM(G_\Lambda^{-1}, Q_\Lambda)\|_\infty < 1/\gamma_{F_2}$. Furthermore, for the robust stability of the overall system, Q_Λ must be contractive

(see Section 4.3). Therefore, to solve our problem, we state the problem as to find a Q_Λ such that

$$HM(G_\Lambda^{-1}, Q_\Lambda) \in \mathcal{RH}^\infty \tag{5.1}$$

$$\|\rho HM(G_\Lambda^{-1}, Q_\Lambda)\|_\infty < 1, \tag{5.2}$$

where $\rho := \gamma_{F_2}$, and

$$\|Q_\Lambda\|_\infty < 1\ , \tag{5.3}$$

which is called as a strong $\mathcal{H}^\infty$ stabilization problem.

In order to find a solution to the problem defined above, let us partition G_Λ^{-1} as $G_\Lambda^{-1} =: \begin{bmatrix} \widehat{G}_{11} & \widehat{G}_{12} \\ \widehat{G}_{21} & \widehat{G}_{22} \end{bmatrix}$, where $\widehat{G}_{11}$ is $n \times n$ and $\widehat{G}_{22}$ is 1×1. Then, $HM(G_\Lambda^{-1}, Q_\Lambda) = (\widehat{G}_{11}Q_\Lambda + \widehat{G}_{12})(\widehat{G}_{21}Q_\Lambda + \widehat{G}_{22})^{-1}$. Thus, by defining

$$G_{\Lambda_\rho}^{-1} := \begin{bmatrix} I_n & 0 \\ 0 & \rho^{-1} \end{bmatrix} G_\Lambda^{-1} = \begin{bmatrix} \widehat{G}_{11} & \widehat{G}_{12} \\ \rho^{-1}\widehat{G}_{21} & \rho^{-1}\widehat{G}_{22} \end{bmatrix}\ , \tag{5.4}$$

(5.2) is equivalent to that

$$S := HM(G_{\Lambda_\rho}^{-1}, Q_\Lambda) \tag{5.5}$$

is contractive.

In order to find a condition that guarantees contractiveness of Q_Λ, let us also partition G_{Λ_ρ} as $G_{\Lambda_\rho} = \begin{bmatrix} \overline{G}_{11} & \overline{G}_{12} \\ \overline{G}_{21} & \overline{G}_{22} \end{bmatrix}$, where $\overline{G}_{11}$ is $n \times n$ and $\overline{G}_{22}$ is 1×1. Then, using (5.5) and (2.7), we obtain

$$Q_\Lambda = HM(G_{\Lambda_\rho}, S) = (\overline{G}_{11}S + \overline{G}_{12})(\overline{G}_{21}S + \overline{G}_{22})^{-1}. \tag{5.6}$$

It follows from [67] that we can introduce a nonzero *tuning parameter* λ, which does not affect the controller but may reduce the conservativeness in the design, so that

$$Q_\Lambda = (\lambda\overline{G}_{11}S + \lambda\overline{G}_{12})(\lambda\overline{G}_{21}S + \lambda\overline{G}_{22})^{-1}\ . \tag{5.7}$$

Let us also define $U := \lambda(\overline{G}_{11}S + \overline{G}_{12})$, $V := 1 - \lambda(\overline{G}_{21}S + \overline{G}_{22})$, and $\Gamma := \sqrt{2}\begin{bmatrix} U \\ V \end{bmatrix}$. Then

$$Q_\Lambda = U(1-V)^{-1} = HM(G_\Gamma, \Gamma)\ , \tag{5.8}$$

where $G_\Gamma := \begin{bmatrix} \begin{bmatrix} I_n & 0 \\ 0 & -1 \end{bmatrix} & 0 \\ 0 & \sqrt{2} \end{bmatrix}$ and it satisfies $G_\Gamma^T J_{n,1} G_\Gamma \leq J_{(n+1),1}$. This property of G_Γ can be used to present a sufficient condition for the contractiveness of Q_Λ. Let us define z_Γ, w_Γ, u_Γ and y_Γ such that $\begin{bmatrix} z_\Gamma \\ w_\Gamma \end{bmatrix} = G_\Gamma \begin{bmatrix} u_\Gamma \\ y_\Gamma \end{bmatrix}$ and $u_\Gamma = \Gamma y_\Gamma$. Then, by (5.8), $z_\Gamma = Q_\Lambda w_\Gamma$. Since $G_\Gamma^T J_{n,1} G_\Gamma \leq J_{(n+1),1}$, then

$$\begin{aligned} \begin{bmatrix} z_\Gamma \\ w_\Gamma \end{bmatrix}^T J_{n,1} \begin{bmatrix} z_\Gamma \\ w_\Gamma \end{bmatrix} &= \begin{bmatrix} u_\Gamma \\ y_\Gamma \end{bmatrix}^T G_\Gamma^T J_{n,1} G_\Gamma \begin{bmatrix} u_\Gamma \\ y_\Gamma \end{bmatrix} \\ &\leq \begin{bmatrix} u_\Gamma \\ y_\Gamma \end{bmatrix}^T J_{(n+1),1} \begin{bmatrix} u_\Gamma \\ y_\Gamma \end{bmatrix} \end{aligned}$$

which gives $z_\Gamma^T z_\Gamma - w_\Gamma^T w_\Gamma \leq u_\Gamma^T u_\Gamma - y_\Gamma^T y_\Gamma$, which implies

$$\|z_\Gamma\|_2^2 - \|w_\Gamma\|_2^2 \leq \|u_\Gamma\|_2^2 - \|y_\Gamma\|_2^2 \,. \tag{5.9}$$

Since $u_\Gamma = \Gamma y_\Gamma$, if Γ is contractive, $\|u_\Gamma\|_2 < \|y_\Gamma\|_2$. Then, from (5.9), $\|z_\Gamma\|_2 < \|w_\Gamma\|_2$. However, since $z_\Gamma = Q_\Lambda w_\Gamma$, this implies contractiveness of Q_Λ. Therefore, Q_Λ is contractive if Γ is contractive. Furthermore, recall that S must also be contractive. These two conditions are simultaneously satisfied if $\left\| \begin{bmatrix} \Gamma \\ S \end{bmatrix} \right\|_\infty < 1$, where

$$\begin{bmatrix} \Gamma \\ S \end{bmatrix} = \begin{bmatrix} \sqrt{2}\lambda \overline{G}_{11} & \sqrt{2}\lambda \overline{G}_{12} \\ -\sqrt{2}\lambda \overline{G}_{21} & \sqrt{2} - \sqrt{2}\lambda \overline{G}_{22} \\ I & 0 \end{bmatrix} \begin{bmatrix} S \\ 1 \end{bmatrix} \,. \tag{5.10}$$

The structure of $\begin{bmatrix} \Gamma \\ S \end{bmatrix}$ given in (5.10), can easily be represented using homographic transformation. For this, let us define

$$G_G := \begin{bmatrix} \sqrt{2}\lambda \overline{G}_{11} & \sqrt{2}\lambda \overline{G}_{12} \\ -\sqrt{2}\lambda \overline{G}_{21} & \sqrt{2}(1 - \lambda \overline{G}_{22}) \\ I_n & 0 \\ 0 & 1 \end{bmatrix} . \tag{5.11}$$

Then, $HM(G_G, S) = \begin{bmatrix} \Gamma \\ S \end{bmatrix}$. Therefore, the condition $\left\| \begin{bmatrix} \Gamma \\ S \end{bmatrix} \right\|_\infty < 1$ is satisfied if and only if $HM(G_G, S)$ is contractive. As a result, the problem of finding Q_Λ which satisfies (5.1)–(5.3) is solved if there exists $\lambda > 0$ and S such that $HM(G_G, S)$ is stable and $\|HM(G_G, S)\|_\infty < 1$. The problem of finding S and λ such that $HM(G_G, S)$ is stable and $\|HM(G_G, S)\|_\infty < 1$ can be solved by using $(\bar{J}, \hat{J})$-lossless factorization of G_G as in [50], where $\bar{J} := J_{(n+1+n),1}$ and $\hat{J} := J_{n,1}$. Utilization of $(\bar{J}, \hat{J})$-lossless factorization of G_G in the problem solving is enabled by the cascade connection property of HM, (2.8), and Theorem 2.1. Let $G_G = \Theta_G \Phi_G$ be a $(\bar{J}, \hat{J})$-lossless factorization of G_G, where $\bar{J} := J_{(n+1+n),1}$, $\hat{J} := J_{n,1}$, Θ_G is $(\bar{J}, \hat{J})$-lossless and Φ_G is bistable [50]. Therefore, by (2.8), $HM(G_G, S) = HM(\Theta_G, HM(\Phi_G, S))$. In addition, since Θ_G is $(\bar{J}, \hat{J})$-lossless, by Theorem 2.1, $\|HM(G_G, S)\|_\infty < 1$ if and only if $\|HM(\Phi_G, S)\|_\infty < 1$. Therefore, if a contractive, but otherwise arbitrary, $Q_G := HM(\Phi_G, S)$ is chosen, then, using (2.7), contractive S is obtained as

$$S = HM(\Phi_G^{-1}, Q_G) \, . \tag{5.12}$$

Then, a Q_Λ which satisfies (5.1)–(5.3) is obtained by (5.6).

In order to find the state-space solution of a $(\bar{J}, \hat{J})$-lossless factorization of G_G, let a minimal realization of G_Λ^{-1} be given as

$$G_\Lambda^{-1} = \left[\begin{array}{c|cc} \widehat{A} & \widehat{B}_1 & \widehat{B}_2 \\ \hline \widehat{C}_1 & I_n & 0 \\ \widehat{C}_2 & 0 & 1 \end{array}\right] , \tag{5.13}$$

where $\lim_{s\to\infty} G_\Lambda^{-1}(s) = I_{n+1}$ (see Section 4.3). Then a minimal realization of $G_{\Lambda_\rho}^{-1}$ is given as

$$G_{\Lambda_\rho}^{-1} = \left[\begin{array}{c|cc} \widehat{A} & \widehat{B}_1 & \widehat{B}_2 \\ \hline \widehat{C}_1 & I_n & 0 \\ \rho^{-1}\widehat{C}_2 & 0 & \rho^{-1} \end{array}\right] . \tag{5.14}$$

Thus, a minimal realization of G_{Λ_ρ} is given as

$$G_{\Lambda_\rho} = \left[\begin{array}{c|cc} \widehat{A} - \widehat{B}_1\widehat{C}_1 - \widehat{B}_2\widehat{C}_2 & \widehat{B}_1 & \rho\widehat{B}_2 \\ \hline -\widehat{C}_1 & I_n & 0 \\ -\widehat{C}_2 & 0 & \rho \end{array}\right] . \tag{5.15}$$

Therefore, a minimal realization of G_G can be obtained as

$$G_G = \left[\begin{array}{c|c} A_G & B_G \\ \hline C_G & D_G \end{array}\right] , \tag{5.16}$$

where $A_G := \widehat{A} - \widehat{B}_1\widehat{C}_1 - \widehat{B}_2\widehat{C}_2$, $B_G := \left[\begin{array}{cc} \widehat{B}_1 & \rho\widehat{B}_2 \end{array}\right]$, $C_G := \left[\begin{array}{c} -\sqrt{2}\lambda\widehat{C}_1 \\ \sqrt{2}\lambda\widehat{C}_2 \\ 0 \\ 0 \end{array}\right]$,

and

$$D_G := \left[\begin{array}{cc} \sqrt{2}\lambda I_n & 0 \\ 0 & \sqrt{2}(1-\lambda\rho) \\ I_n & 0 \\ 0 & 1 \end{array}\right] . \tag{5.17}$$

Since G_Λ is bistable, from (5.13), both $\widehat{A}$ and $\widehat{A} - \widehat{B}_1\widehat{C}_1 - \widehat{B}_2\widehat{C}_2 = A_G$ are Hurwitz. Thus, G_G is stable.

The state-space solution of $(\bar{J}, \hat{J})$-lossless factorization of G_G is given in the following theorem.

Theorem 5.1. *[50] Consider the stable system G_G and its minimal realization given in (5.16). G_G has a $(\bar{J}, \hat{J})$-lossless factorization, $G_G = \Theta_G\Phi_G$, if and only if there exists a nonsingular matrix E_G, such that*

$$D_G^T\bar{J}D_G = E_G^T\hat{J}E_G , \tag{5.18}$$

and a solution $X_G \geq 0$ to the following Riccati equation

$$X_GA_G + A_G^TX_G - Y_G^T(D_G^T\bar{J}D_G)^{-1}Y_G + C_G^T\bar{J}C_G = 0 \tag{5.19}$$

such that $A_\pi := A_G + B_G F_G$ *is Hurwitz, where* $F_G := -(D_G^T \bar{J} D_G)^{-1} Y_G$ *and* $Y_G := D_G^T \bar{J} C_G + B_G^T X_G$. *In that case,* $\Theta_G = \left[\begin{array}{c|c} A_\pi & B_G \\ \hline C_G + D_G F_G & D_G \end{array}\right] E_G^{-1}$ *and*

$$\Phi_G = E_G \left[\begin{array}{c|c} A_G & -B_G \\ \hline F_G & I_{n+1} \end{array}\right] . \tag{5.20}$$

In order to show the existence condition of non-singular E_G, which satisfies (5.18), for D_G in (5.17), let us pursue the following process. $D_G^T \bar{J} D_G = \begin{bmatrix} (2\lambda^2+1) I_n & 0 \\ 0 & -d \end{bmatrix}$, where $d := 4\lambda\rho - 2\lambda^2\rho^2 - 1$. Suppose E_G is nonsingular and let $V := E_G^{-1}$. Then, from (5.18), $V^T D_G^T \bar{J} D_G V = \hat{J}$. Let $y := Vx$, where $x := \begin{bmatrix} 0 & \cdots & 0 & 1 \end{bmatrix}^T$. Then, $y^T D_G^T \bar{J} D_G y = x^T \hat{J} x = -1$, which implies that $D_G^T \bar{J} D_G$ must have at least one negative eigenvalue. However, since $D_G^T \bar{J} D_G = \begin{bmatrix} (2\lambda^2+1) I_n & 0 \\ 0 & -d \end{bmatrix}$, and $2\lambda^2 + 1 > 0$, we must have $-d < 0$ if E_G is nonsingular. Equivalently, E_G is nonsingular only if $d > 0$. On the other hand, if $d > 0$, a nonsingular E_G can be obtained as $E_G = \begin{bmatrix} \sqrt{2\lambda^2+1} I_n & 0 \\ 0 & \sqrt{d} \end{bmatrix}$. Therefore, a nonsingular E_G satisfying (5.18) exists if and only if $d > 0$. However, note that, $d > 0$ if and only if λ is chosen in the interval $\left(\frac{\sqrt{2}-1}{\sqrt{2}\rho}, \frac{\sqrt{2}+1}{\sqrt{2}\rho}\right)$.

Therefore, a controller which solves the problem of Section 4.3 and which is stable apart from the integral action can be obtained by the following algorithm.

Algorithm 5.1.

1. *Find the optimal sensitivity level* γ^{opt}, *given by (4.36), and let* $\gamma = \gamma^{opt}$.

2. *Find* F_1, F_2, *and* G_Λ *(see Section 4.3) for the current sensitivity level* γ. *Also compute* $\gamma_{F_2} := \|F_2\|_\infty$. *Let* $\rho = \gamma_{F_2}$. *Choose a sufficiently large* l *and equally spaced values* $\lambda_1, \lambda_2, \ldots, \lambda_l$ *within the interval* $\left(\frac{\sqrt{2}-1}{\sqrt{2}\rho}, \frac{\sqrt{2}+1}{\sqrt{2}\rho}\right)$. *Let* $i = 1$.

3. *For $\lambda = \lambda_i$, if there exists a solution $X_G \geq 0$ to the Riccati equation (5.19), go to step 6. Otherwise, continue with step 4.*

4. *If $i = l$, go to step 5. Otherwise, set $i = i + 1$ and go to step 3.*

5. *Increase γ by a small amount and go to step 2.*

6. *Let $Q_\Lambda = HM(G_{\Lambda_\rho}, S)$, where, by (5.4), $G_{\Lambda_\rho} = G_\Lambda \begin{bmatrix} I_n & 0 \\ 0 & \rho \end{bmatrix}$ and, by (5.12), $S = HM(\Phi_G^{-1}, Q_G)$, where Φ_G is given by (5.20) and Q_G is contractive but otherwise arbitrary. The desired controller is then given by (see Figure 5.1)*

$$K(s) = F_1(s)H(s)\frac{\kappa(s+\epsilon)}{s(1+F_2(s)H(s))}\,, \tag{5.21}$$

where $H := HM(G_\Lambda^{-1}, Q_\Lambda)$ and $\kappa := \frac{\gamma}{\sqrt{2\sum_{i=1}^{n}\left(\delta_i^+\right)^2}}$.

To design a stable $\mathcal{H}^\infty$ flow controller is not an easy task due to the infinite dimensionality of the controller. However, stability of the infinite dimensional block F_2 resulted to utilize the small-gain theorem in Algorithm 5.1 to design a stable $\mathcal{H}^\infty$ flow controller. Since the small-gain theorem provides only a sufficient condition for the stability of the feedback system, stable $\mathcal{H}^\infty$ flow controllers designed by Algorithm 5.1, may be conservative, when they exist. In addition, there is no guarantee that the proposed algorithm terminates for any sensitivity level, since Algorithm 5.1 is based on the sufficient conditions. However, the stable $\mathcal{H}^\infty$ flow controllers designed by Algorithm 5.1 are obtained for some sensitivity levels, which are not less than two or three folds of γ^{opt}, in general. However, less conservative controllers can be designed by relaxing the small-gain condition in (5.2) as given in the following section.

5.3 Stable $\mathcal{H}^\infty$ Flow Controller Design Methodology by Solving Modified Strong $\mathcal{H}^\infty$ Stabilization Problem

The stable $\mathcal{H}^\infty$ flow controllers designed by Algorithm 5.1 are conservative due to the use of the small-gain theorem. In order to design a less

conservative controller compared to the controller designed by Algorithm 5.1, let us replace (5.2) by

$$\|\rho HM(G_\Lambda^{-1}, Q_\Lambda)\|_\infty < 1, \quad \rho \leq \gamma_{F_2}. \tag{5.22}$$

Now, to design a stable $\mathcal{H}^\infty$ flow controller, a contractive Q_Λ, which stabilizes $HM(G_\Lambda^{-1}, Q_\Lambda)$ and satisfies (5.22) for some $\rho \leq \gamma_{F_2}$, is sought. The sensitivity level γ is increased if a stable controller (apart from the integral term) can not be obtained for any $\rho \in [\rho_{min}, \gamma_{F_2}]$, where $\rho_{min} < \gamma_{F_2}$ is a chosen lower limit. Note that the contractive Q_Λ found by this procedure, given as Algorithm 5.2 below, may not satisfy the small-gain condition, however, it may stabilize the overall controller, except the integral term.

Algorithm 5.2.

1. *Find the optimal sensitivity level γ^{opt}, given by (4.36), and let $\gamma = \gamma^{opt}$.*

2. *Find F_1, F_2, and G_Λ for the current sensitivity level γ. Also compute $\gamma_{F_2} = \|F_2\|_\infty$ and choose a $\rho_{min} \in (0, \gamma_{F_2})$. Let $\rho = \gamma_{F_2}$.*

3. *Choose a sufficiently large l and equally spaced values λ_1, λ_2, ..., λ_l within the interval $\left(\frac{\sqrt{2}-1}{\sqrt{2}\rho}, \frac{\sqrt{2}+1}{\sqrt{2}\rho}\right)$. Let $i = 1$.*

4. *For $\lambda = \lambda_i$, if there exists a solution $X_G \geq 0$ to the Riccati equation (5.19), go to step 8. Otherwise, continue with step 5.*

5. *If $i = l$, go to step 6. Otherwise, set $i = i + 1$ and go to step 4.*

6. *Decrease ρ by a small amount. If $\rho \geq \rho_{min}$ go to step 3, otherwise go to step 7.*

7. *Increase γ by a small amount and go to step 2.*

8. *Let $Q_\Lambda = HM(G_{\Lambda_\rho}, S)$, where, by (5.4), $G_{\Lambda_\rho} = G_\Lambda \begin{bmatrix} I_n & 0 \\ 0 & \rho \end{bmatrix}$ and, by (5.12), $S = HM(\Phi_G^{-1}, Q_G)$, where Φ_G is given by (5.20) and Q_G is contractive but otherwise arbitrary. If $(1 + F_2H)^{-1}$ is stable (this is true if*

$\rho = \gamma_{F_2}$; otherwise, stability can be tested by using the Nyquist criterion), where $H = HM(G_\Lambda^{-1}, Q_\Lambda)$, go to step 9. Otherwise, go to step 5.

9. *The desired controller is given by (see Figure 5.1)*

$$K(s) = F_1(s)H(s)\frac{\kappa(s+\epsilon)}{s(1+F_2(s)H(s))}\,, \tag{5.23}$$

where $\kappa := \frac{\gamma}{\sqrt{2\sum_{i=1}^{n}\left(\delta_i^+\right)^2}}$.

To illustrate the performance of the stable $\mathcal{H}^\infty$ flow controllers designed by Algorithm 5.2, a network with two sources is considered. The controllers are designed for the given parameters in Table 5.1 and ρ_{min} in step 2 of Algorithm 5.2 is chosen as $\gamma_{F_2}/10$. The $\mathcal{H}^\infty$-optimal central flow controllers are also designed considering the same design parameters. The time-domain performance of both controllers are presented by simulations done using MATLAB/SIMULINK package, where the nonlinear effects (hard constraints) are also taken into account. In these simulations, the desired queue length, q_d, is taken 30 packets, the buffer size (maximum queue length) is taken as 60 packets, and the capacity of the outgoing link is taken as 90 packets/tu, where tu stands for the time unit. Moreover, the rate limits for the sources are taken as 150 packets/tu. The uncertain part of the actual time-delays used in the simulations are given in Table 5.2. In this table, Case ka, Case kb, refer to a case where the controller designed for Case k of Table 5.1 is used ($k = 1, 2$). The simulation results are shown in Figures 5.2–5.4, where (a) represents the response of the $\mathcal{H}^\infty$-optimal central flow controller and (b) represents the response of the stable $\mathcal{H}^\infty$ flow controller designed by Algorithm 5.2. In addition, in Figures 5.2–5.4, q (whose scale is on the right) is the queue length $q(t)$, and $\mathrm{r}_i^{\mathrm{s}}$ (whose scale is on the left) is the actual flow rate at source i, for $i = 1, 2$.

The $\mathcal{H}^\infty$-optimal central flow controller designed by the approach of Section 4.3 for Case 1 is unstable and the optimal sensitivity level is $\gamma^{opt} = 2.817$. As shown in Figure 5.2(a), the response of the optimal controller for Case 1a does not stabilize the actual plant, flow rates at sources and queue length at the bottleneck saturate. The unstable response of the designed stabilizing optimal controller may be due to the fact that the unstable controllers

Table 5.1: Controller design parameters

Case	h_1 (tu)	h_2 (tu)	β_1	β_2	β_1^f	β_2^f	δ_1^+	δ_2^+	α_1	α_2	$\sigma_1 = \sigma_2$
Case 1	4	2	0.1	0.2	0.01	0.05	1/4	1/2	2/3	1/3	0.25
Case 2	4	2	0.2	0.3	0.05	0.1	1/4	3/4	2/3	1/3	0.25

Table 5.2: Uncertain part of the actual time-delays

	i	$\delta_i^b(t)$	$\delta_i^f(t)$
Case 1a	1	$0.10+0.25\sin(\frac{2\pi}{50}t)$	$0.05+0.05\sin(\frac{2\pi}{100}t)$
	2	$0.15+0.30\sin(\frac{2\pi}{50}t)$	$0.10+0.05\sin(\frac{2\pi}{100}t)$
Case 1b,2a	1	$0.10+0.50\sin(\frac{2\pi}{20}t)$	$0.10+0.15\sin(\frac{2\pi}{80}t)$
	2	$0.15 + 0.50\sin(\frac{2\pi}{45}t)$	$0.10+0.10\sin(\frac{2\pi}{100}t)$

are highly sensitive to the unmodelled nonlinear dynamics, which are not considered in the controller design, however, taken into account in the simulations. By Algorithm 5.2, a stable $\mathcal{H}^\infty$ flow controller for Case 1 is obtained for $\gamma = 3.590$. As shown in Figure 5.2(b), the response of the stable $\mathcal{H}^\infty$ flow controller for Case 1a robustly stabilizes the actual plant and achieves all the design requirements despite the presence of uncertain time-varying time-delays.

The uncertain part of the actual time-delays in Case 1b vary faster within a wider range compared to the uncertain part of the actual time-delays in Case 1a. As shown in Figure 5.3(a), the optimal controller, which is unstable, does not stabilize the actual system for Case 1b. However, since the stable controllers have better robustness abilities compared to the unstable controllers, as seen in Figure 5.3(b), the stable controller stabilizes the actual system and achieves the tracking (4.5) and fairness (4.6) requirements also for Case 1b. Note that the steady-state oscillations of the queue length in Figure 5.3(b) are greater than the ones in Figure 5.2(b), this is due to the increase in the variation of the uncertain part of the forward time-delays.

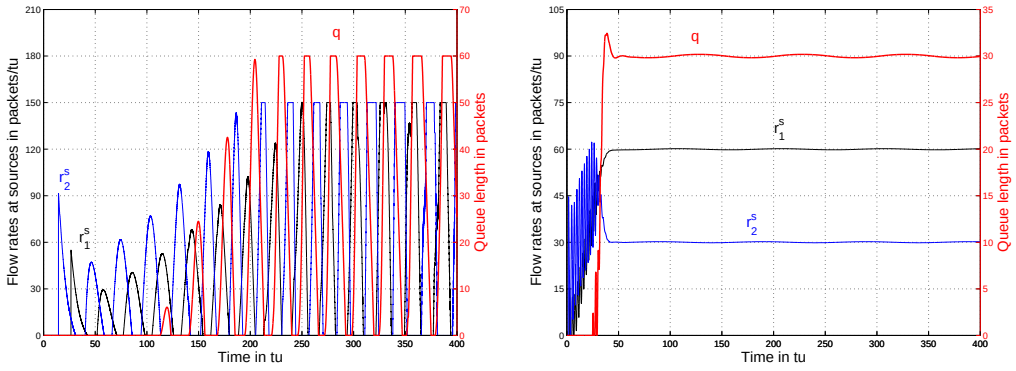

(a) (b)

Figure 5.2: Simulation results for Case 1a

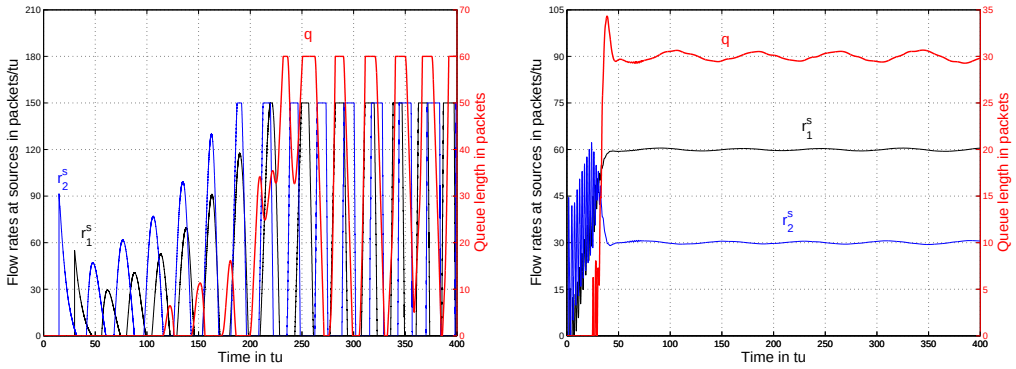

(a) (b)

Figure 5.3: Simulation results for Case 1b

In order to design a controller to provide the actual time-delays varying faster in a wider range compared to the controller designed for Case 1, the controller design parameters β_1, β_2, β_1^f, β_2^f, and δ_2^+ in Case 1 are increased as in Case 2. The $\mathcal{H}^\infty$-optimal central flow controller for Case 2 is obtained at $\gamma^{opt} = 3.433$, however, it is still unstable. The optimal controller designed for Case 2 has better stability margins compared to the optimal controller designed for Case 1, because of the increase in the controller design parameters (see Section 4.5). However, similar to the optimal controller designed for Case 1, the optimal controller designed for Case 2 can not stabilize the actual system for Case 2a as seen in Figure 5.4(a). The stable controller designed by Algorithm 5.2 for Case 2 is obtained at $\gamma = 4.600$. As shown in Figure 5.4(b),

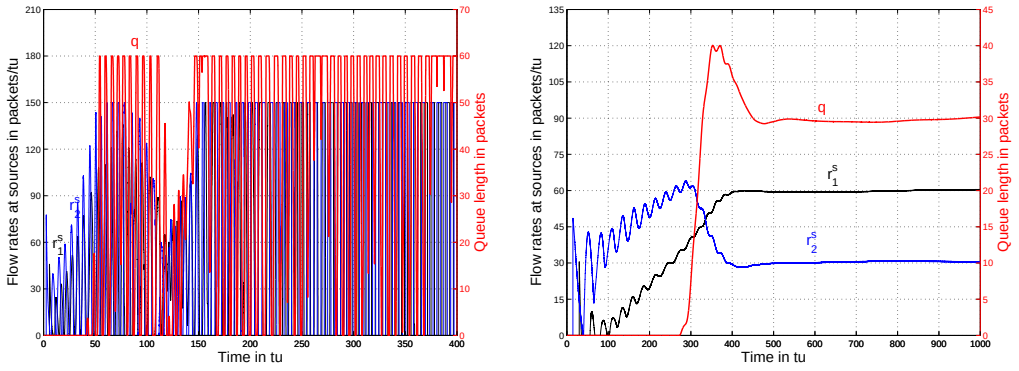

(a) (b)

Figure 5.4: Simulation results for Case 2a

the stable controller stabilizes the actual plant for Case 2a and satisfies both the tracking and the weighted fairness requirements,

As shown in Figures 5.2(b)– 5.4(b), the stable $\mathcal{H}^\infty$ flow controllers designed by Algorithm 5.2 stabilize the actual system and achieve the design requirements despite the presence of uncertain time-varying time-delays. Algorithm 5.2 is based on less stringent conditions compared to Algorithm 5.1. However, there also exists conservativeness in the approach proposed in this section, because there may exist a contractive Q_Λ, which does not satisfy (5.22) for any ρ in the given interval, but results in a stable $\mathcal{H}^\infty$ flow controller. Therefore, it is not guaranteed that Algorithm 5.2 yields a stable $\mathcal{H}^\infty$ flow controller. However, Algorithm 5.2 produces a stable $\mathcal{H}^\infty$ flow controller, in most cases.

5.4 Stable $\mathcal{H}^\infty$ Flow Controller Design Methodology by Utilizing the Stability of the Finite-Dimensional Part of the Controller

In Algorithms 5.1 and 5.2, a contractive Q_Λ is sought to stabilize $HM(G_\Lambda^{-1}, Q_\Lambda)$ and satisfy $\|HM(G_\Lambda^{-1}, Q_\Lambda)\|_\infty < 1/\rho$, for a given $\rho > 0$, by increasing the sensitivity level γ. In Algorithm 5.1, ρ is taken as γ_{F_2}, where $\gamma_{F_2} = \|F_2\|_\infty$. However, the controllers designed by Algorithm 5.1 are conser-

vative, in general. In order to design a less conservative stable controller, ρ is taken less than or equal γ_{F_2} in Algorithm 5.2. Note that, both algorithms try to produce a contractive Q_Λ satisfying two conditions given above. However, a contractive Q_Λ which stabilizes $HM(G^{-1}, Q_\Lambda)$ always makes the $\mathcal{H}^\infty$ norm of $HM(G^{-1}, Q_\Lambda)$ less than for some value. To introduce an upper bound on the $\mathcal{H}^\infty$ norm of $HM(G^{-1}, Q_\Lambda)$ may produce a conservative stable controller, since a contractive Q_Λ, which stabilizes $HM(G^{-1}, Q_\Lambda)$, may not achieve the given $\mathcal{H}^\infty$ norm bound, however, may stabilize the actual controller, except the integral term.

In this section, an alternative approach is presented and the stable $\mathcal{H}^\infty$ flow controller design is based on the stabilization of the finite-dimensional part of the controller. A contractive Q_Λ is sought to satisfy the stability of both $HM(G_\Lambda^{-1}, Q_\Lambda)$ and the closed-loop TFM from $\bar{y}$ to r in Figure 5.1, by increasing the sensitivity level γ.

The controller depicted in Figure 5.1 can be shown as in Figure 5.5, where

$$\Sigma := \begin{bmatrix} \Sigma_{11} & \Sigma_{12} \\ \Sigma_{21} & \Sigma_{22} \end{bmatrix} := \left[\begin{array}{c|cc} A - B_2C_2 & B_2 & B_1 \\ \hline C_1 & 0 & I_n \\ -C_2 & 1 & 0 \end{array}\right], \tag{5.24}$$

where $\left[\begin{array}{c|cc} A & B_1 & B_2 \\ \hline C_1 & I_n & 0 \\ C_2 & 0 & 1 \end{array}\right] := \begin{bmatrix} G_{11} & G_{12} \\ G_{21} & G_{22} \end{bmatrix} := G_\Lambda^{-1}.$

Now, let us consider the closed-loop TFM from $\tilde{y}$ to $\bar{r}$ in Figure 5.5. A contractive Q_Λ stabilizes the closed-loop TFM from $\tilde{y}$ to $\bar{r}$ in Figure 5.5 if and only if it stabilizes the plant $\Sigma_{22} = \left[\begin{array}{c|c} A - B_2C_2 & B_1 \\ \hline -C_2 & 0 \end{array}\right] =: \left[\begin{array}{c|c} A_\Sigma & B_\Sigma \\ \hline C_\Sigma & 0 \end{array}\right]$. Let us assume that Σ_{22} satisfies the following conditions:

a) (A_Σ, B_Σ) is stabilizable and (C_Σ, A_Σ) is detectable

b) A_Σ has no $j\omega$ axis eigenvalues.

The existence of a stabilizing output feedback controller for Σ is guaranteed

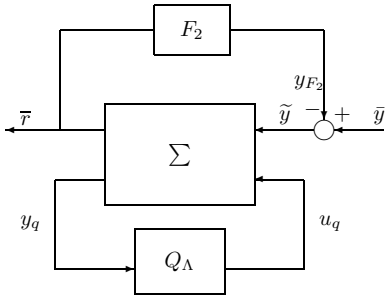

Figure 5.5: Representation of the controller

by (a). Let $X \geq 0$ be the stabilizing solution of

$$A_\Sigma^T X + X A_\Sigma - X B_\Sigma B_\Sigma^T X = 0, \tag{5.25}$$

where $F_\Sigma := -B_\Sigma^T X$ and $A_X = A_\Sigma + B_\Sigma F$ is stable. Since it is assumed that (A_Σ, B_Σ) is stabilizable and A_Σ has no $j\omega$ axis eigenvalues, there exists a unique solution $X \geq 0$ for (5.25). Therefore, Σ_{22} has a right-coprime factorization such as $\Sigma_{22} = N_\Sigma M_\Sigma^{-1}$ [5]:

$$\begin{bmatrix} M_\Sigma \\ N_\Sigma \end{bmatrix} := \left[\begin{array}{c|c} A_X & B_\Sigma \\ \hline F_\Sigma & I \\ C_\Sigma & 0 \end{array}\right], \tag{5.26}$$

where N_Σ, M_Σ are in $\mathcal{RH}^\infty$. Now, a contractive Q_Λ stabilizes Σ_{22} if and only if $(M_\Sigma - Q_\Lambda N_\Sigma)^{-1} \in \mathcal{RH}^\infty$. Following [68], let us define $R_\Sigma := M_\Sigma - I$. Therefore, $M_\Sigma - Q_\Lambda N_\Sigma$ can be written in terms of R_Σ as follows:

$$M_\Sigma - Q_\Lambda N_\Sigma = I + R_\Sigma - Q_\Lambda N_\Sigma. \tag{5.27}$$

By the small-gain theorem [5], if there exists a contractive Q_Λ such that $\|R_\Sigma - Q_\Lambda N_\Sigma\|_\infty < 1$, from (5.27), Q_Λ stabilizes Σ_{22}. To find such a contractive Q_Λ, a two block problem is defined in [68]:

$$\left\| \begin{bmatrix} R_\Sigma & 0 \end{bmatrix} - \varepsilon_r^{-1} Q_\Lambda \begin{bmatrix} \varepsilon_r N_\Sigma & I \end{bmatrix} \right\|_\infty < 1, \tag{5.28}$$

where $\varepsilon_r < 1$. Let us define $\hat{Q}_\Lambda := \varepsilon_r^{-1} Q_\Lambda$ and $\hat{N}_\Sigma := \varepsilon_r N_\Sigma$. Then utilizing LFT,

$$\begin{bmatrix} R_\Sigma & 0 \end{bmatrix} - \hat{Q}_\Lambda \begin{bmatrix} \hat{N}_\Sigma & I \end{bmatrix} = F_l(G_\Sigma, -\hat{Q}_\Lambda), \tag{5.29}$$

where

$$G_\Sigma := \left[\begin{array}{cc|c} \left[\begin{array}{cc} R_\Sigma & 0 \end{array}\right] & I & \\ \left[\begin{array}{cc} \hat{N}_\Sigma & I \end{array}\right] & 0 & \end{array}\right] := \left[\begin{array}{c|cc} A_X & \left[\begin{array}{cc} B_\Sigma & 0 \end{array}\right] & 0 \\ \hline F_\Sigma & \left[\begin{array}{cc} 0 & 0 \end{array}\right] & I \\ \varepsilon_r C_\Sigma & \left[\begin{array}{cc} 0 & I \end{array}\right] & 0 \end{array}\right]. \tag{5.30}$$

Now, the problem in (5.28) can be solved by solving only one algebraic Riccati equation as given in the following theorem.

Theorem 5.2. *[26] There exits a contractive Q_Λ, which stabilizes Σ, if there exists $Y \geq 0$ and a $\varepsilon_r \in (0,1)$, such that*

$$A_X Y + Y A_X^T - Y(\varepsilon_r^2 C_\Sigma^T C_\Sigma - X B_\Sigma B_\Sigma^T X)Y + B_\Sigma B_\Sigma^T = 0. \tag{5.31}$$

Under this condition, the realization of the contractive Q_Λ can be written as:

$$Q_\Lambda = \left[\begin{array}{c|c} A_K & -L \\ \hline F & 0 \end{array}\right], \tag{5.32}$$

where $A_K = A_\Sigma + B_\Sigma F + L C_\Sigma$, and $L = -\varepsilon_r^2 Y C_\Sigma^T$.

Theorem 5.2 is based on the right-coprime factorization over $\mathcal{RH}^\infty$ of Σ_{22}. A stabilizing contractive Q_Λ can also be designed by utilizing the left-coprime factorization of Σ_{22} over $\mathcal{RH}^\infty$.

Since it is assumed that (C_Σ, A_Σ) is detectable and A_Σ has no $j\omega$ axis eigenvalues, there exist a unique $\widetilde{Y} \geq 0$ such that

$$A_\Sigma \widetilde{Y} + \widetilde{Y} A_\Sigma^T - \widetilde{Y} C_\Sigma^T C_\Sigma \widetilde{Y} = 0, \tag{5.33}$$

where $\widetilde{L} := -\widetilde{Y} C_\Sigma^T$ and $\widetilde{A}_Y := A_\Sigma + \widetilde{L} C_\Sigma$ is stable. Now, Σ_{22} has a left coprime factorization over $\mathcal{RH}^\infty$ such as $\Sigma_{22} = \widetilde{M}_\Sigma^{-1} \widetilde{N}_\Sigma$.

Theorem 5.3. *[26] There exits a contractive Q_Λ, which stabilizes Σ, if there exists $\widetilde{X} \geq 0$ and a $\varepsilon_l \in (0,1)$ such that*

$$A_Y^T \widetilde{X} + \widetilde{X} A_Y + \widetilde{X}(\widetilde{Y} C_\Sigma^T C_\Sigma \widetilde{Y} - \varepsilon_l^2 B_\Sigma B_\Sigma^T)\widetilde{X} + C_\Sigma^T C_\Sigma = 0. \tag{5.34}$$

Under this condition, the realization of the contractive Q_Λ can be written as:

$$Q_\Lambda = \left[\begin{array}{c|c} \widetilde{A}_K & -\widetilde{L} \\ \hline \widetilde{F} & 0 \end{array}\right], \tag{5.35}$$

where $\widetilde{A}_K = A_\Sigma + \widetilde{L}C_\Sigma + B_\Sigma\widetilde{F}$, and $\widetilde{F} = -\varepsilon_l^2 B_\Sigma^T \widetilde{X}$.

Now, utilizing the above theorems, two algorithms are given below to design a contractive Q_Λ to obtain a stable $\mathcal{H}^\infty$ flow controller.

Algorithm 5.3.

1. *Find the optimal sensitivity level γ^{opt}, given by (4.36), and let $\gamma = \gamma^{opt}$. Choose a sufficiently large l and equally spaced values $\varepsilon_1, \ldots, \varepsilon_l$ within the interval $(0, 1)$.*

2. *Find F_1, F_2, and G_Λ (see Section 4.3) for the current sensitivity level γ. Let $i = 1$.*

3. *If there exists $X \geq 0$, which solves (5.25), go to step 4. Otherwise, go to step 6.*

4. *For $\varepsilon_r = \varepsilon_i$, if there exists $Y \geq 0$, which solves (5.31), go to step 7. Otherwise, go to step 5.*

5. *If $i = l$, go to step 6. Otherwise, set $i = i + 1$ and go to step 4.*

6. *Increase γ by a small amount and go to step 2.*

7. *If $(1 + F_2H)^{-1}$ is unstable (can be checked by the Nyquist criterion), where $H = HM(G_\Lambda^{-1}, Q_\Lambda)$ and Q_Λ is obtained from (5.32), then go to step 5. If $(1 + F_2H)^{-1}$ is stable, the desired controller is then given by (see Figure 5.1)*

$$K(s) = F_1(s)H(s)\frac{\kappa(s+\epsilon)}{s(1 + F_2(s)H(s))}, \tag{5.36}$$

where $\kappa := \frac{\gamma}{\sqrt{2\sum_{i=1}^n (\delta_i^+)^2}}$.

Algorithm 5.3 is based on the right-coprime factorization of Σ_{22}. If the left-coprime factorization of Σ_{22} is considered, the algorithm can alternatively be written as:

Algorithm 5.4.

1., 2. Same as in Algorithm 5.3.

3. If there exists $\widetilde{Y} \geq 0$, which solves (5.33), go to step 4. Otherwise, go to step 6.

4. For $\varepsilon_l = \varepsilon_i$, if there exists $\widetilde{X} \geq 0$, which solves (5.34), go to step 7. Otherwise, go to step 5.

5., 6. Same as in Algorithm 5.3.

7. If $(1 + F_2 H)^{-1}$ is unstable (can be checked by the Nyquist criterion), where $H = HM(G_\Lambda^{-1}, Q_\Lambda)$ and Q_Λ is obtained from (5.35), then go to step 5. If $(1 + F_2 H)^{-1}$ is stable, the desired controller is then given by (5.36).

Note that, each algorithm proposed in this section solves a different problem to design a stable $\mathcal{H}^\infty$ flow controller. Therefore, Algorithms 5.3 and 5.4 may result in different controllers. In order to obtain a stable controller with a good performance, stable $\mathcal{H}^\infty$ flow controller design may be done utilizing both Algorithms 5.3 and 5.4, and the resulting stable controller having the better performance may be chosen. It should be noted that there is no guarantee for either of the algorithm to produce a desired controller.

To evaluate the performance of the controller designed by the algorithms proposed here, the network introduced in Section 5.3 is considered. A simulation is done using MATLAB/SIMULINK package, where the nonlinear effects (hard constraints) are also taken into account. The controller design is done using the parameters given in Table 5.1. In the simulation, the desired queue length, q_d, the buffer size, the capacity of the outgoing link, and the

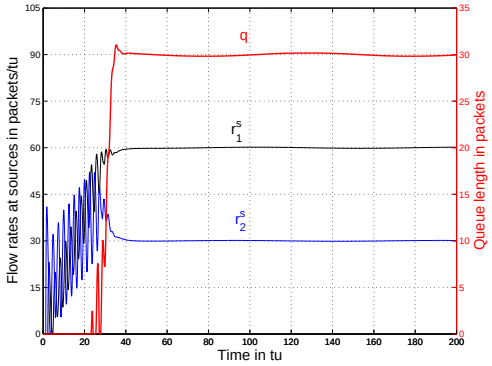

Figure 5.6: Simulation result of the controller designed by Algorithm 5.3 for Case 1a

rate limits for the sources are taken as in Section 5.3. The simulation result of the stable controller designed by Algorithm 5.3 is shown in Figure 5.6. In Figure 5.6, q (whose scale is on the right) is the queue length $q(t)$, and $\mathrm{r}_i^{\mathrm{s}}$ (whose scale is on the left) is the actual flow rate at source i, for $i = 1, 2$.

A stable $\mathcal{H}^\infty$ flow controller for Case 1, given in Section 5.3, is obtained at $\gamma = 3.260$, by utilizing Algorithm 5.3. It should be noted that Algorithm 5.4 produces the same stable $\mathcal{H}^\infty$ flow controller, because A_Σ is stable in this case and $(C_\Sigma, A_\Sigma, B_\Sigma)$ triple satisfies stabilizable and delectable assumptions, a positive definite solution of (5.34), $\widetilde{X}$, exists for all γ [5]. Therefore, the resulting Q_Λ is zero, and the resulting stable controller is the central controller. As shown in Figure 5.6, the response of the designed stable $\mathcal{H}^\infty$ flow controller robustly stabilizes the actual plant and achieves the design requirements despite the presence of uncertain time-varying time-delays. In addition, by comparing Figure 5.2(b) to Figure 5.6, the queue response of the controller designed by Algorithm 5.3 is faster compared to the queue response of the controller designed by Algorithm 5.2. In addition, the queue response in Figure 5.6 makes smaller overshoot compared to the one in Figure 5.2(b).

Algorithms 5.3 and 5.4 are based on the stability of the finite-dimensional part of the mapping from $\overline{y}$ to $\overline{r}$ in Figure 5.1, which is $HM(G_\Lambda^{-1}, Q_\Lambda)$, by a contractive Q_Λ. By comparing Algorithms 5.3 and 5.4 to Algorithms 5.1

and 5.2, a contractive Q_Λ is designed by Algorithms 5.3 and 5.4 to satisfy only (5.1). However, any contractive Q_Λ satisfying (5.1) also yields that $\|HM(G_\Lambda^{-1}, Q_\Lambda)\|_\infty$ is bounded. However, to introduce an upper bound on the $\mathcal{H}^\infty$ norm of $HM(G_\Lambda^{-1}, Q_\Lambda)$ as in (5.2) and (5.22), respectively, in Algorithms 5.1 and 5.2, challenges to design a contractive Q_Λ compared to design a contractive Q_Λ satisfying only (5.1). Therefore, the approach of seeking a contractive Q_Λ, which stabilizes $HM(G_\Lambda^{-1}, Q_\Lambda)$ and the closed-loop TFM from $\bar{y}$ to $\bar{r}$ in Figure 5.1, by increasing the sensitivity level may be less conservative compared to the approaches of Sections 5.2 and 5.3.

5.5 Stable $\mathcal{H}^\infty$ Flow Controller Design by Utilizing the Uncertainty Weighting Function

In this section, an alternative $\mathcal{H}^\infty$ flow controller design algorithm, which is inspired by [65], is given. The algorithm seeks a stable $\mathcal{H}^\infty$ flow controller by changing the gain of the uncertainty weight W_1 in the flow control problem (see Section 4.2). To do this, the uncertainty weight is defined as $\widehat{W}_1 := kW_1$ for $k > 0$ and the $\mathcal{H}^\infty$ controller is designed for $\widehat{W}_1$ while increasing k, starting from $k = 1$, up to finding a stable $\mathcal{H}^\infty$ flow controller. However, it should be noted that instead of increasing the k, alternatively, a stable $\mathcal{H}^\infty$ flow controller can be sought by decreasing k. Therefore, a stable $\mathcal{H}^\infty$ flow controller, which stabilizes the closed-loop system and achieves the design requirements can be obtained by the following algorithm.

Algorithm 5.5.

1. *Let $k = 1$.*
2. *Let $\widehat{W}_1 := kW_1$ (see Section 4.2 for W_1).*
3. *Find the optimal sensitivity level γ^{opt}, given by (4.36), by using $\widehat{W}_1$ instead of W_1.*
4. *Find F_1, F_2, and G_Λ (see Section 4.3) for the current sensitivity level γ.*

5. *If* $(1 + F_2H)^{-1}$ *is unstable (can be checked by the Nyquist criterion), where* $H = HM(G_\Lambda^{-1}, Q_\Lambda)$ *and* Q_Λ *is chosen as* $Q_\Lambda = 0$*, go to step 6. Otherwise go to step 7.*

6. *Increase* k *by a small amount and go to step 2.*

7. *The stable* $\mathcal{H}^\infty$ *flow controller is obtained by (see Figure 5.1)*

$$K(s) = F_1(s)H(s)\frac{\kappa(s+\epsilon)}{s(1+F_2(s)H(s))}\,, \tag{5.37}$$

where $\kappa := \frac{\gamma}{\sqrt{2\sum_{i=1}^{n}\left(\delta_i^+\right)^2}}$.

To illustrate the performance of the stable $\mathcal{H}^\infty$ flow controller designed by Algorithm 5.5, the network introduced in Section 5.3 is considered. The controller is designed for the given parameters in Table 5.1. The time-domain performance of the controller is presented by a simulation done using MATLAB/SIMULINK package, where the nonlinear effects (hard constraints) are also taken into account. In the simulation, the desired queue length, q_d, the buffer size, the capacity of the outgoing link, and the rate limits for the sources are taken as in Section 5.3. The uncertain part of the actual time-delays used in the simulation is as in Case 1a, which is given in Table 5.2. The simulation result is shown in Figure 5.7. In Figure 5.7, q (whose scale is on the right) is the queue length $q(t)$, and $\mathrm{r}_i^{\mathrm{s}}$ (whose scale is on the left) is the actual flow rate at source i, for $i = 1, 2$.

A stable $\mathcal{H}^\infty$ flow controller for Case 1, given in Section 5.3, is obtained for $\gamma = 4.470$ and $k = 2.5$, by Algorithm 5.5. The response of the designed controller is depicted in Figure 5.7. As seen in Figure 5.7, the controller designed by Algorithm 5.5 robustly stabilizes the actual system and achieves the design requirements. The queue length at the bottleneck node is kept at the desired level, and the network capacity is shared fairly among the sources according to (4.6) despite the presence of uncertain time-varying time-delays. As shown by comparing Figure 5.7 to 5.6, the response of the controller designed by Algorithm 5.3 is faster compared to the controller designed by Algorithm 5.5.

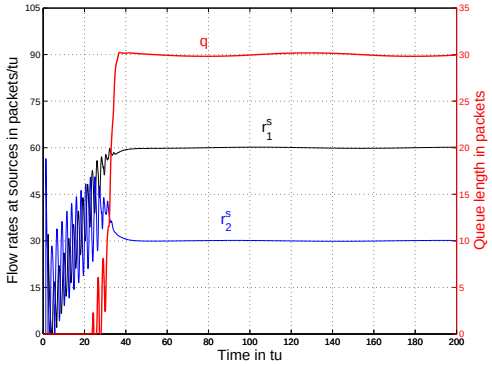

Figure 5.7: Simulation result of the controller designed by Algorithm 5.5 for Case 1a

Algorithm 5.5 seeks an optimal stable $\mathcal{H}^\infty$-central controller, by increasing the gain of the uncertainty weight, starting from 1. Namely, if the optimal central controller is unstable for the given uncertainty weight, apart from the integral term, another optimal central controller is designed by increasing the gain of the uncertainty weight. This process continues up to finding a stable central controller. However, instability of the optimal central controller does not imply that the optimal controller, except the integral term, is unstable for all contractive Q_Λ, since there may be a nonzero contractive Q_Λ, which stabilizes the actual controller, apart from the integral term. Therefore, the proposed approach has a conservative aspect. In addition, the proposed approach does not guarantee to yield a stable $\mathcal{H}^\infty$ flow controller.

5.6 Stable $\mathcal{H}^\infty$ Flow Controller Design by Using Approximation Techniques

Up to this section, five different stable $\mathcal{H}^\infty$ flow controller design algorithms were proposed. None of these algorithms utilize the dynamics of F_2, which is infinite-dimensional, directly. In order to consider the dynamics of F_2 in the stable controller design, different rational approximations of F_2 are considered in this section. Utilizing the rational approximation of F_2, three

different stable $\mathcal{H}^\infty$ flow controller design approaches are proposed. In these approaches, first, a rational approximation of F_2 is obtained and then a strong stabilization problem for the finite-dimensional system is defined and solved. Then, in order to obtain a stable $\mathcal{H}^\infty$ flow controller, it is tested whether Q_Λ, which is obtained from the solution of the strong stabilization problem, stabilizes the actual infinite-dimensional controller. Two different approximation methods will be considered, one of them is inspired by the δ-operator and the other one is based on the bilinear transformation [69]. For brevity, the rational approximation method inspired by the δ-operator is called the *δ-approximation method* and the method based on the bilinear-transformation is called the *bilinear approximation method*. As proved in [69], both of the methods ensure that the rational approximation of the FIR filter

- keeps the low-pass property of the FIR filter
- is stable
- does not contain any unstable pole-zero cancellations
- has the same DC gain with the FIR filter (i.e. $\|F_2(0)\| = \|F_{2_{app}}(0)\|$, where $F_{2_{app}}$ denotes the TFM of the approximation).

In addition, the error between the FIR filter and its rational approximation can be made as small as desired by any one of these methods.

Parts of the results presented in this section have been published in [48], [49]. However, example cases considered here are different than those in [48], [49].

In the following subsection, the two rational approximation methods to be used are presented.

5.6.1 Approximation methods

Let us consider the following FIR filter described by the TFM

$$Z(s) = (I - e^{-(sI - A_z)h_z})(sI - A_z)^{-1}B_z \; . \tag{5.38}$$

In order to obtain the rational approximation of $Z(s)$ by the δ-approximation method, let us define as in [69]

$$\Phi_N^\delta := \left(\int_0^{\frac{h_z}{N}} e^{-A_z \zeta} d\zeta \right)^{-1}, \tag{5.39}$$

where N is the number of approximation steps. Then, let us define

$$\Gamma_N^\delta(s) := (e^{\frac{h_z}{N}(sI - A_z)} - I)\Phi_N^\delta \ , \tag{5.40}$$

where Γ_N^δ satisfies $\lim_{N\to\infty} \Gamma_N^\delta(s) = sI - A_z$, which is called the *limiting property*. Utilizing (5.39) and (5.40), $e^{-(sI-A_z)h_z}$ can be written as

$$e^{-(sI-A_z)h_z} = ((\Phi_N^\delta)^{-1}\Gamma_N^\delta + I)^{-N}. \tag{5.41}$$

Therefore, by (5.41), Z in (5.38) can be written as

$$Z(s) \ = \ (I - ((\Phi_N^\delta)^{-1}\Gamma_N^\delta + I)^{-N}(sI - A_z)^{-1}B_z \ .$$

Utilizing the limiting property of Γ_N^δ, $\Gamma_N^\delta(s) \approx (sI - A_z)$, Z can be approximated by Z_N^δ as given below:

$$\begin{aligned} Z(s) \approx Z_N^\delta(s) &= (I - ((\Phi_N^\delta)^{-1}(sI - A_z) + I)^{-N}(sI - A_z)^{-1}B_z \\ &= \sum_{k=1}^{N} (\Pi_N^\delta)^k(s)(\Phi_N^\delta)^{-1}B_z \ , \end{aligned} \tag{5.42}$$

where $\Pi_N^\delta(s) := (sI - A_z + \Phi_N^\delta)^{-1}\Phi_N^\delta$.

In order to obtain the rational approximation of $Z(s)$ by the bilinear approximation method, let us define as in [69]

$$\Phi_N^b := \left(\int_0^{\frac{h_z}{N}} e^{-A_z \zeta} d\zeta \right)^{-1} \left(e^{-A_z \frac{h_z}{N}} + I \right) \ . \tag{5.43}$$

Then, let us define

$$\Gamma_N^b(s) := (e^{\frac{h_z}{N}(sI - A_z)} - I)(e^{\frac{h_z}{N}(sI - A_z)} + I)^{-1}\Phi_N^b \ . \tag{5.44}$$

Similar to Γ_N^δ, Γ_N^b has also the limiting property, $\lim_{N\to\infty} \Gamma_N^b(s) = sI - A_z$. Utilizing (5.43) and (5.44), $e^{-(sI-A_z)h_z}$ can be written as

$$e^{-(sI-A_z)h_z} = (\Phi_N^b - \Gamma_N^b(s))^N(\Phi_N^b + \Gamma_N^b(s))^{-N}.$$

Therefore, Z in (5.38) can be written as

$$Z(s) \;=\; (I-(\Phi_N^b-\Gamma_N^b(s))^N(\Phi_N^b+\Gamma_N^b(s))^{-N})(sI-A_z)^{-1}B_z\ .$$

By the limiting property of Γ_N^b, $\Gamma_N^b(s)\approx(sI-A_z)$, Z can be approximated to Z_N^b given below

$$\begin{aligned} Z(s)\approx Z_N^b(s) &= (I-(\Phi_N^b-sI+A_z)^N(sI-A_z+\Phi_N^b)^{-N}) \\ &\quad\times(sI-A_z)^{-1}B_z \\ &= \sum_{k=0}^{N-1}(\Pi_N^b)^k(s)\Xi_N^b(s)B_z\ , \end{aligned} \tag{5.45}$$

where $\Pi_N^b(s):=(\Phi_N^b-sI+A_z)(sI-A_z+\Phi_N^b)^{-1}$ and $\Xi_N^b(s)=2(sI-A_z+\Phi_N^b)^{-1}$.

Let us define the approximation error as $E_N:=Z-Z_N$, where Z_N is either Z_N^δ or Z_N^b. As shown in [69], both of the approximations guarantee that $\lim_{N\to\infty}\|E_N\|_\infty=0$. The stability of the rational approximation of $Z(s)$ depends on N. Using numerical calculations, the lower bound for N to satisfy the stability of rational approximation of $Z(s)$ is given in [69] by the following theorem.

Theorem 5.4. *[69] Both Z_N^δ given in (5.42) and Z_N^b given in (5.45) are stable for any $N>\tilde{N}$ with*

$$\tilde{N}=\left\lceil\frac{h_z}{2.8}\cdot\max_i|\lambda_i(A_z)|\right\rceil\ ,$$

where $\lambda_i(A_z)$ denotes the i^{th} eigenvalue of a given matrix A_z.

In each of the following three subsections, a different suboptimal stable $\mathcal{H}^\infty$ flow controller design approach is presented. It should be noted that any one of the approximation methods introduced above can be used for each of these approaches.

5.6.2 Stable $\mathcal{H}^\infty$ flow controller design by using coprime factorizations of the plant

Let $F_{2_{app}}:=\left[\begin{array}{c|c}\widetilde{A}_{F_2} & \widetilde{B}_{F_2}\\ \hline \widetilde{C}_{F_2} & 0\end{array}\right]$ be a rational approximation of F_2 in Figure 5.1. In here, $F_{2_{app}}$ can be obtained either by the δ-approximation method

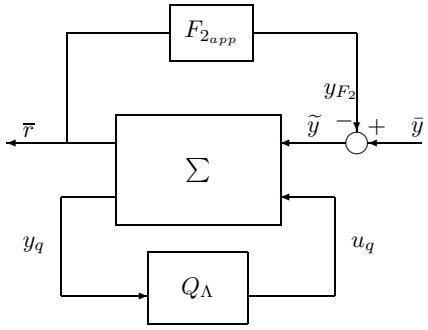

Figure 5.8: Representation with rational approximation of F_2 [48]

or by the bilinear approximation method. Then, replacing F_2 by $F_{2_{app}}$, the system from $\bar{y}$ to $\bar{r}$ can be represented as shown in Figure 5.8, where

$$\Sigma := \begin{bmatrix} \Sigma_{11} & \Sigma_{12} \\ \Sigma_{21} & \Sigma_{22} \end{bmatrix} := \left[\begin{array}{c|cc} A - B_2C_2 & B_2 & B_1 \\ \hline C_1 & 0 & I_n \\ -C_2 & 1 & 0 \end{array}\right], \tag{5.46}$$

where $\left[\begin{array}{c|cc} A & B_1 & B_2 \\ \hline C_1 & I_n & 0 \\ C_2 & 0 & 1 \end{array}\right] := \begin{bmatrix} G_{11} & G_{12} \\ G_{21} & G_{22} \end{bmatrix} := G_\Lambda^{-1}.$

The system in Figure 5.8 can equivalently be represented as in Figure 5.9, where

$$G_p := F_u(\Sigma, F_{2_{app}}) =: \begin{bmatrix} G_{p_{11}} & G_{p_{12}} \\ G_{p_{21}} & G_{p_{22}} \end{bmatrix} := \left[\begin{array}{c|cc} A_p & B_{p_1} & B_{p_2} \\ \hline C_{p_1} & D_{p_{11}} & D_{p_{12}} \\ C_{p_2} & D_{p_{21}} & D_{p_{22}} \end{array}\right]$$

$$:= \left[\begin{array}{cc|cc} A - B_2C_2 & -B_2\widetilde{C}_{F_2} & B_2 & B_1 \\ \widetilde{B}_{F_2}C_1 & \widetilde{A}_{F_2} & 0 & \widetilde{B}_{F_2} \\ \hline C_1 & 0 & 0 & I_n \\ -C_2 & -\widetilde{C}_{F_2} & 1 & 0 \end{array}\right]. \tag{5.47}$$

Now, let us consider the closed-loop TFM from $\bar{y}$ to $\bar{r}$ in Figure 5.9. A contractive Q_Λ stabilizes the closed-loop TFM from $\bar{y}$ to $\bar{r}$ in Figure 5.9 if and only if it stabilizes the plant $G_{p_{22}} = \left[\begin{array}{c|c} A_p & B_{p_2} \\ \hline C_{p_2} & 0 \end{array}\right]$ [5]. Similar to the approach

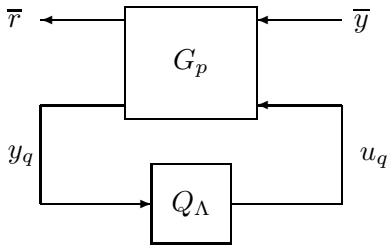

Figure 5.9: Equivalent representation with rational approximation of F_2 [48]

proposed in Section 5.4, to design a stabilizing contractive Q_Λ, let us assume that $G_{p_{22}}$ satisfies the following conditions:

a) (A_p, B_{p_2}) is stabilizable and (C_{p_2}, A_p) is detectable

b) A_p has no $j\omega$ axis eigenvalues.

Let $X_r \geq 0$ be the stabilizing solution of

$$A_p^T X_r + X_r A_p - X_r B_{p_2} B_{p_2}^T X_r = 0, \tag{5.48}$$

where $F_r := -B_{p_2}^T X_r$ and $A_{X_r} = A_p + B_{p_2} F_r$ is stable. Now, the problem of designing a contractive Q_Λ, which stabilizes $G_{p_{22}}$, can be solved by solving only one algebraic Riccati equation as given in the following theorem.

Theorem 5.5. *[26] There exits a contractive Q_Λ, which stabilizes G_p, if there exists $Y_r \geq 0$ and a $\overline{\varepsilon}_r \in (0, 1)$ such that*

$$A_{X_r} Y_r + Y_r A_{X_r}^T - Y_r(\overline{\varepsilon}_r^2 C_{p_2}^T C_{p_2} - X_r B_{p_2} B_{p_2}^T X_r) Y_r + B_{p_2} B_{p_2}^T = 0. \tag{5.49}$$

Under this condition, the realization of the contractive Q_Λ can be written as:

$$Q_\Lambda = \left[\begin{array}{c|c} A_{K_r} & -L_r \\ \hline F_r & 0 \end{array}\right], \tag{5.50}$$

where $A_{K_r} = A_{X_r} + L_r C_{p_2}$, and $L_r = -\overline{\varepsilon}_r^2 Y_r C_{p_2}^T$.

Alternatively, by using a left-coprime factorizations rather than a right coprime factorization (see Section 5.4), let $Y_l \geq 0$ be a stabilizing solution of

$$A_p Y_l + Y_l A_p^T - Y_l C_{p_2}^T C_{p_2} Y_l = 0, \tag{5.51}$$

where $L_l := -Y_l C_{p_2}^T$ and $A_{Y_l} := A_p + L_l C_{p_2}$ is stable. Then a solution can be obtained by using the following theorem.

Theorem 5.6. *[26] There exits a contractive Q_Λ, which stabilizes G_p, if there exists $X_l \geq 0$ and a $\overline{\varepsilon}_l \in (0,1)$ such that*

$$A_{Y_l}^T X_l + X_l A_{Y_l} + X_l (Y_l C_{p_2}^T C_{p_2} Y_l - \overline{\varepsilon}_l^2 B_{p_2} B_{p_2}^T) X_l + C_{p_2}^T C_{p_2} = 0. \tag{5.52}$$

Under this condition, the realization of the contractive Q_Λ can be written as:

$$Q_\Lambda = \left[\begin{array}{c|c} A_{K_l} & -L_l \\ \hline F_l & 0 \end{array}\right], \tag{5.53}$$

where $A_{K_l} = A_{Y_l} + B_{p_2} F_l$, and $F_l = -\overline{\varepsilon}_l^2 B_{p_2}^T X_l$.

Therefore, the following algorithms can be devised to obtain a stable $\mathcal{H}^\infty$ flow controller.

Algorithm 5.6.

1. *Find the optimal sensitivity level γ^{opt}, given by (4.36), and let $\gamma = \gamma^{opt}$. Choose a sufficiently large l and equally spaced values $\overline{\varepsilon}_1, \cdots, \overline{\varepsilon}_l$ within the interval $(0,1)$.*
2. *Find F_1, F_2, and G_Λ (see Section 4.3) for the current sensitivity level γ.*
3. *Compute $\widetilde{N}$ from Theorem 5.4, choose an upper bound $N_{max} > \widetilde{N}$, and let $N = \widetilde{N}$.*
4. *Let $N = N + 1$.*
5. *Find $F_{2_{app}}$ for the current N. Let $i = 1$.*
6. *If there exists $X_r \geq 0$, which solves (5.48), go to step 7. Otherwise, if $N < N_{max}$ go to step 4 else go to step 10.*
7. *For $\overline{\varepsilon}_r = \overline{\varepsilon_i}$, if there exists a solution $Y_r \geq 0$ to the Riccati equation (5.49) go to step 11. Otherwise, go to step 8.*

8. *If $i = l$ go to step 9. Otherwise, set $i = i + 1$ and go to step 7.*

9. *If $N < N_{max}$ go to step 4 else continue with step 10.*

10. *Increase γ by a small amount and go to step 2.*

11. *If $(1 + F_2H)^{-1}$ is unstable (can be checked by the Nyquist criterion), where $H = HM(G_\Lambda^{-1}, Q_\Lambda)$ and Q_Λ is obtained from (5.50), then go to step 8. If $(1 + F_2H)^{-1}$ is stable, the desired controller is then given by (see Figure 5.1)*

$$K(s) = F_1(s)H(s)\frac{\kappa(s+\epsilon)}{s(1+F_2(s)H(s))}\,, \tag{5.54}$$

where $\kappa = \frac{\gamma}{\sqrt{2\sum_{i=1}^{n}\left(\delta_i^+\right)^2}}$.

Algorithm 5.6 is based on the right-coprime factorization of G_{p22}. Based on the left-coprime factorization, the algorithm can alternatively be written if steps 6 and 7 are replaced by:

6. *If there exists $Y_l \geq 0$, which solves (5.51), go to step 7. Otherwise, if $N < N_{max}$ go to step 4 else go to step 10.*

7. *For $\overline{\varepsilon}_l = \overline{\varepsilon_i}$, if there exists a solution $X_l \geq 0$ to the Riccati equation (5.52) go to step 11. Otherwise, go to step 8.*

and "(5.50)" in step 11 is replaced by "(5.53)".

5.6.3 Stable $\mathcal{H}^\infty$ flow controller design by using LMI methods

Different from the above approach, to design a stable $\mathcal{H}^\infty$ flow controller, the approach of [70] can be utilized. To design a contractive Q_Λ, which stabilizes G_p, let us consider the following theorem.

Theorem 5.7. *[70] Let us assume that $G_{p_{22}}$ in (5.47) satisfies the conditions (a-b) given following (5.47). Then G_p is stabilizable by a contractive Q_Λ if*

there exists $V > 0$, $\widehat{X} \geq 0$, $\widehat{Y} > 0$, *a scalar* $\xi > 0$ *and a square matrix* T, *satisfying*

$$A_p^T\widehat{X} + \widehat{X}A_p - \widehat{X}B_{p_2}B_{p_2}^T\widehat{X} = 0 \tag{5.55}$$

$$A_p\widehat{Y} + \widehat{Y}A_p^T - 2\widehat{Y}C_{p_2}^TC_{p_2}\widehat{Y} < 0 \tag{5.56}$$

$$\begin{bmatrix} \Upsilon_{11} & \Upsilon_{12} & \Upsilon_{13} & \Upsilon_{14} \\ \Upsilon_{12}^T & \Upsilon_{22} & \xi\Upsilon_{13} & 0 \\ \Upsilon_{13}^T & \xi\Upsilon_{13}^T & -I & 0 \\ \Upsilon_{14}^T & 0 & 0 & -I \end{bmatrix} < 0, \tag{5.57}$$

where $\widehat{X}$ *is the stabilizing solution of (5.55) such that* $A_{\widehat{X}} := A_p - B_{p_2}B_{p_2}^T\widehat{X}$ *is stable and* $\Upsilon_{11} := A_{\widehat{X}}^T\widehat{Y}^{-1}T^T + T\widehat{Y}^{-1}A_{\widehat{X}} - C_{p_2}^TC_{p_2}T^T - TC_{p_2}^TC_{p_2}$, $\Upsilon_{12} := V - T\widehat{Y}^{-1} + \xi A_{\widehat{X}}^T\widehat{Y}^{-1}T^T - \xi C_{p_2}^TC_{p_2}T^T$, $\Upsilon_{13} := TC_{p_2}^T$, $\Upsilon_{14} := -\widehat{X}B_{p_2}$, $\Upsilon_{22} := -\xi T\widehat{Y}^{-1} - \xi\widehat{Y}^{-1}T^T$.

Then stabilizing contractive Q_Λ *can be constructed as:*

$$Q_\Lambda = \left[\begin{array}{c|c} A_{\widehat{X}} - \widehat{Y}C_{p_2}^TC_{p_2} & \widehat{Y}C_{p_2}^T \\ \hline -B_{p_2}^T\widehat{X} & 0 \end{array}\right]. \tag{5.58}$$

The algebraic Riccati equation (5.55) has a unique stabilizing solution, because $G_{p_{22}}$ satisfies assumptions (a-b) given following (5.47). The matrix inequality (5.56) can be converted to an LMI by pre-post multiplying (5.56) by $\widehat{Y}^{-1}$ and using Theorem 2.2. The matrix inequality (5.57), however, is not an LMI, since Υ_{11}, Υ_{12}, and Υ_{22} consist of summations of product of variables $\widehat{Y}$, T, and ξ. In order to solve (5.55)–(5.57), one of the approaches is as follows: first the algebraic Riccati equation (5.55) is solved for $\widehat{X}$. Once the solution of (5.55) is found, (5.56) can be solved for $\widehat{Y}$ as a feasibility problem by using LMI Toolbox in MATLAB [71]. After substituting the solutions of (5.55) and (5.56) into (5.57), the variables $\widehat{X}$ and $\widehat{Y}$ in (5.57) are eliminated. Now, (5.57) involves only three variables V, T, and ξ to be solved. However, Υ_{12}, $\xi\Upsilon_{13}$, and Υ_{22} consist of the summations of product of ξ and T. To eliminate one of the variables of Υ_{12}, $\xi\Upsilon_{13}$, and Υ_{22}, let us choose a positive number such as ξ_{max}. Now, replacing ξ in (5.57) by a chosen $\bar{\xi}$ in the interval $(0, \xi_{max})$, (5.57)

becomes an LMI in V and T and it can be solved as a feasibility problem. The following algorithm, realizes this approach.

Algorithm 5.7.

1. *Find the optimal sensitivity level* γ^{opt}*, given by (4.36), and let* $\gamma = \gamma^{opt}$*. Choose an upper bound* ξ_{max}*. Choose a sufficiently large* l *and equally spaced values* $\xi_1, \ldots, \xi_l$ *within the interval* $(0, \xi_{max})$*.*

2. *Find* F_1*,* F_2*, and* G_Λ *(see Section 4.3) for the current sensitivity level* γ*.*

3. *Compute* $\widetilde{N}$ *from Theorem 5.4, choose an upper bound* $N_{max} > \widetilde{N}$*, and let* $N = \widetilde{N}$*.*

4. *Let* $N = N + 1$*.*

5. *Find* $F_{2_{app}}$ *for the current* N*. Let* $i = 1$*.*

6. *If there exists* $\widehat{X} \geq 0$*, which solves (5.55), go to step 7. Otherwise, if* $N < N_{max}$ *go to step 4 else go to step 11.*

7. *Solve the feasibility problem (5.56) for* $\widehat{Y}$*. If there exists a solution* $\widehat{Y} \geq 0$ *go to step 8. Otherwise, if* $N < N_{max}$ *go to step 4 else go to step 11.*

8. *For* $\xi = \xi_i$*, solve the feasibility problem (5.57) for* V *and* T*. If there exists a solution* $V > 0$ *and a* T *go to step 12, otherwise, continue with step 9.*

9. *If* $i = l$ *go to step 10 else set* $i = i + 1$ *and go to step 8.*

10. *If* $N < N_{max}$ *go to step 4 else continue with step 11.*

11. *Increase* γ *by a small amount and go to step 2.*

12. *If* $(1 + F_2 H)^{-1}$ *is unstable (can be checked by the Nyquist criterion), where* $H = HM(G_\Lambda^{-1}, Q_\Lambda)$ *and* Q_Λ *is obtained from (5.58), then go to*

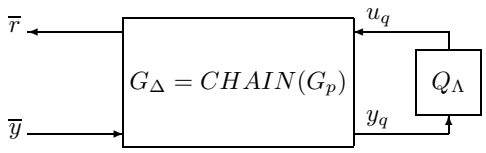

Figure 5.10: Chain-scattering representation [48]

step 9. If $(1 + F_2H)^{-1}$ *is stable, the desired controller is then given by (see Figure 5.1)*

$$K(s) = F_1(s)H(s)\frac{\kappa(s+\epsilon)}{s(1+F_2(s)H(s))}\ , \tag{5.59}$$

where $\kappa = \frac{\gamma}{\sqrt{2\sum_{i=1}^{n}\left(\delta_i^+\right)^2}}$.

5.6.4 Stable controller design using chain-scattering approach

In this subsection, chain-scattering representation is utilized in order to design a stable $\mathcal{H}^\infty$ flow controller. In (5.47), since $D_{p_{21}} = 1$ is invertible, G_p has a chain-scattering representation, $G_\Delta = CHAIN(G_p)$. Therefore, the system shown in Figure 5.9 can be represented as in Figure 5.10, where

$$\begin{aligned} G_\Delta \ &=: \ \left[\begin{array}{cc} G_{\Delta_{11}} & G_{\Delta_{12}} \\ G_{\Delta_{21}} & G_{\Delta_{22}} \end{array}\right] =: \left[\begin{array}{c|cc} \widehat{A} & \widehat{B}_1 & \widehat{B}_2 \\ \hline \widehat{C}_1 & I_n & 0 \\ \widehat{C}_2 & 0 & 1 \end{array}\right] \\ &:= \ \left[\begin{array}{c|cc} A_p - B_{p_1}C_{p_2} & B_{p_2} & B_{p_1} \\ \hline C_{p_1} & D_{p_{11}} & 0 \\ -C_{p_2} & 0 & D_{p_{21}} \end{array}\right], \end{aligned} \tag{5.60}$$

which can be shown to be bistable. The problem can now be defined as to find a contractive Q_Λ such that the closed-loop TFM from $\bar{y}$ to $\bar{r}$ in Figure 5.10, which is $S := HM(G_\Delta, Q_\Lambda)$, is stable. From (5.60), S can be written as $S = \lambda(G_{\Delta_{11}}Q_\Lambda + G_{\Delta_{12}})(\lambda G_{\Delta_{21}}Q_\Lambda + \lambda G_{\Delta_{22}})^{-1}$, for any $\lambda > 0$, which does not affect the stability, however might reduce the conservativeness in the controller design [67]. For any contractive Q_Λ, $\lambda(G_{\Delta_{11}}Q_\Lambda + G_{\Delta_{12}})$ is stable. Furthermore, $(\lambda G_{\Delta_{21}}Q_\Lambda + \lambda G_{\Delta_{22}})^{-1}$ (and thus S) is stable if $\|\lambda(G_{\Delta_{21}}Q_\Lambda + G_{\Delta_{22}}) - 1\|_\infty < 1$.

The problem of finding a contractive Q_Λ which satisfies $\|\lambda(G_{\Delta_{21}}Q_\Lambda + G_{\Delta_{22}}) - 1\|_\infty < 1$ can be defined as a two block problem as shown in [28]:

$$\|HM(T, Q_\Lambda)\|_\infty < 1 \ , \tag{5.61}$$

where

$$\begin{aligned} T &= \left[\begin{array}{cc} \left[\begin{array}{c} \lambda G_{\Delta_{21}} \\ I_n \end{array}\right] & \left[\begin{array}{c} \lambda G_{\Delta_{22}} - 1 \\ 0 \end{array}\right] \\ 0 & 1 \end{array}\right] = \left[\begin{array}{c|cc} \widehat{A} & \widehat{B}_1 & \widehat{B}_2 \\ \hline \lambda\widehat{C}_2 & 0 & \lambda - 1 \\ 0 & I_n & 0 \\ 0 & 0 & 1 \end{array}\right] \\ &=: \left[\begin{array}{c|c} A_T & B_T \\ \hline C_T & D_T \end{array}\right] \ . \end{aligned} \tag{5.62}$$

Finding a contractive Q_Λ which satisfies (5.61) can be solved via a $(\bar{J}, \hat{J})$-lossless factorization of T, where $\bar{J} := J_{(n+1),1}$ and $\hat{J} := J_{n,1}$. Similar to the problem solution in Section 5.2, the necessary condition for the $(\bar{J}, \hat{J})$-lossless factorization of T is the existence of a nonsingular E_T such that $D_T^T \bar{J} D_T = E_T^T \hat{J} E_T = \left[\begin{array}{cc} I_n & 0 \\ 0 & \lambda(\lambda - 2) \end{array}\right]$. This is satisfied for $0 < \lambda < 2$. Moreover, in this case, the nonsingular E_T can be selected as $E_T = \left[\begin{array}{cc} I_n & 0 \\ 0 & \sqrt{\lambda(2-\lambda)} \end{array}\right]$.

Theorem 5.8. *[50] For a given realization of T in (5.62), the two block problem given in (5.61) can be solved if there exists a solution $\overline{X} \geq 0$ for $0 < \lambda < 2$ satisfying*

$$\overline{X} A_T + A_T^T \overline{X} - R(D_T^T \bar{J} D_T)^{-1} R^T + C_T^T \bar{J} C_T = 0 \ , \tag{5.63}$$

where $R := C_T^T \bar{J} D_T + \overline{X} B_T$, such that $A_{F_T} := A_T + B_T F_T$ is stable, where $F_T := -(D_T^T \bar{J} D_T)^{-1} R^T$. In that case, the contractive Q_Λ can be written as

$$Q_\Lambda = HM(\Phi_T^{-1}, \widehat{\Gamma}) \ , \tag{5.64}$$

where $\widehat{\Gamma}$ is any contractive parameter and

$$\Phi_T^{-1} = \left[\begin{array}{c|c} A_T + B_T F_T & B_T E_T^{-1} \\ \hline F_T & E_T^{-1} \end{array}\right] \ .$$

Now, using Theorem 5.8, a stable $\mathcal{H}^\infty$ flow controller, which stabilizes the closed-loop system and achieves the design requirements can be obtained by the following algorithm.

Algorithm 5.8.

1. *Find the optimal sensitivity level γ^{opt}, given in (4.36), and let $\gamma = \gamma^{opt}$. Choose a sufficiently large l and equally spaced values λ_1, λ_2, ..., λ_l within the interval $(0, 2)$.*

2. *Find F_1, F_2, and G_Λ (see Section 4.3) for the current sensitivity level γ.*

3. *Compute $\widetilde{N}$ from Theorem 5.4, choose an upper bound $N_{max} > \widetilde{N}$, and let $N = \widetilde{N}$.*

4. *Let $N = N + 1$.*

5. *Find $F_{2_{app}}$ for the current N. Let $i = 1$.*

6. *For $\lambda = \lambda_i$, if there exists a solution $\overline{X} \geq 0$ to the Riccati equation (5.63) go to step 10, otherwise continue with step 7.*

7. *If $i = l$ go to step 8. Otherwise, set $i = i + 1$ and go to step 6.*

8. *If $N < N_{max}$ go to step 4 else continue with step 9*

9. *Increase γ by a small amount and go to step 2.*

10. *If $(1 + F_2 H)^{-1}$ is unstable (can be checked by the Nyquist criterion), where $H = HM(G_\Lambda^{-1}, Q_\Lambda)$ and Q_Λ is obtained from (5.64), then go to step 7. If $(1 + F_2 H)^{-1}$ is stable, the desired controller is then given by (see Figure 5.1)*

$$K(s) = F_1(s)H(s)\frac{\kappa(s+\epsilon)}{s(1 + F_2(s)H(s))}\,, \tag{5.65}$$

where $\kappa = \frac{\gamma}{\sqrt{2\sum_{i=1}^{n}\left(\delta_i^+\right)^2}}$.

5.6.5 Performance of the designed controllers

In this subsection, the performance of the stable controllers designed by Algorithms 5.6, 5.7, and 5.8 are compared. In order to illustrate and compare the performance of the stable $\mathcal{H}^\infty$ flow controllers designed by Algorithms 5.6–5.8, the network introduced in Section 5.3 is considered. The controllers are designed for Case 1, given in Table 5.1. The upper bound ξ_{max} in step 1 of Algorithm 5.7 is taken as $\xi_{max} = 1000$. The free parameter $\widehat{\Gamma}$ of the stable $\mathcal{H}^\infty$ flow controller, which is designed by Algorithm 5.8, is taken as $\widehat{\Gamma} = 0$. The stable $\mathcal{H}^\infty$ flow controllers designed by Algorithms 5.6–5.8 are obtained for $N = 2$, where $\widetilde{N} = 1$. The γ value, which yields a stable $\mathcal{H}^\infty$ flow controller for each algorithm, is presented in Table 5.3. In Table 5.3, γ^{opt} represents the optimal sensitivity level of the corresponding optimal controller, $\gamma^{5.6}$ represents the γ value, which yields a stable $\mathcal{H}^\infty$ flow controller by Algorithm 5.6, $\gamma^{5.7}$ represents the γ value, which yields a stable $\mathcal{H}^\infty$ flow controller by Algorithm 5.7, and $\gamma^{5.8}$ represents the γ value which yields a stable $\mathcal{H}^\infty$ flow controller by Algorithm 5.8. As seen in Table 5.3, the stable $\mathcal{H}^\infty$ flow controllers designed by Algorithms 5.6 and 5.7 produce smaller sensitivity levels compared to Algorithm 5.8. In addition, the stable $\mathcal{H}^\infty$ flow controllers designed by Algorithms 5.6 and 5.7 are obtained for the same sensitivity level no matter which approximation method is used. In addition, since G_p in (5.47) is stable for Case 1, $X_r = 0$ and $\widehat{X} = 0$ solve (5.48) and (5.55), respectively. Hence, Algorithms 5.6 and 5.7 result in a stable central controller for Case 1. However, the stable controller designed by Algorithm 5.8 is not a central controller. In addition, as shown in Table 5.3, the stable $\mathcal{H}^\infty$ flow controller designed by Algorithm 5.8 using the δ-approximation method is obtained for a smaller sensitivity level compared to the one which yields a stable controller by Algorithm 5.8 using the bilinear approximation method.

For the time-domain performance comparison of the designed controllers, the simulations are done using MATLAB/SIMULINK package, where the nonlinear effects (hard constraints) are also taken into account. For all

Table 5.3: Sensitivity level of the designed stable $\mathcal{H}^\infty$ flow controllers

Case	γ^{opt}	Approximation method	$\gamma^{5.6}$	$\gamma^{5.7}$	$\gamma^{5.8}$
Case 1	2.817	δ-approximation method	3.260	3.260	4.297
		bilinear approximation method	3.260	3.260	4.528

cases, as in the previous sections, the desired queue length, q_d, is taken 30 packets, the buffer size (maximum queue length) is taken as 60 packets, and the capacity of the outgoing link is taken as 90 packets/tu, where tu stands for time unit. Moreover, the rate limits for the sources are taken as 150 packets/tu. The uncertain part of the actual time-delays used in the simulations are as in Case 1a, which is given in Table 5.2. The response of the designed stable $\mathcal{H}^\infty$ flow controllers are presented in Figures 5.11–5.12. As stated above, since Algorithms 5.6 and 5.7 yield the same stable $\mathcal{H}^\infty$ flow controller, the performance of the controller designed by Algorithm 5.6 is compared to the one designed by Algorithm 5.8. In Figure 5.11, (a) represents the response of the controller designed by Algorithm 5.6, and (b) represents the response of the controller designed by Algorithm 5.8 using the δ-approximation method. In order to compare the performance of the obtained stable controllers using the δ-approximation method with the ones obtained using the bilinear approximation method, the response of the stable $\mathcal{H}^\infty$ flow controller, which is designed for Case 1 by Algorithm 5.8 using the bilinear approximation method, is presented in Figure 5.12. In Figures 5.11–5.12, q (whose scale is on the right) is the queue length $q(t)$, and $\mathrm{r}_i^{\mathrm{s}}$ (whose scale is on the left) is the actual flow rate at source i, for $i = 1, 2$.

As seen in Figures 5.11–5.12, all the stable controllers designed by the proposed algorithms here, whether using the δ or the bilinear rational approximation method, stabilize the actual system and achieve the design requirements despite the presence of uncertain time-varying time-delays. The oscillations in the queue length in Figures 5.11–5.12 are due to the variations

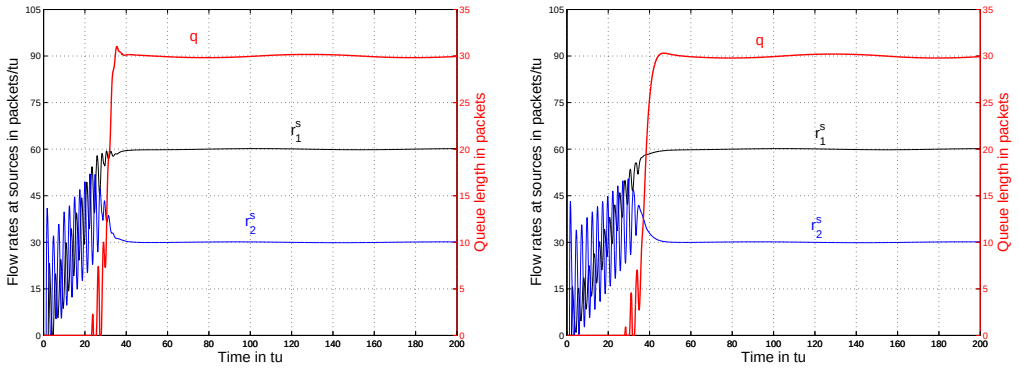

(a) (b)

Figure 5.11: Simulation results of the designed stable controllers for Case 1a

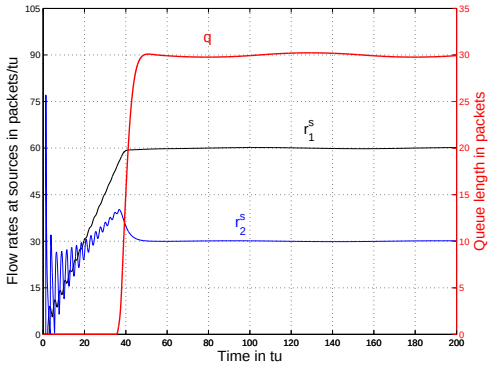

Figure 5.12: Simulation result of the stable controller designed by using the bilinear approximation for Case 1a

of the uncertain part of the forward time-delay. As shown by comparing Figure 5.11(a) to 5.11(b), the stable $\mathcal{H}^\infty$ flow controller designed by Algorithm 5.6 (or 5.7) has faster response compared to the one designed by Algorithm 5.8.

As seen by comparing Figure 5.11(b) to 5.12, the response of the controller designed by Algorithm 5.8 using the δ-approximation method is faster compared to the one designed by Algorithm 5.8 using the bilinear approximation method. This observation was also stated in [49]. Therefore, as seen in Table 5.3, the controllers designed by Algorithm 5.8 using the δ-approximation method results in a less conservative controller compared to the controller designed by using the bilinear approximation method, in general.

In the previous sections, F_2 was used either in the controller design to satisfy a bound on the $\mathcal{H}^\infty$ norm of $HM(G_\Lambda^{-1}, Q_\Lambda)$ or to determine the stability of the controller by the obtained $HM(G_\Lambda^{-1}, Q_\Lambda)$. However, Algorithms 5.6, 5.7, and 5.8 consider the dynamics of the approximated FIR filter F_2 to design a stable $\mathcal{H}^\infty$ controller. In general, Algorithms 5.6, 5.7 and 5.8 yield stable controllers. However, similar to the previous algorithms, these algorithms do not guarantee to yield a stable controller.

5.7 Summary

In this chapter, a number of different stable $\mathcal{H}^\infty$ flow controller design approaches were presented. The first approach uses the small-gain theorem, since finite-dimensional part of the controller is fed back by the stable infinite-dimensional block. In the first approach, since the algorithm produces a conservative controller, due to the use of the small-gain theorem, in Section 5.3, a less conservative approach was presented. The third approach, which was presented in Section 5.4, is based on the stabilization of the finite-dimensional part of the flow controller. In the fourth approach, presented in Section 5.5, stable controller design was based on seeking a stable $\mathcal{H}^\infty$ flow controller by increasing the gain of the uncertainty weight. Each of the last three stable $\mathcal{H}^\infty$ flow controller design approaches, all presented in Section 5.6, were based on a different approach to the stable controller design problem for finite-dimensional systems, where a rational approximation of F_2 is used.

In order to show the performance of the designed controllers by the approaches proposed in Sections 5.3–5.6, simulation studies were carried out using MATLAB/SIMULINK package, where the nonlinearities of the model were taken into account (see Section 4.1). As shown by the simulation results, the actual plant was robustly stabilized and the performance objectives, despite the presence of uncertain time-varying time-delays, were achieved by the suboptimal stable $\mathcal{H}^\infty$ flow controllers, which were designed by Algorithms 5.2–5.8.

As a summary, even though only the sufficient conditions are used to design a stable $\mathcal{H}^\infty$ flow controller, Algorithms 5.1–5.8 produce a stable controller, in many cases. However, it should be noted that none of the proposed algorithms guarantee to produce a stable $\mathcal{H}^\infty$ flow controller.

6 CONCLUSION

In this dissertation, an optimal $\mathcal{H}^\infty$ flow controller design problem for data-communication networks was considered. The controller was designed utilizing the non-causal uncertainty blocks instead of causal blocks to improve the performance of the controller. The $\mathcal{H}^\infty$ flow controllers were designed neglecting the existing nonlinearities. However, since unstable controllers are highly sensitive to unmodelled nonlinear dynamics, the neglected nonlinearities may worsen the performance of the resulting controller, if it is unstable. In order to overcome this problem, stable $\mathcal{H}^\infty$ flow controller design problem was also considered.

In Chapter 3, validity of the small-gain theorem for feedback interconnection of non-causal subsystems was considered. In Section 3.2, the sufficient conditions to satisfy the internal stability of the feedback interconnection of two stable subsystems, at least one of which is non-causal, were given. In order to utilize the small-gain theorem in the robust flow controller design, the result in Section 3.2 was extended and a less conservative result was presented in Section 3.3. Utilization of the non-causal uncertainty blocks in the robust controller design for systems with multiple uncertain time-delays was presented in Section 3.4. In Section 3.4, under different uncertainty representations of the finite-dimensional part of the plant, it was shown that the uncertainty block of the generalized system has a special structure for each representation. It was shown in Section 3.4 that the proposed conditions in Sections 3.2 and 3.3 for the validity of the small-gain theorem under non-causal subsystems may not be sufficient to design a robust controller by the approach of [13]. In order to utilize the non-causal uncertainty blocks in the robust controller design, a new small-gain condition, called strong small-gain condition, was introduced in Section 3.4. In Section 3.5, an alternative robust controller design approach was proposed by replacing the non-causal uncertainty blocks with the causal ones.

In Chapter 3, in order to utilize the non-causal uncertainty blocks to

design a robust controller for multiple time-delay systems by the approach of [13], it was assumed that the nominal plant has a coprime-factorization, where the denominator matrix is diagonal. This assumption brings a conservatism. This assumption was made to factor out the uncertainty part and state the problem in a generalized framework. Another restriction in this study arises in the case of multiplicative input/output uncertainty representation, since either the input or the output uncertainty block must also be diagonal.

In Chapter 4, robust flow control problem for data-communication networks was considered. The network model was given in Section 4.1 and the mathematical model of the overall system was given in Section 4.2. In Section 4.2, the uncertainty block of the overall system was allowed to be non-causal. However, utilizing the results in Section 3.3, these non-causal blocks could be handled. A mixed sensitivity minimization problem was defined in Section 4.3 to design a robust flow controller which keeps the queue length at the bottleneck node at a desired level and allocates the different ratios of the network capacity to different sources. The time-domain performance of the controllers designed by the approach proposed in Section 4.3 was illustrated by simulations using MATLAB/SIMULINK package in Section 4.4. The simulations were done using a discrete model, where the controllers were designed by using a fluid-flow model. In addition, the performance improvements of the controllers designed by the approach of Section 4.3 compared to the controllers designed by the approach of [23] were shown in Section 4.4. In Section 4.5, the performance level and actual stability margins were derived for the designed optimal $\mathcal{H}^\infty$ flow controllers. The advantages of using non-causal uncertainty blocks in the robust flow controller design problem were addressed in Section 4.6. In Section 4.7, sufficient conditions to choose the free parameter Q_Λ were derived such that the controller achieving the robustness and the tracking requirements also achieves the weighted fairness requirement by the chosen Q_Λ.

In Chapter 4, a robust optimal flow controller was designed for data-communication networks with a single bottleneck-node. In this case, since the

network has a single bottleneck-node, which is fed by n sources, the nominal time-delays at the channels were factored out and the approach of [13] was used to design a robust flow controller. To design a robust flow controller for multi-bottleneck networks is not trivial. In this case, there exists n bottleneck nodes, each of which is fed by multiple sources. In addition, each bottleneck node can also send data to other bottleneck nodes. Therefore, the dynamics of the queue length at a bottleneck node depends on the rate of data that is received from the sources, the other bottleneck nodes, and the rate of data that is sent to the other bottleneck nodes from the current bottleneck node [72]. It should be noted that both the rate of data that is received from the sources and the other bottleneck nodes and the rate commands that are sent from any bottleneck node are subject to time-delays. Besides the existence of the time-delays, which are usually uncertain and time-varying, one of the arising problems in the design is: What should be the type of the controller: "centralized" or "decentralized"? If a centralized controller is to be designed, then another question arises: Where it should be implemented? Since there are multiple bottleneck-nodes and the information send from each bottleneck node, except the bottleneck node, where the centralized controller is implemented (if the controller is implemented at a bottleneck node), to the centralized controller is subject to time-delays, different network topologies may require different locations for the implementation of the centralized controller. If a decentralized controller is to be designed, following the lines of [73], the nominal time-delays can be factored out and the approach of [13] may be used to design a robust flow controller. For a future study, using the approach proposed in this dissertation, a decentralized robust flow controller can be designed for data-communication networks with multiple bottleneck nodes following the lines of [73].

In Chapter 5, the stable $\mathcal{H}^\infty$ flow controller design problem was considered. This problem is difficult and stable $\mathcal{H}^\infty$ controller design problem for systems with time-delays up to date have been limited to SISO systems. A number of approaches were given to design a stable $\mathcal{H}^\infty$ flow controller. In all approaches, except the approach of Section 5.5, stable $\mathcal{H}^\infty$ flow controller

design approaches were based on designing a contractive Q_Λ to stabilize the overall controller, apart from the integral term. In Algorithm 5.1, a strong $\mathcal{H}^\infty$ stabilization problem is solved to design a stable $\mathcal{H}^\infty$ flow controller. In Algorithm 5.2, another strong $\mathcal{H}^\infty$ stabilization problem is solved to design a stable $\mathcal{H}^\infty$ flow controller. However, the problem, which is to be solved in Algorithm 5.2, is more relaxed compared to that one in Algorithm 5.1. In Algorithms 5.3 and 5.4, the stable $\mathcal{H}^\infty$ flow controller design was based on the stabilization of the finite-dimensional part of the controller. In Algorithm 5.5, the stable $\mathcal{H}^\infty$ flow controller design was based on seeking a stable stabilizing $\mathcal{H}^\infty$ flow controller by increasing the gain of the defined uncertainty weight. Algorithms 5.6–5.8 were based on solving the strong stabilization problem by utilizing a rational approximation of the FIR block in the feedback loop of the controller structure. Once a rational approximation of the FIR block is found, the contractive free parameter, Q_Λ, is designed to stabilize the approximation of the controller. It is then checked whether this Q_Λ also stabilizes the actual controller. If it does, the desired controller is obtained. If not, a new contractive Q_Λ is sought.

The presented approaches in Chapter 5 are conservative, since these approaches were based on sufficient conditions and may increase the sensitivity level γ, unnecessarily. In addition, since the finite-dimensional term of the controller, except the integral term, is fed back by an infinite-dimensional block, instead of considering the dynamics of the infinite-dimensional block, the dynamics of a rational approximation of this block was considered to design a stable $\mathcal{H}^\infty$ flow controller. Moreover, since all the proposed algorithms were based on sufficient conditions, these algorithms do not guarantee to result in a stable $\mathcal{H}^\infty$ flow controller. However, stable $\mathcal{H}^\infty$ flow controllers were obtained by the proposed algorithms, in general. For a future study, stable $\mathcal{H}^\infty$ flow controller design can be considered by taking into account the dynamics of the infinite-dimensional part of the controller directly.

In summary, robust flow controller design for data communication networks with multiple time-delays utilizing the non-causal uncertainty blocks

was presented in this dissertation. As shown by a number simulations, the performance of the robust flow controllers designed by utilizing the non-causal uncertainty blocks is in general better than the performance of the controllers designed utilizing the causal blocks. In addition, it is indicated by a number of cases that the controllers designed utilizing the non-causal uncertainty blocks have better robustness margins and performance levels compared to the controllers designed by utilizing the causal uncertainty blocks. Since the controller design approach proposed here may result in unstable controllers, which may fail to produce a stable response due to their sensitivity to unmodelled dynamics, stable $\mathcal{H}^\infty$ flow controller design was presented using different approaches. As shown by a number of simulations, while the designed optimal controllers can not produce a stable response, stable $\mathcal{H}^\infty$ controllers, which were obtained by the proposed algorithms, stabilize the actual system and produce a desired response.

BIBLIOGRAPHY

[1] S. I. Niculescu. *Delay Effects on Stability: A Robust Control Approach,* Lecture Notes in Control and Information Sciences, No. 269. Springer-Verlag, London, 2001.

[2] J.-P. Richard. Time-delay systems: an overview of some recent advances and open problems. *Automatica*, 39:1667–1694, 2003.

[3] G. Zames. On the input-output stability of time-varying nonlinear feeedback systems Part I: Conditions derived using concepts of loop gain, conicity, and positivity. *IEEE Transactions on Automatic Control*, AC–11:228–238, 1966.

[4] I. W. Sandberg. On the L_2-boundedness of solutions of nonlinear functional equations. *Bell Syst. Tech. J.*, 43:1581–1599, 1964.

[5] K. Zhou, J. C. Doyle, and K. Glover. *Robust and Optimal Control.* Prentice Hall, Englewood Cliffs, U.S.A, 1996.

[6] O. Toker and H. Özbay. $\mathcal{H}_\infty$ optimal and suboptimal controllers for infinite dimensional SISO plants. *IEEE Transactions on Automatic Control*, 40:751–755, 1995.

[7] R. F. Curtain and H. Zwart. *An Introduction to Infinite-Dimensional Linear Systems Theory.* Springer-Verlag, New York, U.S.A, 1995.

[8] C. Foias, H. Özbay, and A. Tannenbaum. *Robust Control of Infinite Dimensional Systems: Frequency Domain Methods,* Lecture Notes in Control and Information Sciences, No. 209. Springer-Verlag, London, 1996.

[9] S. Gümüşsoy. *Optimal H^∞ Controller Design and Strong Stabilization for Time-Delay and MIMO Systems.* PhD Dissertation, The Ohio State University, Columbus, Ohio, U.S.A., 2004.

[10] K. M. Nagpal and R. Ravi. $\mathcal{H}^\infty$ control and estimation problems with delayed measurements: State-space solutions. *SIAM Journal on Control and Optimization*, 35:1217–1243, 1997.

[11] G. Tadmor. The standart $\mathcal{H}^\infty$ problem in systems with a single input delay. *IEEE Transactions on Automatic Control*, 45:382–397, 2000.

[12] G. Meinsma and H. Zwart. On $\mathcal{H}_\infty$ control for dead-time systems. *IEEE Transactions on Automatic Control*, 45:272–285, 2000.

[13] G. Meinsma and L. Mirkin. $\mathcal{H}_\infty$ control of systems with multiple I/O delays via decomposition to adobe problems. *IEEE Transactions on Automatic Control*, 50:199–211, 2005.

[14] D. Gorinevsky and G. Stein. Structured uncertainty analysis of robust stability for multidimensional array systems. *IEEE Transactions on Automatic Control*, 48:1557–1568, 2003.

[15] R. D'Andrea. A linear matrix inequality approach to decentralized control of distributed parameter systems. In *Proceedings of the American Control Conference*, pages 1350–1354, Philadelphia, PA, U.S.A, 1998.

[16] R. D'Andrea. Linear matrix inequalities, multidimensional system optimization, and control of spacially distributed systems: An example. In *Proceedings of the American Control Conference*, pages 2713–2717, San Diego, CA, U.S.A, 1999.

[17] R. D'Andrea and G. E. Dullerud. Distributed control design for spatially interconnected systems. *IEEE Transactions on Automatic Control*, 48:1478–1495, 2003.

[18] R.S. Chandra and R. D'Andrea. A scaled small gain theorem with applications to spatially interconnected systems. *IEEE Transactions on Automatic Control*, 51:465–469, 2006.

[19] S. Mascolo. Smith's principle for congestion control in high-speed ATM networks. In *Proceedings of the 36th Conference on Decision and Control*, pages 4595–4600, San Diego, CA, U.S.A, December 1997.

[20] S. Mascolo. Congestion control in high-speed communication networks using the Smith principle. *Automatica*, 35:1921–1935, 1999.

[21] H. Özbay, S. Kalyanaraman, and A. İftar. On rate-based congestion control in high speed networks: Design of an $\mathcal{H}^\infty$ based flow controller for single bottleneck. In *Proceedings of the American Control Conference*, pages 2376–2380, Philadelphia, PA, U.S.A, June 1998.

[22] H. Özbay, T. Kang, S. Kalyanaraman, and A. İftar. Performance and robustness analysis of an $\mathcal{H}^\infty$ based flow controller. In *Proceedings of the IEEE Conference on Decision and Control*, pages 2691–2696, Phoenix, AZ, U.S.A, December 1999.

[23] P.-F. Quet, B. Ataşlar, A. İftar, H. Özbay, S. Kalyanaraman, and T. Kang. Rate-based flow controllers for communication networks in the presence of uncertain time-varying multiple time-delays. *Automatica*, 38:917–928, 2002.

[24] B. Ataşlar, H. Özbay, and A. İftar. Comparision of H^∞ and μ synthesis based flow controllers for high-speed networks with multiple time-delays. In *Proceedings. of the American Control Conference*, pages 3787–3788, Arlington, VA, U.S.A, 2001.

[25] B. Ataşlar. *Veri-İletişim Ağlarında Gürbüz Akış Kontrolü*. PhD Dissertation, Anadolu University, Eskişehir, Turkey, July 2004.

[26] M. Zeren and H. Özbay. On the strong stabilization and stable $\mathcal{H}^\infty$-controller design problems for MIMO systems. *Automatica*, 36:1675–1684,

2000.

[27] S. Gümüşsoy and H. Özbay. Remarks on strong stabilization and stable H^∞ controller design. *IEEE Transactions on Automatic Control*, 50:2083–2087, 2005.

[28] P. H. Lee and Y. C. Soh. Synthesis of stable $\mathcal{H}^\infty$ controller via the chain scattering framework. *Systems and Control Letters*, 47:121–127, 2002.

[29] V. Balakrishnan. $\mathcal{H}^\infty$ controller synthesis with time-domain constraints. *IEEE Transactions on Automatic Control*, 42:1179–1186, 1997.

[30] A. M. Mohamed, F. Matsumura, T. Namerikawa, and J.-H. Lee. Q-parameterization control of vibrations in a variable speed magnetic bearing. In *Proccedings of the 1997 International Conference on Control Applications*, pages 540–546, Hartford, CT, U.S.A, October 1997.

[31] M. Vidyasagar. *Control System Synthesis: A Factorization Approach*. M.I.T. Press, Cambridge, MA, U.S.A, 1985.

[32] D.U. Campos-Delgado and K. Zhou. A parameteric optization approach to $\mathcal{H}^\infty$ and $\mathcal{H}_2$ strong stabilization. *Automatica*, 39:1205–1211, 2003.

[33] J. L. Abedor and K. Poola. On the strong stabilization of delay systems. In *Proceedings of the IEEE Conference on Decision and Control*, pages 2317–2318, Tampa, FL, U.S.A, December 1989.

[34] K. Suyama. Strong stabilization of systems with time-delays. In *Proceedings of the 1991 International Conference on Industrial Electronics, Control and Instrumentation*, pages 1758–1763, Kobe, JAPAN, October 1991.

[35] S. Gümüşsoy and H. Özbay. Stable H^∞ controller design for time-delay systems. *International Journal of Control*, 81:546–556, 2008.

[36] H. U. Ünal and A. İftar. A small gain theorem for systems with non-causal subsystems. *Automatica*, 44:2950–2953, 2008.

[37] H. U. Ünal and A. İftar. Utilization of non-causal uncertainty blocks in the robust flow controller design problem for data-communication networks. In *Proceedings of the 17th IEEE International Conference on Control Applications*, pages 61–66, San Antonio, TX, U.S.A., September 2008.

[38] H. U. Ünal and A. İftar. Utilization of non-causal uncertainty blocks in the robust controller design problem for systems with multiple uncertain time-delays. In *Proceedings of the 18th International Symposium on Mathematical Theory of Networks and Systems*, Blacksburg, VA, U.S.A., July 2008.

[39] H. U. Ünal and A. İftar. Robust control design for time-delay systems using non-causal uncertainty blocks. In *Proceedings of the European Control Conference*, pages 567–572, Budapest, HUNGARY, August 2009.

[40] H. U. Ünal, B. Ataşlar-Ayyıldız, A. İftar, and H. Özbay. Robust controller design for multiple time-delay systems: The case of data-communication networks. In *Proceedings of the 17th International Symposium on Mathematical Theory of Networks and Systems*, pages 63–70, Kyoto, JAPAN, July 2006.

[41] H. U. Ünal, B. Ataşlar, A. İftar, and H. Özbay. Çoklu zaman gecikmeli veri iletişim ağları için gürbüz denetleyici tasarımı. In *Proceedings of the National Automatic Control Meeting (TOK'06)*, pages 451–456, Ankara, TURKEY, November 2006.

[42] H. U. Ünal, B. Ataşlar-Ayyıldız, A. İftar, and H. Özbay. H^∞-based flow control in data-communication networks with multiple time-delays. Technical Report, Dept. of Electrical and Electronics Engineering, Anadolu University, Eskişehir, Turkey, 2006.

[43] H. U. Ünal, B. Ataşlar-Ayyıldız, A. İftar, and H. Özbay. Robust flow control in data-communication networks with multiple time-delays. *International Journal of Robust and Nonlinear Control*, 2010. (DOI:10.1002/rnc.1535).

[44] H. U. Ünal and A. İftar. Veri-iletişim ağları için tasarlanan optimal H^∞ akış denetleyicisinin performans seviyesi ve gürbüz kararlılık payları. In *Proceedings of the National Automatic Control Meeting (TOK'08)*, pages 188–193, İstanbul, TURKEY, November 2008.

[45] H. U. Ünal and A. İftar. Performance and robustness of flow controllers designed using non-causal uncertainty blocks. (Submitted for publication).

[46] H. U. Ünal and A. İftar. Veri-iletişim ağlarında adil kapasite paylaşımını sağlayan gürbüz akış denetleyicisi tasarımı. In *Proceedings of the National Automatic Control Meeting (TOK'07)*, pages 212–217, İstanbul, TURKEY, September 2007.

[47] H. U. Ünal and A. İftar. Stable H^∞ controller design for systems with multiple time-delays: The case of data-communication networks. In *Proceedings of the 17th IFAC World Congress*, pages 13348–13354, Seoul, KOREA, July 2008.

[48] H. U. Ünal and A. İftar. Stable H^∞ flow controller design. In *Proceedings of the 8th IFAC Workshop on Time-Delay Systems*, Sinaia, ROMANIA, September 2009.

[49] H. U. Ünal and A. İftar. Kararlı H^∞ akış denetleyicilerinin performansı. In *Proceedings of the National Automatic Control Meeting (TOK'09)*, İstanbul, TURKEY, October 2009.

[50] H. Kimura. *Chain-Scattering Approach to H_∞ Control.* Birkhauser, Boston, U.S.A, 1996.

[51] G. E. Dullerud and F. Paganini. *A Course in Robust Control Theory.* Springer, New York, U.S.A, 1999.

[52] J. F. Kurose and K. W. Ross. *Computer Networking A Top-Down Approach Featuring the Internet.* Addison-Wesley, U.S.A., 2003.

[53] G. Zames. On the input-output stability of time-varying nonlinear feeedback systems Part II: Conditions involving circles in the frequency plane and sector nonlinearities. *IEEE Transactions on Automatic Control*, AC–11:228–238, 1966.

[54] J. C. Williems. *The Analysis of Feedback Systems.* MIT Press, Cambridge Massachusetts, U.S.A, 1971.

[55] M. Vidyasagar. *Nonlinear System Analysis.* Prentice-Hall, New Jersey, U.S.A, 1993.

[56] L. Mirkin and N. Raskin. Every stabilizing dead-time controller has an observer-predictor-based structure. *Automatica*, 39:1747–1754, 2003.

[57] E. Altman, T. Başar, and R. Srikant. Multi-user rate-based flow control with action delays: a team-theoretic approach. In *Proceedings of the IEEE Conference on Decision and Control*, pages 2387–2392, San Diego, CA, U.S.A, December 1997.

[58] L. Benmohamed and S. M. Meerkov. Feedback control of congestion in packet switching networks: the case of a single congested node. *IEEE/ACM Trans. on Networking*, 1:693–708, 1993.

[59] F. Bonomi and K. W. Fendick. The rate-based flow control framework for the available bit rate ATM service. *IEEE Network*, 9(2):25–39, March/April 1995.

[60] S. Floyd. TCP and explicit congestion notification. *ACM Computer Communication Review*, 24:10–23, 1994.

[61] S. Kunniyur and R. Srikant. End-to-end congestion control schemes: Utility functions, random losses, and ECN marks. In *Proceedings of the INFOCOM*, pages 1323–1332, Tel Aviv, ISRAEL, March 2000.

[62] P. K. Laberteaux, C. E. Rohrs, and P. J. Antsaklis. A practical controller for explicit rate congestion control. *IEEE Transactions on Automatic Control*, 47:960–978, 2002.

[63] S. Mascolo. Smith's principle for congestion control in high-speed data networks. *IEEE Transactions on Automatic Control*, 45:358–364, 2000.

[64] K. Ogata. *Modern Control Engineering*. Prentice–Hall, Englewood Cliffs, NJ, U.S.A, 1990.

[65] O. Toker and H. Özbay. On the rational $\mathcal{H}_\infty$ controller design for infinite dimensional plants. *International Journal of Robust and Nonlinear Control*, 6:383–397, 1996.

[66] H. Özbay. Tutorial review $\mathcal{H}_\infty$ optimal controller design for a class of distributed parameter systems. *International Journal of Control*, 58:739–782, 1993.

[67] P. H. Lee and Y. C. Soh. Synthesis of simultaneous stabilizing $\mathcal{H}^\infty$ controller. *International Journal of Control*, 78:1437–1446, 2005.

[68] M. Zeren and H. Özbay. On the synthesis of stable $\mathcal{H}^\infty$ controllers. *IEEE Transactions on Automatic Control*, 44:431–435, 1999.

[69] Q. C. Zhong. *Robust Control of Time-Delay Systems*. Springer-Verlag, London, UK, 2006.

[70] P. Cheng, Y. Y. Cao, and Y. Sun. Strong γ_k-γ_{cl} $\mathcal{H}^\infty$ stabilization with a new slack variable approach. *Automatica*, 45:1861–1867, 2009.

[71] P. Gahinet, A. Nemirovski, A. J. Laub, and M. Chilali. *LMI Control Toolbox, For use with MATLAB*. The MathWorks, Inc., 1995.

[72] E. Biberović, A. İftar, and H. Özbay. A solution to the robust flow control problem for networks with multiple bottlenecks. In *Proceedings of the IEEE Conference on Decision and Control*, pages 2303–2308, Orlando, FL, U.S.A, December 2001.

[73] İ. Munyas, Ö. Yelbaşı, E. Biberović, A. İftar, and H. Özbay. Decentralised robust flow controller design for networks with multiple bottlenecks. *International Journal of Control*, 82:95–116, 2009.